

DEVELOPMENT OF A NOVEL GRADIENT-  
FORCE TAPERED FIBRE OPTICAL TWEEZERS  
SYSTEM FOR 3D OPTICAL TRAPPING AT NEAR  
HORIZONTAL FIBRE INSERTION ANGLES

STEVEN ROSS

A thesis submitted in partial fulfilment of the requirements  
of Liverpool John Moores University for the degree of  
Doctor of Philosophy (Ph.D.)

November 2014

**ABSTRACT**

The use of optical fibre as a mechanism for the delivery of the trapping laser beam to the sample chamber significantly reduces both the size and the build costs of “Optical Tweezers”. Furthermore, the use of fibre facilitates the decoupling of the optical trapping beam from the microscope optics, which provides further scope for the development of a portable optical trapping system, and the potential for uncomplicated integration with other advanced microscopy systems such as an atomic force microscope (AFM) for example. For use with an AFM, the optical fibre must be inserted at an angle of  $10^\circ$  with respect to the sample chamber floor. However, previous literature suggests that 3D optical trapping with a single fibre inserted at an angle  $\leq 20^\circ$  is not feasible. This thesis presents the design, development, build and test of a single beam optical fibre based gradient force optical tweezers system and its associated software. An investigation is conducted to ascertain why optical trapping, using single fibre systems, cannot be achieved at sub  $20^\circ$  insertion angles, the result of which formed the basis of a hypothesis that explains this limitation. This finding led to the development of tapered optical fibre tips that are capable of 3D optical trapping at an insertion angle of  $\leq 10^\circ$ . The optimised optical fibre tapers are presented and their ability to trap both organic and inanimate material in 3D at an insertion angle of  $10^\circ$  is demonstrated. The near-horizontal insertion angle introduced a maximum trapping range (MTR). The MTR of the tips is determined empirically, evaluated against simulated data, and found to be tuneable through taper optimisation. Optical trap characterisation has been undertaken in terms of the optical trapping forces acting on the trapping subjects. Finally, the fibre tapering devices ability to reproduce identical tapers, or not, using the same device parameters, was investigated and the results in terms of geometric profile and optical performance are presented.

# TABLE OF CONTENTS

<b>ABSTRACT</b> .....	<b>II</b>
<b>TABLE OF CONTENTS</b> .....	<b>III</b>
<b>ACKNOWLEDGMENTS</b> .....	<b>VIII</b>
<b>LIST OF FIGURES</b> .....	<b>X</b>
<b>LIST OF TABLES</b> .....	<b>XIV</b>
<b>LIST OF EQUATIONS</b> .....	<b>XV</b>
<b>LIST OF ABBREVIATIONS</b> .....	<b>XVII</b>
<b>1 CHAPTER ONE INTRODUCTION</b> .....	<b>1-1</b>
1.1 AIMS AND OBJECTIVES .....	1-3
<b>2 CHAPTER TWO OPTICAL TRAPPING: ORIGIN, THEORY, DESIGN</b>	
<b>CONFIGURATIONS AND APPLICATIONS</b> .....	<b>2-1</b>
2.1 OPTICAL TRAPPING THEORY .....	2-5
2.2 FORCE MODELLING .....	2-8
2.2.1 <i>MIE REGIME - THE RAY OPTICS MODEL</i> .....	2-12
2.2.2 <i>RAYLEIGH REGIME – POINT DIPOLE MODEL</i> .....	2-13
2.2.3 <i>INTERMEDIATE REGIME – ELECTROMAGNETIC THEORY</i> .....	2-14
2.3 OPTICAL TRAPPING DESIGN CONFIGURATIONS .....	2-14
2.3.1 <i>MULTIPLE TRAPPING SYSTEMS</i> .....	2-15
2.3.2 <i>ALTERNATIVE BEAM MODES</i> .....	2-20
2.4 APPLICATIONS OF OPTICAL TRAPPING .....	2-22
<b>3 CHAPTER THREE FIBRE OPTIC BASED OPTICAL TRAPPING SYSTEM</b>	
<b>CONFIGURATIONS</b> .....	<b>3-1</b>
3.1 COUNTER-PROPAGATING OPTICAL FIBRES .....	3-2
3.2 SINGLE OPTICAL FIBRE BASED TRAPPING SYSTEMS .....	3-6
3.3 SHAPING OPTICAL FIBRE FOR 3D OPTICAL TRAPPING .....	3-10
3.3.1 <i>CHEMICAL ETCHING</i> .....	3-12
3.3.2 <i>LASER MICRO-MACHINING</i> .....	3-13
3.3.3 <i>FOCUSED ION BEAM (FIB)</i> .....	3-14
3.3.4 <i>POLISHING AND GRINDING</i> .....	3-15
3.3.5 <i>PHOTO-POLYMERISATION</i> .....	3-15
3.3.6 <i>GRADED INDEX FIBRE LENS</i> .....	3-16

3.3.7	<i>HEATING AND DRAWING</i> .....	3-16
3.4	BEAM SHAPING DISCUSSION .....	3-18
<b>4</b>	<b>CHAPTER FOUR SYSTEM DESIGN CONSIDERATIONS.....</b>	<b>4-1</b>
4.1	RECAP- OPTICAL TRAPPING DESIGN CONFIGURATIONS.....	4-2
4.2	RECAP-DESIGN SPECIFICATIONS .....	4-2
4.3	ADVANTAGES OF FIBRE OPTIC BASED OPTICAL TRAPPING (FOT) CONFIGURATIONS OVER CONVENTIONAL OPTICAL TWEEZERS (COT) SYSTEMS.....	4-3
4.3.1	<i>SYSTEM SIZE AND COST</i> .....	4-3
4.3.2	<i>TRAP DETECTION</i> .....	4-4
4.3.3	<i>DECOUPLING THE TRAPPING LASER BEAM FROM THE MICROSCOPE'S VIEWING OPTICS</i> .....	4-11
4.3.4	<i>CONVENTIONAL OPTICAL TWEEZERS SYSTEM CONFIGURATION, MANOEUVRABLE DISTANCE AND OPTICAL POWER CONSTRAINTS</i> .....	4-12
4.4	DISADVANTAGES OF FIBRE OPTIC BASED OPTICAL TWEEZERS CONFIGURATIONS OVER COT SYSTEMS.....	4-13
4.4.1	<i>MAINTAINING A TARGET IMAGE DURING SAMPLE ELEVATION</i> .....	4-13
4.4.2	<i>MULTIPLE TRAPPING SITES</i> .....	4-14
4.4.3	<i>REDUCED OPTICAL TRAPPING EFFICIENCY</i> .....	4-16
4.4.4	<i>DISADVANTAGES DUE TO THE PHYSICAL ATTRIBUTES OF OPTICAL FIBRE</i> .....	4-18
4.5	CHOICE OF SYSTEM CONFIGURATION .....	4-19
4.6	PREFERRED OPTICAL FIBRE TRAP CONFIGURATION.....	4-20
4.7	PREFERRED BEAM FOCUSING METHOD .....	4-28
<b>5</b>	<b>CHAPTER FIVE TAPERED FIBRE OPTIC TWEEZERS (T-FOTs) SYSTEM COMPONENTS.....</b>	<b>5-1</b>
5.1	MICROSCOPE.....	5-2
5.2	LASER .....	5-4
5.2.1	<i>BEAM QUALITY</i> .....	5-4
5.2.2	<i>WAVELENGTH</i> .....	5-5
5.2.3	<i>OPTICAL OUTPUT POWER</i> .....	5-8
5.2.4	<i>VENTUS IR LASER</i> .....	5-10
5.3	LASER TO FIBRE COUPLING .....	5-12
5.4	OPTICAL FIBRE CONNECTORS .....	5-18

5.5	SINGLE MODE OPTICAL FIBRE (SMF).....	5-23
5.6	OPTICAL POWER MONITORING.....	5-26
5.6.1	<i>INLINE OPTICAL TAP</i> .....	5-26
5.6.2	<i>OPTICAL POWER METER</i> .....	5-26
5.7	DATA ACQUISITION .....	5-27
5.8	VIDEO ACQUISITION .....	5-28
5.9	MICRO/NANO MANIPULATION TRANSLATION STAGES.....	5-34
5.9.1	<i>MOTORISED LINEAR TRANSLATION STAGES</i> .....	5-34
5.9.2	<i>PIEZO TRANSLATION STAGES</i> .....	5-35
5.9.3	<i>ROTATION STAGE</i> .....	5-35
5.10	MISCELLANEOUS COMPONENTS.....	5-35
5.10.1	<i>LASER INTERLOCK SYSTEM</i> .....	5-36
5.10.2	<i>OPTICAL TRAPPING SHROUD</i> .....	5-37
5.10.3	<i>SAFETY EYEWEAR AND OPTICAL IR FILTERS</i> .....	5-37
5.10.4	<i>SUTTER P2000/F MICROPIPETTE PULLER</i> .....	5-38
5.10.5	<i>OPTICAL FIBRE FUSION SPLICER</i> .....	5-39
5.10.6	<i>THERMAL CYCLER PCR MACHINE</i> .....	5-40
5.10.7	<i>THERMOCOUPLE</i> .....	5-43
<b>6</b>	<b>CHAPTER SIX TAPERED FIBRE OPTIC TWEEZERS (T-FOTs) SYSTEM SETUP AND CALIBRATION.....</b>	<b>6-1</b>
6.1	TAPERED FIBRE OPTIC TWEEZERS (T-FOTs) SYSTEM SETUP.....	6-2
6.2	OPTICAL FIBRE TAPER FABRICATION.....	6-8
6.2.1	<i>HEATING &amp; DRAWING METHOD USING THE SUTTER P/2000F MICROPIPETTE PULLER</i> .....	6-8
6.3	FABRICATION OF TAPERED FIBRE OPTIC TIP FOR 3D OPTICAL TRAPPING .....	6-9
6.3.1	<i>SPLICING OF THE OPTICAL FIBRE TO THE SYSTEM</i> .....	6-9
6.3.2	<i>LOADING THE FIBRE INTO THE MICROPIPETTE PULLER FOR TAPER FABRICATION</i> .....	6-11
6.3.3	<i>TAPERED FIBRE OPTIC TIP INSPECTION</i> .....	6-15
6.4	TAPERED FIBRE OPTIC TWEEZERS (T-FOTs) SYSTEM CALIBRATION .....	6-16
6.4.1	<i>MICROSCOPE AND CAMERA</i> .....	6-16
6.4.2	<i>INLINE OPTICAL TAP</i> .....	6-23
6.4.2.1	<i>CALIBRATION SETUP</i> .....	6-24
6.4.2.2	<i>OPTICAL TAP CALIBRATION METHOD</i> .....	6-29

6.4.3	<i>OPTICAL FIBRE TAPER POSITIONING AND ALIGNMENT</i> .....	6-31
<b>7</b>	<b>CHAPTER SEVEN EXPERIMENTAL PROCEDURES, RESULTS AND DISCUSSION</b> .....	<b>7-1</b>
7.1	VISUAL INSPECTION OF TAPERED OPTICAL FIBRE TIPS .....	7-3
7.2	TEST FOR 3D OPTICAL TRAPPING AT AN INSERTION ANGLE OF 45° .....	7-3
7.2.1	<i>3D TRAPPING TEST FOR TAPERED FIBRE OPTIC TIP NUMBER 44</i> .....	7-5
7.2.2	<i>RESULTS - 3D TRAPPING TEST</i> .....	7-8
7.3	OPTICAL TRAPPING AT 10° INSERTION ANGLE .....	7-10
7.3.1	<i>INVESTIGATIONS INTO TRAPPING DEGRADATION AT INSERTION ANGLES BELOW 20°</i> ...	7-11
7.3.2	<i>FIBRE TAPER OPTIMISATION FOR 3D OPTICAL TRAPPING AT AN INSERTION ANGLE OF 10°</i> .....	7-14
7.3.3	<i>DEVELOPMENT OF NOVEL OPTIMISED TAPERED FIBRE OPTIC TIPS FOR 3D OPTICAL TRAPPING AT AN INSERTION ANGLE OF 10°</i> .....	7-16
7.4	INITIAL OPTICAL TRAPPING OBSERVATIONS .....	7-20
7.4.1	<i>CHANGE IN TRAP DYNAMICS</i> .....	7-21
7.4.2	<i>EXPERIMENT - DETERMINING THE MAXIMUM TRAPPING RANGE</i> .....	7-25
7.4.3	<i>RESULTS: DETERMINING THE MAXIMUM TRAPPING RANGE</i> .....	7-27
7.4.4	<i>FURTHER TESTING TO VALIDATE THE MAXIMUM TRAPPING RANGE</i> .....	7-28
7.4.5	<i>POSSIBLE EXPLANATION FOR THE MAXIMUM TRAPPING RANGE ERROR</i> .....	7-29
7.5	CHARACTERISING THE OPTICAL TRAPPING FORCE .....	7-31
7.6	RESULTS - CHARACTERISING THE OPTICAL TRAPPING FORCE .....	7-35
7.6.1	<i>TAPERED OPTICAL FIBRE TIP NUMBER 44</i> .....	7-37
7.6.2	<i>TAPERED OPTICAL FIBRE TIP NUMBER 92</i> .....	7-39
7.6.3	<i>TAPERED OPTICAL FIBRE TIP NUMBER 94</i> .....	7-41
7.6.4	<i>TAPERED OPTICAL FIBRE TIP NUMBER 96</i> .....	7-42
7.7	EFFECTS OF FRAME RATE ON MEASURED OPTICAL TRAPPING FORCE.....	7-43
7.8	FIBRE TAPER REPEATABILITY TEST .....	7-46
7.8.1	<i>RESULTS – COMPARISON OF THE PHYSICAL DIMENSIONS</i> .....	7-47
7.8.2	<i>RESULTS – COMPARISON OF THE MAXIMUM TRAPPING RANGE</i> .....	7-48
7.8.3	<i>RESULTS – COMPARISON OF THE TAPERS OPTICAL TRAP FOCAL POINTS</i> .....	7-49
7.8.4	<i>RESULTS – COMPARISON OF THE OPTICAL FORCE OUTPUT</i> .....	7-50
7.8.5	<i>DISCUSSION</i> .....	7-53
7.9	TRAPPING OF BIOLOGICAL SAMPLES.....	7-55

<b>8</b>	<b>CHAPTER EIGHT CONCLUSION .....</b>	<b>8-1</b>
<b>9</b>	<b>CHAPTER NINE FUTURE WORK .....</b>	<b>9-1</b>
<b>10</b>	<b>SECTION TEN REFERENCES.....</b>	<b>10-1</b>
<b>11</b>	<b>SECTION ELEVEN APPENDICES .....</b>	<b>11-1</b>
11.1	APPENDIX - A – PUBLICATIONS .....	11-2
11.1.1	<i>NON-PEER REVIEWED .....</i>	<i>11-2</i>
11.1.2	<i>PEER REVIEWED.....</i>	<i>11-3</i>
11.1.2.1	<i>SINGLE-BEAM THREE-DIMENSIONAL OPTICAL TRAPPING AT EXTREMELY LOW INSERTION ANGLES VIA OPTICAL FIBER OPTIMIZATION</i>	<i>11-3</i>
11.2	APPENDIX – B - OPTICAL TRAPPING DATA SOURCES (ON DISK) .....	11-1
11.2.1	<i>DISK 1 VIDEO DATA FOR TIP NUMBER 44.....</i>	<i>11-1</i>
11.2.2	<i>DISK 1 DECOMPILED VIDEO DATA FOR TIP NUMBER 44.....</i>	<i>11-1</i>
11.2.3	<i>DISK 2 VIDEO DATA FOR TIPS NUMBERED 92, 94 AND 96 .....</i>	<i>11-2</i>
11.2.4	<i>DISK 2 DECOMPILED VIDEO DATA FOR TIPS NUMBERED 92, 94 AND 96.....</i>	<i>11-4</i>
11.3	APPENDIX - C – DISK 2 T-FOT'S SYSTEM SOFTWARE PROGRAMS .....	11-7
11.4	APPENDIX - D – DISK 2 SYSTEM COMPONENTS SPECIFICATION SHEETS .....	11-7

## ACKNOWLEDGMENTS

Throughout my Ph.D. there have been many people who have helped my progression upon this arduous, sometimes frustrating and at times lonely, but also challenging, exciting and rewarding journey. Therefore I would like to give thanks and show my gratitude to those who have aided my arrival to this point. First of all I would like to give thanks to my principal supervisor Professor David R. Burton for securing the funding and granting me the “opportunity of a lifetime”. I really appreciate your wide breadth of technical knowledge and your understanding of all things in general that you bring to our student supervisor meetings. I am also grateful for your uplifting words of encouragement during times when things did not go according to plan, your patience and your continued efforts of support in varying capacities throughout my PhD life-cycle. The continued support that you apply to all your students is, in your own words, a legacy of one of the founder members of GERI, Emeritus Professor Michael J. Lalor an advisor and friend to whom I also give thanks and my wholehearted gratitude.

To my second supervisor Dr. Francis Lilley the “go to guy of GERI” you have been a constant vehicle of support in all aspects of research life from technical advisor to proof reader thanks a million Fran for everything. To my third supervisor, mate and fellow Bluenose Dr. Mark F. Murphy the biology man I would like to thank you for all your advice over the years both as a colleague and a friend. But I especially want to thank you for the laughs; you really are a funny man who cheers the place up no end. I would like to give my sincere thanks to Helen who I consider a good friend and who works tirelessly to ensure that GERI runs like clockwork; I hope all your dreams transpire Miss Pottle. I extend this thanks to the since retired Mrs. Margaret Sutton, Prof. Lalor’s sidekick, who was like a mother to all the students during my formative years as a researcher. I would like to thank Dr. Frederic

Bezombes for his expertise and crash course in fibre termination and polishing and Dr. Sasha Skydan for the use of his particle tracking software. There are many other colleagues and friends who have passed through the doors of GERI over the years who have made some contribution, or other, that are just too numerous to mention personally, for which I apologise in advance, but you all know who you are and I extend my gratitude thus. I definitely owe each and every one of you a drink or three.

I would like to thank the Engineering and Physical Sciences Research Council (EPSRC) who supported this research under Grant No. R66311G. I would also like to thank Mr. Adrian Walker and the team at the Engineering Instrument Loan Pool, Rutherton Appleton Laboratory, UK, for the loan of high speed video camera equipment that was critical for this project.

I would like to thank my Mother Lesley for her unwavering belief in me, and my Father John whose dogged determination to carry on come hell or high water has definitely rubbed off on me. It is a quality that I have had to call on countless times to get me to the finish line. I would also like to thank my brother and sister; Ian and Julie and their fantastic families for all of their support and my free haircuts. Finally, but certainly not least I would like to give my truly heartfelt thanks and love to my wife Melanie and two sons Martin and Sonny, who have all sacrificed something in the cause. But especially my wife and best friend whose unconditional love and support has definitely been tested to the maximum. You have been my one pillar of support that I know I can always rely on and for which I am eternally grateful.

## LIST OF FIGURES

Figure 1-1 (a) showing the internal configuration of the AFM head (b) arrangement of how the integrated AFM and optical fibre based trapping system configuration would look and showing an optical fibre tip deployed at an insertion angle of ten degrees.....	1-5
Figure 2-1 electromagnetic radiation pressure forces acting on an off-axis sphere in a weakly focused laser beam.....	2-3
Figure 2-2 (a) counter-propagating laser beam trap (b) optical levitation trap.....	2-6
Figure 2-3 optical tweezers (a) particle located beyond focal point - backwards axial restoring force (b) particle located before the focus – forward axial restoring force (c) particle located off-axis – transverse restoring force.....	2-8
Figure 2-4 particle size regimes (a) Mie regime $d > \lambda$ (b) Intermediate regime $d = \lambda$ and (c) Rayleigh regime $d < \lambda$ .....	2-11
Figure 2-5 single laser source dual-trap optical tweezers system.....	2-16
Figure 2-6 schematic of dual optical tweezers created using two laser sources.....	2-17
Figure 2-7 Tetris arcade game re-created using a fast scanning laser to optically trap 42 x 1 $\mu\text{m}$ glass beads; image courtesy of.....	2-19
Figure 2-8 (a) Gaussian TEM <sub>00</sub> intensity beam profile (b) Laguerre-Gaussian TEM <sub>01</sub> “doughnut mode” intensity profile.....	2-21
Figure 2-9 intensity distributions near the focus for (a) radially polarised beam $\phi = 0^\circ$ and (b) azimuthally polarised beam $\phi = 90^\circ$ .....	2-22
Figure 4-1 showing how the tapered fibre tip points to the trapping zone (a) first frame of optical trapping video sequence (b) last frame of optical trapping video sequence.....	4-5
Figure 4-2 effectiveness of a QPD detection system for (a) COT optical tweezers dual trap system and (b) a single optical fibre based 3D optical tweezers system.....	4-10
Figure 4-3 schematic depicting 2D trapping at a 45° insertion angle. The particle is trapped as the microscope sample chamber slide acts to halt the particle’s migration in the direction of the beam’s propagation.....	4-23
Figure 4-4 diagram depicting 2D manipulation at a at 10° insertion angle. At the near horizontal insertion angle there is no physical impedance provided to the particle by the microscope sample slide thus the particle is accelerated away from the fibre tip by the laser beam.....	4-24
Figure 5-1 (a) plan view of the Ventus IR laser mounted on the bespoke aluminium bracket. The laser to fibre coupler, labelled port 1, is mounted on the right hand side of the 90° angle bracket (b) side elevation of the laser and the bespoke bracket-coupler assembly.....	5-14
Figure 5-2 initial dual port laser to fibre coupling device.....	5-15

Figure 5-3 laser to fibre coupler lens graph showing the focal length of the focusing lens required to provide a focused laser beam spot size $\leq$ the mode field diameter of the fibre.....	5-17
Figure 5-4 graph showing the focal length of the focusing lens required to provide a $NA_{\text{Fibre}} \leq NA_{\text{Rays}}$ .....	5-18
Figure 5-5 original laser to fibre coupling system incorporating a 50/50 beam splitter with built in manual attenuators and dual laser to fibre couplers (b) reconfigured laser to single optical fibre coupling system .....	5-21
Figure 5-6 comparison of optical power oscillation, due the use of high power connectors (HPC), for laser to single fibre and laser to dual fibre coupling configurations.....	5-23
Figure 5-7 diagrams depicting a 3 $\mu\text{m}$ particle with overlay xMag, yMag grid (a) grid showing xMag =130 nm and yMag = 130 nm values for Infinity-X camera (b) grid showing xMag = 250 nm and yMag = 250 nm values for MC-1 camera .....	5-34
Figure 5-8 (a) optical tap and thermocouple set within the lid of the thermo cycler PCR machine to enable the optical tap's local temperature feedback and control (b) magnified image of the optical tap and thermocouple fitted within the lid of the PCR machine.....	5-42
Figure 6-1 basic schematic diagram of the tapered optical fibre tweezers system (T-FOT's) system design setup .....	6-3
Figure 6-2 T-FOTs tapered optical fibre tip entering the microscope sample chamber supported by the steel tod and fibre holder.....	6-4
Figure 6-3 translation assemblies mounted on a tall structure showing 50 mm length mounting post arrangement for a tapered optical fibre insertion angle of $10^\circ$ .....	6-6
Figure 6-4 stripping of Acrylate buffer.....	6-12
Figure 6-5 P2000/F 20W $\text{CO}_2$ laser based micropipette puller.....	6-13
Figure 6-6 (a) showing an SEM image of a "good" tapered fibre tip and (b) showing a higher magnification SEM image of a "bad" snapped and uneven end faced tapered fibre tip.....	6-16
Figure 6-7 image of the stage micrometer under x10 magnification with a x0.5 magnification C-mount adapter, opened in GIMP to calculate the amount of pixels for a given distance of $400\mu\text{m}$ .....	6-18
Figure 6-8 objective lens x40, c-mount lens included giving a real magnification that varies with c-mount adjustment (a) c-mount adjusted fully in the anti-clockwise direction (b) c-mount adjusted in the fully clockwise direction.....	6-20
Figure 6-9 objective lens x40 magnification, c-mount lens extracted giving a real magnification of 34.5 (a) image at full resolution $1280 \times 1024$ pixels (b) image at reduced resolution $640 \times 480$ pixels .....	6-22
Figure 6-10 setup for calibration of the inline optical tap.....	6-25

Figure 6-11 Thorlabs PM100 optical power meter virtual instrument graphical user interface.....	6-26
Figure 6-12 optical tap monitoring virtual instrument (OpticalTap25degrees.vi) developed in the LabView programming language .....	6-28
Figure 7-1 trapping in 2D; as the tapered optical fibre taper is elevated in the +ve Z direction the microsphere is driven away from the tapered optical fibre tip in the direction of the laser beam's propagation and remains seated on the microscope sample chamber floor. ....	7-7
Figure 7-2 X-Y trapping (a) the tapered fibre probe and 3 $\mu$ m diameter silica micro-sphere trapped at the fibre end, (b)-(e) The Piezo translation stage moves the fibre probe, directing sphere A in an anti-clockwise direction around sphere B, in the directional sequence +X, +Y, -X, -Y (f)-(g) Z-Trapping (f) the trapping fibre is moved in the +Z direction and both the fibre and the silica sphere can be seen to be out of focus (image (g) continued on the following page in Figure 7-4(g)).....	7-9
Figure 7-3 (continued from previous page in Figure 7-3 (a)-(f)) (g) the trapping fibre is moved in the -Z direction and both the fibre and particle A are seen to have come back into focus.....	7-10
Figure 7-4 Dimensions of Nufern 1060XP single mode optical fibre .....	7-12
Figure 7-5 large diameter, tapered optical fibre tip at an insertion angle of 45 $^{\circ}$ .....	7-13
Figure 7-6 large diameter tapered optical fibre tip at an insertion angle of 10 $^{\circ}$ .....	7-14
Figure 7-7 proposed optimized optical fibre taper geometry possessing a longer taper length combined with a smaller diameter tip to gain closer proximity to the sample.....	7-15
Figure 7-8 dimensions of the tapered fibre optic tips numbered (a) 44, (b) 92, (c) 94 and (d) 96 .....	7-18
Figure 7-9 SEM Image of (a) slight bend in the needle-like region due to elastic recoil (b) distortion seen in a light microscopy image of a tapered tip with pronounced elastic recoil (c) hand polished finish to the taper end-face (d) taper showing signs of heat distortion.....	7-20
Figure 7-10 tapered optical fibre tips, corresponding to program numbers (a) 92 (b) 94 and (c) 96, optically trapping 3 $\mu$ m silica microspheres, showing their respective trapping zones.....	7-21
Figure 7-11 TFOT's system demonstrating the optical trapping of three microspheres simultaneously due to optical binding.....	7-23
Figure 7-12 change in trapping dynamics with the introduction of a maximum trapping range .....	7-24
Figure 7-13 experimental procedure carried out to determine the maximum trapping range (MTR).....	7-26

Figure 7-14 (a) plot of data with uncharacteristic data spike (b) plot of data after using clipdata1.pro to eradicate the data spike.....	7-35
Figure 7-15 force v optical power gradients for tip number 44 at 45° insertion angle and tips numbered 92, 94 and 96 at an insertion angle of 10° .....	7-36
Figure 7-16 force - distance curves of ascending optical powers for tip numbered 44 at an insertion angle of 45° .....	7-39
Figure 7-17 force - distance curves of ascending optical powers for tip numbered 92 at an insertion angle of 10° .....	7-40
Figure 7-18 force - distance curves of ascending optical powers for tip numbered 94 at an insertion angle of 10° .....	7-42
Figure 7-19 force - distance curves of ascending optical powers for tip numbered 96 at an insertion angle of 10° .....	7-43
Figure 7-20 comparison of alternative frame rates - force - distance curves of ascending optical powers for tip numbered 94 at an insertion angle of 10° (a) 500fps and (b) 1000fps .....	7-44
Figure 7-21 (a) original fibre taper dimensions for tip number 92 (b) attempt to recreate tip 92 - fibre taper dimensions for tip 92a (c) original fibre taper dimensions for tip number 94 (d) attempt to recreate tip 94 - fibre taper dimensions for tip 94a.....	7-48
Figure 7-22 comparison of the optical tweezers trapping zone for (a) tip 92 (b) tip 92a (c) tip 94 and (d) tip 94a .....	7-50
Figure 7-23 comparison of the optical forces produced by the original and replica tapers (a) tip 92 and its replica (b) tip 92a; and the original tip 94 (c) and its replica tip 94a (d).....	7-51
Figure 7-24 force v optical power gradients for tip number 92 and 92a at 10° insertion angle .....	7-52
Figure 7-25 force v optical power gradients for tip number 94 and 94a at 10° insertion angle .....	7-53
Figure 7-26 optically trapped yeast cell elevated above the general population of cells demonstrating 3D trapping in the process .....	7-56
Figure 9-1 particle distribution plot showing the starting position of 3µm silica microspheres recorded during multiple location optical trapping procedures.....	9-4

**LIST OF TABLES**

Table 4-1 memory requirements for 1 second of video footage acquired from the two video cameras employed during this project .....	4-8
Table 4-2 comparison of the resolvable tracking distance that can be achieved by the two video cameras for x20, 35, x40, x60 and x100 magnifications .....	4-8
Table 5-1 comparison of optical power fluctuations in laser to dual optical fibre coupling against laser to single optical fibre coupling using high power optical fibre connectors.....	5-22
Table 5-2 optical fibre comparison .....	5-24
Table 5-3 T-FOTs system insertion loss power budget .....	5-25
Table 5-4 video camera specification comparison.....	5-30
Table 5-5 comparison of camera memory requirements.....	5-31
Table 5-6 field of view and pixel resolution at x40 magnification .....	5-33
Table 5-7 P2000/F micropipette puller, parameters, parameter ranges and functions.....	5-39
Table 6-1 key for Figure 6-5 P2000/F micropipette puller's description .....	6-13
Table 6-2 overall image magnification after c-mount adjustment .....	6-20
Table 7-1 Sutter P2000/F micropipette puller program parameters for the first single tapered fibre capable of 3D optical trapping- taper number 44.....	7-5
Table 7-2 parameter values for the P2000/F Micro-Pipette Puller Used to Fabricate the Optical Fibre Tapers.....	7-16
Table 7-3 trapping range uncertainty .....	7-27
Table 7-4 force v power gradient (FPG) values and optical trapping efficiency (Q) values .....	7-37
Table 7-5 average optical power output of laser for tip 94 at 500fps and 1000fps.....	7-45
Table 7-6 average optical power output of laser for tips and 92, 94 and replica tapers 92a and 94a .....	7-51

**LIST OF EQUATIONS**

(2-1)	.....	2-4
(2-2)	.....	2-9
(2-3)	.....	2-9
(2-4)	.....	2-10
(2-5)	.....	2-11
(2-6)	.....	2-12
(2-7)	.....	2-12
(2-8)	.....	2-12
(2-9)	.....	2-13
(2-10)	.....	2-13
(2-11)	.....	2-13
(2-12)	.....	2-14
(2-13)	.....	2-14
(4-1)	.....	4-11
(4-2)	.....	4-25
(4-3)	.....	4-26
(5-1)	.....	5-16
(5-4)	.....	5-25
(5-5)	.....	5-26
(6-1)	.....	6-17
(6-2)	.....	6-17
(6-3)	.....	6-19
(7-1)	.....	7-26
(7-2)	.....	7-31
(7-3)	.....	7-33

(7-4) ..... 7-33

(7-5) ..... 7-33

(7-6) ..... 7-34

(7-7) ..... 7-34

## LIST OF ABBREVIATIONS

<b>.vi</b>	LabView virtual instrument
<b>2D</b>	Two dimensional
<b>3D</b>	Three dimensional
<b>AFM</b>	Atomic force microscope
<b>AOD</b>	Acoustic optic deflector
<b>COT</b>	Conventional optical tweezers
<b>dB</b>	Decibel
<b>dBm</b>	Decibel-milliwatts
<b>DOE</b>	Diffraction optical element
<b>DPSS</b>	Diode pumped solid state
<b>EPSRC</b>	European Physical Research Council
<b>FC/AFC</b>	Ferrule connector/angled flat connector
<b>FC/APC</b>	Ferrule connector/angled polished connector
<b>FOT</b>	Fibre optic based trapping system
<b>FPG</b>	Force/Power Gradient
<b>FOV</b>	Field of view
<b>fps</b>	Frames per second
<b>GERI</b>	The General Engineering Research Institute
<b>GUV's</b>	Giant unilamellar vesicles
<b>HOTs</b>	Holographic optical tweezers
<b>IR</b>	Infrared
<b>LJMU</b>	Liverpool John Moores University
<b>MMF</b>	Multi mode fibre
<b>NA</b>	Numerical aperture
<b>Nd:YAG</b>	Neodymium doped Yttrium Aluminium Garnet
<b>OT</b>	Optical trapping
<b>OT's</b>	Optical tweezers
<b>PCR machine</b>	Polymerase chain reaction machine
<b>InGaAs</b>	Indium gallium arsenide
<b>PM SMF</b>	Polarisation maintaining single mode fibre
<b>Q</b>	Optical trapping system efficiency
<b>QPD</b>	Quadrant photo diode
<b>RBC's</b>	Red blood cells
<b>SEM</b>	Scanning electron microscope
<b>SLM</b>	Spatial light modulator
<b>SMF</b>	Single mode fibre
<b>T-FOTs</b>	Tapered fibre optic tweezers
<b>TIR</b>	Total internal reflection

# CHAPTER ONE INTRODUCTION

## INTRODUCTION

Light can be considered one of the most fundamental and invaluable resources available to man, especially considering that in its absence life itself could not exist. The Sun is the largest natural energy source servicing planet Earth with heat and light. It provides the light that drives photosynthesis in plants, is the cause of atmospheric and aqueous current flows and supplies the warmth and illumination that makes life and vision possible ([Kalogirou, 2009](#)).

Both natural and artificial light can be used in an endless number of ways. For example it is used to heat and illuminate rooms, transport data in telecommunication systems ([Acampora, 1994](#)) and deliver military missile hardware with pin point accuracy ([Cohen, 1994](#)). It is employed in both medical ([Razaghi et al., 2012](#), [Weber et al., 1997](#)) and superficial beauty treatments alike ([Gallagher et al., 2005](#)). It mimics the action of the stylus on a vinyl record, playing music from compact discs ([Sykes, 1984](#)) and it can be used in sensors to detect changes within systems ([Pitt et al., 1985](#), [Rao et al., 1998](#), [Bezombes et al., 2007](#)). This is by no means an exhaustive list, but provides only a small cross section of natural phenomena and applications of light.

However one of the most astounding of applications, which once could have just been considered the fanciful dream of science fiction writers, is known as optical trapping. Optical trapping is a technique, whereby the forces that are generated during the interaction between light and matter are harnessed and used to manipulate material without making physical contact.

One can appreciate however, that those forces would be appreciably small and so no ordinary light source will suffice. It was not therefore, until the advent of the laser ([Maiman,](#)

[1960](#)) that the use of light as a vehicle for the manipulation of matter was no longer just the dream of the science fictional novelist.

The role of the laser that brought about this change of circumstance can be attributed to its unique and inherent properties, which make possible the delivery of a parallel, coherent and monochromatic beam of light that can be focused to a small, very intense spot size. Such intense irradiation over an appreciably small surface area leads to the generation of radiation pressure forces that are sufficient for optical manipulation to become a reality.

These optical forces, when exerted on a material by the scattering, absorption, emission, or re-radiation of the incident light, can facilitate the acceleration, deceleration, deflection, guidance and stable trapping of mesoscopic scale objects including live biological and inanimate material ([Svoboda and Block, 1994](#)). Such subjects can be manipulated directly by the optical forces generated from the incident beam, or may be manipulated indirectly, whereby objects of interest can be adhered to dielectric<sup>1</sup> microspheres, and these latter can then be optically trapped and used as an ‘optical handle’ ([Block et al., 1990](#)).

## **1.1 AIMS AND OBJECTIVES**

The aim here is to develop an optical trapping system to aid our investigations into the mechanical properties of cells ([Murphy et al., 2006](#), [Murphy, 2007](#), [Randall and Murphy, 2008](#), [Randall, 2009](#), [Doyle et al., 2010](#), [Madden et al., 2010](#), [Doyle et al., 2011](#), [Johnston et al., 2011](#), [Murphy et al., 2012](#)). Atomic force microscopy (AFM) is currently used to carry out

---

<sup>1</sup> A dielectric is an electrical insulating material, which can be polarised by applying an electric field. Its ability to be polarised is determined by the relative permittivity formerly known as the dielectric constant of the material.

force-indentation experiments on adherent cells. However, we would also like to use AFM to study the force response of non-adherent cells, e.g. blood cells.

In order to achieve this, a single non-adherent cell would be required to be held in place whilst the AFM cantilever is brought into contact with it. This is one of the driving forces behind the design of our optical trap. The system should be physically decoupled from the microscope, and exhibit a certain degree of portability to ensure its interoperability with other such advanced microscopy systems. With this in mind an optical fibre based system configuration has been proposed here.

The AFM head houses the optical lever detection system, which consists of the cantilever, laser and photo detector, as shown in Figure 1-1 (a). The head is situated directly above the sample chamber, as depicted in Figure 1-1 (b), which shows how the trapping system would be incorporated within the AFM; hence the possible insertion angle for an optical fibre to pass beneath it is limited to  $10^\circ$ , or less, with respect to the plane of the sample chamber. However, existing literature suggests that using a single optical fibre inserted at an angle  $<20^\circ$ , to the plane of the sample chamber floor, full 3D optical trapping is not possible ([Taguchi et al., 2012](#)). Previously single optical fibre traps have also shown a significant reduction of trapping efficiency at insertion angles of less than  $40^\circ$  to the plane of the sample chamber ([Hu et al., 2004](#)).

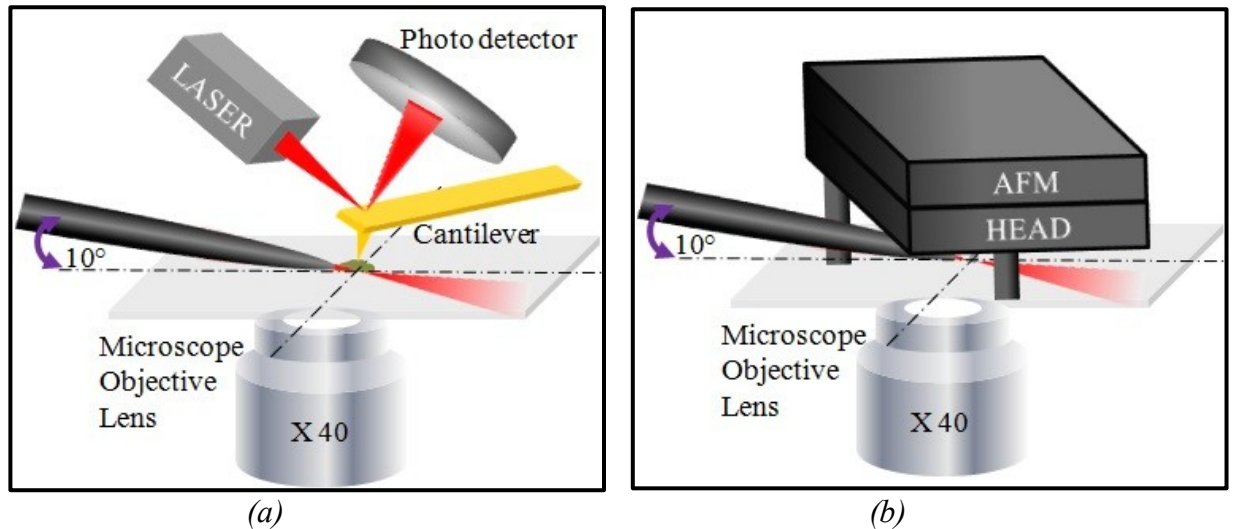


*Figure 1-1 (a) showing the internal configuration of the AFM head (b) arrangement of how the integrated AFM and optical fibre based trapping system configuration would look and showing an optical fibre tip deployed at an insertion angle of ten degrees.*

To date these limitations of single optical fibre optical traps have not been investigated in order to discover their cause. This thesis investigates these limitations and proposes a hypothesis that is based on the geometric profile of the optical fibre's distal end. Consequently a solution is proposed, whereby the geometry of the tapered optical fibre's distal end is optimised, to allow 3D optical trapping at an insertion angle of  $10^\circ$  for silica particles of  $3 \mu\text{m}$  in diameter. To the authors' knowledge this is the first time that a single-optical fibre-based 3D optical trapping system has been employed at such extremely low insertion angles for the particle sizes given above. Thus the findings in this thesis provide experimental proof that the system developed here could easily be incorporated with other advanced microscopy applications such as that envisaged with the AFM.

**CHAPTER TWO OPTICAL  
TRAPPING: ORIGIN, THEORY,  
DESIGN CONFIGURATIONS AND  
APPLICATIONS**

## **OPTICAL TRAPPING: ORIGIN, THEORY, DESIGN CONFIGURATIONS AND APPLICATIONS**

The origins of optical trapping can be traced back to 1969 when Arthur Ashkin, a scientist working for Bell Laboratories, commenced investigations into the effects of electromagnetic radiation pressure upon microscopic particles ([Ashkin, 1970](#)). It was during these experiments that unusual and extraordinary phenomena were observed. As expected the initial observations verified that when the laser light was incident upon a particle, the particle was propelled in the direction of the laser beam's propagation. However on closer inspection it was found that any particles which were located at the fringes of the Gaussian laser beam were pulled into the high intensity region of the laser beam's central axis following the activation of the laser.

Once on axis, the particle would then be pushed along in the direction of the beam's propagation. When the laser was deactivated, the particles would stop moving in the direction of the beam's propagation and drift away from the central axis due to Brownian motion. If the laser was reactivated, then the particles would again be pulled into the high intensity region before being propelled in the direction of the beam's propagation, as previously described. This demonstrated that the particle was in fact being guided by the laser beam, as if it was being transported within an "optical conduit".

It was these observations of the radiation pressure force effects that prompted Ashkin to decompose the total optical forces acting upon the particle into two force components; namely the scattering force and the gradient force. Figure 2-1 shows Ashkin's decomposition of the electromagnetic (EM) radiation pressure force acting on a dielectric particle in a weakly focused laser beam. The two rays (a) and (b) are from a laser beam with

a Gaussian TEM<sub>00</sub> profile. Since ray (a) is nearer to the high intensity region of the Gaussian beam's central axis then it is of a greater intensity than that of ray (b). This is depicted in the image by the thicker line being attributed to ray (a).

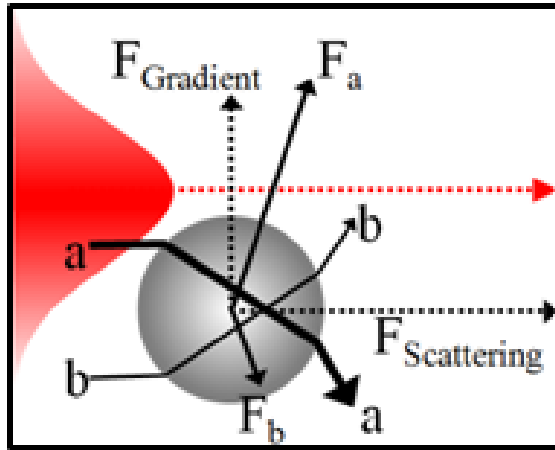


*Figure 2-1 electromagnetic radiation pressure forces acting on an off-axis sphere in a weakly focused laser beam*

Consider a dielectric particle, many wavelengths in diameter and with a greater refractive index than that of its surrounding medium that is located off axis at the fringes of the laser beam's width. The pair of rays, (a) and (b), strikes the particle symmetrically, either side of its central axis. The change in refractive index at the particle-medium interface causes a change in the rays' momentum and so the rays refract within the particle. This change in momentum results in the generation of forces, depicted as ( $F_a$ ) and ( $F_b$ ) in Figure 2-1, which act in the opposite direction to the momentum change. Since ray (a) is of a higher intensity than ray (b) then the resulting force ( $F_a$ ) is greater than ( $F_b$ ). The particle then is pulled into the high intensity region of the laser beam's axis due to  $F_a$ , which is a combination of the weaker scattering force and the dominant gradient force.

The gradient force ( $F_{\text{Gradient}}$ ) is due to refraction and is proportional to the spatial gradient in light intensity and acts in the transverse direction towards the high intensity region of the laser beam's central axis. The scattering force ( $F_{\text{Scattering}}$ ) is due to reflection, is proportional to the intensity of the laser beam and acts in the axial direction of the laser beam's propagation. Once the particle has moved into the laser beam's central axis, then  $F_{\text{Gradient}} = F_{\text{Scattering}}$ , and hence there is no longer a net gradient force and so the scattering force dominates. The particle is propelled by the scattering force in the direction of the beam's propagation.

One further noteworthy observation is that the particle, with a higher refractive index than the surrounding medium yielding an effective index ( $m$ )  $>1$ , acts as a focusing lens. The effective index  $m$  is given by;

$$m = \frac{n_p}{n_m} \quad (2-1)$$

where  $n_p$  is the refractive index of the particle and  $n_m$  is the refractive index of the surrounding medium.

In the contrary situation, where the refractive indices of the particle and its surrounding media are reversed (so that the effective index  $<1$ ), then the particle acts as a diverging lens. Therefore the particle will not be drawn into the high intensity region of the laser beam's central-axis, but instead will be driven out of the laser beam entirely. Nevertheless optical trapping of low index particles is still achievable and this issue is discussed further in Section 2.4.

## 2.1 OPTICAL TRAPPING THEORY

It was this simple decomposition and understanding of the optical forces at play, during the interaction between light and matter, which led Ashkin to develop his first optical trapping systems. Ashkin reasoned that, in order to develop a stable optical trap, he had to find a way to eliminate the effects of the dominant scattering forces that propel the particle in the direction of the beam's propagation.

This realisation led to the development of two contrasting optical trapping configurations in quick succession. In the first optical trap design, Ashkin used two counter-propagating laser beams, as shown in Figure 2-2 (a). The counter-propagating beams create a balance between the two opposing scattering forces, which result in a net force that is at an equilibrium point (E) where stable 3D trapping may be observed. The position of the equilibrium point is determined by the intensity difference between the two beams. For example if both beams were of equal intensity, then the equilibrium point would occupy the central position between the opposing beams ([Ashkin, 1970](#)).

Figure 2-2 (b) shows Ashkin's second optical trap design, known as the optical levitation trap ([Ashkin and Dziedzic, 1971](#)). In this configuration Ashkin employed a vertically orientated laser beam. The scattering force, which is perpendicular to the horizontal sample chamber, is opposed by the naturally occurring physical force of gravity. A stable 3D trap is achieved at the equilibrium point (E), where the scattering and gravitational forces balance.

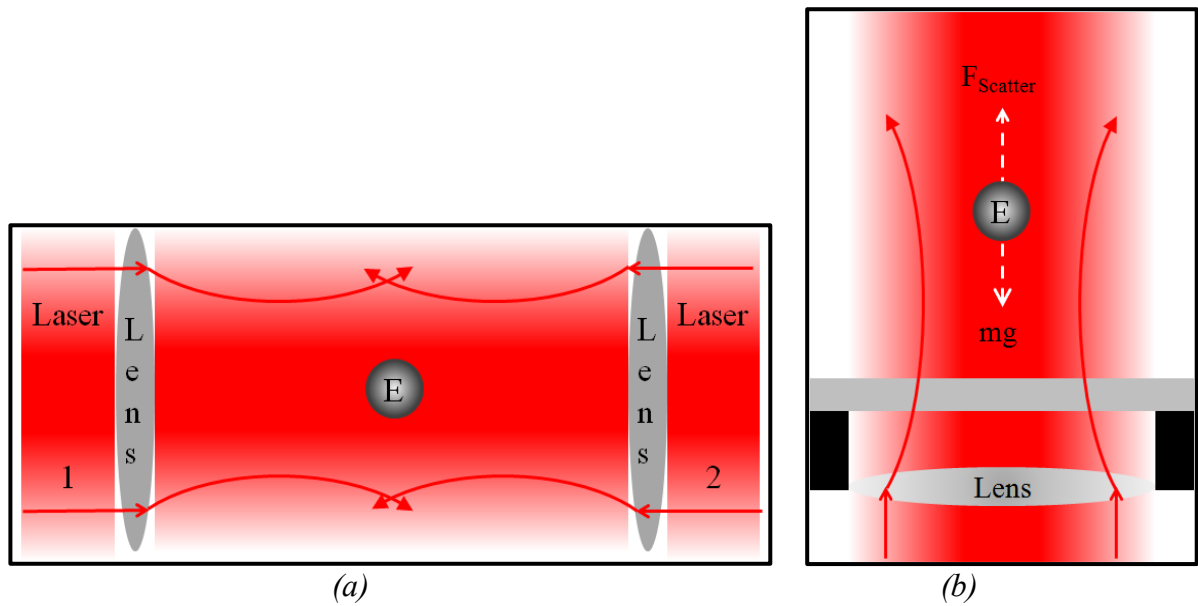


Figure 2-2 (a) counter-propagating laser beam trap (b) optical levitation trap

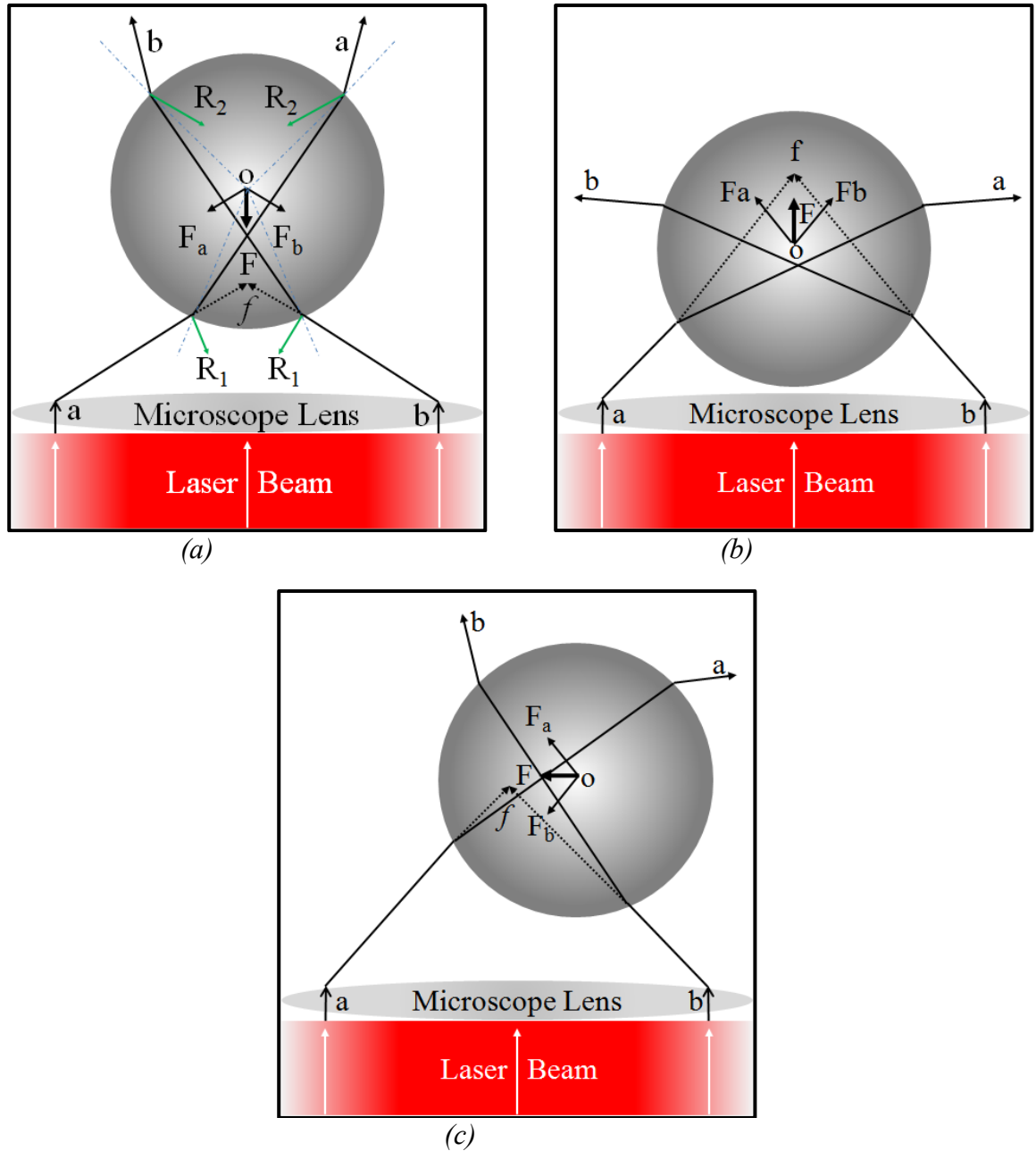
Later Ashkin discovered that by creating a steep intensity gradient by tightly focusing the laser beam, using a high numerical aperture (NA) microscope objective lens, resulted in a transverse gradient force that is much larger than the axial scattering force. This arrangement created a single beam, all optical, 3D gradient force optical trap ([Ashkin et al., 1986](#)). These devices, have since become universally known as “optical tweezers”, a term coined by Ashkin himself ([Ashkin and Dziedzic, 1987](#)).

Figure 2-3 shows the ray optics force diagram for “optical tweezers”. The images portray the existence of negative radiation pressure, or a backwards restoring force component, that is due to the steeper axial intensity gradient. Figure 2-3 (a) shows two rays, (a) and (b), passing through the particle. Because most of the light is expected to transmit through the particle then the surface reflections at  $R_1$  and  $R_2$  are considered to be infinitesimal and thus can be neglected. It is assumed that the particle medium combination yields an effective index  $m > 1$  and so the particle acts as a focusing lens. Therefore the rays are both refracted in a focused manner which instigates the reaction forces  $F_a$  and  $F_b$  that are due to the change

in momentum of the rays. These forces result in a negative axial radiation pressure force ( $F$ ), that drives the particle towards its focal point ( $F_p$ ).

Figure 2-3 (b) is of a particle located before the focal point. Here the axial force ( $F$ ) acts to push the particle towards the laser's  $F_p$ . However once it is located in the trapping zone at  $F_p$  the particle is halted and is not driven away by the scattering force, but instead is now held in a stable 3D trap.

Figure 2-3 (c) shows a particle located off-axis with respect to the laser beam's width; in this scenario the transverse restoring force ( $F$ ) drives the particle in a transverse direction back towards the laser's  $F_p$  ([Ashkin, 1992](#)).



*Figure 2-3 optical tweezers (a) particle located beyond focal point - backwards axial restoring force (b) particle located before the focus – forward axial restoring force (c) particle located off-axis – transverse restoring force*

## 2.2 FORCE MODELLING

When trying to understand the phenomenon of radiation pressure forces, theoretical models can be adopted for their computation and simulation. However such is the nature of optical

trapping, that it becomes extremely difficult for computational models to predict exactly what is happening within a given system. Nevertheless such models can be useful for predicting improvements to trapping systems, or for comparisons with measured results; they are also useful for exposing the generation of additional forces, such as for example radiometric forces.

A photon has energy ( $h\nu$ ) and momentum ( $h/\lambda$ ), where  $h$  is Planck's constant and  $\nu$  is frequency. The forces in optical trapping occur due to the momentum transferred by the light, of power ( $P$ ), incident upon an absorbing particle, the reaction to which leads to a force ( $F$ ) being transferred to the particle and is defined by;

$$F = \frac{n_m P}{c} \quad (2-2)$$

where  $n_m$  is the refractive index of the surrounding medium and  $c$  is the speed of the light in a vacuum ([Molloy and Padgett, 2002](#)).

The dimensionless quantity  $Q$ , which is used to describe the efficiency of an optical trapping system, can be determined by the fraction of the power utilised to exert a force. The  $Q$  value can be affected by parameters such as the beam convergence angle, spot size, wavelength, polarisation and beam profile, so therefore the  $Q$  value must be taken into consideration for the computation of the optical forces, as given by;

$$F = Q \frac{n_m P}{c} \quad (2-3)$$

where  $Q$  is defined as the ratio between the generated optical trapping forces and the optical power taken to produce the forces ([Kauppila et al., 2012](#)).

$$Q = \frac{Fc}{n_m P} \quad (2-4)$$

It has already been expressed that changes afforded to the optical geometry can play a role in the optical trapping efficiency ( $Q$ ) and this consequently affects the outcome of the resultant forces. Additionally, due consideration must be taken with regard to the prevalent environmental conditions, such as temperature, particle size, particle shape, particle refractive index, medium refractive index and viscosity. All of these are important experimental parameters and if there were any fluctuations in these, they would impart an influence on any results. This is before one even considers the use of biological specimens as the trapping subject, as unlike silica microspheres that generally exhibit relatively uniform size, shape and index of refraction, cells are morphologically complex, inhomogeneous with respect to refractive index, dynamic in that they are nomadic in vitro, and are capable of morphological adaptation and reproduction.

Choice of the correct computational model is also strongly dependent upon which size regime the particle of interest fits into. Figure 2-4 depicts the three size regimes, showing that each, of the regimes, is dependent on particle size with respect to the wavelength of the incident light. Figure 2-4 (a) shows the Mie regime, defined by the condition that the diameter of the particle is greater than the wavelength of the light ( $d \gg \lambda$ ). In this size regime the optical forces can be sufficiently well explained by using a simple Ray optics approach, in which ray diagrams are adopted, as first depicted in Figure 2-1 and Figure 2-3.

Figure 2-4 (c) shows the Rayleigh regime, the opposite of the Mie condition, where the diameter of the particle is smaller than the wavelength of the light ( $d \ll \lambda$ ). Here the light can no longer be usefully represented by rays; instead objects in this size regime are best represented using point dipole scatter theory.

Shown in Figure 2-4 (b), and lying in between these two polar regimes, is the Intermediate regime, where the diameter of the particle is equal to the wavelength of the light ( $d \approx \lambda$ ) and to model in this scenario the use of electromagnetic theory is required.

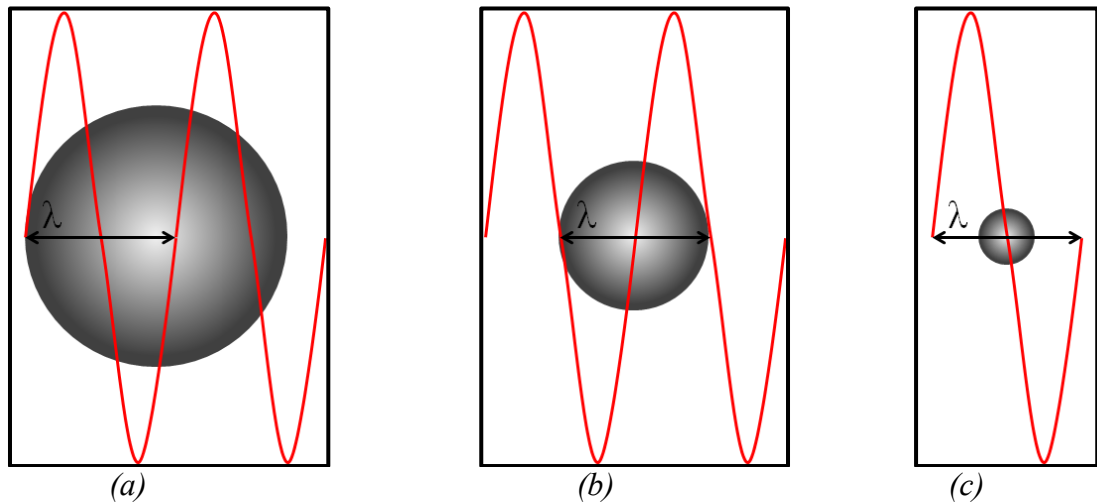


Figure 2-4 particle size regimes (a) Mie regime  $d > \lambda$  (b) Intermediate regime  $d = \lambda$  and (c) Rayleigh regime  $d < \lambda$

The criteria for Rayleigh scattering is that  $\alpha \ll 1$ , where  $\alpha$  is the dimensionless size parameter and is expressed as;

$$\alpha = \frac{2\pi a}{\lambda} \quad (2-5)$$

where  $a$  is the radius of the spherical particle, and  $\lambda$  is the relative scattering wavelength defined as;

$$\lambda = \frac{\lambda_0}{n_m} \quad (2-6)$$

where  $\lambda_0$  is the incident wavelength and  $n_m$  is the refractive index of the surrounding medium ([Hahn, 2009](#)).

For example for a particle of diameter size = 250 nm, laser wavelength = 1064 nm and with the medium being water with a refractive index of 1.33; this would result in  $\alpha = 0.98$ , hence being in the Rayleigh scattering regime. The smallest particle that was employed during this research programme has been 3  $\mu\text{m}$  diameter silica microspheres. Using the same laser and medium with 3  $\mu\text{m}$  diameter particles yields  $\alpha = 11.78$ , which, falls well within the limits for the Mie scattering regime and therefore the use of a Ray Optics approach will suffice here.

### 2.2.1 *MIE REGIME - THE RAY OPTICS MODEL*

Particles with a diameter that is larger than the wavelength of the incident light ( $d > \lambda$ ) can be modelled using the Ray Optics approach, where the scattering force may be given as;

$$F_S = Q \frac{n_m P}{c} \left\{ 1 + R \cos 2\theta - \frac{T^2 [\cos(2\theta - 2r) + R \cos(2\theta)]}{1 + R^2 + 2R \cos(2r)} \right\} \quad (2-7)$$

where  $F_S$  is the scattering force in the direction of the beam's propagation;  $R$  and  $T$  are the Fresnel reflection and transmission coefficients of the surface at  $\theta$  the angle of incidence and  $r$  the angle of refraction respectively. The gradient force  $F_G$  is given as;

$$F_G = Q \frac{n_m P}{c} \left\{ R \sin 2\theta - \frac{T^2 [\sin(2\theta - 2r) + R \sin(2\theta)]}{1 + R^2 + 2R \cos(2r)} \right\} \quad (2-8)$$

The total force is then;

$$F_T = \sqrt{F_S^2 + F_G^2} \quad (2-9)$$

Equations (2-7) - (2-9) are reproduced from ([Ashkin, 1992](#), [Svoboda and Block, 1994](#)).

### 2.2.2 **RAYLEIGH REGIME – POINT DIPOLE MODEL**

When the trapping laser wavelength is far greater than the size of the particle that is to be trapped ( $d < \lambda$ ), then the ray optics approach is no longer valid. In the Rayleigh scattering regime, calculation of the optical forces is achieved by treating the particle as a point dipole. The focus of the beam, on the other hand, cannot be represented as a point, but must take the form of a diffraction limited area that is of a similar size to the wavelength. The scattering and gradient force components are split, such that the scattering force is due to the absorption and re-radiation of light by the dipole. The scattering force may be calculated by;

$$F_{Scatter} = \frac{I_0 \sigma n_m}{c} \quad (2-10)$$

where  $I_0$  is the incident light intensity,  $n_m$  is the refractive index of the medium,  $c$  is the speed of light in a vacuum and  $\sigma$  is the scattering cross section of the particle, which is given by;

$$\sigma = \frac{128\pi^5 a^6}{3\lambda^4} \left( \frac{m^2 - 1}{m^2 + 2} \right)^2 \quad (2-11)$$

where  $a$ , is the radius of the particle,  $\lambda$  is the wavelength of the trapping laser and  $m$  is the effective refractive index, as given in Equation (2-1). The time averaged gradient force is then given by;

$$F_{Gradient} = \frac{2\pi\alpha}{cn_m^2} \nabla I_0 \quad (2-12)$$

where  $\alpha$  is the sphere's polarising ability, which is given by;

$$\alpha = n_m^2 a^3 \left( \frac{m^2 - 1}{m^2 + 2} \right) \quad (2-13)$$

Equations (2-10) - (2-13) are reproduced from ([Neuman and Block, 2004](#)).

### **2.2.3 INTERMEDIATE REGIME – ELECTROMAGNETIC THEORY**

The geometric and Rayleigh approximations provide an intuitive understanding of the physical principles of optical trapping for particles that are either larger, or smaller, than the wavelength of the light being used. However their quantitative validity for trapped particles with diameters that are equal in length to the laser wavelength ( $d = \lambda$ ) is of no consequence. In this Intermediate size regime a correct description of optical tweezers can only be made using electromagnetic theory.

## **2.3 OPTICAL TRAPPING DESIGN CONFIGURATIONS**

Ever since the birth of Ashkin's pioneering optical trapping systems, researchers have striven to improve upon and further develop the efficiency, functionality and practicality of those primary systems. These endeavours have led to the creation of a vast array of optical trapping system configurations, providing systems that offer multiple and flexible optical trapping sites, as well as the capability to trap material of a low refractive index.

One of the simplest implementations of optical tweezers is the single beam trap, in which the trapping beam is static ([Ashkin et al., 1986](#)). ([Jong et al., 1995](#), [Kumar De et al., 2008](#))

built simple single static beam optical tweezers around commercially available inverted microscopes. Visscher and Brakenhoff ([1991](#)) combined an optical trap with the 3D imaging capabilities of a confocal microscope. This configuration allowed the viewing and trapping optics to be decoupled from each other, permitting the 3D displacement of the focusing objective, and thus the capability for the optical trap's position to be moved.

Kroner et al. ([2006](#)) utilised a vertical-cavity surface-emitting laser with a photo-resist micro-lens fabricated onto the output facet. This simple arrangement successfully trapped 10  $\mu\text{m}$  polystyrene particles and substantially reduced the system footprint by removing the usual tweezers' bulk optics.

### ***2.3.1 MULTIPLE TRAPPING SYSTEMS***

A simple two beam trap is easily be achieved by dividing the trapping beam using a polarising beam splitter, and later recombining both beams using a second polarising beam splitter as shown in Figure 2-5. The second polarising beam splitter is positioned before the entrance to the microscope's high NA objective, resulting in two orthogonally polarised and independently steerable optical traps ([Misawa et al., 1992](#), [Fallman and Axner, 1997](#)).

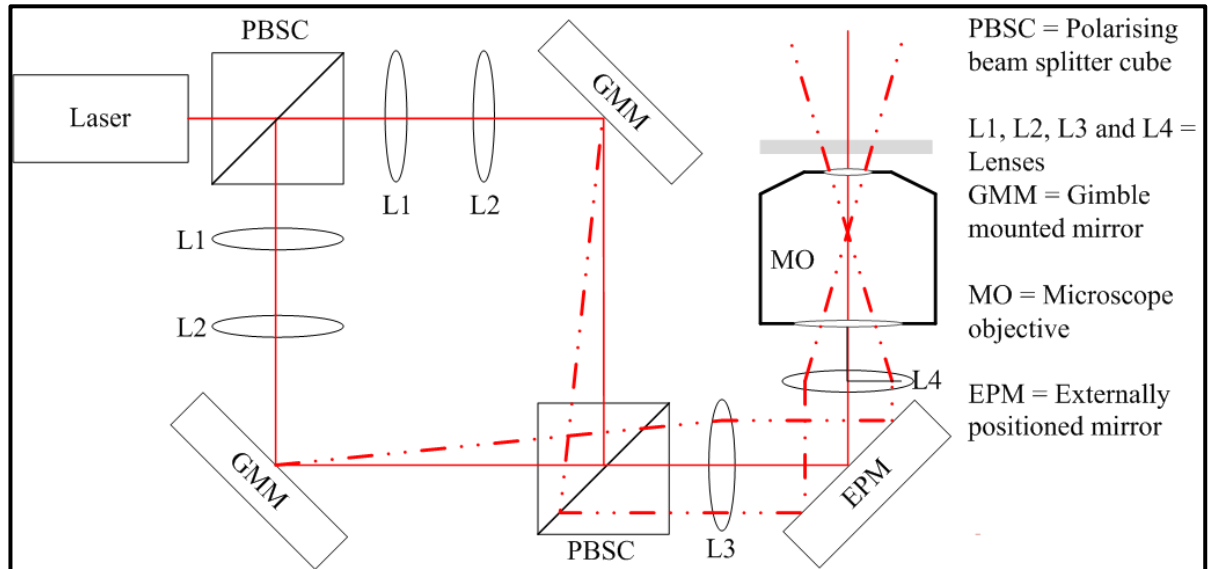


*Figure 2-5 single laser source dual-trap optical tweezers system*

Figure 2-6 shows how two laser sources were used to form a dual optical tweezers configuration by ([Soni et al., 2002](#)). The trapping lasers shown in the schematic are the 1064nm ND: YAG laser and 830nm diode laser, whilst the 635 nm diode laser was used for detection purposes only. This type of configuration would result with a considerably greater overall system cost when compared to simply dividing a single laser beam.

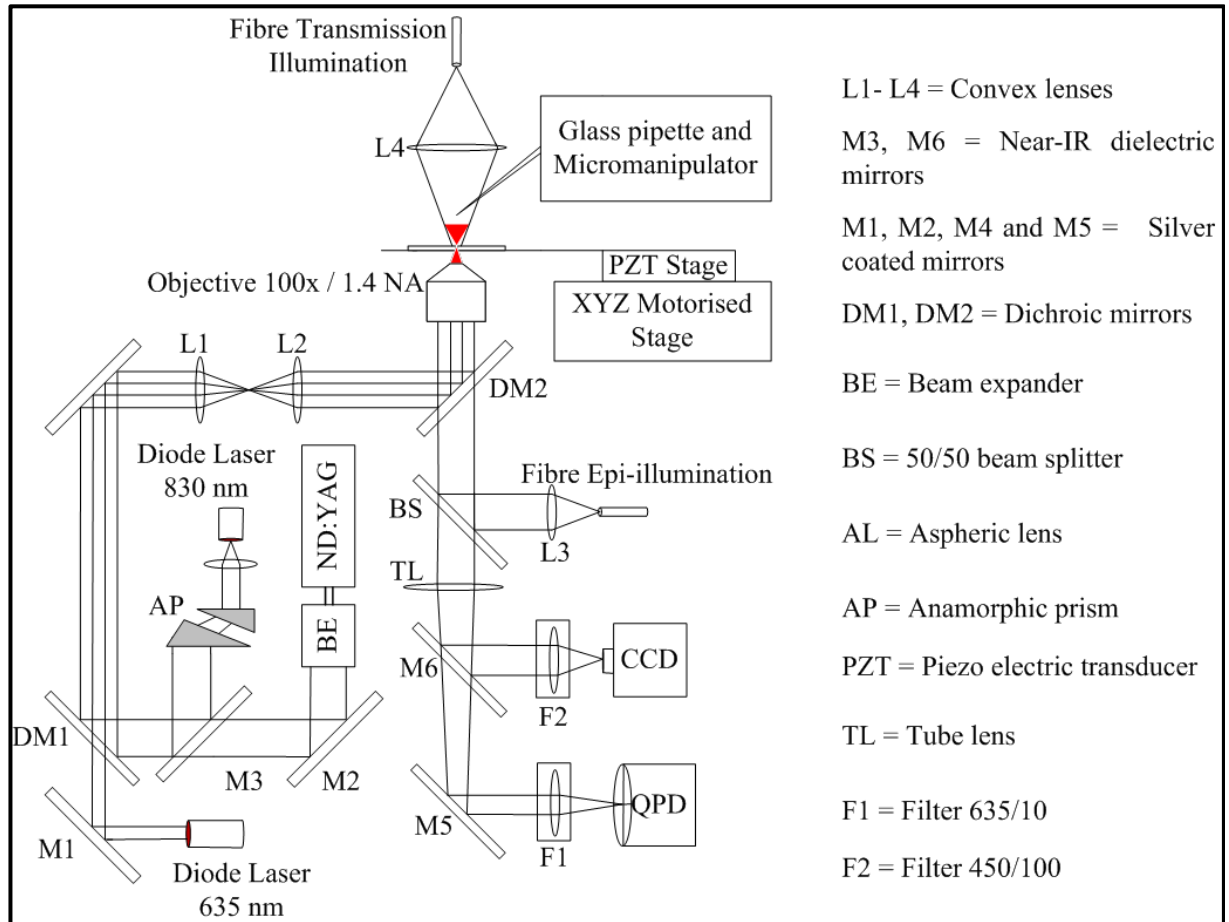
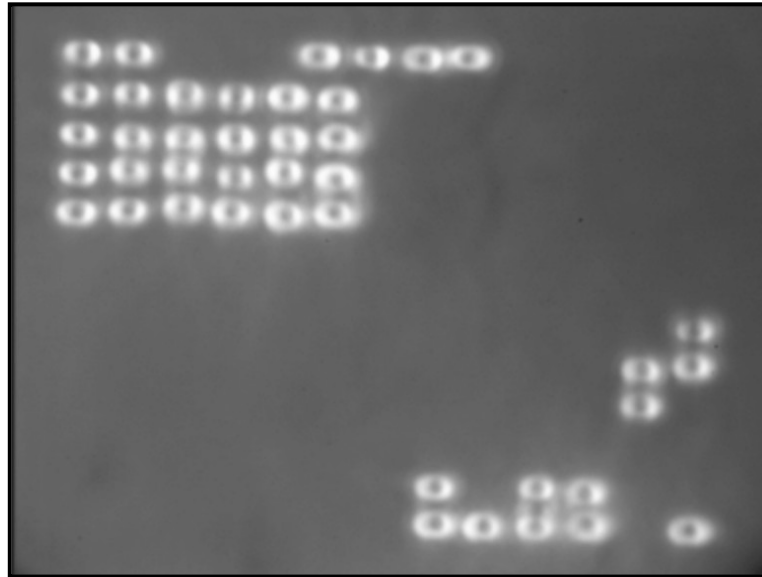


Figure 2-6 schematic of dual optical tweezers created using two laser sources

Multiple trap tweezers have also been developed by employing a fast scanning laser, whereby the single laser beam is time shared amongst the trapping sites. One such case, building on their earlier single trap design, incorporated the system with 3D imaging via a bilateral confocal scanning laser microscope (CSLM) ([Visscher et al., 1993](#)). This system used an acousto-optic modulator (AOM), to provide fast shuttering of the beam, enabling the beam to be switched off whilst moving between optical trapping sites. Scanning of the beam itself was achieved using two galvanometric mirrors, one for each of the X and Y directions, with a typical scan rate of 50Hz, thereby giving a period of 20 ms during which the particle is illuminated for about 4 ms, representing about 1/5<sup>th</sup> of the whole scanning duration.

Visscher et al ([1996](#)) later replaced the galvanometric mirrors with acousto-optic deflectors, hence providing an increased scanning rate of 20 KHz and thus increasing the number of available system traps in the process. The scanning rates must be faster than the roll off frequency of the power spectrum for position, which are typically in the range between 250 Hz and 1500 Hz for micrometre sized particles. This allows the laser to re-visit all of the designated optical trapping sites, re-trapping its targets, before they have a chance to diffuse out of the trapping range due to Brownian motion. For example the time taken for a 1 $\mu$ m diameter spherical particle to diffuse by a distance of 100 nm is about 10 ms ([Capitanio et al., 2007](#)). The particle should be illuminated for a suitable duration and with a frequency such that the particle appears to be under constant control, i.e. not deviating far from the original trapping location. Therefore the amount of trapping sites in an optical trapping system, comprising a fast scanning laser beam, is limited firstly by the response times for switching the laser on and off between trapping sites and secondly by the scan rates of the deflection equipment used for the focused beam deflection.

A good visual example of such a fast scanning laser multiple tweezers system has been demonstrated in a video that was produced a decade ago by a team from Amsterdam University ([Mameren et al., 2011](#)). The video captures the use of a multiple trap OT's system being used to play a microscopic version of the popular arcade game Tetris, as shown in Figure 2-7. The system employs an acoustic optic deflector (AOD) to create a fast scanning beam. During the video 42 silica micro-spheres, of 1  $\mu$ m diameter appear to be simultaneously trapped and independently manoeuvred by what would appear to be 42 individual trapping beams. However the reality is that there is just a solitary time shared trapping beam that traps one micro-sphere at a time.



*Figure 2-7 Tetris arcade game re-created using a fast scanning laser to optically trap  $42 \times 1 \mu\text{m}$  glass beads; image courtesy of ([Mameren et al., 2011](#))*

Conventional optical tweezers systems COT systems are based on Ashkin's initial design ([Ashkin et al., 1986](#)), and rely on bulk optics to shape and direct a laser beam in free space. In the late 1990's new methods for providing multiple optical traps in COT based setups were demonstrated as a result of technological advancements of optical components. Dufrense and Grier ([1998](#)) used a commercially available diffractive optical element (DOE), to split a single laser beam, thereby creating an array of optical traps. The array of  $4 \times 4$  optical traps could not realise the manipulation of individual traps, instead the 16 traps could only be moved together as a single entity. Building on this work ([Grier and Roichman, 2006](#)) developed computer generated holographic optical traps (HOT's), using spatial light modulators (SLMs), capable of generating in excess of 100 optical tweezers and which were each capable of operating independently of one another.

### 2.3.2 *ALTERNATIVE BEAM MODES*

The systems discussed thus far use laser beams with a  $TEM_{00}$  Gaussian beam mode to trap material that meets the effective refractive index criteria  $m > 1$ . Failure to meet this decisive criterion results in an expelling, rather than a trapping action. Recalling the earlier discussion when  $m < 1$ , the transition of light is altered in such a way that the sphere behaves as a concave (diverging) lens. This configuration drives the particle away from the high intensity region of the beam's axis and out of the beam altogether and so it is incapable of being optically trapped.

The preceding statement is true for OT using focused laser beams of  $TEM_{00}$  Gaussian intensity. However, trapping of particles with a refractive index that is less than that of their surrounding medium ( $n_p < n_m = m < 1$ ) is still attainable, regardless of the rules as set out above. By altering the properties of the laser beam's shape and intensity, it is possible to trap particles of low refractive index. The beam properties can be reversed by creating a transverse electromagnetic mode Laguerre-Gaussian ( $TEM_{01}$ ) otherwise known as a doughnut mode. In this mode the intensity minimum occupies the centre of the beam along its axis with the intensity maxima circling around the axis similar in shape to that of a doughnut.

Figure 2-8 shows a comparison of the beam profiles for both the Gaussian  $TEM_{00}$  (a) and Laguerre – Gaussian  $TEM_{01}$  beam modes (b).

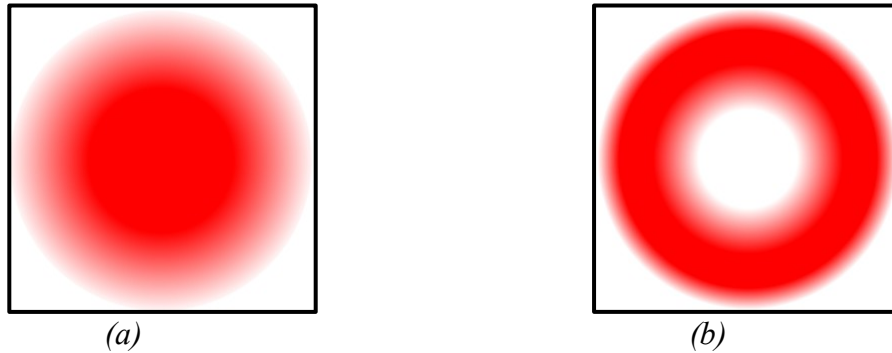


Figure 2-8 (a) Gaussian  $TEM_{00}$  intensity beam profile (b) Laguerre-Gaussian  $TEM_{01}$  “doughnut mode” intensity profile

Gahagan and Swartzlander ([1996](#)) used a holographically generated and strongly focused Laguerre-Gaussian  $TEM_{01}$ , or the so called “stationary dark optical vortex” laser beam, to achieve 3D optical trapping of low index particles<sup>2</sup>. Zhan ([2003](#)) stably trapped dielectric spheres of low refractive index (hollow glass spheres with  $n_p \approx 1$ ) by employing a focused azimuthally polarised beam and by reverting back to a radially polarised beam he was able to stably trap high index ( $n_p = 1.59$ ) particles. Radial polarisation occurs when the polarisation vector points towards the beam axis as shown in Figure 2-9 (a). The intensity for a highly focused radially polarised beam has a strong peak at the centre. Azimuth polarisation occurs when the polarisation vector is tangential to the beam as shown in Figure 2-9 (b). The intensity for a highly focused azimuthally polarised beam has intensity minima at the centre.

<sup>2</sup> The low index particles consisted of hollow glass spheres with a diameter of 20  $\mu\text{m}$  and with an effective index of  $n_p \approx 1.1$

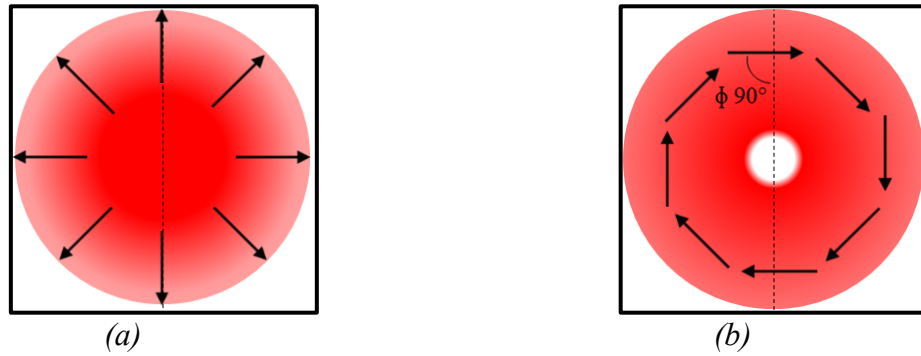


Figure 2-9 intensity distributions near the focus for (a) radially polarised beam  $\phi = 0^\circ$  and (b) azimuthally polarised beam  $\phi = 90^\circ$

A Laguerre - Gaussian  $TEM_{01}$ , or doughnut mode beam, was used to perform 2D optical trapping of metal particles by ([Sakai and Noda, 2007](#)). O’Neil and Padgett from the University of Glasgow also successfully adopted such a beam within an inverted optical tweezers system to trap micron sized metallic particles ([O’Neil and Padgett, 2000](#)). Alternatively dual line parallel optical tweezers, similar in nature to an interference pattern, have also been utilised for the confinement of low refractive index microscopic particles ([Mohanty et al., 2007](#)).

A Bessel laser beam was employed for the stacking and manipulation of multiple spheres, alignment of long rod-like shapes and to guide micron sized spheres by a distance that exceed the Rayleigh range of a Gaussian beam by more than an order of magnitude ([Arlt et al., 2001](#)). These types of manipulations are made possible as the beam is propagation invariant, that is, the central maximum propagates without appreciable spreading over this distance.

## 2.4 APPLICATIONS OF OPTICAL TRAPPING

Ashkin’s pioneering work in optical trapping is not limited to just the invention of the devices themselves, but also in their application across a wide variety of research areas.

Since they are capable of generating optical forces in excess of 100 pN with sub nanometre resolution, whilst simultaneously measuring the displacement of particles with diameters ranging between the Rayleigh and Mie regimes ([Grier, 2003](#)), optical trapping systems have become invaluable tools within the physical and biological sciences.

It was Ashkin's collaborations with Stephen Chu, and others, that led to Chu ([Chu, 1998](#)), Claude Cohen-Tannoudji ([Cohen-Tannoudji, 1998](#)) and William D. Phillips ([Phillips, 1998](#)) sharing the Nobel Prize in Physics 1997 for "the development of methods to cool and trap atoms with a laser". The first observations of optically trapped atoms were recorded shortly after the development of optical tweezers ([Chu et al., 1986](#)). Ashkin also pioneered the optical trapping of biological material, demonstrating the trapping and manipulation of individual and orientated arrays of tobacco mosaic viruses, single live motile bacteria and *Escherichia coli* (E-Coli) bacteria ([Ashkin and Dziedzic, 1987](#)).

Ashkin then went on to use IR laser traps and reported significantly less damage being caused to biological material. During this investigation active biological processes, such as E-coli reproduction and the budding of yeast cells, were observed whilst under the influence of the optical trap. The trapping of blood cells and of organelles within spirogyra cells was also achieved ([Ashkin et al., 1987](#)). Optical trapping was also used to manipulate structures internal to a cell, without inflicting physical damage to the cell membrane. So called artificial filaments were pulled from different regions of a plant cell as a means to observe the viscoelastic properties of the cell cytoplasm. Successful manipulation of large organelles, such as chloroplasts and nuclei, was also demonstrated along with the trapping and confinement of collections of small particles that move within well defined channels found inside scallion cells ([Ashkin and Dziedzic, 1989](#)).

Optical tweezers have also been used to fashion, assemble and drive micro machines and motors. Fabrication of the micro devices is achieved by photo polymerisation of resin via two photon absorption. The devices included optically held and driven rotary motors ([Galajda and Ormos, 2001](#), [Maruo et al., 2003](#)) and a nano spring that was extended and released, using optical tweezers, to cause oscillation ([Kawata et al., 2001](#)).

A comprehensive review of the history and applications of optical trapping spanning 30 years from 1970 is covered in two review articles by Ashkin ([Ashkin, 1997](#), [Ashkin, 2000](#)). A substantial guide to the literature on optical tweezers up to 2003 is provided by ([Lang and Block, 2003](#)).

A single beam COT system was used to stretch and deform red blood cells (RBC's) ([Liao et al., 2008](#)). After confining a single red blood cell, an AOM was used to deflect the trapping beam periodically between two fixed points. The scanning distance was increased in discrete steps and ranged from 1.23 $\mu\text{m}$  to 3.03 $\mu\text{m}$ . At low-frequency scan rates ( $\sim 1\text{Hz}$  to a few the tens of Hz), the cell oscillated between the scan points and its deformity was negligible. However, for scan rates at frequencies  $\geq 100\text{Hz}$ , the action of the optical tweezers, jumping from site to site, caused the single red blood cell to significantly deform as if it had been pulled apart by two independent trapping beams. The greatest deformities were observed at a scanning distance of 2.67 $\mu\text{m}$ , and it was also found that increasing the optical output power from 10 mW to 20 mW had no additional effect.

The mechanical property changes of RBC's, with respect to their stored time in Alsever's solution, have been studied using a COT system and 5 $\mu\text{m}$  polystyrene microspheres employed as optical handles ([Li et al., 2009](#)). The microsphere and the sample cell substrate

had previously been treated in a polylysine solution, which promotes cell adhesion to solid substrates. In this investigation, one pole of an RBC and the sample chamber adhered, whilst a polystyrene microsphere was first optically trapped and then brought into connection with the opposing pole of the RBC. Following the cell-sphere adhesion, the specimen stage was moved and caused the RBC to stretch. The maximum force, which was imparted to the RBC, was recorded to be 315 pN and was achieved using laser powers of 2000mW. The elasticity of the RBC, with respect to its time stored in Alsevers solution, was investigated for cells stored for 2 days, 5 days, 7 days and 14 days. The results of the investigation concluded that the shear modulus increased with the storage time, thus the elasticity decreased.

Similarly, a polylysine-coated bead was bound to one end of a growing *Escherichia coli* (E-coli) bacteria cell. However, in this case optical tweezers were used to confine and manipulate the bead causing the cell to bend, rather than stretch ([Wang et al., 2010](#)). During the investigation, the addition of the antibiotic drug A22 revealed a reduction in bending stiffness from  $(2.8 \pm 0.5) \times 10^{-20} \text{ Nm}^2$  to  $(2.0 \pm 0.4) \times 10^{-20} \text{ Nm}^2$ . The results show that MreB, a bacterial actin homologue, contributes nearly as much to the stiffness of a cell as to the peptidoglycan cell wall, and demonstrates the fact that the cytoskeleton contributes the mechanical integrity of a bacterial cell just as in eukaryotes.

Counter-propagating fibre traps have also been employed to deform RBC's ([Guck et al., 2000](#)) and have since become known as optical stretchers ([Guck et al., 2001](#)), which are discussed in Chapter 3.1. More recently ([Bellini et al., 2010](#)) have created what they term a “monolithic chip” which is a purpose built optical stretcher combined with a micro fluidic system. The chip has been produced using a frequency-doubled cavity dumped YB-KYW

femto-second laser to perform both laser irradiation and laser writing of fused silica. The micro fluidic channel fabrication was accomplished using 230 fs pulses at 600 KHz repetition rate with a pulsed energy of 290 nJ at  $\lambda = 515$  nm. Writing of the optical waveguide in the fused silica sample is realised using the same laser, but using a repetition rate of 1MHz.

Optical tweezers have been used to conduct many additional studies concerning the mechanical properties of RBC's. For example they have been applied to measure the apparent overall elasticity, apparent membrane viscosity, zeta potential (electro-kinetic potential in colloidal dispersions), thickness of the double layer of electrical charges and adhesion ([Fontes et al., 2011](#)).

An assessment of the elasticity of RBC's which have been dispersed in different fluid media, commonly used to dilute RBC samples has been conducted by ([Barnes et al., 2013](#)). The types of media included foetal bovine serum (FBS), newborn bovine serum (NBBS) and phosphate buffer (PBS) solution. The results showed evidence of much higher elasticity values for FBS in comparison to both NBBS and PBS, of which the recorded values were similar.

Optical tweezers have been applied to establish the step size of class V myosin (myosin-V) ([Watanabe et al., 2010](#)). Myosin-V is a molecular motor that transports cargo with large successive steps of  $\sim 36$ nm along actin filaments. The hand over hand model, a popular mechanism that describes the myosin-V stepping motion, indicates that successive large steps are only possible if the myosin-V has two heads. However, it has been shown by the

results of the study that myosin-V, consisting of a single head, is also capable of successive large steps as long as the actin-myosin interaction angle is optimised.

The viscosity and elasticity of fibroblast cells have been recorded using both AFM and optical tweezers ([Nawaz et al., 2012](#)). The optical tweezers were employed in the same manner as the AFM in that a microsphere was optically trapped and used as an optical force probe similar to that of the AFM cantilever. The AFM was used to investigate the cellular response at forces from 30-600 pN, in which indentations of between 0.2 and 1.2  $\mu\text{m}$  were recorded. In comparison the optical tweezers were used to investigate the cellular response at forces up to 10 pN. As a result average indentations of 255nm were recorded over 90 different cells with an average of 9.1 pN being applied.

**CHAPTER THREE FIBRE OPTIC  
BASED OPTICAL TRAPPING  
SYSTEM CONFIGURATIONS**

## **FIBRE OPTIC BASED OPTICAL TRAPPING SYSTEM CONFIGURATIONS**

COT optical tweezers systems, i.e. those that use a free-space laser beam that is directed through a high numerical aperture (NA) microscope objective lens to focus the laser light, are relatively large and bulky systems in comparison to the miniaturized arena in which they were built to serve. In an effort to reduce both the build costs and the size of optical trapping systems, researchers began employing optical fibre to deliver the trapping laser light directly into the sample arena. The use of optical fibre decoupled the trapping system from the microscope and removed the need for the associated optics that are required to shape and direct the beam in the process. This chapter provides a comprehensive review of the various optical fibre based optical trapping system configurations that have evolved since their invention.

### **3.1 COUNTER-PROPAGATING OPTICAL FIBRES**

The first optical fibre based optical trapping system was demonstrated by ([Constable et al., 1993](#)). In this configuration two cleaved, counter-propagating, single mode optical fibres are used to create an adaptation to Ashkin's first optical trapping system that utilised dual counter-propagating beams ([Ashkin, 1970](#)). The dual fibre trap was used to confine polystyrene spheres ranging in size between 100 nm and 10  $\mu\text{m}$  in diameter. Perfect alignment of the two optical fibres is crucial for stable 3-D trapping. The alignment here was achieved using a rudimentary, but research effective setup, consisting of capillary tubes adhered to a microscope slide in such an arrangement as to act as a v-groove for the optical fibres. The empirically measured forces highlighted a weak axial confinement in the longitudinal direction.

The negative characteristic of requiring exact fibre alignment was turned into a positive application, as researchers created what has been termed "the fibre-optic spanner". Black

et al. positioned the opposing fibres with a slight transverse offset. The effect of this caused the optical trap to rotate human smooth muscle cells ([Black and Mohanty, 2012a](#)) and dielectric microstructures ([Black and Mohanty, 2012b](#)) due to the effects of the opposing and offset scattering forces. Black and Mohanty believe that the system could be potentially used for a diverse range of future applications, which include the uncoiling of DNA strands or for the analysis of spinning cells to determine whether they are cancerous, or not.

Controlled rotation of a cell was achieved, in a counter-propagating trap that used opposing single mode and dual mode fibres, by rotating the dual mode fibre about its axis ([Kreysing et al., 2008](#)).

Plastic micro objects in the shape of a bar and a cross were confined and rotated by three tapered fibres with hemispherical lenses. The three fibres were inserted at an angle of  $35^\circ$  to the sample chamber floor, arranged around a central trapping zone, in which the particle to be trapped was located, and separated by  $120^\circ$ . Switching the laser on and off between the three fibres in one circular direction caused the bar to rotate in the opposite direction, i.e. by switching the laser on and off in a clockwise direction around the bar moved it in a counter-clockwise direction. In the case of the cross shaped object, the opposite effect occurred, in that switching the laser on and off in the clockwise direction rotated the cross in the clockwise direction ([Ikeda et al., 2004](#)).

To counteract the relatively weak confinement in the longitudinal direction two approaches were taken. In the first instance Lyons and Sonek ([1995](#)) employed hemispherically lensed dual counter-propagating tapered optical fibres. In this case it was found that the axial stability is very much dependent on both particle size and fibre lens spacing. It was also evident that critical fibre spacing and particle size can cause, in

addition to the expected central equilibrium point, bi-stable equilibrium trapping points located near the focus of each of the lenses.

For the second method, additional fibres were included to create a crosshair configuration at the beam centre ([Sidick et al., 1997](#)). In order to ensure exact alignment of the four fibres, and in an effort to create a high precision optical micro-instrument, ([Collins et al., 1999](#)) fashioned precisely aligned V-grooves in which the fibres could be seated. The V-grooves were etched into silicon wafers using an aqueous 22.5% potassium hydroxide solution at 60 °C. The four fibre arrangement was employed to complete several tasks other than just optical confinement. Two counter-propagating fibres were indeed used for confinement. However the additional two fibres were each employed to do additional tasks, the third being employed as an optical probe, or pump, whilst the fourth fibre was engaged as a sensor for optical detection ([Jensen-McMullin et al., 2005](#)).

Gauthier and Frangioudakis ([2000](#)) combined the counter-propagating dual optical fibre trap with the optical levitation trap, which had been previously designed by ([Ashkin and Dziedzic, 1971](#)), in a novel method for isolating single particles . In this set-up single particles could be isolated within the levitation trap and elevated to the trapping zone of the counter-propagating fibre trap, thus negating interference from additional particles and consequently offering the opportunity for solitary particle analysis.

It would be natural to assume that the total forces in a counter-propagating configuration, acting upon a trapped subject, would be of a compressive nature. However ([Guck et al., 2000](#)) found this not to be the case whilst trapping material that is sufficiently elastic. During these studies it was found that any soft dielectric material, consisting of a higher refractive index to that of its surrounding medium, could be stretched, and thus Guck et al. coined the term the “optical stretcher”([Guck et al., 2001](#)). By combining the

counter-propagating optical trap with a micro-fluidic system, Guck et al., then developed a system for the diagnosis of diseased cells. The system was capable of investigating the mechanical properties of a single red blood cell as an inherent cell marker for cancer. The system was extremely fast in comparison to other single cell elasticity techniques, which can only process a few cells per day, processing cells at a frequency of one per minute ([Guck et al., 2005](#)). The optical stretcher configuration, complete with micro-fluidic capability, has been employed to study the mechanics of giant unilamellar vesicles (GUVs) and to characterise the membrane response to a step stress ([Solmaz et al., 2012](#)).

Wei et al. ([2006](#)) also adopted the dual beam configuration to trap 15  $\mu\text{m}$  diameter Chinese hamster ovary cells and also silica particles. Force calibration of the counter propagating trap was achieved using the particle displacement method. Although, in this instance the position of a trapped particle, acquired from the video analysis, has been combined with its position that was acquired using the scattered light projected onto a pair of quadrant photodiodes (QPD). This was sufficient for directly calibrating the axial displacement, but it was said to be impossible to apply this to the transverse displacement. This shortcoming was overcome by applying a Fourier transform to the QPD output voltage in order to obtain its power spectrum, then fitting it to a Lorentzian form. This combined method also overcomes the limitations set by the resolution of the camera.

The counter-propagating fibre configuration was used by a team from St. Andrews University to hold and manoeuvre large objects of approximately 30  $\mu\text{m}$  in diameter in the form of human keratinocytes. The arrangement was coupled with a micro-fluidic system to ensure an even flow of samples and was arranged orthogonally to a microscope objective, which was used to acquire the Raman spectra from local parts of a trapped cell ([Jess et al., 2006](#)).

The counter-propagating optical fibre arrangement has also been used to trap aerosols. However, this study experimented not just with single-mode fibre (SMF), but also with multi-mode fibre (MMF) ([Rudd et al., 2008](#)). During MMF trapping, particles were trapped in different locations and under different forces. This was evident when displacing the particles, as they moved irrationally, at different amounts and at different rates, whereas, under SMF trapping, there was only a single equilibrium point and more control was observed during displacement.

### **3.2 SINGLE OPTICAL FIBRE BASED TRAPPING SYSTEMS**

To truly replicate optical tweezers, optical trapping should be realised by a single optical fibre. The difficulty here though is that the laser beam exiting a cleaved optical fibre is divergent. This for all intents and purposes goes against the basic physics of optical tweezers, as a highly focused beam is required for single beam 3D trapping. To overcome this limitation, the distal end of the fibre could be positioned at the input to the microscope objective. This course of action will indeed reduce the overall system size, since the use of optical fibre eliminates the requirement for the usual large array of bulk optics. However, by taking this action, then the optical trapping system will still be married to the viewing optics of the microscope and thus using such a system limits its potential for integration with additional microscopy applications.

Therefore the optical fibre should be adapted such that the exiting beam is sufficiently focused to facilitate 3D optical trapping. There are several techniques available that enable the fibre tips to be adapted to create lens-like outputs at the fibre tips, and these approaches are discussed further in Section 3.3.

Taguchi et al., ([1997](#), [2007](#)) and ([Hu et al., 2004](#), [Hu et al., 2005](#), [Hu et al., 2006](#), [Hu et al., 2007](#)) employed single fibre probes that had a polished hemispherical lens on the

optical fibre output face. However the gradient forces that were generated were not sufficient to cause 3D trapping and only 2D trapping was realised.

Hu *et al* adopted two methods to measure the optical trapping forces as a function of position. Firstly the static measurement method, whereby the sample chamber is driven and the force acting on the particle by the flow of the surrounding medium displaces the particle from the trap. The particle's position is recorded using a CCD camera and the optical force is calculated using a revised Stokes equation. The second method is a dynamic method, where the particle is trapped instantaneously and its position, as it moves to the trapping zone, is recorded with a CCD camera and the force is then calculated from Newton's second law and the revised Stokes equation.

The effects of the fibre's insertion angle have also been investigated by ([Hu et al., 2004](#), [Hu et al., 2006](#), [Hu et al., 2007](#)), only 2D trapping could be achieved in this single lensed fibre configuration, where the insertion angle was tested between 55° - 30°. It was found that for insertion angles of 55°, 50°, 45° and 40° trapping was achievable. However, at 35° it was found that although there was an equilibrium position, the small optical forces that were generated were less than those due to Brownian motion, and so the particle was not maintained within the trap. At an insertion angle of 30° there was no equilibrium position reported and thus no trapping was experienced.

By applying two hemispherical lensed fibres, not counter-propagating, but inserted at an angle such that the two beams intersect, Taguchi *et al* achieved 3-D trapping and were able to levitate particles ([Taguchi et al., 2000](#), [Taguchi and Watanbe, 2007](#)). The optical forces acting on the particles were theoretically calculated using the ray optics approximation<sup>3</sup> for fibres inserted at angles of 30°, 35°, 45° and 60°, with 45° identified as being the

---

<sup>3</sup> See chapter 2.3 Force Modelling – Mei Regime – The Ray Optics Model

optimum insertion angle ([Taguchi et al., 2001](#)). Liu and Yu ([2009](#)) found that 3D trapping using dual lensed fibres was dependent upon the angle of the fibre insertion. Here it was found that only 2D trapping could be achieved at insertion angles  $\leq 45^\circ$ , but 3D trapping was possible for those insertion angles  $\geq 50^\circ$ .

The hemispherical lensed approach failed to provide 3-D trapping using a single fibre, since the necessary high numerical aperture could not be achieved. In an attempt to replicate optical tweezers, the first single optical fibre based 3-D trap was subsequently developed ([Taylor and Hnatovsky, 2003](#)). In this arrangement 2D optical trapping was achieved by an annular light distribution from a chemically etched, tapered, and hollow tipped, metallised fibre probe. 3D particle confinement was achieved by balancing an electrostatic force of attraction towards the tip with the opposing scattering force.

A 3D single beam 3D all-optical trap was demonstrated by ([Liu et al., 2006](#)). The distal end of the optical fibre is tapered using a two stage heating and drawing process to create a reduced diameter lens-like end face, causing a suitable focus for 3D trapping. Brambilla and Xu ([2007](#)) also used the heating and drawing technique to develop a single fibre optical trap by creating a tapered adiabatic<sup>4</sup> tip profile to convert the mode size. However the insertion angle of the fibre is not discussed in this paper and it is unclear whether, or not, 3D trapping was achieved.

Cabrini *et al* employed an axicon<sup>5</sup> micro-lens that was fabricated directly onto a cleaved fibre end, using Focussed Ion Beam milling, to create a single fibre trap from a Bessel beam output. It is unclear if the trap was capable of 2D or 3D trapping. The paper

---

<sup>4</sup> An adiabatic process involves the gradual changing of external conditions of a quantum mechanical system that allows the system to adapt its configuration. In this context the gradual tapering of the optical fibre reduces the spot size of the laser beam without incurring significant losses.

<sup>5</sup> An axicon lens is a plano-convex lens (one conical surface and one flat surface) creating a ring shaped approximation of a Bessel beam.

discusses the axicon lens fabrication and its optimisation to achieve a focal point ( $Z_{\max}$ ) at a distance of about 50  $\mu\text{m}$  from the fibre end ([Cabrini et al., 2006](#)).

Researchers in Italy have created two separate 3D trapping configurations using a four fibre bundle and fibre with an annular core ([Liberale et al., 2007](#), [Minzioni et al., 2008](#), [F. Bragheri et al., 2008](#), [F Bragheri et al., 2008b](#)). In both configurations the core of the fibre is cut at its end-face using focused ion beam milling, with an angle such that the propagating light exiting the fibre is reflected to a common focal point. The resulting numerical aperture (NA) is said to be close to that of the NA objectives used in COT OT's ( $\sim 1.06$ ). This is achieved by the use of strategically placed cuts that cause reflection at the fibre medium interface and provide 3D optical trapping with efficiency ( $Q$ ) that is equal to that of COT systems. Taguchi et al. ([2012](#)) developed a single optical fibre 3D trap using a dynamic chemical etching technique to bring the fibre's distal end to a sharp conical taper.

Following on from their first trap ([Liu et al., 2006](#)), Yuan *et al* ([2008](#)) developed a second fibre based optical trap. In this set-up twin core fibre that is abruptly tapered by a heating and drawing method is used to form a high intensity focal spot at the point where both beams converge, creating a stable 3-D optical trap. Multi-core fibre has also been shaped using chemical etching to create a sharp point that is then melted, using an arc discharge process, into a parabolic lens geometry at the end of the fibre tip ([Yu et al., 2012](#)). Other techniques using 2 ([Zhang et al., 2012a](#)), 3 and 4, multi-cores with an annular distribution and annular core fibres have been exploited to create 3D fibre traps ([Zhang et al., 2012b](#)). In both instances the method used to shape the fibre's end face was grinding and polishing.

### 3.3 SHAPING OPTICAL FIBRE FOR 3D OPTICAL TRAPPING

The optical output from a cleaved optical fibre end-face is of a divergent nature. This type of output poses no problem for the counter-propagating optical fibre trapping configuration, such as those proposed by ([Constable et al., 1993](#), [Scott D. Collins et al., 1997](#), [Guck et al., 2000](#)), since this type of configuration relies on the cancellation of the scattering force by an opposing scattering force. However, for optical tweezers-like configurations, akin to a single output beam that is capable of 3D optical trapping, whilst being unaided by additional external forces, then a focused optical output is a prerequisite in order to produce a gradient force that dominates the orthogonally aligned scattering force.

In a COT set-up the required steep intensity gradient is provided by tightly focusing the laser beam via a high numerical aperture (NA) microscope objective. This could also be achieved by using optical fibre to guide the light to the back aperture of the microscope's objective lens. However this course of action does not offer the opportunity to decouple the optical trapping system from the microscope and thus limits the possibility of ever developing a portable system via such an approach.

One solution to this challenge is to adapt the optical fibre's end-face, creating a lens effect, in order to alter the optical output from a divergent to a focused beam. This has been attempted in a number ways, with varying degrees of success, a subject which has been previously discussed in the review of optical fibre trapping configurations presented in Chapter 3.2. For instance, it has previously been reported that some types of fibre end-face lens-like configurations are only capable of 2D trapping. Whereas, other fibre end-face lens-like configurations are capable of efficient 3D optical trapping.

However, what are of interest here is the various techniques that are employed to create a lens-like effect at the fibre end-face, rather than the optical properties and trapping performance of the lenses themselves. There are many methods by which an optical fibre may be tailored to create a working lens. This section reviews the methods that are available and critically analyses their suitability for shaping fibre, for not only 3-D single beam optical trapping, but also within the context of its proposed application, namely integration with the AFM and other microscopy systems.

Manipulating optical fibre to shape the exiting laser beam has many applications in telecommunications and in the development of photonic devices. However the same methods can be adopted for applications in optical trapping. There are three key ‘manufacturing’ processes that are employed to influence the optical output from an optical fibre.

The first process concerns erosion of the fibre material, which can be achieved in several ways including the use of specialist technology and the use of chemical substances, or abrasives, to remove the material. The second method deposits or “grows” material onto the fibre’s end-face, whereas, the third method adapts the morphology of the optical fibre tip, through the application of heat and subsequent manipulation of the viscous material.

Erosion, ablation and polishing are all techniques that are concerned with the removal of material. Erosion requires chemical reactions to ‘eat away’ at the material. Ablation is the process whereby the solid material absorbs electromagnetic radiation, which causes it to heat and evaporate, or sublime at low flux levels. At high flux levels the material is converted to plasma. Polishing, on the other hand, relies upon the physical contact of abrasive materials to scratch, grind and polish the surface of the material.

### 3.3.1 *CHEMICAL ETCHING*

Chemical etching is one of the techniques employed to develop a tapered finish to an optical fibre's end-face. Generally the optical fibre end-face is dipped into a vessel of Hydrofluoric (HF) acid. Usually there is a layer of organic solvent floating on top of the HF to provide control of the meniscus. Taguchi et al. ([2012](#)) employed a dynamic chemical etching technique to produce an optical fibre taper with a  $17^\circ$  apex angle, that was capable of 3D trapping at an insertion angle of  $50^\circ$ . Here the optical fibre was dipped into Hydrofluoric acid (HF), which was contained by an overlying layer of Toluene. The optical fibre was then subjected to controlled movements within the HF. An assortment of tip shapes could be achieved by varying the speed at which the fibre was moved within the HF.

Chemical etching was the process adopted by ([Xin et al., 2006](#)) to create an optical fibre probe suitable for near field imaging and biomechanical sensing. However, in order to reduce the volume of material to be etched, the optical fibre was first subjected to a heating and drawing process. The heat was generated, in this instance, by using an electric arc. Supplementary to the reduced etching time afforded by this method, was the development of tips with a larger cone angle and shorter taper length, when compared to tapers fabricated using chemical etching alone.

Alternatively optical fibre dipped in a solution of ammonium bifluoride (AB), that is allowed to evaporate during the etching process, provides a natural tapering procedure. This is because the amount of the fibre that is being etched increases towards the end of the fibre, since the fluid level drops. Thus the amount of time for which a section of the fibre is etched is controlled by the rate of evaporation. This latter method was employed by ([Barnard and Lit, 1991](#)) to create a taper at the end of an optical fibre. The tapered tip was then subjected to heating, by using a CO<sub>2</sub> laser to create a spherical drop that solidified

when cooled and thus acted as a lens. This lens was fabricated to improve coupling efficiency between a laser diode and SMF.

### 3.3.2 *LASER MICRO-MACHINING*

Presby et al. ([1990](#)) employed a laser ablation process, using short intense laser pulses, to “machine” a spherical lens on the end of an optical fibre. The technique requires the optical fibre to be spun, in a manner that is similar to that of a work piece in a metal worker’s lathe. However, rather than cutting the work-piece using a steel cutting tool, which would be the case in a traditional lathe setup, the system employs a 25 W CO<sub>2</sub> laser to achieve the “cut” via ablation. The short duration laser pulses ensure that controlled amounts of the outside material are vaporised, and ensure that the internal structure of the optical fibre is unaffected by heat.

Deep ultraviolet lasers, at a wavelength of 157 nm, have also been employed to micro-shape lenses onto the end of an optical fibre. Li et al. ([2007](#)) demonstrated two methods; in the first instance the fibre was placed at a right angle to the laser beam and rotated around its axis. The Fluorine Excimer (F<sub>2</sub>) laser beam was then shaped by a mask and cut the spinning fibre to give a conical shape to its end-face. In the second method the laser was aligned with the face of the optical fibre’s end-face. As the optical fibre was rotated about its axis, the laser beam spot was scanned across the fibre face to create a micro-lens at the fibre’s tip.

Pulsed, short wavelength, 248 nm, Excimer lasers have been used to develop concave and convex microstructures using a scanning method known as the “planetary scanning method”. In this approach a “self-spinning photo-mask” is employed and simultaneously revolved in an orbital manner about the sample to create both spherical and aspheric refractive type micro-lenses. Three aspheric and three spherical lenses were developed and

tested in terms of their focusing ability. The results showed that the aspheric lenses demonstrated significantly greater focusing ability compared to the spherical types ([Lee and Wu, 2007](#)).

A novel approach to producing micro-lenses on the end of an optical fibre was exploited by a team of researchers in Italy. The intention here was to be able to quickly and easily produce lenses, in situ, for medical applications, such as for endoscopic laser treatment and surgery. The method is so simple that it is thought that a surgeon could quickly make a lens whilst in theatre. The method requires the end of the fibre to be heated by the laser to form a bulbous lens-like structure at its end. However, heating of the fibre end is not achieved via an external source, as in the above techniques. Instead the heat is generated by the laser that propagates within the fibre. The fibre is orientated in a downwards vertical direction, pointing towards a low thermally conducting target material. The exiting laser beam, on contact with the target material, results in fusion of small portions of the material. This reaction causes the generation of heat, as a small incandescent furnace is produced and a large part of the energy is re-emitted in the middle infrared region. It is within this mid-infrared region that the fibre core material is highly absorbing. Thus resulting with melting of the fibre tip to form a spherical lens on the optical fibre's end-face ([Russo et al., 1984](#)).

### **3.3.3 FOCUSED ION BEAM (FIB)**

FIB is a technique that employs a tightly focused beam of gallium ions. FIB is capable of locally milling away atoms by physical sputtering with sub 10 nm resolution. This technique is known as FIB milling, or subtractive lithography. Alternatively it is possible to locally deposit material with sub 10 nm resolution and this approach is known as FIB lithography, or additive lithography ([Wazenboeck and Wade, 2011](#)).

FIB milling was employed to create an axicon lens directly onto the end of an optical fibre, allowing a Bessel beam output to create an optical trap ([Cabrini et al., 2006](#)).

Fibre based optical tweezers with a trapping efficiency ( $Q$ ) equal to that of a COT system have been created using FIB Milling of the fibre end-face, as previously discussed in Chapter 3.2 ([Liberale et al., 2007](#), [Minzioni et al., 2008](#), [F. Bragheri et al., 2008](#), [F Bragheri et al., 2008b](#)).

### **3.3.4 POLISHING AND GRINDING**

Polishing and grinding techniques employ abrasive materials, such as optical fibre lapping film, the micrometer equivalent to sand-paper, or emery cloth, that are used to remove excess material from wood and steel respectively.

Effective lenses have been fabricated onto the end of a single mode fibre for laser diode coupling. The lens was created by polishing the fibre end-face using a four axis micro-lapping machine developed by ([Lin, 2005](#)). Ying-Chien et al. ([2008](#)) used a commercially available fibre lens polisher to create optical fibre with varying types of end-face lenses, with coupling efficiencies of up to about 83% being recorded.

In order to reduce polishing time, single mode optical fibre was initially subjected to the heating and drawing process. The heating and drawing process produced a tapered fibre with a reduced diameter end-face. The polishing of the end-face produced a micro-axicon lens that was capable of delivering a Bessel beam output ([Grosjean et al., 2007](#)).

### **3.3.5 PHOTO-POLYMERISATION**

The self-writing process of photo-polymerisation of light curing resin has also been used to “grow” an optical tip at the end of an optical fibre. The method has been used to develop a reduced size counter propagating optical trap ([Valkai et al., 2009](#)). In a similar vein,

([Bear, 1980](#)) created a micro-lens at the fibre core, by first dipping the fibre end-face into a negative photoresist. This is followed by propagating HeNe laser light, at 632.8 nm, within the optical fibre, to cure the resin at the fibre end-face. Alternatively optical fibre was heated and drawn down to a diameter of 20  $\mu\text{m}$  before cleaving. To create a hemispherical micro-lens at the end-face it is applied with a small drop of photosensitive polymer, which is then cured ([Liu and Yu, 2007](#)).

### **3.3.6 GRADED INDEX FIBRE LENS**

A micro-lens with a long working distance was fabricated, for the coupling of polarisation maintaining (PM) fibre, with 1.55  $\mu\text{m}$  quantum dot devices. This was achieved by fusion splicing graded index fibre onto the end of PM fibre. The graded index fibre was then cleaved to the required length. A droplet of silica is then added to the face of the graded index fibre. The silica droplet was deposited by heating a tapered SMF in the fusion splicer and bringing it into contact with the graded index end-face ([Thual et al., 2005](#)).

### **3.3.7 HEATING AND DRAWING**

Heating and drawing of the optical fibre, until fracture, can result in the production of a tapered optical fibre that can focus an exit beam sufficiently for 3D optical trapping. Usually the fibre is held at either end and the heat is applied at the centre point. When the fibre's material becomes sufficiently viscous, then translation equipment at either end is driven to pull the fibre apart forming two nearly identical tapers either side of the point of fracture.

Heating of the fibre can be achieved in a number of ways, including gas flame, electric arc discharge, or laser. When compared to the use of lasers as the heat source, gas offers some disadvantages. Firstly maintaining a constant and suitable temperature requires the gas flow rate to be precisely regulated. The second drawback is with regard to the purity of

the gas flame. If the gas is not of certain purity, then it is understood that contaminants could be deposited onto the optical fibre, the result of which is that the deposited impurities would have an adverse effect on the fibre's optical properties. Additionally the heat transfer from a gas flame is conductive. Therefore the flame heats the material from the outside-in and can lead to non-uniform heating of the fibre, which can result in an inconsistent taper profile.

Finally since heating does not occur from absorption due to radiation, as in the case of the laser, translation of the gas flame along a section of the optical fibre can lead to non-uniform heating due to air currents affecting the direction and intensity of the gas flame ([Ward et al., 2006](#)).

CO<sub>2</sub> lasers offer the best source of heat to make the optical fibre viscous. Since the heat is generated through the radiation and absorption of the electromagnetic waves by the material, then the heat transfer occurs in a uniform manner. Moreover the optical properties of the optical fibre are not altered, since there are no external contaminants being transferred to the optical fibre. Also the method of heat transfer, due to the absorption of electromagnetic radiation, eliminates the possibility of air currents having a negative effect on the heat transfer process, since the propagation of light is impervious to such occurrences.

Tapering of SMF through the heating and drawing process has been adopted, for optical trapping and other applications, using different heat sources on various optical fibre configurations. Brambilla and Xu ([2007](#)) employed a commercially available micropipette puller that uses a CO<sub>2</sub> laser to taper optical fibre for optical trapping.

A homemade tapering rig was used to form a “biconical” tapered fibre. The rig consists of a 1mm wide oxy-butane torch flame with stepper motors employed to control the movement of the flame and translation stages ([Harun et al., 2013](#)).

Abdelrafik et al. ([2001](#)) used a CO<sub>2</sub> laser in a process whereby the optical fibre is twice heated using two different approaches that together form a spherical micro-lens on the fibre end-face. Firstly the fibre is tapered using a heating and drawing process. Subsequently the spherical micro-lens is created by rotating and melting the tapered tip.

### **3.4 BEAM SHAPING DISCUSSION**

Chemical etching, polishing, laser ablation and FIB milling all have one thing in common in that they alter the fibre’s shape by removal of outer material. This can be detrimental to the optical fibre’s integrity, since light propagates within an optical fibre due to total internal reflection (TIR). This therefore could pose challenges in that there could be optical losses prior to the exit point of the fibre. A further problem associated with chemical etching is its use of toxins that can be damaging to both the health of the user and the environment.

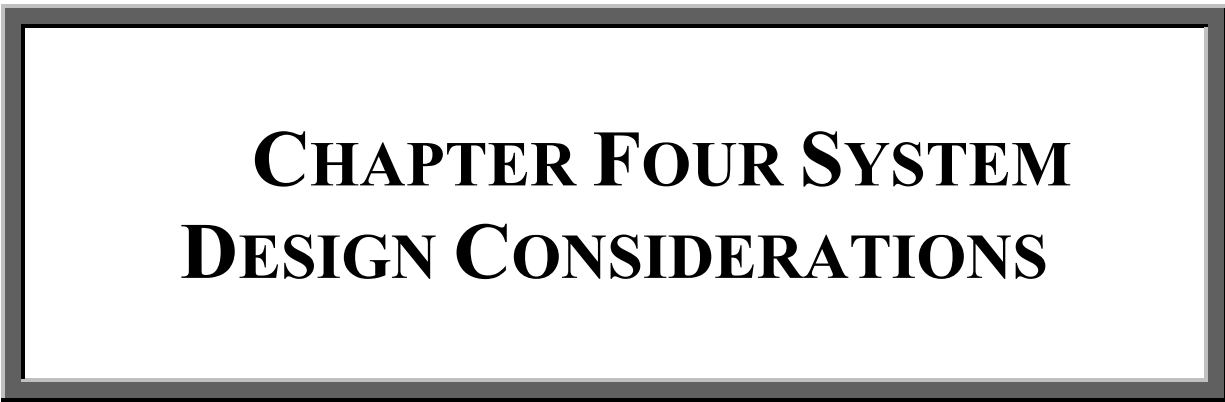
The heating and drawing process however, does not rely on removal of the material and instead maintains the ratio between the core and the cladding diameters of the optical fibre<sup>6</sup>, helping to maintain its integrity and facilitate a reduction in lossless light propagation. Furthermore no small particle waste material is produced and harmful toxins are not employed during the process. Therefore, it poses no health risks due to the inhalation, or splashing, of toxic chemicals, such as HF for example, onto the skin.

Of the two main sources of heat the laser offers the best solution for the heating and drawing method. The reason for this is that the heat is transferred via radiation and

---

<sup>6</sup> Core and cladding diameters of 1060XP high power SMF are 5.8µm and 125µm respectively

absorption by the material and so the laser is not negatively affected by air currents and homogeneous heating of the fibre is maintained. Additionally, the laser does not transfer contaminants to the fibre in the process.



**CHAPTER FOUR SYSTEM  
DESIGN CONSIDERATIONS**

## **SYSTEM DESIGN CONSIDERATIONS**

This chapter investigates the design considerations that were influential during the selection process to find an appropriate optical trapping (OT) system configuration for this research project. During this process the pros and cons for both the conventional optical tweezers based systems (COT) and the fibre optic based systems (FOT) have been collectively explored along with the system design specifications. This evaluation has enabled the appropriate choice of optical trapping system configuration to be made.

### **4.1 RECAP- OPTICAL TRAPPING DESIGN CONFIGURATIONS**

There are two main categories of optical trapping system configurations reported in the literature. First of all there are the (COT), which are those that employ a free space laser beam that is introduced into the sample chamber via the optical pathway of the microscope. The second type of configuration employs optical fibre to deliver the laser beam into the sample chamber. The use of fibre optic based trapping systems (FOT) decouples the trapping system from the microscope, since the optical fibre provides an alternative route to the microscope's optical pathway. However the reader will recall that the configurations here are not just limited to these two types, as each of the two main configurations, as discussed above, can be further divided into a myriad of alternative configurations and setups, which were reviewed in Chapters 2 and 3.

### **4.2 RECAP-DESIGN SPECIFICATIONS**

The major driving force behind this optical tweezers development is that the system is required to be integrated with other advanced microscopy applications. Therefore the system is required to be decoupled from the microscope, whilst being of suitably small dimensions

such as to allow easy transportation of the system between additional applications. In addition to the above requirements for system detachment and physical size constraints, further unavoidable restrictions were imposed upon the proposed OT system. These were in the form of the allotted total maximum budget of £50,000, secured for its design, build, development, test and implementation.

### **4.3 ADVANTAGES OF FIBRE OPTIC BASED OPTICAL TRAPPING (FOT) CONFIGURATIONS OVER CONVENTIONAL OPTICAL TWEEZERS (COT) SYSTEMS**

This section reviews the advantages of employing optical FOT based systems over their COT counterparts. The reader will recall that COT systems use a free space laser beam that is required to be directed into the microscope's optical pathway using bulk optics. Whereas FOT based systems employ optical fibre to deliver the laser light directly into the sample chamber, thereby decoupling the system from the microscope.

#### ***4.3.1 SYSTEM SIZE AND COST***

The sheer physical size of a COT system will preclude the possibility of straightforward system portability. This is due to the large surface area and heavy optical table that is required to arrange the essential bulk optics, which are necessary to shape and direct the laser beam. Furthermore the high relative cost to build a COT system, when compared to a FOT system, is also a limiting factor, which eliminates the possibility of building more than one COT system to service individual, advanced microscopy applications.

In addition the extreme sensitivity of such a bulk optical component set-up to any external vibrations or the mechanical jolting of the system, brought about by its transportation, would probably warrant a complete optical system re-alignment after every system move. With a

fibre based system however, complete system re-alignment would not be a requirement, to such an extent, since there are fewer components. In its basic form a FOT system consists only of a laser and an optical fibre in which to deliver the laser light to the sample. In such a set-up the only component realignment that may be required would be at the laser to fibre coupling device and at the fibre's distal end within the sample plane.

In addition to improving the robustness of the system, the elimination of the bulk optical components, which are employed in a COT system, would provide improved system flexibility, whilst significantly reducing the total capital expenditure associated with its development. Therefore a fibre based configuration would provide a system that offers the required portability, flexibility and robustness with the possibility of being delivered within the specified finite budget.

### **4.3.2 TRAP DETECTION**

Optical trapping systems require a method of detecting and monitoring a trapped particle. In COT systems this is usually in the form of a quadrant photo diode (QPD). In a FOT system the requirement for a photo-detection system is removed. This is due to the optical fibre's distal end visibly acting as a pointer to the trapping zone.

Two examples of the optical fibre taper pointing towards the trapping zone can be seen in Figure 4-1 (a) and (b). Figure 4-1(a) shows the first frame of an actual trapping sequence prior to laser activation. Here the tapered optical fibre tip is lined up in front of a  $3\mu\text{m}$  silica microsphere in preparation for optical trapping. Figure 4-1 (b) shows the last frame in the same optical trapping sequence. In this frame the  $3\mu\text{m}$  silica microsphere is observed at the end of the tapered optical fibre, as it is being optically trapped in 3D. In both images it is apparent

that the end of the tapered optical fibre clearly indicates the local proximity of the trapping zone.

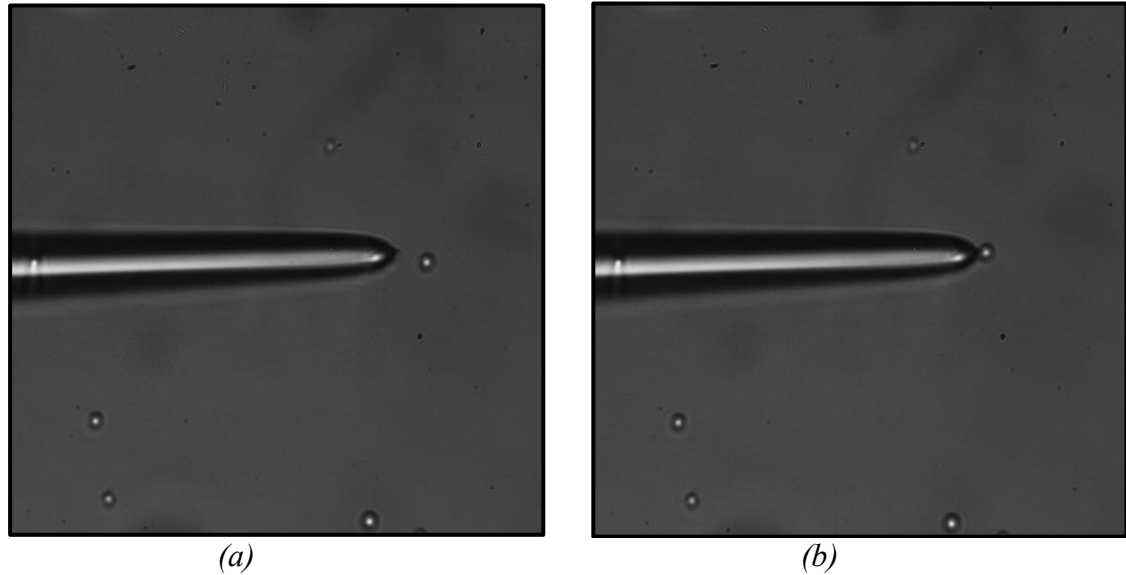


*Figure 4-1 showing how the tapered fibre tip points to the trapping zone (a) first frame of optical trapping video sequence (b) last frame of optical trapping video sequence*

The visual position detection provided by the tapered distal end of the optical fibre is of a great advantage when trying to integrate an OT system with an AFM for example. The reason for this advantage stems from the fact that the QPD that is typically employed by a COT system would be rendered useless for this application, since the AFM head would block the optical path of the laser beam from the sample to the QPD. Thus the inherent visual position detection that is offered by the optical fibre's distal end would be ideally suited for use in a combined optical trapping/AFM system.

Since the distal end of the optical fibre points to the trapping position, then it is obvious that visualisation of the optical trap's position can be easily accomplished simply by using standard video equipment. However standard video equipment alone is no substitute for the

high bandwidth and sub-millisecond resolution of a QPD, which are the required specifications for the successful tracking of a particle's trajectory during optical trapping.

Typically, standard video equipment provides basic frame rates in the range of 25-30 frames per second (fps). The DeltaPix Infinity X camera can provide an improved 60 fps frame rate depending upon the image resolution and the exposure time used. However a maximum of 55 fps could only be achieved at a reduced image resolution of 640 x 480 pixels, whilst using a maximum x40 magnification objective lens for imaging of the specimen plane. The successful tracking of a particle's displacement during an optical trapping procedure would require a larger frame rate than the 55 fps of the DeltaPix Infinity X camera. Therefore a high speed video camera with a frame rate in the range of 100's of fps range would be required.

The addition of a high speed video camera to the system would come at a relatively higher capital expense in comparison to the cost associated with either standard video equipment, or a QPD. However, in the absence of a QPD, a high-speed video camera is likely to be a necessity for two fundamental reasons, both of which are linked to the ability to be able to accurately characterise the optical trap. Firstly the time that it takes for a particle to move through a specific distance, as it is pulled into the trapping zone, for example by a distance of 10 $\mu$ m, can be of the order of milliseconds to seconds. The timeframe here depends upon the viscosity of the medium and particularly upon the optical powers employed, with much shorter timeframes in evidence due to the higher optical powers. For standard video running at 30 fps, 1 second of video provides just 30 data points for any given particle trajectory. The individual data points represent the centre of the tracked particle within a given video frame. Secondly the image of any particle that is travelling at relatively high velocities recorded using

standard video equipment will be subject to motion blur. This can cause serious problems when attempting to characterise the trap during later video analysis, which typically involves particle tracking. Here the tracking of the particle will fail, since the particle's shape will have become distorted due to motion blur and hence will be unrecognisable to the pattern matching template of the particle tracking software. High speed video will therefore provide many frames of data over which to track a particle's trajectory and will all but eliminate the effects of motion blur. The resulting increase in the volume of the data sets being recorded, coupled with the elimination of the effects of motion blur, would provide significantly improved tracking of a trapped particle's trajectory.

However, the inclusion of a high speed video camera within the system design is not without its disadvantages. It has already been mentioned that there is a relatively high capital cost associated with high speed video capturing equipment, when compared to the cost of a simple position detector QPD. For example the valuation of a Photron Fastcam MC-1 was £11,000 (as provided by the EPSRC for insurance purposes), which is relatively expensive when compared to a position detection QPD such as the PDQ30C which costs £572 (Thorlabs, UK).

Moreover, the increased frame rate of a high speed video imager lends itself to a corresponding increase in the required computer memory that is used to store and process the recorded video. In Table 4-1 it can be seen that the DeltaPix Infinity X camera requires the least amount of memory for 1 second of recorded video, at 50 MB, due to its low 55 fps frame rate. Whereas the Photron Fastcam MC-1 high speed camera requires 125 MB of memory for 1 second of video at 500fps.

*Table 4-1 memory requirements for 1 second of video footage acquired from the two video cameras employed during this project.*

<b>Camera</b>	<b>Resolution (pixels)</b>	<b>Frame size (MB)</b>	<b>Frame rate (fps)</b>	<b>1 second of video (MB)</b>
DeltaPix	640 x 480	0.9	55	50
MC-1	512 x 512	0.25	500	125

A further weakness, inherent in the use of video over QPD as a means of particle position detection, is the inferior resolution. The spatial resolution of video is governed by the amount of pixels, their effective size and the distance between the target and the sensor. The smallest resolvable distance or the highest resolution with which a particle can be tracked during its trajectory is determined by the size of the pixel and the magnification of the microscope's objective lens. The highest resolution for the two video cameras tested here can be seen in Table 4-2, which takes into account a range of microscope objective magnifications of between x20 and x100 for comparison. Here the table provides the theoretically highest resolution for values of magnification between x20 and x100. It is evident that x100 magnification offers the highest resolution of 52 nm, which is provided by the smaller pixel area of the Infinity X camera. This can be considered to be a considerably poorer resolution compared to the demonstrated resolution of 0.1 nm provided by a QPD ([Nugent-Glandorf and Perkins, 2004](#)).

*Table 4-2 comparison of the resolvable tracking distance that can be achieved by the two video cameras for x20, 35, x40, x60 and x100 magnifications*

<b>Camera</b>	<b>Pixel Size at the Sensor (<math>\mu\text{m}</math>)</b>	<b>Mag</b>	<b>Mag</b>	<b>Mag</b>	<b>Mag</b>	<b>Mag</b>	<b>Mag</b>
		<b>x20</b>	<b>x30</b>	<b>x35</b>	<b>x40</b>	<b>x60</b>	<b>x100</b>
		<b>Resolvable tracking distance (nm)</b>					
Infinity X	5.2 x 5.2	260	173.3	148.6	130	86.6	52
Fastcam MC-1	10 x 10	500	333.3	285.7	250	166.6	100

Most of the experimental data, collected during this research project, was acquired using a microscope objective with a magnification of x40, which actually turned out to be closer to x35 and is discussed in greater detail in Chapter 6. The previous example was chosen using a

magnification of x100, as this is the magnification usually associated with high NA microscope objectives. High NA microscope objectives are usually employed in a COT system; therefore the likely magnification used to cast an image on to a QPD would be x100.

The best resolution provided by the high speed MC-1 camera at x40 magnification was theoretically 250 nm. However the resolution was in fact found to be nearer to 286 nm, since the magnification was actually x35, as previously mentioned. Table 4-2 shows that improved theoretical resolutions can be gained through the use of a higher magnification. However, there are additional compromises associated with an increase in the magnification factor. Firstly there is a reduction in the field of view (FOV) at the sample plane, a problem that is discussed further in Section 4.3.3. Secondly at increased magnifications the amount of light reaching the camera sensor is significantly reduced. The consequence of this is poorly contrasting images that are ineffective during later processing and analysis.

However position detection of an optically trapped particle, provided by a QPD for an integrated OT/AFM system, cannot be totally ruled out. This is due to recent advances in AFM design that sometimes now incorporates a light path passing through the AFM head and which would facilitate such a set up. Indeed the head of the Asylum Research Molecular Force Probe-3D AFM here at GERI possesses one such light path passing through it. However this light path is currently adapted to provide illumination to the sample arena from above the sample, as this set up improves the quality of the acquired images. The reason for this is that illumination from below the sample chamber is reflected back down the microscope objective by the gold coated AFM cantilever contaminating the image with scattered light in the process.

Another factor that should be taken into account is that normally, in a COT system, the propagation direction of the trapping laser is in a vertical orientation as it passes through the microscope's objective lens and into the sample chamber. The vertical direction of the laser beam's propagation allows the corresponding trap locations, in the X and Y planes, to be captured by the QPD position detection system in the back focal plane, as is depicted in Figure 4-2 (a). In this image the dual trapping locations of a COT system are projected onto a QPD in the back focal plane of the microscope.

This is in stark contrast to the case for a FOT based system, as shown in Figure 4-2 (b). Here the laser beam bypasses the microscope objective, since the optical fibre delivers the beam directly into the sample arena at an insertion angle of about  $10^\circ$  to the sample plane. Consequently the  $80^\circ$  angular change in laser beam orientation that is employed by the FOT based system compared to the COT system, results in the laser beam no longer being directed onto the target of the QPD, effectively rendering the QPD redundant.

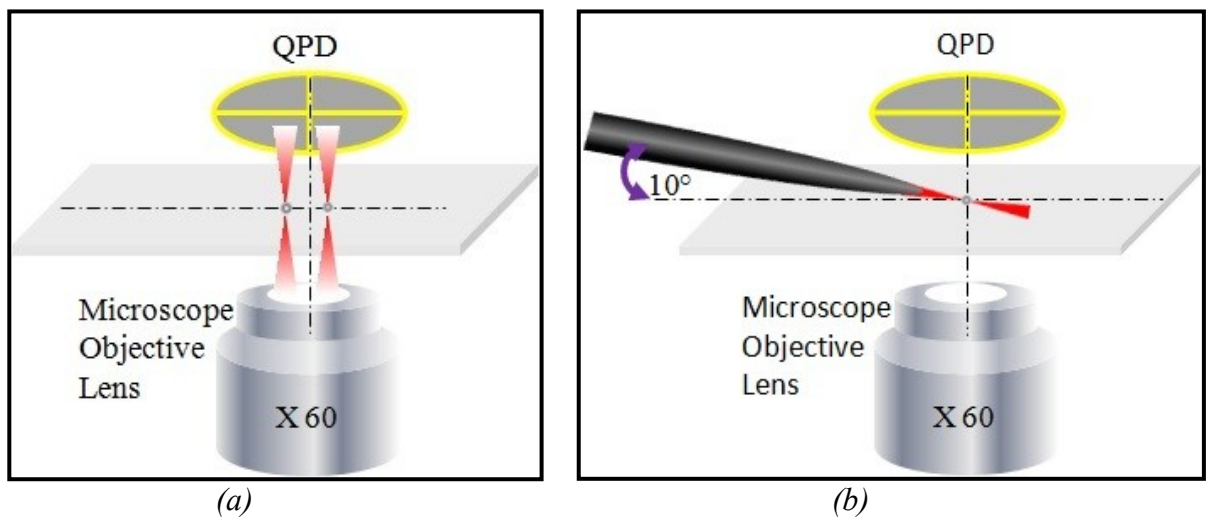


*Figure 4-2 effectiveness of a QPD detection system for (a) COT optical tweezers dual trap system and (b) a single optical fibre based 3D optical tweezers system*

### 4.3.3 ***DECOUPLING THE TRAPPING LASER BEAM FROM THE MICROSCOPE'S VIEWING OPTICS***

An added benefit when employing an optical fibre configuration is that the system becomes decoupled from the microscope, as the trapping laser light is delivered into the microscope sample chamber via the optical fibre. Therefore, an expensive high NA microscope objective lens is no longer a necessity and further reduces the system cost. A further advantage associated with not using a high NA microscope objective lens is an increased field of view (FOV) ([F Bragheri et al., 2008b](#)). Imaging of the sample plane with an improved FOV is readily achievable via standard microscope objectives. To demonstrate this, the Photron Fastcam MC-1 high speed video camera has an effective sensor area of 5.12 X 5.12 mm (figures provided by the camera manufacturer). The size of the effective sensor area is calculated from the multiplication of the sensor pixels (512 x 512) with the effective pixel area of 10µm x 10µm. The FOV for a camera image at the specimen plane, when viewed via the x40 microscope objective, is 128µm x 128µm and is 146.3µm x 146.3µm at x35 magnification. This may be compared with the FOV of an image plane provided by a high numerical aperture (NA) microscope objective, with a x100 magnification, which has a FOV of 51.2µm x 51.2µm, as given by;

$$FOV_{sample} = \frac{E_{sen}}{Mag} \quad (4-1)$$

where  $FOV_{sample}$  is the field of view at the sample,  $E_{Sen}$  is the effective sensor size and  $Mag$  is the given magnification of the viewing optics.

In a COT system the high NA microscope objective has a dual purpose; firstly it forms an image of the sample plane, secondly it is the means for tightly focusing the laser beam, which

is a necessary function for 3D optical trapping to occur. This secondary function of the microscope objective lens actually constitutes a further problem for the optical trap designer. This is because the laser beam, which is located exterior to the microscope, has to be introduced into the microscope's optical path.

Introduction of the laser beam into the optical path of the microscope presents a problem that may require re-engineering of the microscope. However, the purchase costs associated with the atomic force and laser scanning confocal microscopes are quite substantial, in the region of £160,000 and £250,000 respectively. The deployment of a fibre optic based system would eliminate the need for any major re-engineering of these expensive pieces of capital equipment and therefore removes the potential for any damage to be caused to them in the process. This is because the optical trapping laser beam is delivered directly to the sample arena, via the optical fibre, and for that reason avoids the requirement for the laser beam to negotiate the optical pathway through the microscope.

#### ***4.3.4 CONVENTIONAL OPTICAL TWEEZERS SYSTEM CONFIGURATION, MANOEUVRABLE DISTANCE AND OPTICAL POWER CONSTRAINTS***

A further advantage offered by a fibre optic based OT system is that, since the laser beam emanates from the optical fibre tip, the optical power output is maintained constant wherever the optical fibre is transferred to within the X and Y horizontal plane of the microscope's field of view. In contrast COT systems have a limited degree of manoeuvrability within the field of view, before optical power losses are observed. According to ([Brouhard et al., 2003](#)) for example, the area in which an optical trap can be moved, within which the optical output never drops below a 95% threshold is 45  $\mu\text{m}$  x 25  $\mu\text{m}$ .

One course of action to overcome the above problem would be to manoeuvre the microscope sample stage, rather than, or in conjunction with, the trapping beam. However this option would only serve to increase the overall system cost, as additional computer controlled translation stages would be required to drive the microscope's sample stage, at the very least, in the X and Y directions.

#### **4.4 DISADVANTAGES OF FIBRE OPTIC BASED OPTICAL TWEEZERS CONFIGURATIONS OVER COT SYSTEMS**

The discussion thus far has mainly described the advantages that an optical fibre based system configuration offers over that of the COT systems. However there are also some drawbacks associated with fibre optic based OT system configurations when compared to the more conventional COT systems, some of which have already been discussed. These disadvantages vary from system to system and depend upon the specific applications to which they are being applied. To enable an informed and correct choice of system, the negative aspects of fibre optic based systems are also explored here.

##### **4.4.1 MAINTAINING A TARGET IMAGE DURING SAMPLE ELEVATION**

One such disadvantage concerns the ability to maintain a clear focused image of the optically trapped sample whilst it is being elevated in the Z plane. Elevation of an optically trapped particle in a FOT based system requires the optical fibre itself to be moved in the vertical +Z direction. However as the optical fibre and the optically trapped sample operate independently to the microscope objective, when they are manoeuvred in the Z space, they are moved outside the focal region of the microscope objective. In order to maintain a focused image of the optically trapped sample during elevation, continual adjustments to the height of the objective lens must be made by altering the microscope focusing control knob.

Some COT systems on the other hand, employ the microscope objective to not only focus the trapping laser and view the samples at the specimen plane, but to also provide height control for the optical trap. This requires arrangement of the optics so that the trap is in focus with the specimen, hence allowing trapped objects to be readily visualised. This kind of an arrangement improves the quality of the trap as the microscope optics' are designed to minimise aberrations at the specimen plane. Movement in the Z-plane can be achieved by focusing the objective up or downwards ([Svoboda and Block, 1994](#)). Therefore, when making adjustments to the optical trap height in the vertical +Z direction, a clear focused image is maintained.

Although there was some irritation caused to the author whenever the trapped subject was lost from view during elevation, the fact that the user now controls what is actually being imaged turns this negative into a possible positive trait. For example it may be that a general cell population is the subject of interest, after a single trapped cell has been elevated from view. In contrast it could be that the isolated cell itself is the subject of interest after removal from the general cell population. No matter which scenario holds true, the fact is that the user now has control and can dictate the matter to suit the experiment. This kind of task cannot be performed with COT systems in which the optical paths of the trapping laser beam and viewing optics are not separated, such as in the system previously proposed by ([Svoboda and Block, 1994](#)) for example.

#### **4.4.2      *MULTIPLE TRAPPING SITES***

A further shortcoming that is associated with FOT based systems lies in the relative difficulty for the provision of multiple trapping sites. The very nature of optical fibre based trapping systems implies that any additional trapping sites that are to be implemented within a system

must necessarily present increased complexity and cost. The reason for this is due to optical fibre being a physical entity, and it is inevitable therefore that inclusion of more trapping sites within the system would inherently require the inclusion of additional optical fibres. At best for a single beam FOT system, one additional fibre would be required for each additional trapping site. For other system types, such as the counter-propagating FOT system, at least two optical fibres per additional trapping site would be required.

Any additional optical fibres would require mechanical fixing in place at the correct position about the sample chamber. Furthermore in order for every trapping site to be operated independently, then each fibre trap would require its own method for attenuating, or shuttering, the individual trapping laser beams. A further requirement would be the addition of dedicated mechanical translation equipment to provide manipulation, through the X, Y and Z spatial planes, for each individual trapping fibre. Moreover there could be a requirement for rotary manipulation, such as in the cases of dual-lensed optical fibre OT systems ([Taguchi et al., 2001](#), [Taguchi and Watanbe, 2007](#)) and single optical fibre OT's systems ([Liu et al., 2006](#), [Taguchi et al., 2012](#)), to provide a means of adjusting the optical fibre insertion angle. Therefore the system complexity and cost would increase with each additional trap.

In COT systems however, multiple trapping sites are relatively easy to achieve, a subject that was previously covered in Chapter 2. Let us recall the multiple trapping system example by ([Mameren et al., 2011](#)) given in Chapter 2. It would be impracticable to achieve this kind of multiple trap operation using optical fibre for the beam delivery method. This is because the system would require 42 optical fibres, translation devices and the means for switching the 42 individual beams on, or off, independently of each other. All of which would enable the 42 optical traps to operate with the equivalent independence of its COT counterpart. Such a set-

up however, would become bulky, unwieldy and expensive, if being at all possible, when one considers the limited spatial confines of the microscope's specimen plane.

In theory one rapidly scanned optical fibre could mimic the above multiple trapping system. But such a system brings with it a fundamental design flaw, as the action of scanning an optical fibre through the liquid medium would have profoundly negative effects rendering the possibility of multiple trapping sites unattainable. One such negative outcome is the fact that the optical fibre would be prone to collisions with the samples intended for optical trapping. Moreover, the physical disturbances, caused by the relatively large optical fibre being repeatedly and rapidly dragged through the liquid medium, would only serve to cause the particles to diffuse with greater influence than that due to the effects of Brownian motion alone. Finally rapidly scanning an optical fibre and then abruptly bringing it to a halt would cause oscillation of the end of the tapered optical fibre. The vibrating tapered optical fibre end would result in the optical trapping becoming unstable, especially when one considers the short illumination durations required for the re-trapping of diffused particles between the various trapping sites.

A fixed array of optical traps has been created using a bundle of optical fibres, with each having a focusing element on its end-face to create individual optical traps ([Tam et al., 2004](#)). This set up can be considered to be a fibre version of the fixed optical trap array that was created using a diffractive optical element (DOE) ([Dufresne and Grier, 1998](#)).

#### **4.4.3      *REDUCED OPTICAL TRAPPING EFFICIENCY***

Literature suggests that using a single fibre to optically trap particles results in a trapping efficiency ( $Q$ ) that is an order of magnitude less than the  $Q$  value of COT systems.  $Q$  is

defined as the ratio of the optical trapping forces generated and the optical power taken to produce the forces, as given in Equation (2-4).

The  $Q$  values for COT systems have been recorded by ([Malignino et al., 2002](#)).  $Q$  values for the scattering force were recorded between 0.341 to 0.535, which was dependent on the effective index ( $m$ ) of the trapped bead and medium as given in Equation (2-1), where the  $m$  value for polystyrene beads in air and water is given as 1.2 and 1.6 respectively. However, the trapping efficiency varies only slightly, changing from 0.506 to 0.570 respectively, due to the contribution of the gradient force ([Malignino et al., 2002](#)).

A trapping efficiency of 0.07, on the other hand, was recorded by Hu *et al* for their 2D single lensed optical fibre trapping system ([Hu et al., 2007](#)). This is an order of magnitude less than the trapping efficiency attributed to COT systems. The reduced  $Q$  values for fibre based systems are attributed to the difficulties in achieving a sufficiently high NA, a prerequisite for the generation of the steep intensity gradient required if single beam 3D trapping is to be realised.

However, recent advances in optical fibre delivery systems have seen this tendency reversed, through the development of novel solutions that demonstrate optical trapping efficiencies comparable to that of COT systems ([F. Bragheri et al., 2008](#), [F Bragheri et al., 2008a](#), [Liberale et al., 2007](#), [Minzioni et al., 2008](#)). These novel solutions have been discussed earlier in Chapter 3.

However in light of what we are trying to do here, which is to implement the system with the AFM requiring an insertion angle below  $10^\circ$ , these new advances in fibre technology are not applicable, as the fibre end faces remain large. This leads the author to suspect that using

such fibres would give rise to similar problems to those experienced during this research project, which are presented in Chapter 7, and concern the size and geometric profile of the fibre tips produced here.

#### **4.4.4      *DISADVANTAGES DUE TO THE PHYSICAL ATTRIBUTES OF OPTICAL FIBRE***

Further disadvantages associated with the use of optical fibre originate from the fact that it is a physical entity employed within an aqueous arena that may contain adherent biological material. The optical fibre's distal end can therefore be prone to acquiring biological debris, and/or being coated with a layer of bio-film after extended use. Consequently the optical output may be adversely affected.

The optical fibre itself may also play a role in affecting the outcome of force measurements. Movement of the fibre through the medium will undoubtedly cause disturbances within the medium that will not have been previously witnessed during optical trapping using COT systems, and as a result this could lead to added complexity during force determination and calibration.

There is a further difficulty related to the material properties of optical fibres, in that glass is a brittle substance. To improve the material properties of optical fibre, it is shrouded in an outer coating of acrylate buffer, which adds strength and flexibility. However in some cases, this outer buffer has to be removed, to allow the silica fibre end-face to be altered, in order to create the lens effect for focusing the light. This in turn leaves the 'naked' fibre tips vulnerable to damage that can be inflicted by colliding with the microscope sample chamber floor. Alternatively, damage may result due to the periodic cleaning that is required to remove any debris, or bio-film that may have been deposited on the optical fibre during use.

Cleaning the tapered end of an optical fibre, from which the laser beam emanates, is achieved by wiping it with an optical grade paper wipe soaked in Isopropanol 99.5+%, A.C.S. Reagent (Sigma Aldridge, UK), a difficult task when one considers firstly the fragile properties of the material and secondly the small size of the object to be cleaned. For example the size of a tapered optical fibre end can be of the order of anywhere between a few 10's of  $\mu\text{m}$  down to a few 100's of nm in diameter. Any damage to the fibre optic tips would render them useless for optical trapping. Consequently a new lens effect structure would have to be re-formed at the fibre end and all the relevant system calibrations re-executed.

#### **4.5 CHOICE OF SYSTEM CONFIGURATION**

After due consideration of the advantages and disadvantages offered by both the COT and FOT based system configurations, it was decided that a FOT based system design should be adopted. Such a design would reduce the physical footprint of the overall system and in turn would greatly enhance the prospects of facilitating the required level of portability. The nature of such a system would also lead to a substantial reduction in build costs, when compared to the expenditure expected for that of a COT system approach.

Multiple trapping sites at this stage of the project are not yet required. The initial aim is to construct a working 3D single beam trap that is capable of operating at a sufficiently low fibre insertion angle to allow AFM integration. However, if further trapping sites were required in the future, at least one additional trapping site could be realised with relative ease and at low cost.

Dual optical fibre trapping sites could be achieved with the acquisition of a 1 x 2, 50% fused optical fibre coupler, turning a single optical fibre into two separate optical fibre

pathways. By opting for manually operated micrometre controlled X, Y & Z translation stages, manipulation of the additional optical trap could be realised at a fraction of the cost that would be associated with the original single fibre set up. The manually controlled manipulation would provide initial set up functionality for the optical fibre, and once in position this could be maintained as a static trapping site to be used in conjunction with the dynamic trapping site. However for both traps to be able to act independently of each other, this would require both beams to be operated separately. Independent beam control could easily be achieved using two commercially available, in-line, electronically controlled and variable fibre optic attenuators.

#### **4.6 PREFERRED OPTICAL FIBRE TRAP CONFIGURATION**

Selection of optical fibre for conveyance of the laser light to the sample chamber posed further design problems. The first of these was deciding which optical fibre trapping system configuration would be a suitable choice for this project, a solution which can only be arrived at after careful consideration of the available configurations, as discussed in Chapter 3. The application in which the system is to be employed must also be taken into consideration here, as some optical fibre trapping configurations may not be a suitable fit for certain applications.

For example COT dual optical tweezers were employed to hold silica microspheres attached to red blood cells ([Hénon et al., 1999](#)). The silica microspheres, which were being employed as ‘optical handles’, were drawn apart in an attempt to stretch the cells to derive the elastic shear modulus of the cell membrane. However, in this method the red blood cells could only be deformed to about 15% of their overall size. In contrast the use of a counter-propagating optical fibre configuration yielded deformities of up to 160% of the red blood cells’ original size, before rupturing them ([Guck et al., 2000](#)). Moreover, to reach such

relatively high deformities, extreme optical powers were required, up to a maximum of 700 mW per fibre, i.e. 1400 mW of optical power was incident upon the cells. This is in direct contrast to the case where optical handles were employed, where optical powers in the region of 200 mW were employed with beams that were not directly incident upon the cells ([Hénon et al., 1999](#)). However, optical traps, consisting of counter-propagating beams, do not require highly focused laser beams, unlike their optical tweezers counterparts, and as such, operate at reduced irradiance per illuminated area. Therefore they can afford the use of higher optical powers, without running the risk of causing damage to the sample.

Of the entire range of optical fibre trap configurations investigated in Chapter 3, a single optical fibre approach was deemed to be the least complex approach, whilst also offering the greatest flexibility in terms of offering 3D optical trapping and manoeuvrability. However, the single FOTs approach requires sufficient focusing of the beam to enable 3D optical trapping. Therefore such an approach would also require a suitable technique for shaping optical fibre in order to focus the beam.

Looking at the decision to opt for a single beam optical fibre trap, the author first considered various alternatives, such as multiple optical fibre traps, for example the counter-propagating fibre traps ([Constable et al., 1993](#), [S.D Collins et al., 1997](#), [Guck et al., 2001](#)). The problem with the counter-propagating fibre configurations is that the dual fibres have to be exactly aligned, require two, or more, fibres and are usually of a rigid design fixed to the bed of the sample chamber.

To add dynamism to the trap, that is being able to freely move the trapping zone about the sample chamber, both of the counter-propagating optical fibres would have to be manoeuvred

simultaneously, whilst maintaining exact alignment for stable trapping ([Constable et al., 1993](#)). For this reason the counter-propagating optical trap is generally a static trap and therefore does not have the capability to target specific objects within the sample chamber. Instead, with this technique samples that are to be trapped tend to drift into the trapping area, or are coerced using a micro-fluidic device ([Jess et al., 2006](#)) and thus lack the flexibility of movement and control required for this project.

An alternative type of dual beam trap ([Liu and Yu, 2009](#), [Taguchi et al., 2000](#)) for example, consists of two opposing lensed fibres inserted at steep angles of about  $45^\circ$  -  $55^\circ$  to the sample chamber floor. When the two fibres are employed together they are capable of elevating a trapped particle ([Taguchi et al., 2001](#), [Taguchi and Watanabe, 2007](#)). Nevertheless, when operating alone, each trapping fibre is only capable of 2D trapping ([Taguchi and Watanabe, 2007](#)). However, as previously discussed, the employment of two fibres for a single optical trapping site adds to both system complexity and cost. Furthermore, the steep insertion angles required (the previous authors used insertion angles of between  $45^\circ$ - $55^\circ$ ) mean that integration with external systems such as the AFM is impossible. This is due to the reasons stated previously that insertion angles greater than  $10^\circ$  would not allow the fibre to pass under the AFM head.

Single beam optical fibre traps consist of both 2D and 3D traps, with the 3D traps providing varying levels of trapping efficiency. The 2D traps can be discounted for use in this research programme, as system requirements are not met, in that a full range of particle manoeuvrability is not possible as Z displacement of a particle cannot be achieved with single fibre 2D systems.

Moreover, at lower insertion angles, for example  $\leq 10^\circ$ , which is the required angle for AFM integration the beam of a 2D trap, is now at an almost horizontal plane with respect to the sample chamber floor. This near horizontal insertion angle acts only to cause the particle to accelerate in the direction of the beam's propagation, rather than confine it within an optical trap. The reason for this can be explained by using the two images which are shown in Figure 4-3 and Figure 4-4.

Figure 4-3 shows that at higher optical fibre insertion angles, for example  $45^\circ$  as shown here, the tapered optical fibre is almost vertical with respect to the horizontal sample chamber floor. Consequently the microscope sample chamber floor acts as a barrier preventing acceleration of the particle in the direction of the beam's propagation.

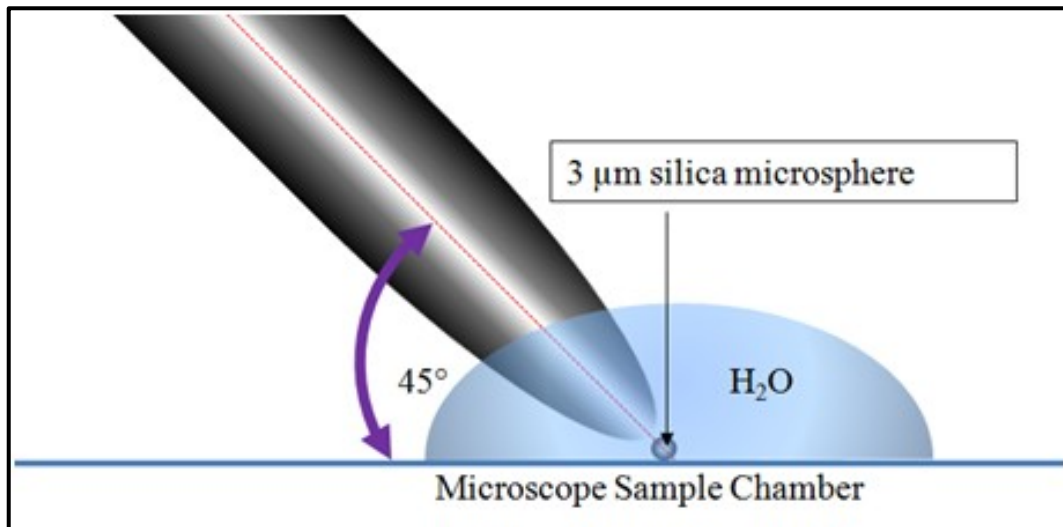


*Figure 4-3 schematic depicting 2D trapping at a  $45^\circ$  insertion angle. The particle is trapped as the microscope sample chamber slide acts to halt the particle's migration in the direction of the beam's propagation*

Such is not the case at lower optical fibre insertion angles, where the beam is almost parallel to the horizontal microscope sample chamber floor, as depicted in Figure 4-4, here the particle is subject to propulsion away from the fibre tip and in the direction of the beams

propagation. The reason for this is that there is no longer any impedance offered to the particle by the microscope sample chamber, which is now at a near parallel plane to the laser beam.

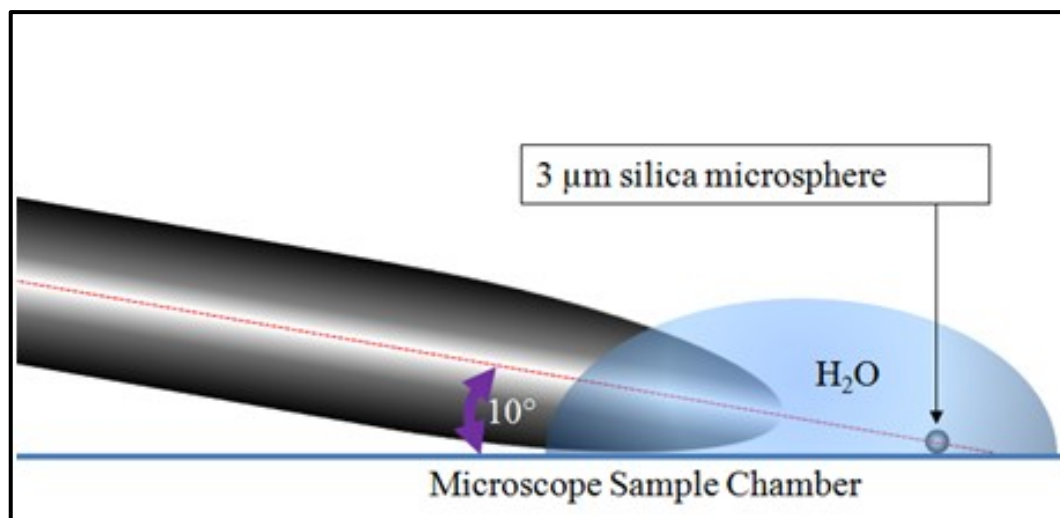


*Figure 4-4 diagram depicting 2D manipulation at a  $10^\circ$  insertion angle. At the near horizontal insertion angle there is no physical impedance provided to the particle by the microscope sample slide thus the particle is accelerated away from the fibre tip by the laser beam*

The 3D trapping single fibre configurations, such as those discussed in Chapter 3, fall into two main categories, namely those with a  $Q$  value that is equal to that of COT systems ([F. Bragheri et al., 2008](#), [F Bragheri et al., 2008a](#)) and those with a  $Q$  value that is an order of magnitude less than that of COT systems ([Liu et al., 2006](#)).

Firstly looking at the category of high  $Q$  value FOT based systems; these consist of speciality fibres, with either an annular core, or an optical fibre bundle consisting of multiple fibres. Both types of configuration require custom machining processes, such as focused ion beam milling (FIB), to shape the optical fibre's distal end, allowing the exiting beam to be focused ([F. Bragheri et al., 2008](#)). However, as FIB milling machines cost about eight times

the budget available to this research project, somewhere in the region of about £400,000, then this method for shaping the optical fibre end is precluded.

Alternatively optical traps with  $Q$  values that are equal to that of COT systems have been developed by tapering speciality fibres that include multi-core fibres, or those with an annular core. Nonetheless such speciality fibres are not available “off the shelf” and therefore have to be developed in-house ([Liberale et al., 2007](#), [Minzioni et al., 2008](#)), or alternatively purchased to order through speciality optical fibre manufacturers, usually at considerably increased cost.

3D optical trapping via a single tapered optical fibre has also been achieved by ([Liu et al., 2006](#)) with the taper being created using the heating and drawing method. This method is said to have a  $Q$  value of an order of magnitude less than that of COT systems (as calculated from the relevant data from ([Liu et al., 2006](#))). As far as the author of this thesis is aware, no previous research has been conducted to explore the possibility of improving the optical trapping efficiency of such tapered optical fibre tips. It is believed that this could be achieved through the optimisation of the tapered optical fibre’s geometric profile for a single core optical fibre. Furthermore, critical analysis of the tapered fibre employed by Liu et al reveals that the fibre  $V$  number, a normalized frequency parameter, which determines the number of modes of a step-index optical fibre, is such that single mode operation is deemed to be improbable ([Liu et al., 2006](#)), with the  $V$  number given by the following formula ([Gambling et al., 1976](#));

$$V = \frac{2\pi}{\lambda} a \text{NA} \quad (4-2)$$

where  $V$  is the normalised frequency parameter, which determines the number of modes of a step index fibre,  $\lambda$  is the wavelength of light in a vacuum,  $a$  is the radius of the fibre core and  $NA$  is the numerical aperture, which is given as;

$$NA = \sqrt{n_{core}^2 - n_{cladding}^2} \quad (4-3)$$

where  $n_{core}$  is the refractive index of the optical fibre's core and  $n_{cladding}$  is the refractive index of the fibre's cladding.

The V-number must be  $< 2.405$  for optical fibre that supports only a single mode ([Agrawal, 1989](#)). In the case of ([Liu et al., 2006](#)), this is not the case. The V number could be in the region of about 3.462. This is larger than the 2.405 limit for single mode operation and is dependent upon the NA of the fibre employed. [of the parameters required to calculate the V number, only the fibre core diameter of 9  $\mu\text{m}$  and laser wavelength  $\lambda=980$  nm were explicitly stated by Liu et al in their paper; they neglected to offer a value for the optical fibre NA. Therefore, for the purpose of this thesis an optical fibre with an NA value of 0.120 has been assumed to be representative of a typical value for 'SM-9/105/125-20A a NuPower single mode optical fibre, (Nufern, UK). This optical fibre was chosen as an example for its core diameter of 9  $\mu\text{m}$  and for its cut-off wavelength that is closest to the required 980 nm wavelength, although not ideal at 1250-1600 nm].

The resultant high V number implies that it is possible that more than a single mode would be supported using their configuration and suggests that a Gaussian  $TEM_{00}$  laser beam is not evident. If this is the case, then there may be scope to add improvements to the trapping efficiency of the system. This could be achieved by employing a SMF with a suitable core diameter to allow single mode propagation of the laser beam. However, since it is well known

that lasers with poor pointing stability and beam shape can be spatially filtered to give Gaussian outputs after coupling into single mode fibre ([Constable et al., 1993](#)), then it might be the case that tapering the optical fibre creates a spatial filter for the higher order modes. If this is the case, then the incident beam could be a fundamental TEM<sub>00</sub> mode Gaussian laser beam after all, although Liu *et al* do not explicitly discuss this issue.

Taguchi et al ([2012](#)) developed a single fibre optical trap capable of 3D optical trapping by shaping the fibre using a dynamic chemical etching method. Many tapered tips were produced in this way, with taper angles between 7° and 37° being formed. However it was found that a tip with a 17° taper angle was the best suited for 3D trapping and was capable of trapping a yeast cell. The cell size was not provided in the literature; however yeast cells can typically vary in size between 2µm -10µm in diameter.

The insertion angle of the tapered optical fibre adopted during these investigations is given as 50°. It is assumed here by the author that ([Taguchi et al., 2012](#)) neglected to attempt trapping at low insertion angles, instead opting for the tried and tested insertion angle of 50°. This strategy may have been the result of previous investigations by Taguchi et al ([Taguchi et al., 1997](#), [Taguchi and Watanabe, 2007](#)), in which only 2D optical trapping, using a single lensed optical fibre, was demonstrated. During these investigations it was also established that optical trapping below an insertion angle of 20° could not be achieved and that the most efficient optical trapping occurred at an insertion angle of 50°.

However from the author's own experiences detailed in this thesis and after considering the profile of the tip produced by Taguchi, a tapered fibre with a profile and size, which has not been explicitly presented by Taguchi et al., but garnered by the author using the assumption

that the optical fibre employed was a SMF with a 125  $\mu\text{m}$  diameter, the taper would have had a maximum taper length of  $\sim 418 \mu\text{m}$ . Such a profile suggests that it may be capable of optical trapping at insertion angles lower than the tested  $50^\circ$  insertion angle.

It is believed that 3D optical trapping at extremely low insertion angles can be possible via a tapered single mode fibre (SMF), with a single core of suitable diameter and capable of single mode propagation. Furthermore, it may be possible to improve the optical trapping efficiency through the optimisation of the geometric profile of the optical fibre taper. This would improve the trapping performance of this most simple of optical designs, making it equivalent to that of the bulky, complex and expensive alternative configurations.

#### **4.7 PREFERRED BEAM FOCUSING METHOD**

Normally the light emanating from a cleaved optical fibre is divergent. However, for a single fibre optical tweezers system configuration, such as that chosen for this project, the divergent light requires altering to convergent form. To enable 3D optical trapping the gradient force must be dominant over the scattering force. To achieve this, the divergent laser beam that exits the optical fibre's distal end must be transformed into a convergent focused beam.

Focusing of the exiting beam from the optical fibre's distal end requires the optical fibre to be shaped so as to alter the course of the propagating beams or to create a lens effect, since this effectively determines whether, or not, the fibre can optically trap in 3D. Therefore, this can be considered to be the most important part of a single beam 3D FOT based system. In order to make an informed choice concerning the best method to shape the optical fibre and hence focus the exiting light beam, an appreciation of currently available methods for shaping the fibre ends is required. After due consideration of all such methods for shaping the beam

exiting an optical fibre, reviewed in Chapter 3, it was decided that the heating and drawing method would be employed during this project.

The logic behind this decision was the result of a number of factors; first and foremost it has already been proven to be a successful method, allowing 3D trapping ([Liu et al., 2006](#)). Secondly the heating and drawing method does not entail erosion, etching, or ablation of the optical fibre material to achieve a tapered profile, which in turn maintains the optical fibre's integrity, as the core/cladding ratio is not altered ([Zhang et al., 2000](#)). Being able to preserve the core/cladding ratio of the optical fibre is an important characteristic, considering lights mode of propagation within it.

Additionally the heating and drawing method can be performed quickly, for example using a device such as the Sutter P2000/F micropipette puller (Intracel, UK). The bulk of the time required to taper an optical fibre is due to the initial preparation and mounting of the optical fibre within the device. The preparation involved includes removal of the outer acrylate buffer, followed by cleaning of the exposed cladding layer. Once correctly prepared, the optical fibre is then mounted into position within the device. The preparation of the fibre usually takes about 5 minutes to complete, with the actual time required to taper an optical fibre, once it is appropriately mounted within the device, taking only a matter of seconds.

The heating and drawing process is said to also offer a reasonable degree of repeatability. This is a desirable characteristic when one considers the difficulties that are associated with employing optical fibre, as damage may be caused to the fragile tapered optical fibre tips, particularly in biological applications, often resulting in the requirement to produce replacement optical fibre tips with nominally 'identical' tapers. However, in practice the

degree of repeatability was found to be somewhat ambiguous, as exact environmental conditions for the puller device must be maintained. Any deviation in such conditions, for instance the ambient room temperature, results in unwanted variations in taper profiles. A comparative study of two original tapered fibres and their replica counterparts has been conducted and is presented in Chapter 7.

Optical fibre tapering by the heating and drawing method can also be achieved at a relatively low capital expenditure when compared to that of alternative methods, such as focused ion beam (FIB) milling for example. In fact with FIB milling machines costing in the region of £400,000 and the P2000/F micropipette puller (Intracell Ltd, UK) having been obtained for only £8,000, this equated to just 1/50<sup>th</sup> of the cost of the FIB milling machine.

The heating and drawing method possesses an additional advantage in that the process is relatively safe and toxin free, unlike that of chemical etching for example, where harmful chemicals such as hydrofluoric acid are routinely employed ([Hoffmann et al., 1995](#), [Xin et al., 2006](#), [Chaigneau et al., 2007](#)).

**CHAPTER FIVE TAPERED FIBRE  
OPTIC TWEEZERS (T-FOTs)  
SYSTEM COMPONENTS**

## **TAPERED FIBRE OPTIC TWEEZERS (T-FOTs) SYSTEM COMPONENTS**

This chapter provides an overview of the individual components that, when assembled collectively, compose the tapered fibre optic tweezers (T-FOTs) system that has been designed and developed as part of this research programme. The specifications of the constituent parts are detailed and discussed with regard to their suitability for use within the system. The major system components are the items that collectively form the T-FOTs system and include such items as the microscope, laser, laser to fibre coupler, optical fibre, optical power output monitoring equipment, optical fibre translation equipment and video and data acquisition equipment. In addition to the major system components, there are many other miscellaneous components and devices that are required and the most significant of these are also discussed here.

### **5.1 MICROSCOPE**

The reader will recall that the reason for developing an optical trapping system, during this project, is for its integration with other microscopy applications. Hence the system should be portable and therefore decoupled from a microscope. However for the design, setup, calibration and characterisation of the system and its corresponding tapered optical fibres, a simple optical microscope was required. This inverted light microscope forms the foundation of the overall optical trapping system and it is around this generic microscope platform that the fibre-trapping system is built.

The microscope that was chosen for this purpose was the GDX-30 trinocular inverted biological microscope (Mazurek Optical Services, UK). The GDX-30 is a relatively low cost microscope, acquired for a cost of £2,443. It is equipped with a camera port with a C-mount

adapter of x0.5 magnification and a range of microscope objective lenses, including x4, x10, x20, x40 and x60 magnifications, which are mounted onto a rotating five position objective nosepiece turret. The microscope also has a sample chamber translation stage, which has a large 160mm x 250mm working area with coaxial X and Y direction manual control.

The inverted optical microscope format was selected over its upright design counterpart for a number of reasons. First and foremost COT systems are designed around an inverted microscope, as this allows the laser to be introduced into the optical path before the microscope objective ([Neuman and Block, 2004](#)). Although in this system the laser beam is to be delivered directly into the sample chamber, effectively removing the requirement to direct the laser via the optical path of the microscope. There are additional advantages, inherent in using an inverted format instrument that also influenced the design choice. For instance an inverted optical design offers better access to the sample stage, which can also be used as a platform for additional micro-manipulation devices. This is a desirable property, as unlike the case with COT systems, the laser beam will be delivered directly into the sample chamber via the optical fibre. Hence there is ample space above the sample chamber of the microscope, which is suitable for the positioning of the tapered optical fibre so that it is free from interference from, or to, the microscope optics.

The inverted microscope design is also better suited for investigations concerning live biological samples such as cells. The reason for this is that there is sufficient space for samples to sit in larger containers such as culture dishes. This is not true for conventional format microscopes where space is typically much more restricted on the specimen stage due to the 'overhead' microscope optics. The use of larger volume culture dishes removes the requirement to transfer cells to smaller glass microscope slides. A problem associated with

the use of smaller vessels, such as microscope slides, is caused by medium evaporation over time, which requires continual medium replenishment during experimentation. Alternatively experimentation can be performed in a fully saturated atmosphere – which is not good for the instrument. Therefore the use of larger volume containers mean that live cells can be monitored over larger durations of time. This is because an environment can be created that is closer to their physiological conditions and hence reduces the possibility of compromising the cell's viability.

Finally the design of the inverted microscope is such that its centre of mass is closer to the lab bench. This low centre of mass design lends itself to a reduction in sensitivity to any vibrations from outside influences and is therefore ideal for a vibration sensitive application such as OT ([Murphy and Davidson, 2012](#)).

## **5.2 LASER**

The laser is at the crux of an optical trapping system, hence careful consideration must be observed when selecting the appropriate type of laser for OT. There are several laser characteristics that determine the suitability of a laser for OT and these are discussed throughout this section.

### **5.2.1 BEAM QUALITY**

Beam quality is one of the basic requirements of a laser for optical trapping, in that it should deliver a single mode output. Normally, COT systems require a Gaussian beam profile transverse electromagnetic mode (TEM<sub>00</sub>) output, as this facilitates focusing to the smallest diameter beam waist, the result of which is the steep intensity gradient that is required for producing an efficient 3D optical trap. However optical trapping is not limited to this mode of

beam, as other beam modes have been successful in alternative trapping arrangements, as discussed previously in Chapter 2.

The laser must possess good pointing stability, without which the optical trap will be prone to unwanted optical trap position displacements within the specimen plane. The laser must also be stable in terms of power fluctuations, as changes of laser power can lead to changes of the trap's stiffness. An advantage of employing optical fibre as a delivery mechanism is the fact that lasers with poor pointing stability can still be used in the system, as the fibre spatially filters the beam to produce a well shaped Gaussian output beam ([Constable et al., 1993](#)), and therefore improves the pointing stability in the process. However, there is a downside to this behaviour, in that the coupling of the laser to the fibre will also inherently introduce unwanted fluctuations to the output power ([Neuman and Block, 2004](#)).

### **5.2.2      *WAVELENGTH***

Choice of laser wavelength must also be considered and this is a very important factor when one considers the application in which it is to be employed. Take the trapping of inanimate dielectric material for instance. Here, the suitability of lasers in the visible region of the electromagnetic spectrum would not be called into question. In fact the use of shorter wavelength light for optical tweezers can be advantageous, due to the fact that higher gradients and better trapping efficiencies can be achieved as the focused spot size of a focused beam is about half the wavelength of the light used ([Guck et al., 2001](#)).

However, for trapping specimens of a biological nature, such as live cells for example, trapping at wavelengths within the visible range can be detrimental to their survival. For improved cell viability, the use of laser wavelengths in the near infrared (NIR) region of the

electromagnetic spectrum are typically preferred, specifically within the 700 nm - 1200 nm region. The reason for such a preference is that at other wavelengths, particularly in the visible and ultraviolet (UV) range of the electromagnetic spectrum, there is an increase in the transmittance of energy from the laser light through to the target biological specimen. Ashkin and Dziedzic ([1987](#)) describe how for viruses, such as the Tobacco Mosaic Virus (TMV), optical absorption is most prevalent within the ultraviolet range of the electromagnetic spectrum (10 nm - 400 nm). Whereas in the case of bacteria, such as the microorganism *Escherichia coli*, for example, absorption of non-ionising radiation most readily occurs in the visible region of the electromagnetic spectrum (400 nm - 800 nm).

This led to Ashkin & Dziedzic postulating that, since different biological materials absorb at different wavelengths, selection of a suitable wavelength would reduce the danger of damage occurring. As a result ([Ashkin et al., 1987](#)) employed the use of a 1064 nm Nd:YAG laser, conducting various experiments on a number of different biological specimens. During the investigations, Ashkin et al. witnessed the reproduction of *Escherichia coli* whilst it was being optically trapped over a 5 hour period. No observable damage was recorded to the *Escherichia coli* whilst being optically trapped, right up to the maximum output power of the laser of 80 mW. Optical trapping of yeast cells was demonstrated over a range of optical powers of between 5-80 mW. Here the yeast cells, confined in the optical trap, were observed to bud into clumps of up to 8 cells, with diameters between 5  $\mu\text{m}$  and 10  $\mu\text{m}$ , over a time span of 5 hours. Human red blood cells were trapped using 40 mW at 1064 nm without any damage being reported. However, at 80 mW some loss of the cell's flexibility was witnessed after being optically trapped for a period of about 10 minutes.

In contrast, it was reported by Ashkin that optical damage occurred to both the *Escherichia coli* and the yeast cells after switching to a visible Argon laser-light trap at 514.5 nm during the same investigation. Furthermore the damage was seen to occur during the application of lower manipulation forces than were applied when using the Nd: YAG laser. The red blood cells were subject to catastrophic damage under illumination by the Argon laser, at low force levels, using just a few mW of power. Ashkin et al irradiated and trapped other species using both the Nd: YAG and Argon lasers during this investigation, which resulted in results comparable to those discussed above, where the Nd: YAG proved to be the less harmful of the two lasers.

The IR region offers a reduction in the absorption of energy from the incident laser light by the biological specimen. This factor is an important issue for this application, as larger levels of energy absorption lead to increased localised heating effects within the cells. It is such excessive heating of proteins and water within the cell which can ultimately lead to cell damage and even “optocution” a term that was first used by Ashkin to describe the irreversible damage caused to biological specimens by laser irradiation ([Ashkin, 1997](#)). Apart from the reduction in absorption by the particles, NIR laser traps possess a further advantage over the visible laser types in that they possess a four-fold reduction in intensity, due to the larger spot size, without a reduction in force. Furthermore, Neuman et al. ([1999](#)) found that the introduction of oxygen scavenging systems can further reduce damage and increase the cell’s viable lifetime by reducing oxygen tension, since the damage is also related to the presence of oxygen.

Since these early discoveries by Ashkin et al., there have been a number of studies conducted to determine the best IR wavelength for biological applications. Liu et al., ([1995](#))

investigated the effects of cell heating induced by IR optical tweezers at a wavelength of 1064nm. The assay consisted of optically trapping liposomes and Chinese hamster ovary (CHO) cells, whilst collecting temperature-dependent Stokes-shifted fluorescence spectra from dye-labelled membranes. The membranes had been labelled with environmentally and temperature sensitive Laurdan (6-dodecanoyl-2-dimethyl amino naphthalene) molecules. An ultraviolet (UV) beam (365 nm wavelength) is employed collinearly with the IR trapping laser to excite the fluorescence from the liposomes, or the CHO cell membrane region. The results show temperature rises of  $1.45 \pm 0.15^\circ\text{C}/100 \text{ mW}$  and  $1.15 \pm 0.25^\circ\text{C}/100 \text{ mW}$  for the liposomes and CHO cells respectively.

It was already demonstrated by Ashkin that UV exposure was damaging to viruses such as the TMV. Therefore, is it possible that the use of UV light, as in the previous study, could also have been having an effect on the liposomes and CHO cells? König et al., (1996) conducted single cell photo-stress experiments on sperm cells exposed to low-power ( 1.5 mW, 5.3 W/cm<sup>2</sup>) UVA radiation at a 365 nm wavelength. From the 580 samples observed  $109 \pm 30$  samples resulted in paralysis and  $310 \pm 110$  samples succumbed to cell death. This shows that it is not only viruses, such as the TMV, that are susceptible to damage due to UV irradiation.

### **5.2.3 OPTICAL OUTPUT POWER**

Optical power considerations must also be assessed before choosing a suitable optical trapping laser source. For example subjecting organic material, such as living human cells and organelles, to relatively high optical intensities of focussed, non-ionising irradiation during optical trapping will typically result in cell damage or cell death, as discussed earlier Ashkin observed damage to red blood cells after 10 minutes of irradiation at 80 mW. This example

and the others given, serve to illustrate that the optical damage is not only a consequence of high irradiating powers, but is also contributed to by the duration of such incidence, the type of biological specimen, and as previously discussed, the wavelength of the laser.

In contrast when relatively low output optical powers are employed, i.e. sub-mW, this may result in a situation where optical trapping is not possible, since the optical forces are insufficient to perform the basic optical trapping tasks. For example during the author's own experience a 3 $\mu$ m silica microsphere could easily be trapped and manipulated. Using as little as 10's of mW's of optical power at the sample, the silica microsphere could be easily elevated in the +z plane. Once in position the optical output power could be reduced to 1 mW. At this point some Brownian motion of the particle could be observed, whilst the particle was still maintained within the optical fibre trap. However further reduction of the optical output power, to about 600 $\mu$ W, proved insufficient for the generation of the required forces to be capable of maintaining the silica microsphere within the optical trap. Hence, the silica microsphere was able to escape the hold of the optical trap and drift back down to the microscope's sample chamber floor.

Additionally a further example taken from literature explains that motor proteins are responsible for the transportation of intracellular components, including vesicles and organelles such as mitochondria. The optical forces required to halt a single molecular motor range between 1 pN required to halt the movement of lipid droplets, and 6 pN required to halt the Kinesin motor proteins ([Jäckle and Jahn, 1998](#), [Welte et al., 1998](#)). Since it usually takes in the region of about 5 Kinesin motor proteins to move a vesicle's cargo, the resultant maximum optical force required to halt this cargo transportation is about 30 pN, a force that was generated using 300 mW of optical power at the sample in a COT setup ([Gross, 2003](#)).

Ashkin et al. demonstrated that it takes between 1 and 4 motors to transport mitochondria along a microtubule<sup>7</sup>. To stop a moving mitochondria being carried by 4 molecular motors required 220 mW at the sample, equating to an in vivo force of about  $2.6 \times 10^{-7}$  Dynes, or  $2.6 \times 10^{-12}$  N per (Dynein like) molecular motor, or  $10.4 \times 10^{-12}$  N to halt four motors ([Ashkin et al., 1990](#)).

The specific application for which the intended OT's system is designed will dictate the optical power requirement of any given system. Recalling the previous example that was discussed in Chapter 4 concerning the counter propagating optical trap ([Guck et al., 2000](#)). This system required optical output powers of about 700 mW per beam to achieve the goal of stretching red blood cells. That is five times the optical power that is required to halt the transportation of a vesicle's cargo, as detailed above.

#### **5.2.4 VENTUS IR LASER**

The laser that was selected for this project was the Ventus IR (Laser Quantum, UK). The device is a Diode Pumped Solid State (DPSS) Neodymium doped Yttrium Aluminium Garnet (Nd: YAG) laser. The Ventus IR is a continuous wave (CW), class IV laser providing a single mode TEM<sub>00</sub> infrared beam. It is capable of delivering up to 3 W at a wavelength of 1064 nm.

It must be noted that 3 W is excessive and far more power than is required for a single trapping site. However, such excess offers sufficient power to facilitate future expansion through the realisation of additional optical trapping locations, made possible by splitting the beam between additional optical fibre tapers. Furthermore there will be inevitable optical

---

<sup>7</sup> To aid in visualising how such molecular motors transport cargo and organelles along the microtubules the reader is guided to watch from 3.38 minutes of the video that is accessible from <http://www.youtube.com/watch?v=FzcTgrxMzZk>.

losses incurred across the various optical interfaces within the trapping system. For example in the original design the beam was split using a 50/50 beam splitter, prior to being coupled into two different optical fibres via two separate optical fibre couplers. This laser to fibre coupling system has an optical efficiency of 50% resulting in an immediate loss of at least half of any optical power being throughput, equating to 1500 mw at the laser's full operational power. Further optical losses will also be accumulated at any additional optical interfaces throughout the system, such as optical connectors, or fusion splices, which are discussed further in Chapter 6. Therefore the relatively high maximum laser power output of 3W that is provided by the Ventus IR laser, provides sufficient compensation for such system losses and for future facilitation of dual optical tweezers capability.

The Ventus IR's NIR wavelength of 1064 nm is ideal for optical trapping of biological material, as previously discussed. Additionally the relatively low cost and exceptional beam quality of the Nd: YAG laser make it one of the most popular choices for optical trapping systems. For comparison, the Titanium Sapphire laser (Ti:Al<sub>2</sub>O<sub>3</sub>) is a tuneable laser operating within the 650-1100 nm wavelength range, a band that covers a small portion of the visible red region and the NIR region of the electromagnetic spectrum. However, the Ti Sapphire laser is prone to amplitude instability ([Neuman et al., 1999](#)) and its cost compared to the Nd: YAG is far greater, as it requires the use of an additional laser as its pump source, such as a frequency doubled Nd:YAG laser.

The Ventus IR laser has a compact design that is ideal for portability, and has an excellent beam quality with an M<sup>2</sup> factor of 1.5. The M<sup>2</sup> parameter is defined as the divergence ratio between the laser beam of interest, in this case the Ventus IR, and an ideal Gaussian beam, with the ratio determining how tightly the beam can be focused ([Liao et al., 2009](#)). For an

ideal Gaussian beam the  $M^2$  value = 1 ([Siegman, 1993](#), [Siegman, 1998](#), [Roundy, 1999](#)). The  $M^2$  value given for diode pumped solid state (DPSS) lasers can be as low as 1.1. At the other extreme the  $M^2$  value for Nd:YAG lasers that use a flash lamp as their pump source, and suffer from poor beam quality, can have  $M^2$  values in the region between 15-100 ([Steen and Mazumder, 2010](#)). This latter statistic only serves to highlight the excellent beam quality provided by the Ventus IR device.

The Ventus laser offers excellent pointing stability, with a beam divergence of 0.6 mrad and a pointing stability value that is a fraction of the beam divergence angle, at 5  $\mu$ rad. It provides a highly stable power output, with a power stability of 0.2 % rms and low noise of 0.2 % rms. The stability is further enhanced as the laser is controlled via an external power supply, a design feature which supports the elimination of any adverse thermal effects within the laser cavity, caused by the external electronic components. Without such steps being taken this could lead to heating of the lasing medium and thus cause fluctuations in the output wavelength. In addition, excessive heating may cause thermal expansion resulting in misalignment of the cavity mirrors, leading to power fluctuations, or even cessation of lasing action altogether, depending upon the severity of any misalignment.

### **5.3 LASER TO FIBRE COUPLING**

The laser to fibre coupler was chosen because of its small package size and its ability to provide high performance at a fraction of the cost of bench top micro-positioning stage alignment systems. These are ideal qualities when one is concerned with the development of an optical tweezers system, incorporating both reduced size and build costs.

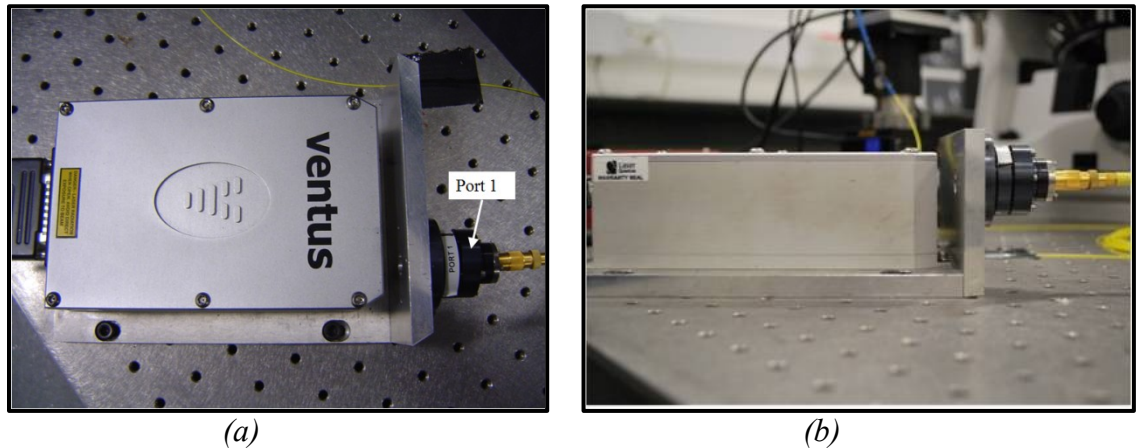
The coupling system comprises a lens to focus the laser beam to a spot that matches the size of the fibre core. The coupling optics are precisely aligned with respect to the laser beam, through the use of three fine tilt adjustment screws, together with an O-ring that is used as a pivot. Once the coupler is aligned for maximum efficiency, it is locked in position using three locking screws (OZ Optics, Canada). The coupler can be attached directly to the laser head, however to avoid any re-engineering of the laser head itself, the laser and the coupling device are mounted onto a custom made aluminium bracket, which also serves as a heat sink to the laser.

Figure 5-1 (a) shows a plan view of the Ventus IR laser mounted on the bespoke aluminium bracket. The laser to fibre coupler, labelled port 1, is mounted on the right hand side of the 90° angle bracket. Figure 5-1 (b) shows the side elevation view of the Ventus IR laser and the laser to fibre coupler mounted upon the bespoke aluminium 90° angle bracket. The laser to fibre coupler is mounted onto the vertical front plate of the 90° angle bracket, shown to the right of the laser head.

The flexible design of the laser to fibre coupler offers four alternative basic configurations.

- Physical contact style receptacle source couplers, which are designed for lasers with a CW output power that is less than 400 mW
- Non-contact style receptacle source couplers, which are most suitable for applications where the input powers are greater than 400mW, as they can handle up to 100 W of CW laser power

- Pigtail style couplers, which are recommended for permanent or semi-permanent situations, where optimum coupling efficiency, output stability, and minimum back reflection are desired. In these couplers the fibres are permanently glued to the focusing lens
- Adjustable focus source couplers, which are ideal for situations where optimum coupling efficiency is critical. Here a special connector allows the spacing between the fibre and the lens to be precisely controlled without rotating the fibre. This allows the user to compensate for any changes in the wavelength, or the beam waist location, thus further optimizing the coupling efficiency.



*Figure 5-1 (a) plan view of the Ventus IR laser mounted on the bespoke aluminium bracket. The laser to fibre coupler, labelled port 1, is mounted on the right hand side of the 90° angle bracket (b) side elevation of the laser and the bespoke bracket-coupler assembly*

The second option, the non-contact style receptacle source coupler was selected for use within the T-FOTs system for its power handling capability in addition to non-permanent fixing of the fibre to the focusing lens, which is inherent with the pigtail style. This is a flexibility that was necessarily required during the research and design stages that formed part of this research programme. However, the maximum coupling efficiency, output stability, and

reduced back reflection of the pig tail style coupler would provide an improvement to the system once all design issues have been fully settled and a permanent solution can be applied.

The overriding problem that would be present with a pigtail style coupling during the design stages is that if the fibre were to be damaged in any way, since it is attached to the lens, it cannot be easily replaced. Replacing a damaged fibre would require a return to the manufacturer, since a replacement lens would also probably be required. Contrast this with the non-contact style coupler that has been used here, where any damaged fibre can be replaced in-house, hence reducing both time-frames and cost.

Figure 5-2 shows the initial T-FOTs system that was originally designed with the scope to deliver two individual optical trapping fibre tips. To facilitate this design feature the laser to fibre coupler incorporated a 50/50 non-polarising beam splitter to divide the beam prior to coupling into two individual optical fibres via receptacle style non-contact source couplers. However due to technical problems associated with back reflection, which are discussed further in Chapter 5.4, this initial design was revised to incorporate only a single fibre coupling system.

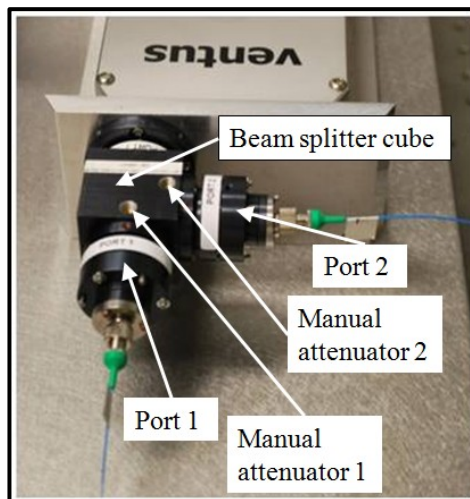


*Figure 5-2 initial dual port laser to fibre coupling device*

To enable good coupling efficiency, the light from the source must be focused precisely onto the core of the optical fibre. The focused laser beam must match the parameters of the fibre for optimum coupling efficiency. In particular two conditions should be met for maximising coupling efficiency; firstly the focused spot diameter of the laser beam should be  $\leq$  the mode field diameter (MFD) of the fibre being used, as given by.

$$SD = f \times DA \leq \text{MFD} \quad (5-1)$$

where ( $SD$ ) is the focused spot size ( $\mu\text{m}$ ) of the laser beam, ( $f$ ) is the focal length (mm) of the lens, ( $DA$ ) is the laser beam full divergence angle (mrad) and ( $a$ ) is the mode field diameter of the fibre being used.

Secondly the numerical aperture of the focused laser rays should not exceed the NA of the fibre being used, as given by.

$$NA_{\text{Rays}} = BD / 2f \leq NA_{\text{Fibre}} \quad (5-2)$$

where ( $NA_{\text{Rays}}$ ) is the numerical aperture of the focused rays, ( $BD$ ) is the laser beam diameter (mm) and ( $NA_{\text{Fibre}}$ ) is the numerical aperture of the optical fibre being used. With regard to Equation (5-1), the focal length of the lens lies between 10 mm and 10.3 mm, which is the distance that allows the focused spot size to be  $\leq$  the mode field diameter of the fibre, as shown in Figure 5-3.

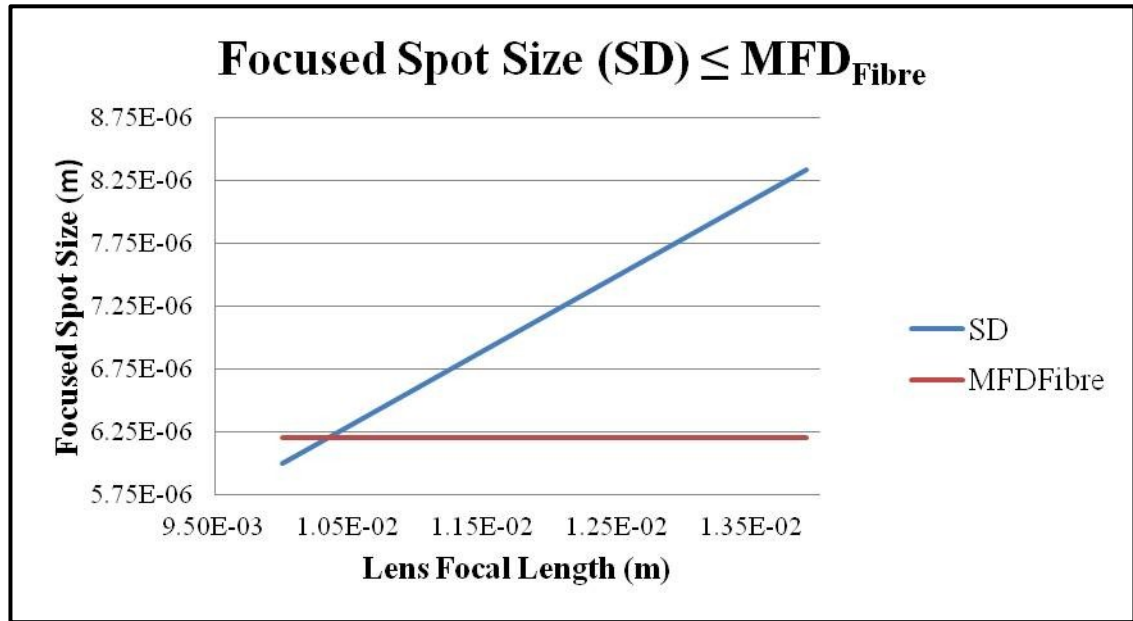


Figure 5-3 laser to fibre coupler lens graph showing the focal length of the focusing lens required to provide a focused laser beam spot size  $\leq$  the mode field diameter of the fibre

Whereas, the focal length of the lens, that allows the numerical aperture (NA) of the fibre to be  $\leq$  the NA of the rays, as given in Equation (5-2) can be between 10 mm and 11.8 mm, as shown in Figure 5-4.

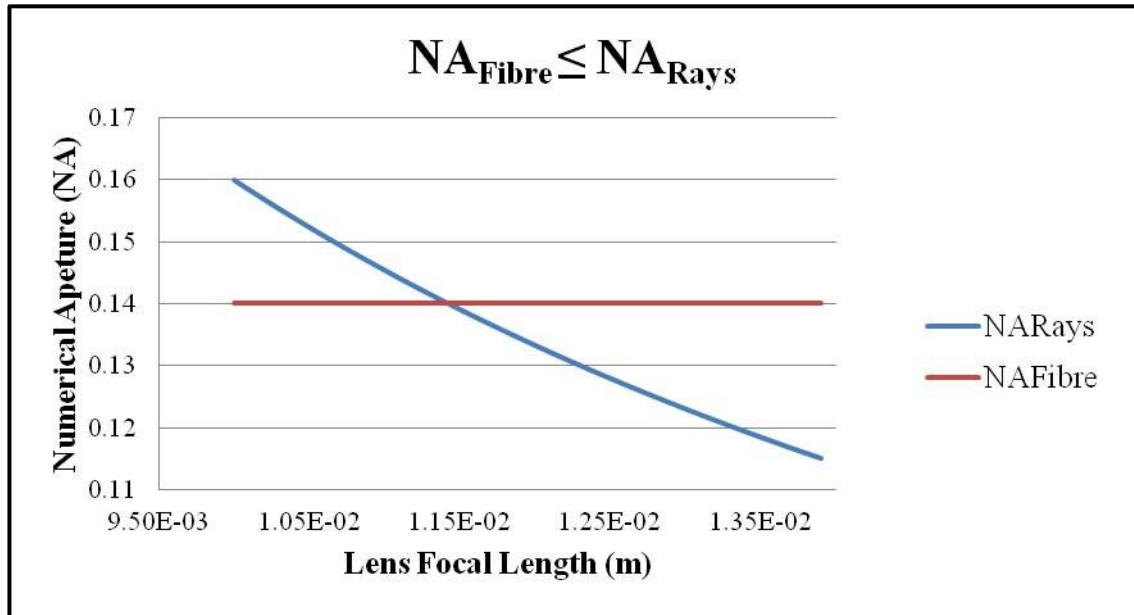


Figure 5-4 graph showing the focal length of the focusing lens required to provide a  $NA_{Fibre} \leq NA_{Rays}$

The impracticality of custom manufacturing a lens to match every laser criterion means that the manufacturer only offers a set of standard of lenses. The lens that best suited this system, from the selection list that was provided by the manufacturer, is an aspheric lens that has a 13.9 mm focal length. The decision to choose this lens configuration was taken after consultation with the manufacturer.

## 5.4 OPTICAL FIBRE CONNECTORS

Optical fibre connectors are a quick and easy method of adding optical fibre components to a system. In this system they are used to connect an optical fibre to the laser to fibre coupler. Initially all of the system fibre optic interfaces, of the various optical fibre components, were unified using mechanical optical fibre connectors. However, the final design of the optical trapping system employs mechanical fibre optic connectors only at the laser to fibre coupling interface. At all other optical fibre interfaces within the system mechanical optical connectors have been replaced by fusion splicing.

Optical connectors come in a variety of types, for example two of the three types that have been employed during this project are, ferrule connectors/angled polished connectors (FC/APC), or ferrule connectors/angled flat connectors (FC/AFC). FC/APC fibre connectors are used for patch cords that have been built in-house here at GERI and were primarily used to connect the custom tapered optical fibre tips to the T-FOTs system. FC/AFC connectors are specialty fibre connectors supplied with purchased patch cords (OZ Optics, Canada). FC/AFC connectors were initially selected for use at the laser to fibre interface. The reason for this is that there is a significant variation in the end face geometries of FC/APC polished connectors, which affects the spacing between the end face of the fibre and the lens. This variation can be minimised using FC/AFC polished connectors, as this connector type features a bevelled end face, where the fibre itself is angled, but the tip of the ferrule is flat and provides optimum repeatability between connections. The FC/APC and FC/AFC connectors both consist of a ceramic ferrule, within which the optical fibre is fixed using an epoxy resin. The fibre is then polished flush with the surface of the connector ferrule. Initially the laser source was coupled into SMF connected to the coupler using FC/AFC type optical fibre connectors.

However, the use of these connector types with high power lasers results in heat being generated at the tip of the fibre. The heat causes the surrounding epoxy resin to break down and emit gases, which proceed to burn onto the tip of the fibre, the result of which causes catastrophic damage to the fibre's end face and massively increases attenuation to the point of inhibiting laser propagation. The aforementioned problem was not only witnessed at the connector located at the laser to fibre coupling stage, but also at additional fibre interface locations where mechanical fibre connections had also been employed. One possible cause of these additional optical fibre 'burn sites' could have been as a direct result of moisture

entering the system. It is believed that condensation build up, during periods of laser inactivity, causes microscopic water droplets to develop on the fibre's end face, at the interface between two connectors, the result of which is that the water droplets cause a lens effect, redirecting the beam and causing the epoxy to heat and burn the fibre.

To overcome the burning of the fibre end faces, at the laser to fibre coupling stage, a new high power optical fibre connector was introduced. This connector type consists of a hollow metal ferrule that features an air gap design. The air gap is located between the optical fibre and the surrounding hollow metal ferrule at the connector end face. The hollow metal ferrule allows the fibre to extend into free space by about 1.1 mm to 1.5 mm, providing an epoxy free region which allows thermal energy to be safely dissipated, without burning the surrounding fibre. However, unlike the standard FC/APC connectors, which were assembled in-house, these new high powered connectors are specialty items which had to be purchased from Canada, with long lead times, and were therefore deemed unpractical for use beyond the laser to fibre coupling interface due to the associated time and cost implications.

FC/AFC connectors are designed specifically to limit back reflection within the optical system, which is the reason why they were initially commissioned for use at the laser to fibre coupler interface. However, the introduction of the high power metal ferrule connectors, led to increased and unwanted back reflections. This problem served to undermine the stability of the optical trap through the fluctuation of the output optical power. To reduce these effects, the laser to fibre coupler design required modification to facilitate improved system stability.

The initial laser to optical fibre coupler design is shown in Figure 5-2 and consists of a 50/50 beam splitter with built in manual attenuators. The beam splitter divides the beam into

two separate paths before being launched, via dual non-contact style receptacle source couplers, into independent SMF's terminated with FC/AFC connectors. The modified laser to optical fibre coupler design is shown in Figure 5-5; here the 50/50 beam splitter and one of the receptacle style non-contact couplers have been removed. The laser is coupled into a single high powered, hollow, metal ferrule optical connector via a single receptacle style non-contact source coupler.

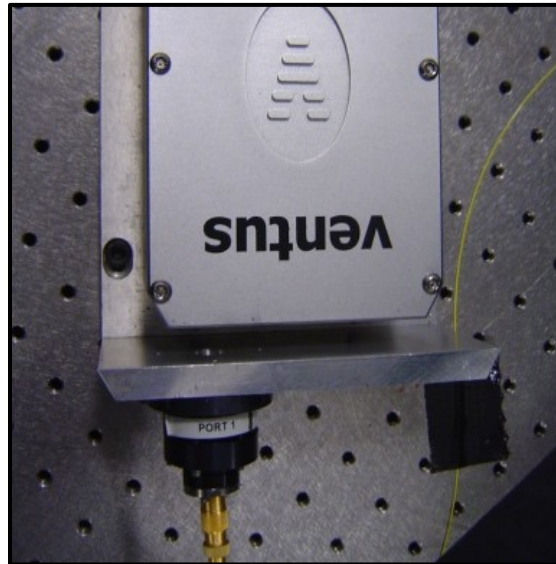


*Figure 5-5 reconfigured laser to single optical fibre coupling system*

Reconfiguration of the laser to fibre coupling system significantly reduced the degree of back reflection and therefore, reduced the associated power fluctuations to an acceptable level. The optical power outputs for both the dual fibre and single fibre coupling configurations are tabulated in Table 5-1. In each case the maximum and minimum optical power output values have been recorded to establish the different optical power oscillations that occur for each of the configurations.

*Table 5-1 comparison of optical power fluctuations in laser to dual optical fibre coupling against laser to single optical fibre coupling using high power optical fibre connectors*

Laser output %	Dual Fibre Launch				Single Fibre Launch	
	Output 1 power fluctuation (mW)		Output 2 power fluctuation (mW)		Output Power Fluctuation (mW)	
	min	max	min	max	min	max
25	14	19	8	12	39	40
30	42	48	27	32	95	99
40	95	104	68	77	220	228
50	149	170	103	125	352	362
60	169	220	135	173	464	481
70	202	267	173	216	590	623
80	254	332	207	264	678	726
90	329	415	262	328	827	873
100	369	476	343	421	-	-

The first noticeable difference between the two configurations is the overall output power. For the dual coupling configuration the maximum optical output power is given as 476mW and 421mW for fibre launches 1 and 2 respectively. This equates to a combined total output of 897 mW, achieved at 100% of the laser's output power, and which provides an average output per fibre of 448.5mW.

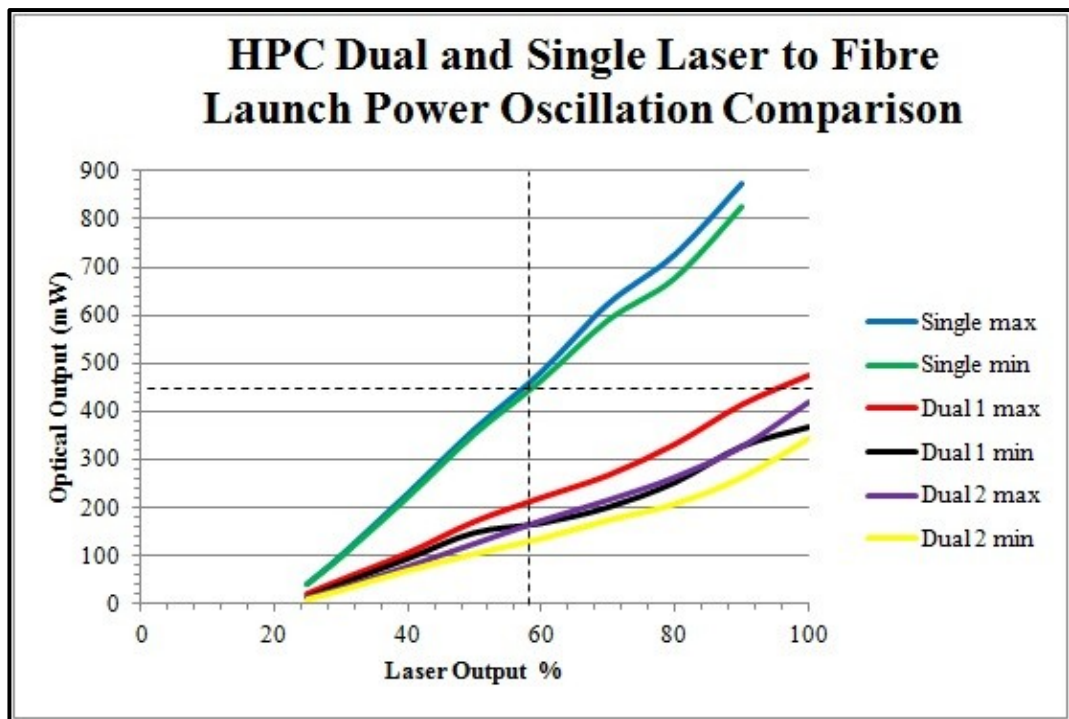
In comparison the single fibre configuration yields a maximum output of 873 mW, achieved using only 90% of the laser's total output power. In this configuration 448mW could be achieved using less than 60% of the laser output power<sup>8</sup>. Crucially however, switching from the dual laser to fibre to the single laser to fibre coupling configuration improved the optical trap stability, as the overall optical power fluctuations were significantly reduced to a difference of about 17 mW at 60% of the laser output.

Figure 5-6 shows in graphical form the differences in optical power fluctuations. At the maximum output the dual fibre configuration exhibits optical power oscillations ranging between 369 and 476mW and 343-421mW for optical fibre launches 1 and 2 respectively.

<sup>8</sup> Denoted by the crosshairs in Figure 5-6

Therefore at 100% of the laser's output power, the dual fibre setup has an average power fluctuation of about 92.5mW per fibre launch.

At 90% laser power, at which the single fibre configuration reached a maximum optical power output of 873 mW, the total power fluctuation witnessed was only 47 mW. This is considerably less than the combined 187 mW of optical power fluctuations resulting from the dual optical fibre coupling configuration. The use of an optical isolator could further reduce the optical power fluctuations, due to back-reflection, however this would undoubtedly be offset by power density losses.



*Figure 5-6 comparison of optical power oscillation, due the use of high power connectors (HPC), for laser to single fibre and laser to dual fibre coupling configurations*

## 5.5 SINGLE MODE OPTICAL FIBRE (SMF)

A comparison of the characteristics for two types of optical fibres used within the system can be seen in Table 5-2. They include a standard single mode fibre (SMF) supplied by (Oz Optics, Ottawa, Canada). This optical fibre is used for the high power connector patch cords

and the input and output fibres for the inline optical tap. The second optical fibre is Nufern's 1060-XP SMF (Thorlabs LTD, Cambridge, UK) and this is used at the distal end of the tapered optical fibre trap. The refractive indices of the 1060-XP core and cladding are 1.4631 and 1.4542 respectively. The 1060-XP SMF's core diameter is stated by the manufacturer as being 5.8  $\mu\text{m}$  therefore, providing a normalised frequency or V-number of 2.398 at 1064 nm, as given by Equation (4-2). Since this V-number is less than 2.405, then it meets the required condition for single mode operation ([Gambling et al., 1976](#)).

*Table 5-2 optical fibre comparison*

Specification	Optical Fibre	
	Oz Optics Standard SMF	Nufern 1060 XP
Wavelength ( $\lambda$ )	980-1550 nm	980-1600 nm
Cut off ( $\lambda$ )	970 nm	920 $\pm$ 30 nm
Core Diameter ( $\mu\text{m}$ )	6.0 $\mu\text{m}$	5.8 $\mu\text{m}$
Cladding Diameter ( $\mu\text{m}$ )	125 $\mu\text{m}$	125 $\mu\text{m}$
Mode field Diameter (MFD)	6.2 @ 1060 nm	6.2 @ 1060 nm
Numerical Aperture (NA)	0.14	0.14

As discussed previously, optical losses occur at all of the optical interfaces within the system, such as at the laser to fibre coupling stage, the connection between two fibres, or the insertion of an optical component, for example the optical tap. The total losses for the system are derived from the summation of the entire individual system interface losses. Other insertion losses can occur due to mismatches in optical fibre specifications, for example if the core diameter, or the NA, of the transmitting fibre is larger than the core diameter, or NA, of the receiving fibre losses will be incurred, which can be calculated using Equations (5-5) and (5-6) respectively.

$$L_{Dia} = 10 \log_{10} (dia_r / dia_t)^2 \quad (5-3)$$

where:  $L_{Dia}$  is the loss diameter,  $dia_r$  is the diameter of the receiving fibre and  $dia_t$  is the diameter of the transmitting fibre.

$$L_{NA} = 10 \log_{10} (NA_r / NA_t)^2 \quad (5-4)$$

where  $L_{NA}$  is the loss on optical fibre,  $NA_r$  is the numerical aperture of the receiving fibre and  $NA_t$  is the numerical aperture of the transmitting fibre ([Cisco, 2005](#)).

Using the information provided in Table 5-2 at the interface between the two different fibres, which have been employed within this system, there is a loss of 0.29 dB derived from Equation (5-2). The loss can be explained due to the mismatched fibre cores. No losses occur due to the NA of the fibres, as they had equal NA's, as described in Equation (5-4). Table 5-3 shows the insertion loss power budget for the T-FOT system. The given insertion losses for the system components are totalled to be 2.105 dB. This equates to a possible maximum output power at the sample of  $\approx 1376 \text{ mW}^9$ , which is an overall power loss of  $\approx 54\%$ .

*Table 5-3 T-FOTs system insertion loss power budget*

<b>Component</b>	<b>Insertion Loss (dB)</b>	<b>Quantity</b>	<b>Total Insertion Loss (dB)</b>
Laser to fibre coupler	1.25	1	1.25
HP Patch-cord	0.3	1	0.3
1060 XP single mode fibre	1.5/km	10 m	0.015
In-line optical tap	0.15	1	0.15
Fusion splice	0.05	2	0.1
Fibre to fibre interface loss	0.29	1	0.29
<b>Total System Losses</b>			<b>2.105</b>

<sup>9</sup> This Value could not be measured empirically due to the limitations imposed by the PM100 optical power monitor's detection sensor. The integrating sphere sensor is limited to a maximum power of 1000mW.

## 5.6 OPTICAL POWER MONITORING

### 5.6.1 *INLINE OPTICAL TAP*

Monitoring of the optical power at the sample is achieved using an inline optical power monitor with a 1% optical tap (OZ Optics, Ottawa, Canada). The semiconductor sensor that is employed within the optical power monitor is an Indium Gallium Arsenide (InGaAs) type. The sensor operates at a wavelength of 1064 nm and can tolerate input powers of between -25dBm and 33dBm, equating to a range of optical powers from as low as 3.16  $\mu$ W up to 1.99 W, converted from dBm to Watts using:

$$P(\text{watt}) = \frac{10^{\left(\frac{P(\text{dBm})}{10}\right)}}{1000} \quad (5-5)$$

where  $P(\text{watt})$  is the power in Watts and  $P(\text{dBm})$  is the power ratio in dBm.

Therefore, the inline optical tap sensor operates within an optical power range that encompasses the Ventus IR laser's maximum output, after taking into account the optical losses incurred at the laser to fibre coupling device.

### 5.6.2 *OPTICAL POWER METER*

A PM100 optical power meter, combined with an S144A integrating sphere sensor (Thorlabs LTD, Cambridge, UK) are used to monitor the output power of the optical fibre during calibration of the optical tap. The integrating sphere sensor enables precise measurements regardless of beam shape, or incident angle, and is therefore ideal for measuring the divergent beams emanating from the optical fibre. The sensor itself consists of an InGaAs sensor with a wavelength range of 800-1700 nm and is capable of measuring optical powers within the

range of  $1\mu\text{W}$  to  $1\text{W}$ . Hence during calibration of the in-line optical tap care was taken to never allow the optical output power of the laser to reach  $1000\text{mW}$ . This precaution was taken to ensure that the damage threshold for the integrating sphere sensor was never breached. Maintaining a safe level of optical output power required the total output power of the laser to never exceed 74% of its total output capacity, which is in the region of about  $980\text{mW}^{10}$  at the sample.

## 5.7 DATA ACQUISITION

The acquisition of data, such as the inline optical tap voltage and temperature data provided by two K-type thermocouples is achieved using the USB-2404-UI data acquisition card (MC Measurement Computing, USA). The DAQ module provides four channels of 24-bit universal analogue input with integrated signal conditioning. The device can be used to measure a variety of sensor types including Resistance Temperature Detectors (RTD's), thermocouples, load cells and other powered sensors. The four channels are individually configurable, so a different measurement type can be performed on each channel. All channels are measured simultaneously at up to 100 samples per second per channel.

The USB-2404-UI can perform the following measurements:

- Voltage
- Current
- Temperature
- Resistance Temperature Detector (RTD) (4-wire and 3-wire)
- Resistance (4-wire and 2-wire)

---

<sup>10</sup> This improved output, compared to earlier data found in Table 5-1, was attained following the removal of Polarisation maintaining fibre from the system and improved alignment after the laser to fibre coupling modification was made.

## 5.8 VIDEO ACQUISITION

A practical solution to viewing the microscope sample chamber, rather than viewing via the microscope's binocular eyepieces, is to employ a video camera and viewing monitor. This method of viewing the sample arena offers two further advantages over and above practicality; Firstly, it offers the optical trap user an added safety barrier, eliminating the possibility of injury, or loss of sight, due to accidental exposure of the eyes to invisible NIR irradiation. Secondly, it provides the means for recording a particle's position for later analysis, as the particle travels along its course during optical trapping. The camera that was initially selected for this role was a DeltaPix Infinity-X microscopy video camera. However analysis of the recorded video footage revealed that the theoretical maximum frame rate of 60 frames per second (fps) was a limiting factor for two distinct reasons.

Firstly, it was found that when the optical output power of the laser exceeded 30 mW, the velocity of the particle being drawn into the optical trap was such that the recorded images were tainted by the effects of motion blur. Motion blur renders the shape of the previously circular particle to become distorted. The problem here is that the particle tracking software is no longer able to track the particle's course. The reason for this is that the particle image no longer resembles the original particle shape, as it can become elongated. Therefore, the circular pattern that the particle tracking software endeavours to match in each video frame is no longer discernible. Secondly the time that it takes for a particle to be drawn into the optical trap can be of the order of milliseconds. This short duration lends itself to a video sequence consisting of a low frame count when standard video rates are employed. The overall frame count depends upon the optical output power of the laser that is being used, i.e. the higher the optical power being used results in fewer frames being used to record the particles trajectory.

Since each frame of video footage holds the co-ordinate data for the particle's trajectory during an optical trapping sequence, the acquisition of insufficient co-ordinate data points limits the accuracy of results, such as the velocity of the particle during its journey, and therefore ultimately the optical forces acting upon the particle.

For example, during optical trapping of a 3  $\mu\text{m}$  silica microsphere, a laser optical output power of 537 mW was applied and the trapping sequence was recorded using the Infinity-X microscopy camera, at a frame-rate of 55 frames per second. The author found that the resultant optical trapping video sequence lasted for duration of 0.11 seconds. During this time the particle was seen to travel a distance of 5.5  $\mu\text{m}$  along the x axis. This sequence resulted in a total of 6 video frames being recorded. However, by replacing the DeltaPix Infinity-X camera with the Photron MC-1 Fastcam high speed video camera, the number of recorded frames produced, at a frame-rate of 500 fps, would have been in the region of about 55 frames. This comparison shows the obvious deficiency of the Infinity-X, which would clearly be surmounted through the use of a higher speed camera.

This realisation prompted an application to the Engineering and Physical Sciences Research Council (EPSRC) Portable Engineering Instrument Loan Pool for a short term loan of a high speed video camera. A Photron Fastcam MC-1 camera was successfully obtained over a three month loan period and was acquired to increase the likelihood of accurately characterising the optical forces of the optical trapping system. Table 5-4 shows a comparison of the specifications for both the DeltaPix infinity-X and the Photron Fastcam MC-1 cameras.

The Photron Fastcam MC-1 is capable of 2000 fps at a maximum resolution of 512 x 512 pixels. This video frame-rate is more than sufficient for the experiments that are to be

conducted here since it was thought that 500 fps would be a sufficient frame-rate so in that respect the MC-1 camera was deemed suitable.

*Table 5-4 video camera specification comparison*

Specification	Camera Model	
	DeltaPix Infinity X	Photron Fastcam MC-1
Sensor Type	CMOS	CMOS
Colour/Monochrome	Monochrome	Monochrome
Maximum Resolution (pixels)	1280 x 1024 <sup>11</sup>	512 x 512
Frame Rate (Max Res) (fps)	60	2000
Max Recording Time (Seconds)	Unlimited	4
Pixel size ( $\mu\text{m}$ )	5.2 x 5.2	10 x 10
Camera Depth (mm)	98	35
Camera Width (mm)	70	35
Camera Height (mm)	54	35
Shutter Speeds (ms)	0.1 - 6000	20– 6000
Field of View (mm)	6.656 x 5.3248	5.12 x 5.12
FOV Mag X40 ( $\mu\text{m}$ )	166.4 x 133.12	128 x 128
X Mag (nm)	130	250
Y Mag (nm)	130	250

The Infinity-X is small and compact, as one would expect from a dedicated microscopy camera. However the Photron Fastcam MC-1 high speed camera is somewhat smaller in its physical dimensions, and thus its suitability for mounting onto a microscope equals, if not surpasses, that of the Infinity X.

A further advantage offered by the MC-1 camera over that of the Infinity X is the pixel size. The pixel size of the MC-1 camera,  $10\mu\text{m} \times 10\mu\text{m}$ , is almost double that of the Infinity-X at only  $5.2 \mu\text{m} \times 5.2 \mu\text{m}$ . The advantage of this is that the larger pixel can harvest more light and thus provide images with less noise, an ideal characteristic given that as the magnification of the image and the camera shutter speeds are increased the illuminating light is significantly reduced.

<sup>11</sup> In order to achieve a maximum frame rate of 55 fps, which is less than the theoretical maximum of 60 fps, the resolution for the DeltaPix Infinity X camera had to be reduced from its maximum of 1280 x 1024 pixels down to 640 x 480 pixels.

The two advantages which the Infinity-X camera holds over the high speed MC-1 camera both stem from the sheer memory requirements demanded by the MC-1 camera. However Table 5-5 shows that a single image produced by the DeltaPix is 50 times more memory intensive than a single image formed using the MC-1, when both are operating at full resolution. This is due in part to the superior pixel resolution, and also to the 24-bits of information assigned to each pixel. This is in comparison to the 8-bits that are assigned to the pixels of the MC-1 camera. However, due to its lower frame rate of 55 fps, the amount of memory required to record and store 1 second of video, is about 2.5 times less than that required for the MC-1 when it is operating at 500 fps.

*Table 5-5 comparison of camera memory requirements*

<b>Camera</b>	<b>Resolution (Pixels)</b>	<b>Frame size (Bytes)</b>	<b>Image size (MB)</b>	<b>Frame rate (fps)</b>	<b>Memory per 1 second of video (MB/s)</b>
DeltaPix <sup>12</sup>	1310720	3932160	3.75	15	56.25
DeltaPix <sup>13</sup>	307200	921600	0.88	55	48.3
Fastcam MC-1	262144	262144	0.25	500	125

It is this high computational cost afforded to the MC-1 high speed camera which leads to the second advantage offered by the DeltaPix Infinity-X camera. Here the recording time is continuous for the Infinity-X, computer memory permitting. However, in comparison, transmitting and storing the vast amounts of rapidly acquired video data from the MC-1 limits the available recording time to about 2 minutes and 43 seconds. This is because the minimum recording frame rate is 50 fps and the maximum number of frames that can be recorded, before transferral to an external memory device, is 8,184 frames. The reason for this limitation is that the images captured by the sensor are initially stored to the fast DRAM memory (2 GB memory) inside the MC-1 processor. The stored data is transferred later to the

<sup>12</sup> DeltaPix camera at full resolution of 1280 x 1024 maximum achievable frame-rate 15 fps

<sup>13</sup> DeltaPix camera at reduced resolution of 640 x 480 required to attain a frame-rate of 55 fps

control PC, over a Gigabit Ethernet interface, since the data rates from the camera are too high to allow images to be stored direct to a hard drive in real time.

Therefore, the Infinity-X would provide the best results during experimental procedures in which the capture of images over a long duration is more important than the high speed capture of images over short durations. For example, during the budding assay conducted to monitor the effects of a yeast cell's ability to reproduce during IR Irradiation, Ashkin and Dziedzic ([1987](#)) optically trapped a yeast cell for 5 hours continuously. Since this yeast budding assay is an observational investigation, then 5 hours of imaging was required using time lapse imaging, and thus the need for a high speed camera is unwarranted in such an experimental situation.

It can be seen in Table 5-6 that theoretically the DeltaPix camera provides a larger field of view (FOV)<sup>14</sup>, at the sample, and can also discern the displacement of a particle in steps of 130 nm compared to steps of 250 nm for the MC-1, assuming both cameras are operating at full resolution and imaged using a microscope objective with a magnification of x40. The smaller pixel size of the Infinity-X offers an advantage over the larger pixel of the MC-1 in that it offers higher resolution and therefore increased accuracy during particle tracking procedures. For example if a particle is moved a distance of 3 $\mu$ m, at the sample when using the DeltaPix camera, the centre of the particle can be located on 23 occasions, providing that the frame-rate is sufficient with respect to the particle velocity. The MC-1 on the other hand can only locate the centre of the particle on 12 occasions, which is highlighted in Figure 5-7.

---

<sup>14</sup> FOV determined by Equation 4-1 in Chapter 4

*Table 5-6 field of view and pixel resolution at x40 magnification*

Camera	Pixel Size ( $\mu\text{m}$ )		Full Image Resolution (pixels)		Field of View at x40 Magnification ( $\mu\text{m}$ )		Individual Pixel Dimensions (nm) at x40 magnification	
	x	y	x	y	xMag	yMag	xMag	yMag
DeltaPix	5.2	5.2	1280	1024	166.4	133.12	130	130
MC-1	10	10	512	512	128	128	250	250

Figure 5-7 depicts a spherical particle of 3  $\mu\text{m}$  diameter with an overlay grid showing the xMag and yMag pixel values. Figure 5-7 (a) represents the xMag and yMag values for the Infinity-X camera. Figure 5-7 (b) represents the xMag and yMag values for the MC-1 camera. During particle tracking, the particle tracking software locates the centre of the particle in each frame of video. Therefore it is clear that smaller displacements of a particle's motion can be recorded between frames when using the Infinity-X camera.

However, this apparent advantage is made null and void on two counts; firstly, by the Infinity-X camera's low frame rate, in view of the fact that sufficient amounts of data points cannot be recorded, as discussed earlier. Secondly, at high magnifications of the image plane, i.e.  $> x40$ , the illuminating light levels are lower, which inherently introduces poor contrast images. Images suffering from poor contrast are difficult to analyse since particle tracking becomes increasingly difficult. Improving the light levels and the contrast of the images, for the Infinity-X camera, results in further reductions to the possible maximum frame rate, which only compounds the limited frame-rate issues of the DeltaPix.

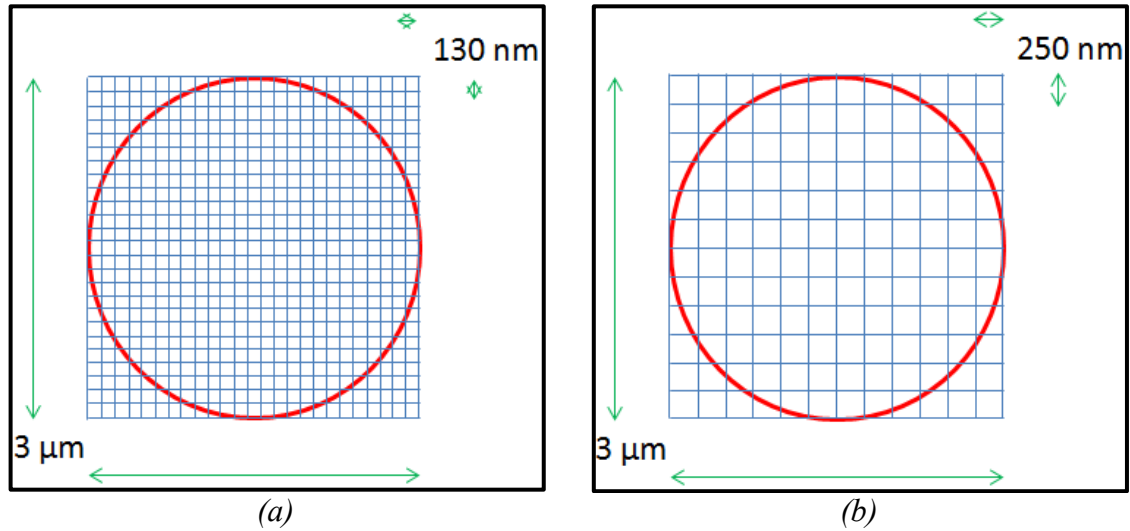


*Figure 5-7 diagrams depicting a 3 μm particle with overlay xMag, yMag grid (a) grid showing xMag = 130 nm and yMag = 130 nm values for Infinity-X camera (b) grid showing xMag = 250 nm and yMag = 250 nm values for MC-1 camera*

## 5.9 MICRO/NANO MANIPULATION TRANSLATION STAGES

Translation stages are used to manoeuvre the tapered optical fibre's distal end within the sample arena. This needs to be performed accurately over precise distances and with controlled speed. The system here required two different types of linear translation stages to provide the optical trapping system with appropriate movement, of the tapered optical fibre tip, around the microscope sample chamber in the X, Y & Z directions. The different types of linear translation stages that were employed are DC-motor types and piezo electric types, for coarse and fine travel respectively. In addition to the two varieties of linear translation stages, a MicroLab-rotation stage is employed to provide precise variation of the insertion angle of the tapered optical fibre with respect to the sample chamber.

### 5.9.1 MOTORISED LINEAR TRANSLATION STAGES

Three motorized compact Physik Instrumente (PI) DC-motor M-110.1DG micro translation stages (Lambda Photometrics, UK), configured for X, Y, Z axis translation allow the tapered

optical fibre to be manoeuvred within the sample chamber in the X, Y and Z planes, over distances of up to 5 mm of coarse travel, with a minimal incremental travel step of 0.05  $\mu\text{m}$  and a maximum velocity of 1 mm/second.

### **5.9.2      *PIEZO TRANSLATION STAGES***

Movement of a finer nature is achieved over 100  $\mu\text{m}$  distances, providing 0.3 nm of resolution in the closed loop mode, in both the X and Y directions, using the P-261.2CD PIHera XY Piezo stage and in the Z direction using the P-621.ZCD PIHera Precision Z stage (Lambda Photometrics, UK). The advantages of the nano positioning stages over the motor driven types include their higher resolution, their rapid response to input changes and their fast and precise settling behaviour to a typical accuracy of 10 nm in 30 msec.

### **5.9.3      *ROTATION STAGE***

A MicroLab rotation stage, 07 TRT 508 (CVI Laser Optics & Melles Griot, UK) is utilised to provide quick and accurate changes to the insertion angle of the tapered optical fibre tip with respect to the microscope sample chamber. The rotation stage provides 360° of manual rotation. However, when the locking screw is engaged, only 15° of precision rotation is permitted. The rotation of the stage is driven by a micrometer which includes a 360° scale that is equipped with a vernier scale that is readable to an accuracy of 1°. The resolution is 18 arc seconds or  $18 \times 1/3600$  of a degree = 0.005°.

## **5.10      MISCELLANEOUS COMPONENTS**

The components listed above describe the major elements of the T-FOTs system. However there are additional components whose importance within the system should not be

undervalued, as they all contribute significantly to the success of the system. First of all to guarantee a successful and working system it must first be deemed safe for human operation.

The dangers of working with exposed, high intensity beams of invisible laser light in the near infrared region of the electromagnetic radiation spectrum, specifically at a wavelength ( $\lambda$ ) of 1064 nm, are well known ([Mainster et al., 2004](#)). The Ventus IR laser is deemed a class IV laser system. This classification is reserved for lasers with optical output powers in excess of 500 mW and with the potential to cause permanent and severe injury to eyes, or skin, even without magnification by external optics. Therefore, a number of engineered defences are introduced to the overall T-FOTs system design in order to facilitate a reduction of risk to individuals during its operation.

### ***5.10.1 LASER INTERLOCK SYSTEM***

A laser interlock system is required for any laser system containing a class 3B laser and above. Since the Ventus IR laser is of a class 4, then a laser interlock system is required to provide a further safety mechanism to the overall system. The Intellilock portable Laser Interlock system was selected for use with the T-FOTs system. The prime driver in terms of its suitability was its portability, which was one of the T-FOTs original design criteria. Its features include, as its first line of defence, a ‘laser on’ warning light above and external to the door of the optical trapping laboratory. This warns people of the potential hazards that may be encountered by entering through the door, and is activated automatically whenever the laser is in operation. If for any reason the door is opened when the laser is in operation, a magnetic door switch is activated and the control unit immediately disengages the laser output.

### **5.10.2 OPTICAL TRAPPING SHROUD**

In addition to the laser interlock system a further mechanical safety feature has been built around the optical trapping system in the form of a physical shroud. The shroud offers protection to the laser user and additional persons within the microscopy laboratory environment, from exposure to the non-ionising radiation of the laser. The shroud was built here at LJMU and consists of 8 bench guard panels configured to provide a box enclosure. The panels are made of black anodised, light diffusing, and textured EVER-GUARD material (Laser Physics, UK). The panels are designed to absorb and diffuse laser beams and they are rated to provide protection from laser irradiance in excess of 1200 watts/cm<sup>2</sup> for at least 180 seconds.

### **5.10.3 SAFETY EYEWEAR AND OPTICAL IR FILTERS**

Laser safety goggles offer the last line of defence should there be some mishap with the laser. The Glendale IR LS 696 goggles, (Laser Physics UK Ltd, UK) are specifically chosen for the Ventus laser operation as they provide the required level of protection with an optical density (O.D.) of 5+ at wavelengths between 1040 and 1550 nm, whilst also providing the user with 75% visible light transmission (VLT).

Optical infrared (IR) filters provide protection at the microscope. The filters consist of Schott KG5 short pass filter glass, 25 mm diameter, 2mm thick and offer a high transmission in the visible region of the electromagnetic spectrum with low transmission at IR regions (UQG Ltd, UK). For example the transmittance is given as  $3 \times 10^{-5}$  at 1060 nm compared to 0.68 for the visible wavelength of 630 nm. Two additional 25 mm diameter circular glass IR filters are fitted into the microscope binocular eye-pieces. However, they are not employed to allow the user to safely look down the microscope binocular eyepieces during “laser on”

procedures; they are only employed as a “last line of defence” safety measure. The microscope binocular eyepieces are used only for set up procedures when the laser is deactivated. During “laser on” procedures the binocular eye pieces are completely blacked out, mechanically, using eyepiece caps. The optical trapping shroud offers additional protection against operator error in this regard. Safe viewing of the optical trapping arena during optical trapping procedures is therefore made possible via the camera and a remote monitor.

It is at the entrance to the camera sensor that a third IR optical filter is employed for two reasons firstly to protect the camera sensor from the damaging IR rays and secondly only light from the visible region of the electromagnetic spectrum is used for imaging of the optical trapping procedures. Therefore the scattered IR rays are denied access to the optical pathway prior to the camera sensor. The reason for this is that when the laser beam is incident upon a trapped particle, the resultant scattered IR light obscures the images of the trapped particle, which prohibits accurate analysis of the recorded optical trapping video footage.

#### ***5.10.4 SUTTER P2000/F MICROPIPETTE PULLER***

The most important component of the T-FOTs system is the tapered optical fibre end-face that is used to focus the laser beam and facilitate 3D optical trapping. The Sutter P2000/F is a device that is usually employed to create micropipettes via the heating and drawing process, whereby the heat is generated by a 20W CO<sub>2</sub> laser. It has been specially adapted to enable the pulling of optical fibre and glass with an outer diameter of  $\leq 0.6$  mm.

The P2000 can store up to 100 programmes, each consisting of 8 command lines. Control of the tapered fibre’s geometry is governed by five input parameters that are set within each of

the command lines. The parameters, shown in Table 5-7, are given in discrete values only, and are not assigned SI units of measure.

*Table 5-7 P2000/F micropipette puller, parameters, parameter ranges and functions*

<b>Parameter</b>	<b>Range</b>	<b>Function</b>
Heat	0-999	(HEAT) Specifies the output power of the laser, and consequently the amount of energy supplied to the optical fibre.
Filament	0-15	(FIL) Specifies the scanning pattern of the laser beam that is used to heat the optical fibre. The P2000 is pre-programmed with 0-15 (16) scanning pattern values, each of which defines the longitudinal length and rate of the scan.
Velocity	0-255	(VEL) parameter specifies the velocity at which the glass/optical fibre carriage must be moving before the hard pull is executed. The velocity of the glass carriages during the initial pull is dependent on the viscosity of the glass and the viscosity of the glass is dependent on its temperature.
Delay	0-255	(DEL) parameter controls the timing of the start of the hard pull relative to the deactivation of the laser.
Pull	0-255	(PULL) parameter controls the force of the hard pull.

### **5.10.5 OPTICAL FIBRE FUSION SPLICER**

Optical fibre fusion splicing was chosen as the replacement method for connecting the optical fibre components of the T-FOTs system. The system that was acquired to carry out the fusion splicing is the Fase II compact fusion splicer and the accompanying HSO II Heat shrink oven for the application of the splice protectors (Tritec Developments Ltd, UK)

The use of an optical fibre fusion splicer removed the physical breaks within the optical fibre system and thus eradicates the points of vulnerability from the possibility of burning at the connector interfaces. In addition, fusion splicing offers a reduction in optical insertion losses, typically 0.05 dB. This compares to 0.25 dB for a mechanical angled physical contact (FC/APC) connector that is connected to a second FC/APC connector via a sleeve, through which is a mechanical interface device that allows the connection of two optical connectors such as FC/APC's for example. However it must also be noted that the above insertion losses are consistent only with optical fibre of the same diameter core. Optical fibre variances within

the system will also increase the insertion losses within the system, as discussed earlier ([Cisco, 2005](#)).

There is however a downside to replacing the mechanical connectors with fusion splicing, which is due to the difficulty associated with incorporating new optical fibre components within the system. For example the replacement of a damaged optical fibre tapered tip requires the optical fibre's distal end to undergo some preparatory work before being assembled within the micropipette puller. Using the mechanical connector method the fibre can be easily disconnected from the system and a new fibre taper can then be easily pulled at a location away from the system. However, to disconnect a fusion spliced section of fibre requires the fibre to be cut and then re-spliced once the remedial work has been carried out. The pipette puller can be taken to within close proximity of the system however, if the optical fibre has been reduced to a length of less than say 2.5 meters, which is an insufficient length to reach the pipette puller, then an additional length of fibre must be added.

#### **5.10.6 THERMAL CYCLER PCR MACHINE**

A significant problem that continually occurred during the early optical trapping experiments was that during the course of the day the optical power output would appear to be prone to large optical losses. This particular anomaly appeared to coincide with a rise in the ambient room temperature of the small lab, where the system was originally located, prior to its move to a new microscopy lab. At first it was thought that the rise in the ambient room temperature caused thermal expansion of the aluminium plate, which holds the laser to fibre coupler in place, resulting in misalignment of the laser to fibre coupling interface. Therefore every time the system appeared to lose optical power, it was deemed necessary to re-align the fibre coupling mechanism. This course of action seemed to offer little, or no, improvement and only

really served to cause detrimental wear to the coupling device tilt screws and threads, causing a reduction in the alignment sensitivity of the coupling system.

The true nature of the problem became apparent, whilst working during one bitterly cold weekend, at time during which the building's heating system was not in operation. On this occasion, rather than witness the usual optical power losses due to the increase in the ambient room temperature, the significantly reduced ambient room temperatures caused the system to appear to exhibit output optical power values far above those which could be physically achieved by the laser. These observations led to a complete change in thought, as it now appeared that misalignment could no longer be the cause of the optical power losses. Instead, attention was turned to the optical tap that is employed to monitor the optical power within the optical fibre. After completing a few tests, it soon became apparent that the voltage output from the optical tap was heavily influenced by temperature. Such was the effect that warmer temperatures produced corresponding lower voltage outputs while conversely colder temperatures resulted with higher voltage outputs.

As a pragmatic solution it was deemed more cost effective to control the optical tap's temperature at a local level, rather than install costly climate control for the whole room. To achieve the required temperature control a Techne TC-312 thermal cycler, PCR machine was acquired. The optical tap was set up inside the lid of the instrument, along with a thermocouple to monitor the local temperature, as shown in Figure 5-8.

Figure 5-8 (a) shows the PCR machine with the lid open and Figure 5-8 (b) shows a magnified image of the inside of the lid which houses the inline optical tap and the K-type thermocouple. The input optical fibre of the optical tap enters at the top right hand corner and

the output optical fibre exits at the bottom left hand corner of the PCR lid. The optical tap itself is located on the centre of the PCR lid. The red and black in-line optical tap output signal wires can be seen in the centre of the image, exiting the optical tap and leaving the PCR machine at the bottom left hand corner of the lid. The thermocouple can just be made out (green wire) entering the lid of the PCR machine at the top right hand corner located behind, and attached to the back of the in-line optical fibre tap.

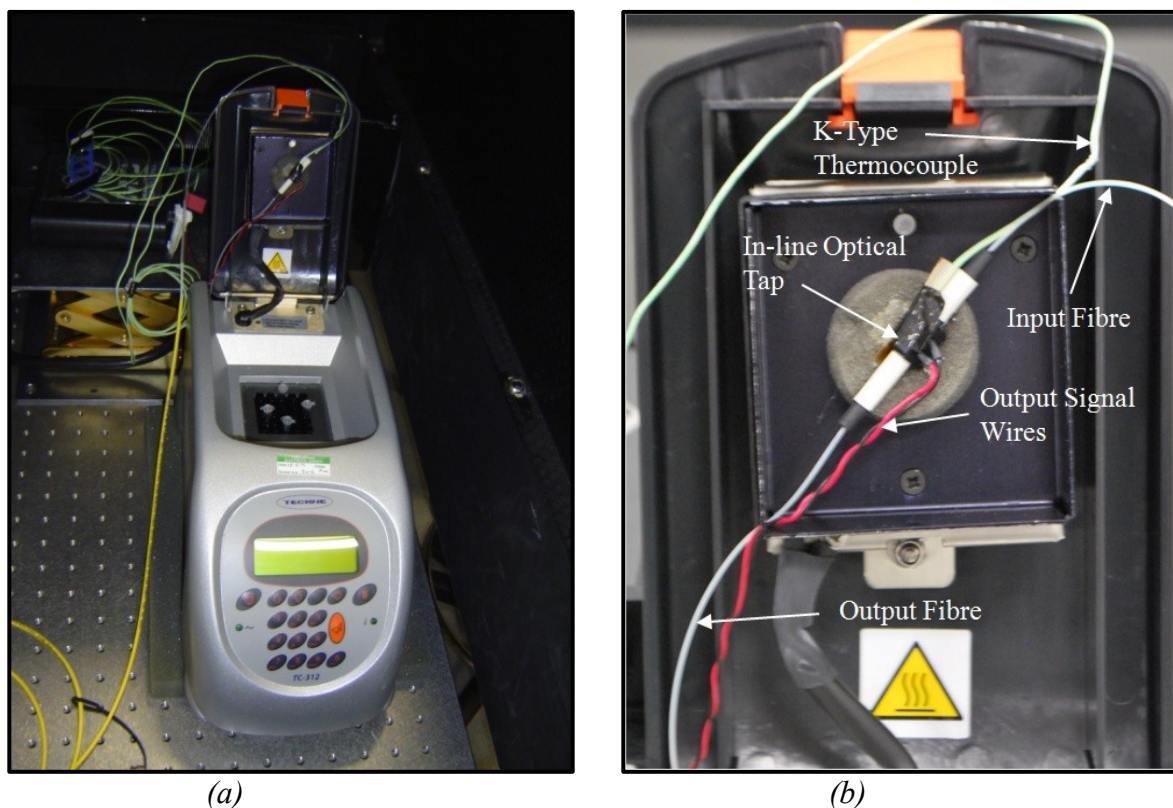


*Figure 5-8 (a) optical tap and thermocouple set within the lid of the thermo cycler PCR machine to enable the optical tap's local temperature feedback and control (b) magnified image of the optical tap and thermocouple fitted within the lid of the PCR machine.*

During trapping experiments the temperature could be monitored and the temperature of the PCR machine adjusted accordingly, so as to maintain the optical tap's temperature within the

given temperature range, of between 24.9°C and 24.95°C,<sup>15</sup> which was deemed the temperature best suited for quick and reliable stabilisation of the optical tap temperature.

### **5.10.7 THERMOCOUPLE**

The working temperature range for the K-type thermocouples lies nominally between -73°C and 260°C and they have a response time of less than 0.3 seconds. The K-type thermocouple consists of a positive lead of Nickel-Chromium (Ni-Cr) alloy and a negative lead of Nickel Aluminium (Ni-Al) (Omega Engineering Limited, UK).

Two K-type thermocouples are employed to monitor the ambient temperature at two locations; firstly the ambient airspace surrounding the T-FOTs system, within the optical trapping system shroud; secondly from within the lid of the thermal cycler PCR machine, which is the location of the inline optical tap. The acquired temperature data provides critical feedback such that temperature adjustments can be made to provide optical tap stability.

---

<sup>15</sup> The above temperature range of between 24.9 and 24.95 was determined as the most suitable range that would allow rapid temperature stabilisation of the optical tap and it was determined through a process of trial and error.

**CHAPTER SIX TAPERED FIBRE  
OPTIC TWEEZERS (T-FOTs)  
SYSTEM SETUP AND  
CALIBRATION**

## **TAPERED FIBRE OPTIC TWEEZERS (T-FOTs) SYSTEM SETUP AND CALIBRATION**

This chapter describes how all of the individual constituent components, which have been discussed in detail throughout Chapter 5, are arranged and assembled together to complete the tapered fibre optic tweezers (T-FOTs) system. It will show the method used to create the optical fibre taper and how it is connected to the system set-up using fusion splicing. Also explained are the procedures that have been undertaken to calibrate the video camera and the inline optical tap. Finally, the method for aligning the optical fibre taper within the microscope sample chamber is presented. 18

### **6.1 TAPERED FIBRE OPTIC TWEEZERS (T-FOTs) SYSTEM SETUP**

Figure 6-1 shows the basic schematic diagram for the tapered fibre optic tweezers (T-FOTs) system that has been developed by the author here at GERI. The system consists of a Ventus IR, diode pumped solid state (DPSS), Neodymium doped Yttrium Aluminium Garnet (Nd:YAG) optical trapping laser source operating at a wavelength ( $\lambda$ ) of 1064 nm (Laser Quantum, UK). The exiting laser beam is coupled into a single mode fibre (SMF) patch cable via a non-contact style receptacle laser to fibre coupler. The optical fibre patch cable is terminated, at its proximal end, with a high power connector that has a hollow metal ferrule design to eliminate burning of the optical fibre.

The output end of the high power optical fibre patch cable is fusion spliced to the input optical fibre of a high power 1 % in-line optical tap that is used to monitor the laser's optical output power at the sample. The output optical fibre of the inline optical tap is fusion spliced to a length of 1060XP single mode fibre (SMF). The distal end of the 1060XP SMF is tapered

using a heating and drawing method in order to deliver a focused beam of laser light to the sample and is further discussed later in this chapter.

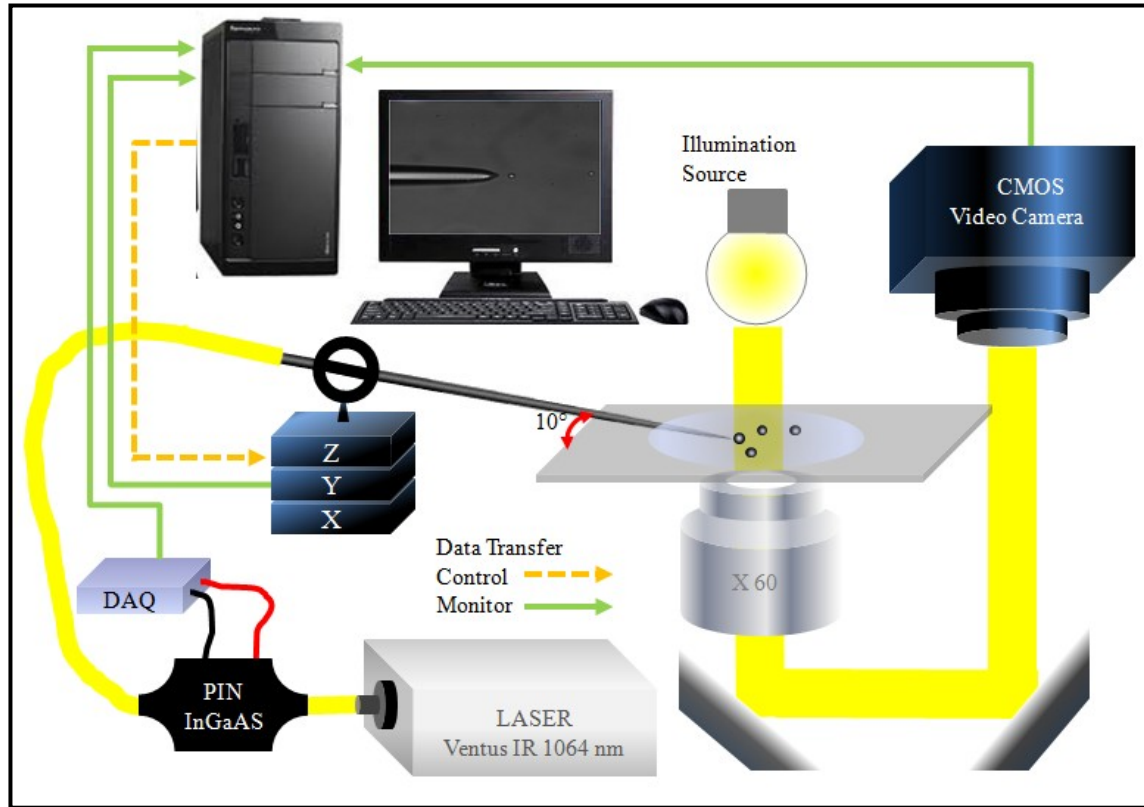


*Figure 6-1 basic schematic diagram of the tapered optical fibre tweezers system (T-FOT's) system design setup*

The fusion splices within the optical fibre system were formed using a combination of the Fase II compact fusion splicer and its accompanying HSO II heat shrink oven. The role of the heat shrink oven is to heat and cure a shrinkable, reinforced splice protector to the fragile fusion splice region (Tritec Developments Ltd, UK). The optical tap is employed to monitor the optical power propagating within the SMF (Oz Optics, Canada). It is mounted within a Techne TC-312 PCR machine for local control of the device temperature. The temperature of the optical tap is measured using a K-type thermocouple (Omega Engineering Ltd, UK). The output current from the optical tap, and the temperature data from the K-type thermocouple,

are received by the USB-2404-UI DAQ module (Adept Scientific, UK) and transmitted to the custom built PC, which is used for control and monitoring of the T-FOTs system.

The tapered distal end of the 1060XP SMF sits tightly within an Asslint Al<sub>2</sub> O<sub>3</sub> 99.7% ceramic tube (W. Haldenwanger Technische Keramik GmbH Co. KG, Germany) to improve lateral support as shown in Figure 6-2. The ceramic tube has internal and external diameters of 300 µm and 800 µm respectively and provides the inner component of a double sleeve structure designed as a fibre holder. The outside sleeve consists of a 50 mm length of Pitot tube. The pitot tubing is attached to a length of steel bar, which offers rigid support for the optical fibre as it is directed into the sample chamber of the GXD-30 inverted microscope (Masarek Optical Systems Ltd, UK). The tapered distal end of the 1060XP SMF protrudes from the end of the fibre holder by about 15 mm.

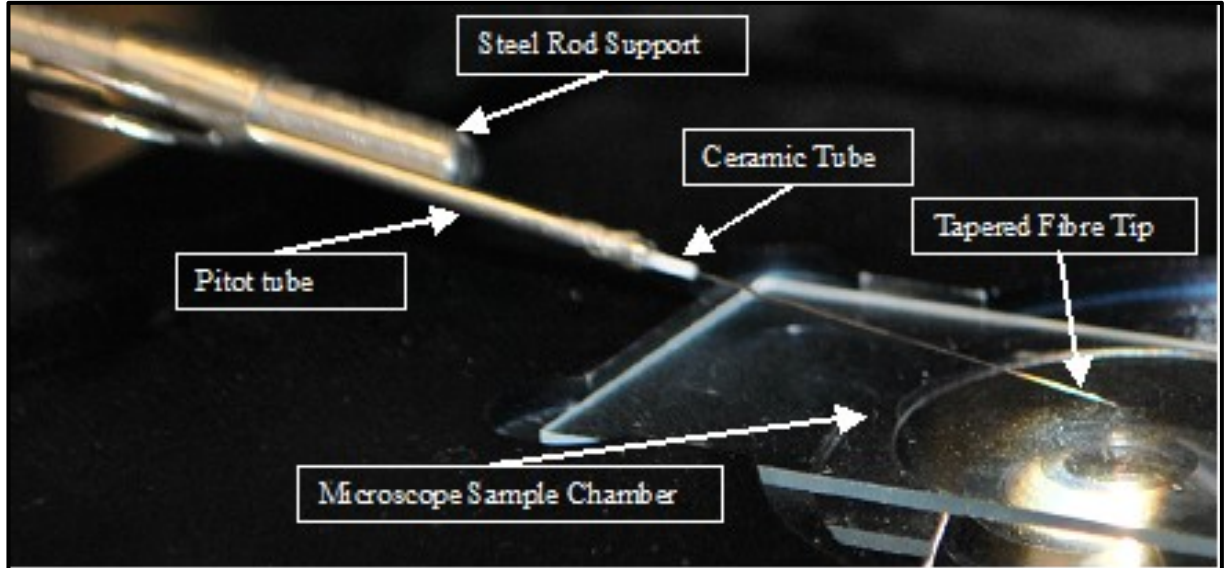


*Figure 6-2 T-FOTs tapered optical fibre tip entering the microscope sample chamber supported by the steel rod and fibre holder*

Figure 6-3 shows the arrangement of the optical fibre assembly and the translation devices. The steel bar that supports the optical fibre is fixed to a miniature rotation stage 07 TRT 508

(CVI Laser Optics & Melles Griot, UK). The miniature rotation stage is mounted on top of the motorised and piezo translation stage assemblies, allowing quick and accurate changes to the insertion angle of the tapered optical fibre to be made. The tapered optical fibre tip is manoeuvred within the sample chamber in the X, Y and Z planes, by using a combination of translation devices. Three motorised M-110.1DG micro translation stages, configured for X, Y and Z axis translations respectively, provide 5mm of coarse travel. Alternatively, movement of a finer nature can be achieved over 100  $\mu\text{m}$  distances, in the X, Y and Z directions, using the P-261.2CD PIHera XY Piezo stage and the P-621.ZCD PIHera precision Z stage (Lambda Photometrics, UK).

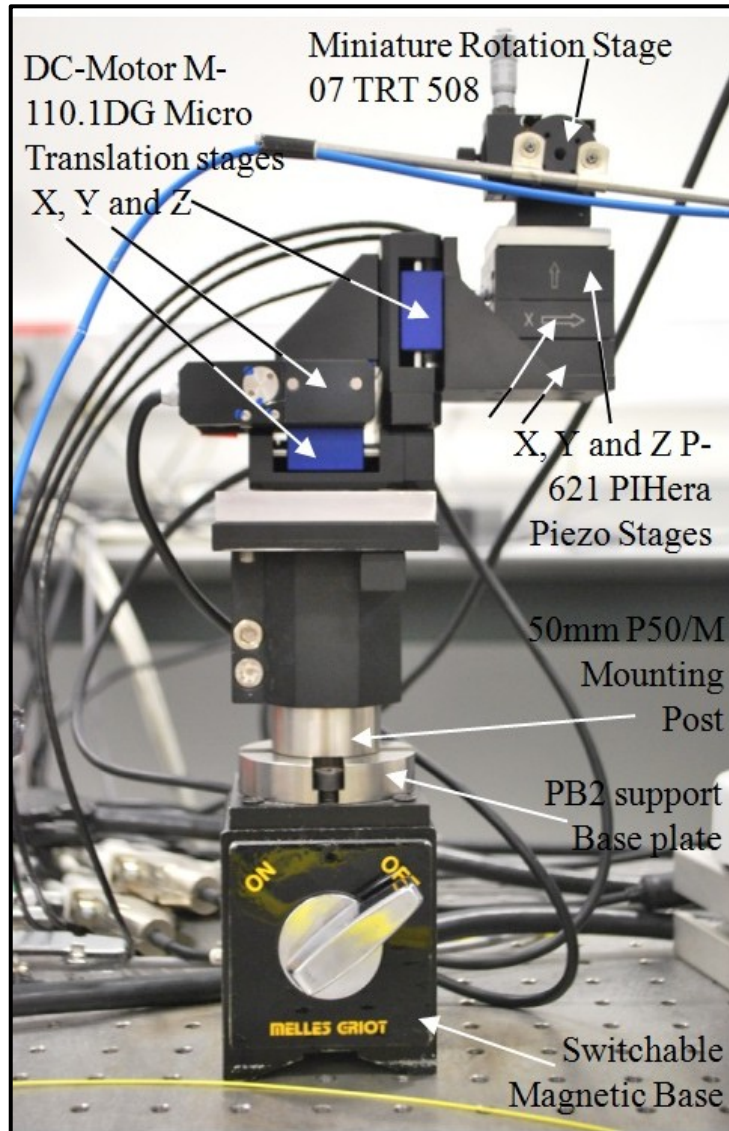


*Figure 6-3 translation assemblies mounted on a tall structure showing 50 mm length mounting post arrangement for a tapered optical fibre insertion angle of  $10^\circ$*

The translation assemblies are mounted on a tall structure to provide a sufficient height for the optical fibre insertion into the microscope sample chamber at the desired angle. The structure consists of a switchable heavy duty magnetic base (CVI Laser Optics & Melles Griot, UK) with a PB2 support base plate fixed to the top. The PB2 support base plate is the foundation that allows a 1.5 inch diameter mounting post of either 50 mm (P50/M), or a 125 mm (P125/M) length (Thorlabs, UK), to be fixed in position.

The shorter mounting post is employed when the tapered optical fibre is to be inserted at an angle of  $10^\circ$  with respect to the microscope's sample chamber. For insertion angles of  $>30^\circ$ , then the longer mounting post is used to provide the additional required height. The translation equipment is mounted onto a C1506/M adjustable mounting platform (Thorlabs LTD., UK) that sits on top of the mounting post. The translation devices consist of two different assemblies, as previously discussed. The first is composed of three DC-motor M-110.1DG micro translation stages. An angle bracket is fixed to the DC-motor translation stage that is used for motion in the vertical Z direction. The second assembly of motion devices sits within the aforementioned angle bracket and consists of the P-261.2CD PIHera XY Piezo stage and the P-621.ZCD PIHera Precision Z directional stage.

Imaging of the sample chamber can be executed via the microscope eyepieces, providing the laser is deactivated. If the laser is active, then in the interests of health and safety, the sample chamber must be viewed via the video camera and PC monitor. Initially the video camera employed was a CMOS DeltaPix Infinity X (Kane computing, UK). However, in light of the Infinity-X's relatively low frame rate, an additional camera, the Photron Fastcam MC-1 high speed video camera, was acquired and used during system characterisation processes. The high speed camera was acquired, by way of a short duration loan from the Engineering & Physical Sciences Research Council (EPSCR) portable instrument loan pool, as previously discussed in Chapter 5. An adjustable C-mount adapter, with an x0.5 magnification lens, is used to couple either of the two cameras to the microscope. However, the lens of the C-mount was removed, theoretically increasing its magnification from x0.5 to x1 magnification. A detailed discussion about the reasons behind this modification is provided in Section 6.4.

The optical pathway prior the C-mount and camera entrance is fitted with a Schott K5, 25mm diameter, 2mm thick, circular glass IR low pass blocking filter to eliminate possible damage to the camera sensor and to improve imaging by blocking out the scattered laser light during experiments. As a precautionary safety measure, two additional and identical Schott K5 IR blocking low pass filters were fitted within the optical pathway prior to the binocular eye pieces.

## **6.2 OPTICAL FIBRE TAPER FABRICATION**

The most crucial component of a fibre based optical tweezers system is the fibre end that is used to deliver and focus the laser light at the sample. For single beam 3D optical trapping to be realised, the optical trapping laser beam must be tightly focused in order to create a steep intensity gradient. This ensures that the gradient force exceeds the scattering force, and thus produces an equilibrium point just beyond the focal point of the beam, where 3D trapping is exploited.

### ***6.2.1 HEATING & DRAWING METHOD USING THE SUTTER P/2000F MICROPIPETTE PULLER***

The heating and drawing method was selected as the best means for developing a tapered optical fibre end face that would be suitable for 3D optical trapping. The reasons for this selection have previously been discussed in Chapters 3 and 4.

Tapering of the optical fibre was performed using the Sutter P2000/f micropipette puller (Intracell LTD, UK). The P2000/f is a modified version designed for pulling optical fibre and glass of diameters less than 0.6mm. The P2000/f micropipette puller is a micro-controlled device utilising a 20W CO<sub>2</sub> laser heat source. The use of a laser as the heat source was the

preferred method over that of a gas flame, due to the inherent technical challenges associated with the latter method, as discussed earlier in Chapter 3.

### **6.3 FABRICATION OF TAPERED FIBRE OPTIC TIP FOR 3D OPTICAL TRAPPING**

The first part of the task requires the assembly of the bare single mode fibre (SMF) (1060XP Nufern) and the outer protection, 900 $\mu$ m diameter optical fibre furcation tubing (FT900M, Thorlabs, UK). A 5 meter length of the single mode optical fibre and a 4.85 meter length of furcation tube are cut from their respective reels. The inner Kevlar threads are removed from inside the furcation tubing to allow easy insertion of the optical fibre. The SMF is then threaded into the furcation tubing until it protrudes from both ends. A Fase II fusion splice machine (Tritec Developments Limited, UK) is then employed to connect one end of the fibre length to the inline optical tap's exit fibre.

#### **6.3.1 *SPLICING OF THE OPTICAL FIBRE TO THE SYSTEM***

Before two fibres can be connected they must first be prepared for fusion splicing. The first task is to slide a splice protector over the end of one of the two fibres that are to be connected. A 25mm length of acrylate buffer is then stripped from the end of both of the fibres using a tight buffer stripping tool. The stripped ends are then cleaned with Isopropanol prior to being cleaved using a TCA8 optical fibre cleaver, (Tritec Developments Ltd, UK). Cleaving both ends of the fibres provides two straight end-faces for precise alignment<sup>16</sup>. The ability precisely to align and mate both end-faces together results in most efficient splice connection, and thus is a crucial element in the process.

---

<sup>16</sup> The TCA8 optical fibre cleaver is capable of producing a fibre end face angle of less than 1°.

Each of the two fibre ends is transversely aligned within the fusion splice machine, along the X axis, using the fixed V-grooves and held in place by the magnetic clamps that are located on either side. Axial translation of the two fibres along the X axis is required to bring the two end-faces together and this is achieved by using thumbwheel driven translation stages. The axial translation stages are capable of driving each fibre a total distance of 5mm enabling the end-faces to be brought into contact. A microscope built-in to the splicer system, with a magnification of x75, is used to view the scene when alignment of the fibres is being conducted. Once the fibres are in position, the electric arc is activated and the fusion splice connection is made.

A fibre optic protection sleeve is employed to protect the fusion spliced joint. The sleeve consists of a cross linked polyolefin heat-shrinkable tube, hot melt tube and a stainless steel rod that runs the length of the sleeve for added support. Following the successful splicing of the two fibres, the splice protector is carefully manoeuvred into position, whilst ensuring that an even distribution of the splice protector is maintained on either side of the joint. Care is taken to ensure that the loose protective furcation tube is supported within both ends of the splice protector prior to heat shrinking. The spliced assembly is carefully placed into the heat shrinking oven and secured in place using the fibre clamps that are located at either side of the heating vessel. The HSOII heat shrink oven (Tritec Developments Ltd, UK) is then activated and the splice protector encompassing the splice is allowed to shrink and cure.

Before fabrication of the optical fibre taper can commence, the inline optical fibre tap has to be calibrated. This calibration is performed prior to any new tapered lens being fabricated. It would however, be more suitable to calibrate the optical tap after the optical fibre tapered lens has been fabricated. However, this practice is not a viable option because, for calibration

purposes, the optical fibre end has to be inserted into a temporary optical fibre connector ferrule. The temporary optical fibre connector is used to hold the fibre in place at the interface of the PM100 optical power monitor's integrated sphere sensor, which is used to measure the intensity of the laser light exiting the optical fibre. Trying to insert a tapered optical fibre tip into the temporary connector often resulted in the tapered optical fibre lenses becoming damaged, which renders them useless. The reason that damage is so easily inflicted to the optical fibre taper are twofold; firstly the fibre is now devoid of its protective acrylate outer buffer, and secondly; the tapering of the fibre significantly reduces its diameter. When combined, these two facts render the tapered silica optical fibre tip brittle and thus extremely fragile.

However, inserting a cleaved optical fibre end into the fibre holder is a simple matter, since the optical fibre is considerably more robust at its natural diameter, which reduces the likelihood of damage occurring. Moreover, any damage that may occur can be neglected, since the optical fibre will undergo tapering following the inline optical tap calibration procedure. For the sake of continuity, a detailed discussion concerning the calibration of the optical tap is postponed until Section 6.6. Consequently the method used to fabricate the tapered optical fibre lenses was as follows.

### ***6.3.2      LOADING THE FIBRE INTO THE MICROPIPETTE PULLER FOR TAPER FABRICATION***

Following the splicing of the optical tap output with the optical fibre that is to be tapered, and the subsequent optical tap calibration which is discussed further in detail in Section 6-6, the distal end of the SMF is tapered using the Sutter P2000/F micropipette puller. Before the fibre is prepared for pulling, the distal end of the fibre is inserted into the ceramic/pitot tube

assembly fibre holder. This ensures that that the subsequent tapered tip will not be damaged whilst trying to negotiate the tight confines of the fibre holder post tapering.

Figure 6-4 shows a schematic where a 25mm section of the optical fibre's acrylate buffer has been removed, at a distance of 125mm away from the distal end of the optical fibre, using a tight buffer stripping tool. It is this exposed 25mm section of fibre that is to be subjected to the heating and drawing process. The exposed fibre cladding region is cleaned, using an optical grade paper wipe that has been doused in Isopropanol solvent, to remove any unwanted residue, or debris, that may be infused into the fibre during the heating process.

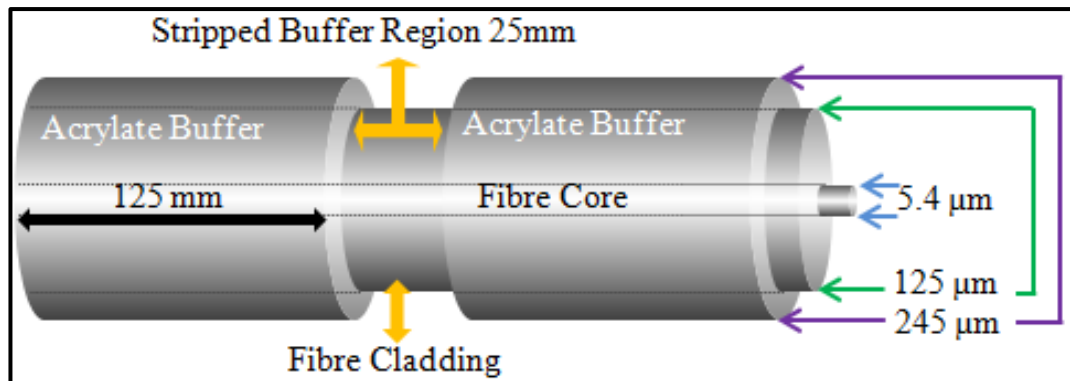


*Figure 6-4 stripping of Acrylate buffer*

Following the stripping and cleaning of the optical fibre's acrylate outer buffer, the optical fibre is loaded into the P2000/f micropipette puller. Figure 6-5 shows the front panel and puller mechanism of the P2000/F micropipette puller. The key to Figure 6-5 describing the micropipette puller's puller bars assembly can be seen in Table 6-1.

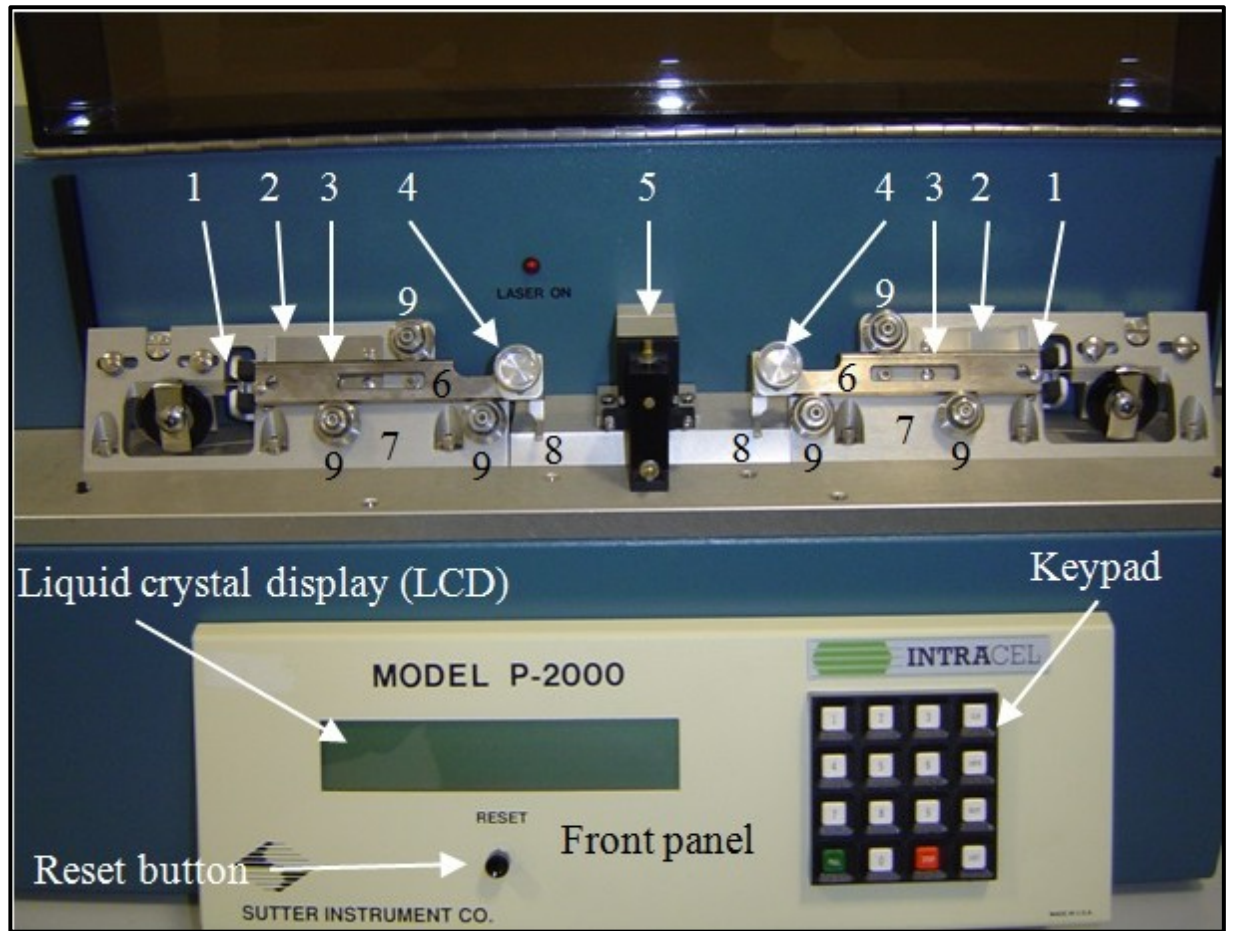


Figure 6-5 P2000/F 20W CO<sub>2</sub> laser based micropipette puller

Table 6-1 key for Figure 6-5 P2000/F micropipette puller's description

Key Number	Description
1	Bumpers – stops the motion of its associated puller bar and prevents impact forces from breaking the tapered optical fibre.
2	Spring stops are one way catches that prevent optical fibre tip collision by catching the puller bars as they rebound off the bumpers.
3	V-groove for precise optical fibre alignment and loading.
4	Glass clamp and clamping knob for clamping the optical fibre into position.
5	Shroud, which encloses the retro mirror and the optical pathway of the laser beam. The shroud protects the user from exposure to the laser beam. Access holes in the side of the shroud allow the optical fibre to be loaded into the optical pathway of the laser.
6	Puller bars – the assembly consists of the puller bars, glass clamp, clamping knob (4) and cable retaining screw.
7	Angled surface panels that provide mountings for the puller bars and their bearings, spring stops, bumpers and the upper cable pulley assemblies.
8	Finger bar used for pulling both puller bars together when loading optical fibre.
9	These are the bearings that guide the puller bars' motion.

The process begins by first releasing the puller bar spring stop catches, on either side of the puller bar mechanism, to release the puller bars. The distal end of the fibre is then loaded from the left hand puller bar, along the v-groove, and through the holes in the side of the shroud, towards the right hand puller bar.

The right hand puller bar is pulled to the left, and towards the centre between the two puller bars, as far as it can go towards the safety shroud. The distal end of the fibre is then placed in position along the V-groove, ensuring that the stripped acrylate buffer section of the fibre is located evenly within the safety shroud, before securing the optical fibre in place by tightening the glass clamping knob. The left hand and the right hand puller bars are then both pulled towards the centre of the pipette puller, held in position, at either side of the protective shroud, using the finger bars. At this point the left hand side of the fibre is placed within the v-groove and secured to the left hand puller bar by tightening the left hand glass clamping knob. The stripped acrylic buffer region of the optical fibre is now secured within the confines of the safety shroud ready for the heating and drawing process to be executed.

The safety lid that covers the puller bar region of the micropipette puller is closed and the required program is selected. To activate the selected program, the PULL button located on the control keypad is pushed and the pulling process is initiated.

After a few seconds the heating and drawing process ends and the fibre has been divided into two, almost identical tapered tips. The clamping knobs are released and the two tapered optical fibre tips are carefully removed from the puller bars. The taper created on the right is of a short length,  $\approx 125$  mm, and will not be connected to the trapping system. However it can be used as an indicator of the taper's success during imaging and analysis purposes. The left

hand taper is already connected to the optical system, and if deemed suitable after a visual inspection, it can be fixed and aligned within the microscope's sample chamber ready to test its suitability for 3D trapping.

### **6.3.3      *TAPERED FIBRE OPTIC TIP INSPECTION***

Immediately after the pulling of a tapered fibre tip, using the P2000/f micropipette puller, the taper located on the left hand side is imaged, using the GX-30 inverted light microscope, as an initial check to verify its suitability for 3D optical trapping. This visual inspection serves only to determine if the fibre was tapered correctly.

A comparison of good and bad tapers can be seen in Figure 6-6, where (a) shows a “good” tapered tip with a parabolic taper and a secondary needle-like component. Figure 6-6 (b) on the other hand shows a magnified image of an unusable taper that has been snapped during the heating and drawing process. The snapped profile could have been obtained as a result of a lack of heat during the heating and drawing operation, rendering the silica optical fibre insufficiently viscous at the point of separation. Nevertheless it is a poor finish that will not result in 3D optical trapping and thus can be discarded.

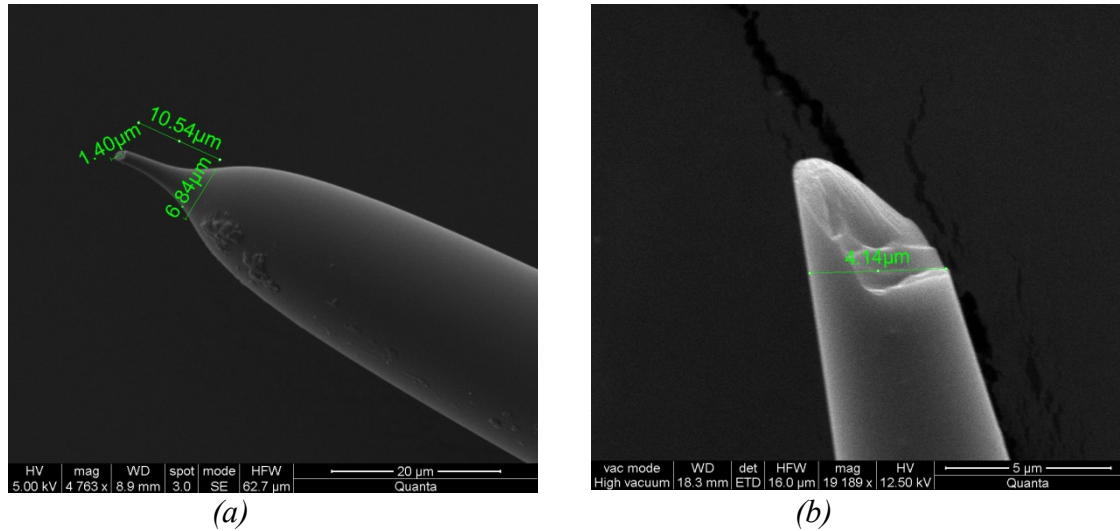


Figure 6-6 (a) showing an SEM image of a “good” tapered fibre tip and (b) showing a higher magnification SEM image of a “bad” snapped and uneven end faced tapered fibre tip

## 6.4 TAPERED FIBRE OPTIC TWEEZERS (T-FOTs) SYSTEM CALIBRATION

This section is concerned with the calibration of components of the T-FOTs system. First to be discussed is the calibration of the microscope’s optical system and camera set-up. Calibration is required to allow accurate measurements to be obtained from the recorded optical trapping images. This is followed by a description of the method employed to calibrate the inline optical tap to allow the real time monitoring of the optical output power at the sample. Finally the chapter is concluded with a description of how the optical fibre taper is positioned and aligned within the microscope’s sample chamber prior to optical trapping.

### 6.4.1 MICROSCOPE AND CAMERA

Calibration of the microscope and camera is required to enable the precise measurement of objects within the acquired microscopy images. This is achieved by recording an image of a stage micrometer at the magnification of interest. The stage micrometer is a 1mm length ruler embedded into a microscope slide, which has increments of 0.01 mm, or 10 μm intervals. To

calibrate the viewing optics the number of pixels along a known distance, measured using the stage micrometer, are determined using software. For example, Figure 6-7 shows an image of the stage micrometer that was taken using the DeltaPix Infinity-X microscopy camera at x10 magnification. The image has been opened in the GIMP 2.8.6 GNU Image Manipulation Program. The program allows the user to measure the amount of pixels that are located within a given distance. The distance being measured here is 400 $\mu\text{m}$ , which corresponds to 428 pixels, which is the measured value given at the bottom of the screenshot.

The individual pixel size of the image at the sample is given as;

$$P_S = \frac{D}{NP_i} \quad (6-1)$$

where  $P_S$  is the size of the pixel at the sample in the image,  $D$  is the measured distance in the image plane (400  $\mu\text{m}$  in Figure 6-7) and  $NP_i$  is the number of pixels in the measured region of the image (428 in Figure 6-7). When the individual pixel size is known the total field of view at the sample is given by;

$$\text{FOV} = S_{\text{Res}} \times P_S \quad (6-2)$$

where FOV is the field of view at the sample measured from the image by multiplying the camera sensor resolution  $S_{\text{Res}}$  with the pixel size  $P_S$  at the sample.

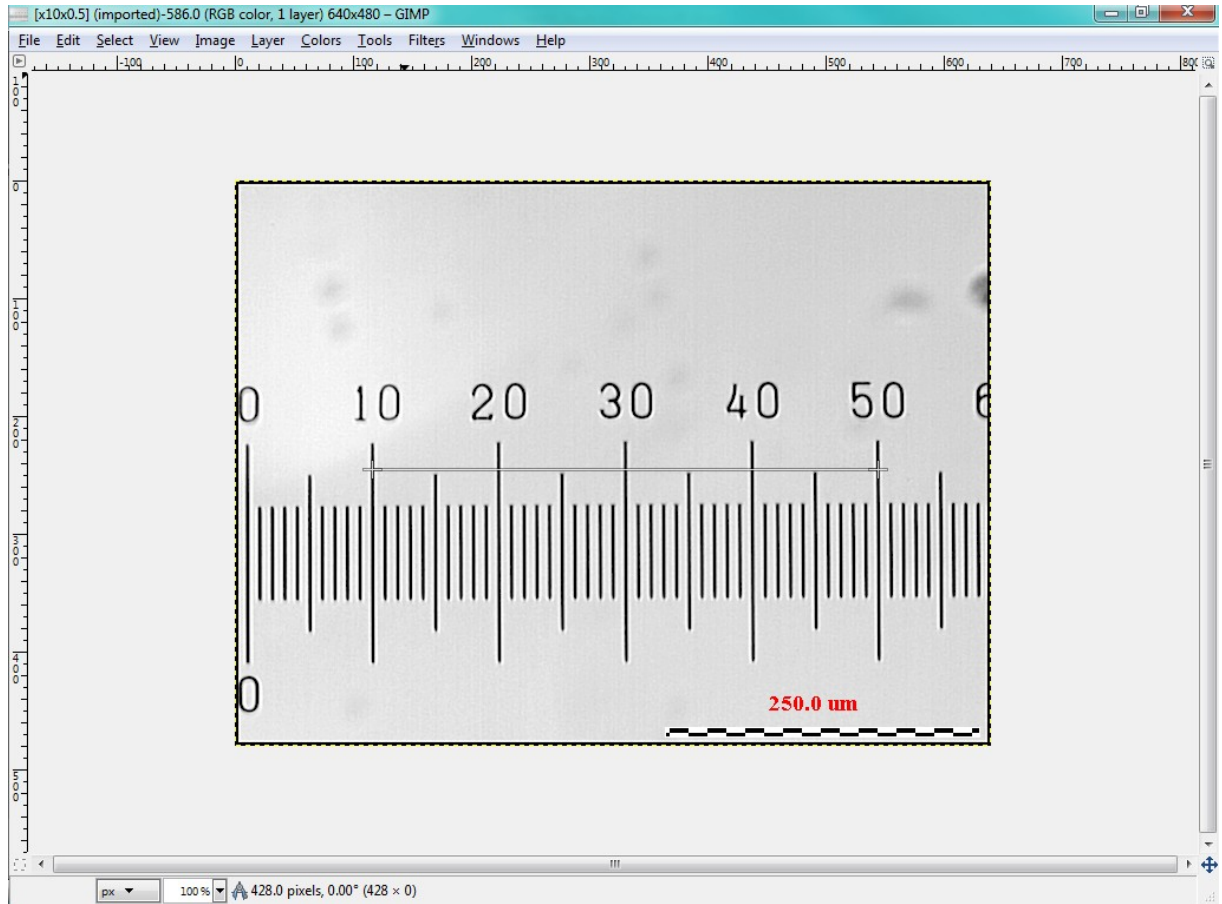


*Figure 6-7 image of the stage micrometer under x10 magnification with a x0.5 magnification C-mount adapter, opened in GIMP to calculate the amount of pixels for a given distance of 400 $\mu$ m*

There is only a requirement to measure a distance, using the stage micrometer, in one direction since the pixels used in both cameras are of a square format, thus determining the width of a pixel also gives us its height. Therefore in Figure 6-7 the individual pixel size at the sample is given as 934.6nm x 934.6nm, and as the image is 640 pixels wide and 480 pixels high, then the field of view at the sample is given as 598.1 $\mu$ m x 448.6 $\mu$ m. Since the image was taken using the x10 magnification microscope objective and the x0.5 magnification camera c-mount adapter, then it is assumed that the magnification may be approximately given by  $10 * 0.5 = x5$ . However rearranging the Equation given in (4-1) actually gives the true magnification;

$$Mag = \frac{E_{Sen}}{FOV_{sample}} \quad (6-3)$$

where  $Mag$  is the given magnification of the viewing optics,  $E_{Sen}$  is the effective sensor size and  $FOV_{sample}$  is the field of view at the sample. It is found that the magnification is not actually x5 but really x5.5.

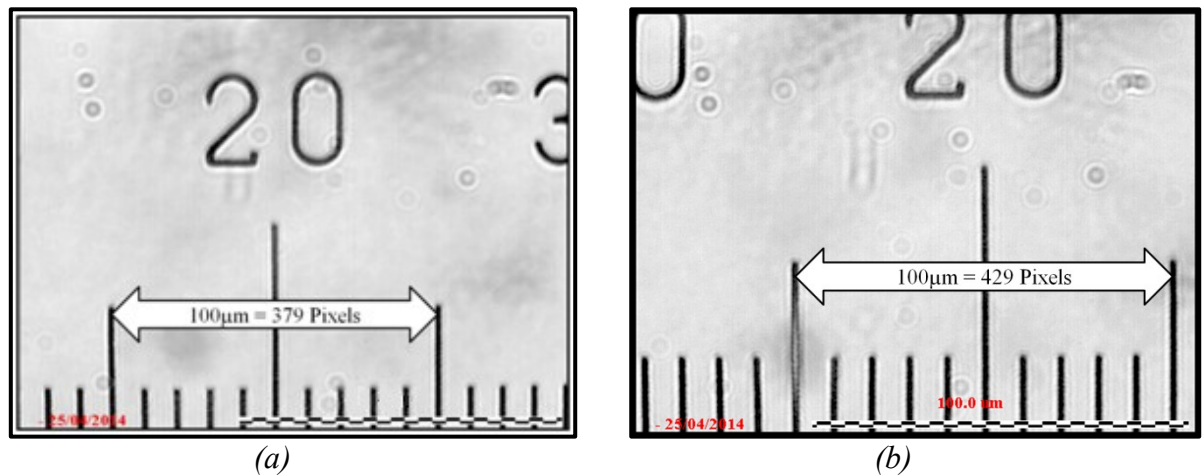
The reason for this discrepancy is as follows. The microscope objective turret is equipped with 5 microscope objective lenses, with magnifications of x4, x10, x20, x40 and x60. The digital video camera is fixed to the camera viewing port of the microscope via an adjustable c-mount camera adapter. The c-mount adapter is fitted with a lens of x0.5 magnification and a mechanism that allows adjustment to the lens height to be made.

Table 6-2 shows that when the x0.5 c-mount lens is fitted the microscope objective, the magnification should nominally be halved since it is being multiplied by x0.5. However, by adjusting the c-mount adapter fully in the anticlockwise direction, the overall magnification falls just short of the given objective magnification multiplied by the given c-mount magnification. Conversely, by adjusting the c-mount lens adapter fully in the clockwise direction, the overall magnification is greater than the given objective magnification multiplied by the given c-mount magnification. Therefore the exact theoretical magnification calculated from the objective lens magnification multiplied by the c-mount lens magnification lies somewhere in between the fully clockwise and anticlockwise positions.

*Table 6-2 overall image magnification after c-mount adjustment*

Objective	C-mount with x0.5 lens fitted		C-mount with no lens fitted	
	Anti-clockwise	Clockwise	Anti-clockwise	Clockwise
x4	x1.9	x2.1	x3.2	x3.2
x10	x4.9	x5.5	x8.6	x8.6
x20	x9.8	x11.2	x17.3	x17.3
x40	x19.7	x22.3	x34.5	x34.5

Figure 6-8 shows two images (a, b) of the stage micrometer that were captured using the DeltaPix Infinity X camera at the reduced resolution of 640 x 480 pixels. The images were magnified onto the camera sensor using the x40 magnification microscope objective lens, in conjunction with the x0.5 magnification c-mount lens. Figure 6-8 (a) was recorded with the c-mount adapter adjusted fully in the anti-clockwise direction. In this instance the annotated arrow depicts a distance of 100 $\mu$ m, which equates to 379 pixels in length. Figure 6-8 (b) was recorded with the c-mount adjusted fully in the clockwise direction. In this instance the annotated arrow depicts a distance of 100 $\mu$ m which equates to 429 pixels in length. The measured magnifications are x19.7 and x22.3 respectively.



*Figure 6-8 objective lens x40, c-mount lens included giving a real magnification that varies with c-mount adjustment (a) c-mount adjusted fully in the anti-clockwise direction (b) c-mount adjusted in the fully clockwise direction*

When the c-mount x0.5 magnification lens is removed from the c-mount adapter, any adjustments that are made in either the anti-clockwise or clockwise direction have no effect on the system. The reason for this is that the adjustment only affected the lens height, which is no longer in place. In theory the removal of the c-mount lens should provide a magnification of x1. However in reality this is not the case. The overall magnification can be seen to have fallen short of this value, due to the c-mount providing an adjustment to the microscope objective magnification by about a magnification factor of x0.86.

Figure 6-8 (a) and (b) were taken at reduced resolution, since it is only at this resolution that the maximum frame-rate of 55 fps could be achieved. The following discussion shows that there is no difference in the magnification calculations due to the difference in resolution. Figure 6-9 shows two images (a) and (b) of a microscope stage micrometer. Both images were acquired using the DeltaPix Infinity-X digital camera. The image was magnified onto the camera sensor using the x40 magnification objective lens, and the lens of the c-mount adapter was removed. The camera has an effective sensor size of 6.656mm X 5.325mm, provided by the 1280 x 1024 pixels at full resolution. Figure 6-9 (a) was recorded at full resolution and the annotated arrow depicts a region of 100 $\mu$ m, as measured using the stage micrometer.

Figure 6-9 (b) was recorded at the reduced resolution of 640 x 480 pixels and here the annotated arrow depicts a region of 50 $\mu$ m. These distances are equal in length to 664 and 332 pixels respectively, and were previously measured using the GIMP GNU Image Manipulation Software Program Version 2.8.6. Therefore, this equates to a pixel length of 150.6nm at the sample. Multiplying this value by 1280 pixels gives the image width at the sample as 192.77 $\mu$ m for Figure 6-9 (a) and 96.38 $\mu$ m for Figure 6-9 (b). The true magnification of the

imaging system can then be found by dividing the width of the effective sensor size by the image width at the sample. Therefore in both cases the magnification is approximately  $\times 34.5$ .

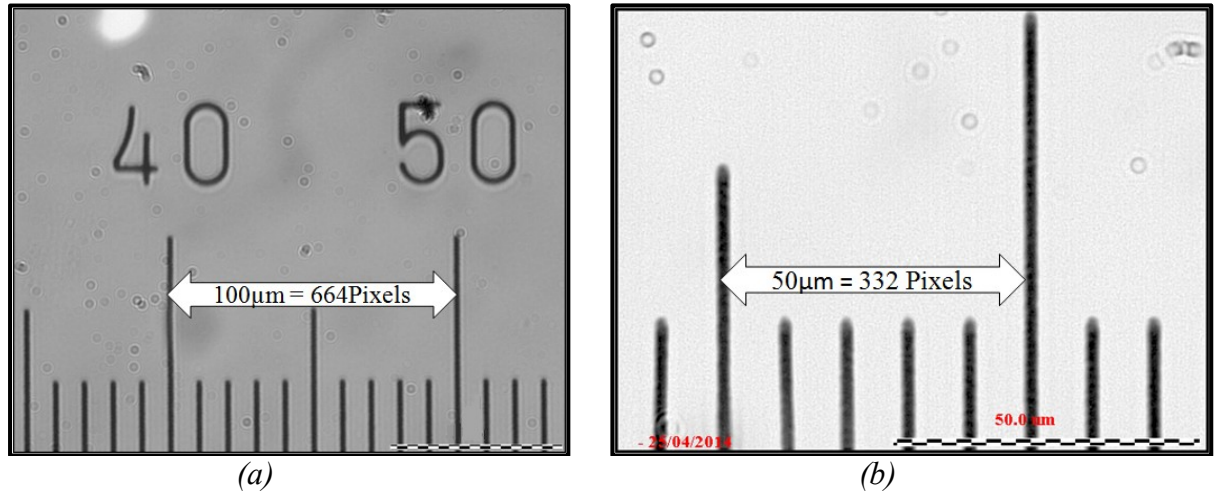


*Figure 6-9 objective lens  $\times 40$  magnification, c-mount lens extracted giving a real magnification of 34.5 (a) image at full resolution 1280 x 1024 pixels (b) image at reduced resolution 640 x 480 pixels*

These fine tuning adjustments mean that the user must calibrate the system before every use to ensure correct measurements at all times, since the adjustments to the c-mount may be altered by other users, etc. It can be seen that through the removal of the c-mount lens the system only requires a single calibration. The reason for this is that the c-mount adjustment has no effect on the magnification outcome and therefore a single magnification is maintained regardless of where the adjustment screw position lies. Therefore it can be altered by other users, etc., but this will never change the system magnification. Whereas with the c-mount lens present, it can be seen that a range of different magnifications are possible, for example when using the  $\times 40$  magnification objective lens, this would result in a possible magnification range lying somewhere between  $\times 19.7$  and  $\times 22.3$ .

A further advantage, and the initial reason for removing the c-mount lens, was to provide improved magnification of the sample. Prior to its removal, the highest magnification that

could be achieved was  $\times 22.3$  when using a  $\times 40$  objective lens. Removal of the c-mount adapter the lens was thought to increase the c-mount magnification from  $\times 0.5$  to  $\times 1$ , which has been found to be not the case. The best magnification that could be achieved using the  $\times 40$  microscope objective combined with the lens-less c-mount adapter was  $\times 34.5$ . This makes the revised c-mount magnification nearer to  $\sim \times 0.86$ , rather than  $\times 1.0$ .

A visual inspection of the microscope's optical pathway shows that the microscope and camera images are not parfocal. That is to say that a user can view a sharp and focused image of the sample plane through the microscope's binocular eye pieces. However, the corresponding image of the sample plane, displayed on the computer monitor, is found to be not "in focus". The image displayed on the monitor can be brought into sharp focus by adjusting the height of the microscope's objective lens. Inevitably this course of action renders the image, as viewed through the binocular eye pieces, to be now no longer "in focus". The images from the binocular eye pieces and the camera show that there is a length difference between the two optical pathways, which manifests in observable differences in the focused image that is provided by the alternate viewing optics. Therefore this suggests that the revised c-mount adapter magnification of  $\times 0.86$  could be improved to provide a true  $\times 1$  magnification, via the use of spacers to lengthen the optical pathway and in the process improve the parfocality of the microscope and camera viewing optics. It was found that the addition of a 35mm length spacing tube, fitted to the c-mount adapter, created a real magnification of  $\times 40$ .

#### **6.4.2     *INLINE OPTICAL TAP***

The inline optical tap is used to monitor the optical power at the sample. The optical tap photo detector receives 1% of the laser beam's output power and produces an output in terms of a

voltage. The output voltage from the tap must be calibrated against the output from an optical power monitor. The output from the optical power monitor and the output from the optical tap are combined and interpolated in a LabView virtual instrument (.vi), thereby allowing the optical tap output to be converted from volts to power in Watts in real time.

Although the optical tap is employed to measure the optical intensity at the sample, its location within the system is not immediately prior to the sample, but is actually located at a certain distance before the light exits the tapered optical fibre tip to irradiate the sample. The distance that the optical tap is located from the sample is dictated by the length of fibre that has been fusion spliced to the output optical fibre of the inline optical tap. This initial length of fibre is inherently reduced during the process of the fabrication of new tapers applied to the distal end. The new tapers are formed either to replace damaged tapers, or to make improvements in the optical output properties of the taper.

#### ***6.4.2.1 CALIBRATION SETUP***

Figure 6-10 shows the set-up of the optical components and monitoring equipment required for calibration of the inline optical tap. The electrical output cables from the inline optical tap photo detector are connected to a USB-2404-UI DAQ data acquisition module, which is linked to a PC via a USB connection. The remaining 99% of the optical output from the optical fibre's distal end is collected by the S144A PIN InGaAs integrating sphere optical sensor, which is linked to the PM100 optical power monitor via an RS232 interface. The PM100 optical power monitor provides real-time measurements of the optical output power that is exiting the optical fibre's distal end. The measurements are also transmitted from the PM100 optical power monitor, via a RS232 to USB interface converter, for display on a PC.

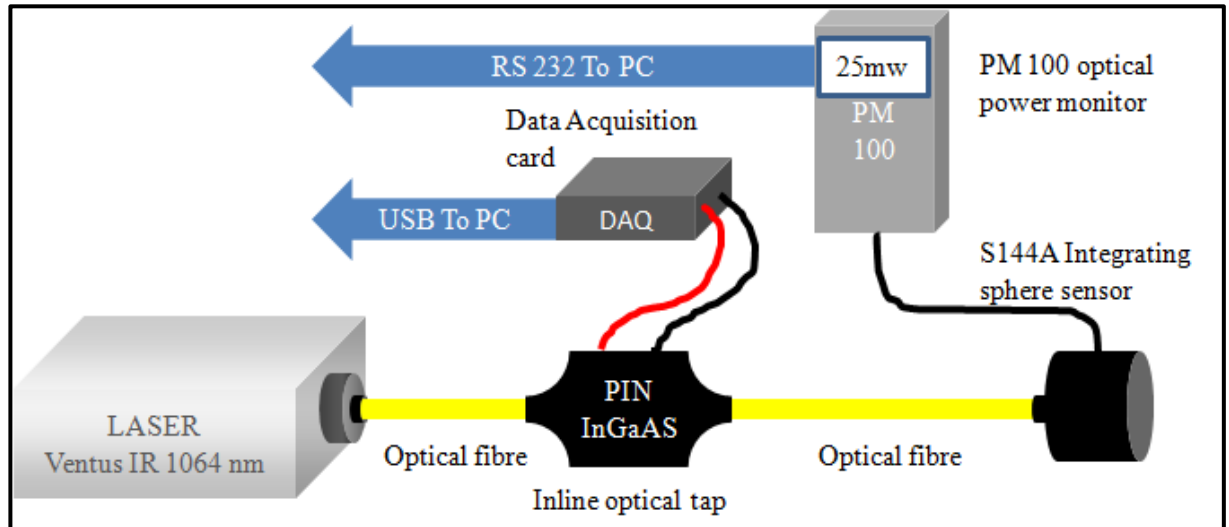


*Figure 6-10 setup for calibration of the inline optical tap*

Two LabView virtual instrument (.vi) programs for data monitoring and analysis are installed on the PC. The first is proprietary software that is shipped with the PM100 optical power monitor, offering remote monitoring of the device via the graphical user interface as shown in Figure 6-11<sup>17</sup>.

<sup>17</sup> The PIN InGaAs detector with integrating sphere is an optical sensor that is specifically designed for detecting and measuring optical power measurements independent of beam shape, entrance angle and polarisation. The PM 100 is a digital optical power meter that displays the output recorded by the sensor. (see Section 5.6.2)

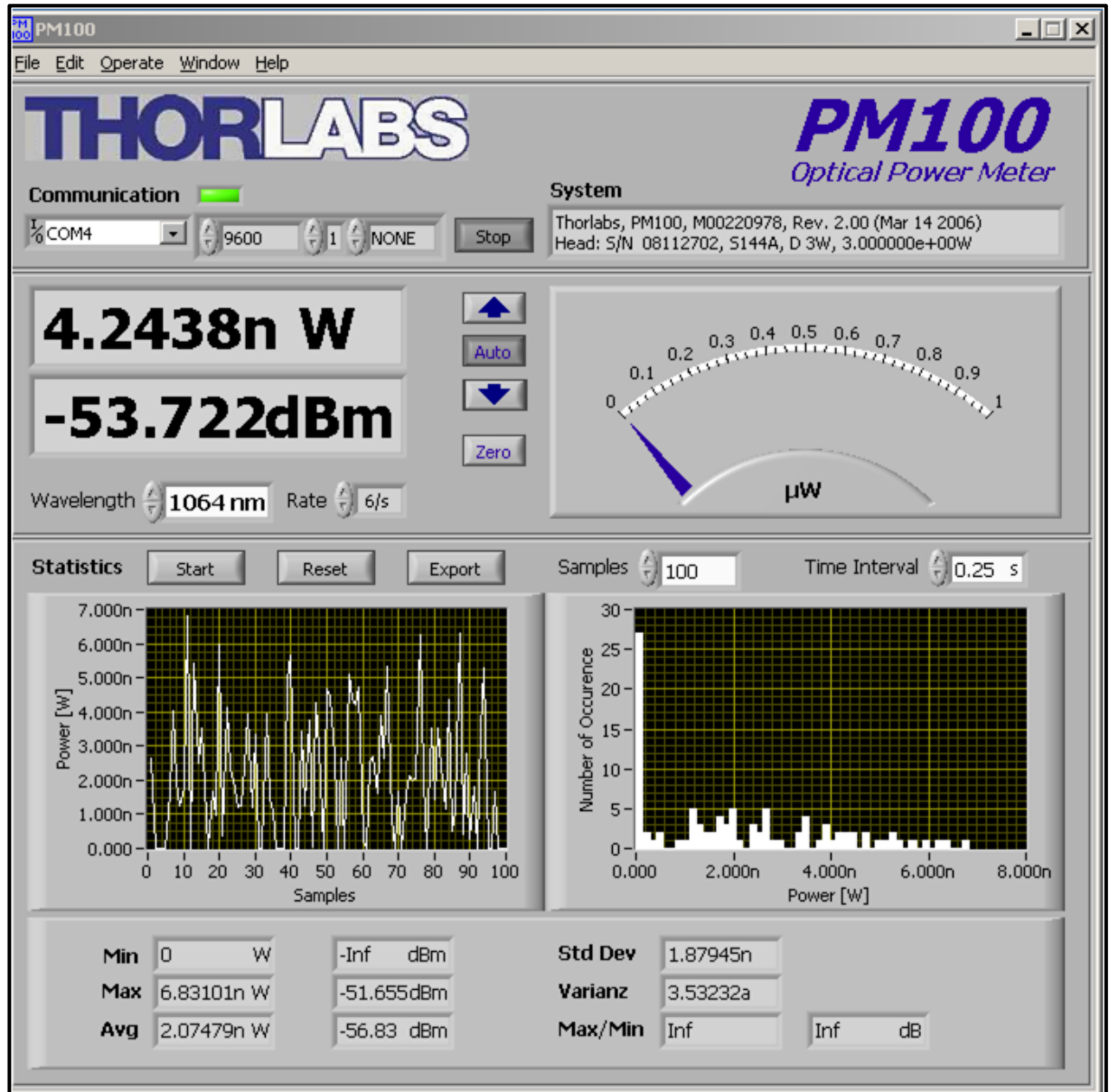


Figure 6-11 Thorlabs PM100 optical power meter virtual instrument graphical user interface

The second virtual instrument was developed in house ([Ross, 2011](#)), and serves three purposes namely to;

1. Receive, record and display the output voltage data from the inline optical tap

2. Interpolate the voltage data and the optical power data, from the inline optical tap and the optical power monitor respectively, and to display the resultant optical power that is interpreted to be at the sample
3. Display temperature data for both the optical trapping shroud and the PCR machine lid, and to provide an “out of limit” temperature warning to the user

Figure 6-12 illustrates the graphical user interface for the second .vi. This .vi receives the optical tap voltage data. The two sets of maximum value data, taken from the optical tap and the optical power monitor, are then interpolated within the LabView code. The interpolation of the two data sets allows the voltage data to be mapped with the corresponding optical power monitor data, and displayed for laser power monitoring in real time by the optical tap.

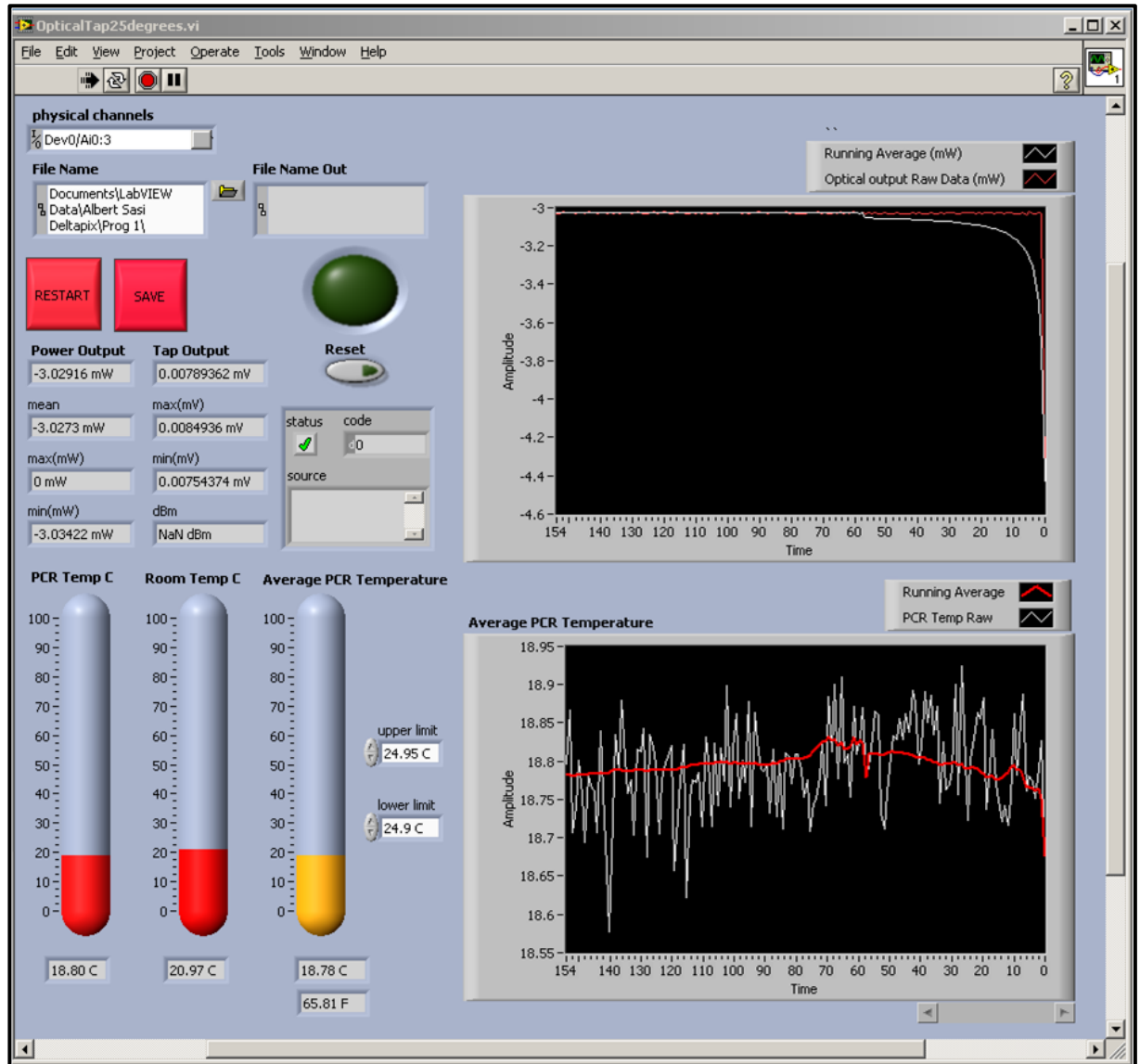


Figure 6-12 optical tap monitoring virtual instrument (*OpticalTap25degrees.vi*) developed in the LabView programming language

The additional temperature acquisition functionality of this .vi receives and displays temperature data from two locations within the optical trapping system; the first of these being the ambient temperature recorded in the optical trapping system protective shroud, whilst the second temperature measurement concerns the area within the access lid of the PCR machine, which is where the optical tap is housed.

The PCR temperature is critical to maintaining the optical tap's accuracy and must be monitored and sustained within a temperature range of between 24.95 - 25°C. If the temperature should deviate from this range, then a visible warning alert is executed to inform the user. The visible temperature alert is evident in Figure 6-12, which shows the average PCR Temperature to be 18.78°C. The alert changes the virtual thermometer's colour from red, its original colour when at the target temperature, to amber which is the alert colour when outside of the given temperature range. This visual warning gives the user a rapid indication that the temperature is out of range. This alert prompts the user to apply the necessary adjustments to the PCR machine's temperature control to bring it back into the acceptable range.

#### ***6.4.2.2 OPTICAL TAP CALIBRATION METHOD***

Prior to any device readings being made, the desired temperature within the PCR machine's lid must first be attained. After first switching on the system, a period of approximately 5 minutes is required to enable the temperature readings, from the thermocouples, to stabilise. When the temperature remains steady, adjustments are made to the PCR machine's temperature control. These temperature adjustments are made either to raise, or lower, the PCR temperature within the lid that houses the in-line optical tap, and thus maintain the in-line tap's temperature within the required temperature range of 24.9 - 24.95°C.

Maintaining the optical tap's temperature is critical to its performance accuracy. Consequently, the above practice is not limited to just the calibration procedure alone, and is a necessity before, and during, all procedures that involve acquiring the optical tap's data accurately.

The laser is activated and is initially set to 19.8% of its output corresponding to an output power of below 1 mW  $\approx$  0.2 mW. The system is then left to run for a period of ten minutes, allowing the laser to stabilise. This also serves to ensure that the maximum values for both the optical tap voltage and the PM100 power monitor data are both recorded. The two virtual instruments are equipped with a function that automatically records these maximum values. These values are manually logged into a table along with the PCR temperature readings. Once satisfied that the maximum values have been recorded, the laser output is subsequently increased. After every increment the laser is left to run for about ten minutes, during which time the desired laser output level is maintained. This is to ensure that, firstly, the laser is stable and secondly that the maximum values of the optical tap and power monitor, have been attained for that laser output % level, whilst allowing sufficient time to stabilise the temperature. The first increase is from the initial 19.8% to 20%  $\approx$  0.7 mW; the increments that are made after 20% occur in 2% step increases. The increases in laser power continue until 74% of the laser's output capacity is reached. This output level is chosen as it prevents the output power at the fibre taper's end-face exceeding the 1 W limit of the integrating sphere sensor of the PM100 optical power monitor.

The collated maximum output voltage and optical power data are manually input, as constant data values, into the interpolation data table located within the optical tap monitoring.vi code. The real-time optical tap voltage data is then interpolated with the voltage and optical power monitor data constants. This provides the optical tap monitoring.vi with the capability to interpret and display in real time the optical tap's voltage data as laser output power, measured in mW, at the sample during optical trapping procedures.

### 6.4.3 *OPTICAL FIBRE TAPER POSITIONING AND ALIGNMENT*

Once a fabricated tapered optical fibre tip has been passed as being fit for purpose, via the initial visual inspection procedure, its ability to be able to conduct 3D optical trapping must then be tested. In order to carry out the 3D trapping assessment, the optical fibre is required to be set up at the correct insertion angle to the microscope sample chamber, and aligned so that it is located centrally in the microscope's optical field of view.

First of all the double sleeve structured fibre holder is carefully guided down the optical fibre towards the optical fibre taper. The optical fibre is secured within the optical fibre holder using adhesive tape at the end furthest from the distal end of the fibre. A length of about 15mm of the tapered fibre's distal end is left protruding from the fibre holder at the opposite end to the taped region. The optical fibre holder is then secured to the length of steel bar, which provides the rigid support for the optical fibre taper, using a quick release clip fashioned from a metal cable cleat. The steel support bar is connected to a miniature rotation stage that is initially set to 0°, and thus holds the bar in a horizontal orientation. This allows the support bar and optical fibre taper to be manoeuvred without inflicting damage to the tapered end, via collisions with the microscope, when moving the fibre into position. At this point the z translation stages, of both the motorised and piezo devices, are set to their highest position in the +ve z direction. When the optical fibre taper is in position and the z translation devices are set, the thumb screw of the miniature rotation stage is adjusted, thereby rotating the support bar to the required insertion angle. When the support bar is at the correct insertion angle, the z translation devices are moved towards their lowest levels in the -ve z direction. This moves the tapered optical fibre towards the microscope sample chamber and the procedure can be observed using the camera. Care must be taken not to drive the tapered tip into the

microscope's sample chamber floor i.e. the glass microscope sample slide, because a broken taper usually results as a consequence of this action. To aid in reducing this possibility, the velocities of the z direction translation devices are reduced from  $10^{-6}$  m/s down to  $10^{-9}$  m/s.

If the taper has not reached the sample chamber floor by the time both the fine travel and coarse travel negative limits have been exhausted, then both of the z translation devices are returned in the +ve z direction to their highest settings and the rotary translation device is returned back to  $0^\circ$ . This elevates the taper away from the microscope's sample chamber, to protect it from inadvertent damage, whilst height adjustments can be made to the C1506/M adjustable mounting platform.

When the mounting platform has been sufficiently adjusted, the above method is repeated. When manoeuvring the optical fibre taper at the reduced velocity of  $10^{-9}$  m/s contact with the microscope's sample chamber floor is possible without damage being caused to the tip. Instead the optical fibre bends rather than breaks, since the contact is made by gently manoeuvring the tip rather than subjecting it to a relatively high velocity impact. As the fibre bends it begins to translate in a +ve x direction. The distance that the fibre moves in the +ve x direction is dependent upon its translation distance in the -ve z direction. Thus its course in the +ve x direction is maintained, providing that translation in the -ve z direction continues. This is visible on the PC monitor via the camera. This forward motion of the fibre taper in the +ve x direction is more prevalent at the higher insertion angle of  $45^\circ$ . However, at an insertion angle of  $10^\circ$  the movement in the +ve x direction is still detectable. Therefore, this is still a valid method for determining when the fibre initially becomes into contact with the microscope sample slide.

By slowly moving the fibre taper in the +ve z direction the taper begins to move back in the -ve x direction. Eventually the taper will stop traversing in the -ve x direction and proceed to move in the +ve z direction. This becomes evident as the taper begins to move out of view from the focal plane of the microscope's optical system. This point is taken as a reference with regard to the taper and microscope slide and allows the user to determine the correct height, at which the taper is positioned above the sample. This ensures that the fibre taper and thus the trapping zone are directly above the target particle, when at an insertion angle of  $45^\circ$ , ready for optical trapping. The fibre should be elevated to a height that is slightly higher than the target particle's diameter, for example a height of  $\approx 4\mu\text{m}$  is required for a  $3\mu\text{m}$  diameter silica microsphere and  $\approx 11\mu\text{m}$  for  $10\mu\text{m}$  diameter silica microsphere.

At an insertion angle of  $45^\circ$ , the height that the tapered optical fibre should sit above the sample depends on the actual size of the target samples which are under consideration. For example, if the sample to be optically trapped was a yeast cell with a diameter of  $6\mu\text{m}$ , then the taper height must be greater than the yeast cell diameter, at say  $7\mu\text{m}$ . This is because the taper is inserted at a near vertical orientation to the sample and ideally should sit directly above the target.

At an insertion angle of  $10^\circ$  the height of the taper can be kept near to the contact point of reference, either touching, or just above, the microscope slide. This is because the tapered optical fibre's insertion angle is now at a near horizontal orientation to the sample and will be targeting samples from their side elevation, rather from above.

When the height of the tapered optical fibre has been correctly established, the x and y position must be calibrated. This is achieved by first moving the tapered fibre in the +ve z

direction, until it is not in contact with the sample chamber floor. Then the x and y translation devices are set to their midway positions. These correspond to 2.5 mm for the x and y motorised translation devices and 50  $\mu\text{m}$  for the x and y piezo devices.

At this point the lowest possible microscope objective magnification is selected, which is x4 in this case. Then the switchable heavy duty magnetic base of the translation assembly's tall support structure is switched off. This allows the tall support structure to be manually manoeuvred to allow the optical fibre taper to be directed to the region within the sample chamber that corresponds to the centre of the field of view of the image plane.

The microscope objective is then increased to the next available magnification, which is x10 in this case, and the above procedure is repeated. This formal procedure is continued until the optical fibre taper has been centred within the field of view, for the requisite optical trapping magnification of x40.

This arrangement of the optical fibre taper coupled with the setting of the x and y translation devices at their mid-points, allows the maximum range and symmetrical freedom of movement for the optical fibre taper, so that it can be located anywhere within the region of the field of view of the microscope optics and the camera. In this manner the maximum amount of travel afforded to the tapered optical fibre, in the x and y directions of in the sample plane, is 5.1mm.

**CHAPTER SEVEN**  
**EXPERIMENTAL PROCEDURES,**  
**RESULTS AND DISCUSSION**

## **EXPERIMENTAL PROCEDURES, RESULTS AND DISCUSSION**

This chapter presents the experimental procedures and results that were obtained during the development and characterisation of the T-FOTs system, the first of which is the visual inspection of tapered optical fibre tips. This procedure permits the early exclusion of any damaged tapered optical fibre tips from any further test procedures. Tapers that qualify from this early quality check via the initial visual inspection are integrated into the optical system and are subsequently tested for their suitability to optically trap in 3D.

The initial optical trapping tests were conducted at an optical fibre insertion angle of  $45^\circ$ . This was followed by an investigation as to why 3D optical trapping using a single optical fibre is believed to be impossible at a fibre insertion angle of  $<20^\circ$  with respect to the sample chamber floor. From this investigation a hypothesis is proposed here, which led to the development and testing of three optimised tapered optical fibre tips, each of which were capable of 3D optical trapping at an insertion angle of  $10^\circ$ .

The observed changes in the optical trapping dynamics, whilst trapping at an insertion angle of  $10^\circ$  in comparison to optical trapping at an insertion angle of  $45^\circ$ , were the precursor to a further experiment, which was designed to determine the maximum optical trapping range for the optimised tapered fibres.

Optical trap characterisation experiments have been conducted here to determine the ratio of the optical trapping forces, with respect to the trapping laser intensity. This was followed by an examination of the T-FOT system's ability to trap live biological cells of varying compositions and sizes.

The final testing regime in this section involved recreating the optimised tapered tips to check the micropipette puller's ability to reproduce the tapered optical fibre tips' geometric profiles, with the aim of generating optical performances that are comparable to the originals.

## 7.1 VISUAL INSPECTION OF TAPERED OPTICAL FIBRE TIPS

The criteria sought during the visual inspection concerns the tip formation. For example a potentially 'good' tip will have a completely formed taper that exhibits a parabolic profile, such as that shown earlier in **Error! Reference source not found.**(a). In contrast a definite 'bad' taper is one that has been abruptly snapped, such as that shown in **Error! Reference source not found.**(b). Such a taper possesses a rough and uneven end-face, and in all probability, is due to a lack of heat and thus viscosity at the point of fracture.

The visual template for a good taper was initially taken from literature, for example ([Liu et al., 2006](#)). In this example 3D optical trapping had been achieved using a solitary SMF that had been tapered using the heating and drawing method. However, the visual inspection method is only useful for distinguishing between the potentially 'good' and 'bad' tapers, such as those shown in **Error! Reference source not found.** (a) and (b) respectively. However, it offers no guarantee that a tapered tip can actually perform 3D optical trapping, regardless of the fact that its appearance may be of an ideal profile. The reality is that the only viable test that is capable of determining the suitability of a tapered tip is to incorporate the tapered optical fibre tip into the optical system and physically test whether, or not, it can optically trap in 3D.

## 7.2 TEST FOR 3D OPTICAL TRAPPING AT AN INSERTION ANGLE OF 45°

The literature suggests that optical trapping, using a single optical fibre, cannot be performed at insertion angles below 20°. Optimal optical trapping efficiencies have previously been

recorded at insertion angles of between 40°-50°. Therefore it was within this insertion angle-range that the first attempts, at 3D optical trapping, would be made within this research programme. The reasoning behind this rationale was that a working 3D optical trapping taper would be initially required to be able to form an investigation as to why trapping at lower insertion angles is not possible.

The development of suitable tapered fibre tips, for 3D optical trapping via the heating and drawing process, can be considered to be something of a black art, relying mainly on a process of trial and error. This in itself is a very time-consuming enterprise, especially when immediate positive results fail to materialise. It is the integration of the tapered fibre tip within the system that consumes much of the time, the reason being that in order to physically test the fibre taper's ability to create a 3D optical trap, the tapered tip has to first be fusion spliced within the optical system, inserted at the correct insertion angle and aligned centrally within the microscope's sample chamber FOV, all of which takes place after the inline optical tap has been calibrated, which is a further time consuming procedure in itself.

Development of the first tapered fibre optic tip was a frustrating endeavour, as every tip that was initially pulled all failed to produce a functional 3D optical trap. Indeed it took two years and the disposal of 100's of meters worth of unusable optical fibre tapers before the first 3D optical trapping taper was demonstrated.

Table 7-1 shows the program parameters that were applied to the Sutter P2000/F micropipette puller device to produce the first tapered optical fibre tip that was capable of 3D optical trapping. This tip is named tapered tip number 44, which is the program number of the Sutter P2000/F micropipette puller, the device that is used to fabricate the taper. Throughout this

thesis all additional optical fibre tapers that are discussed will also be identified by their corresponding P2000/F program number.

*Table 7-1 Sutter P2000/F micropipette puller program parameters for the first single tapered fibre capable of 3D optical trapping- taper number 44*

<b>Program Number</b>	<b>Heat</b>	<b>Filament</b>	<b>Velocity</b>	<b>Delay</b>	<b>Pull</b>
44	320	002	022	128	000
	320	002	022	128	175

### **7.2.1 3D TRAPPING TEST FOR TAPERED FIBRE OPTIC TIP NUMBER 44**

Due to the arrangement of the optical fibre, which is at an insertion angle of  $45^\circ$  with respect to the microscope's sample chamber, there may be occasions when an optically trapped microsphere is not under the influence of 3D optical trapping. The reason for this is that at such an insertion angle the tapered optical fibre is at an almost vertical orientation to that of the microscope sample chamber. When in this orientation a weakly focused laser beam might at first appear to be trapping a microsphere in a stable 3D trap. However, the microsphere might only really be under the influence of the radiation pressure force, which is only capable of 2D manipulation. Recalling previous discussions a weakly focused laser will pull a microsphere, which is located at the fringes of the beam, into the high intensity region of the laser beam's central axis due to the gradient force. Once on axis, the microsphere is propelled in the direction of the laser beam's propagation due to the dominant scattering force. However because of the near vertical orientation of the fibre taper the microsphere's movement in the direction of the laser beams propagation is halted by the microscope sample chamber floor. This action traps the microsphere and allows the microsphere to be manoeuvred in both the X and Y spatial planes, but not in the Z plane.

Therefore, each taper was subjected to a physical test to determine its suitability for 3D optical trapping and the first of these to successfully negotiate this test was tip number 44.

The tapered optical fibre tip was set up and arranged within the sample chamber as previously discussed in Chapter 6. A sample solution was prepared consisting of 3 $\mu$ m silica microspheres (Bangs Laboratories) diluted 1:600 parts of de-ionised water. A drop of Triton-X 100 surfactant was added to the diluted solution to eliminate microsphere coagulation. To reduce the density of the sample microspheres 400 $\mu$ l of deionised water is first applied to the microscope sample slide and then a single drop, of the diluted microsphere solution is then added to the 400 $\mu$ l of water using a micro-pipette dispenser. This ensures that the sample is not overly saturated with target microspheres and permits the trapping and isolation of a single microsphere without interference from its neighbours. The reduction in microsphere density within the medium also has the advantage of simplifying the analysis of the recorded video footage.

The tapered optical fibre tip is manoeuvred about the sample chamber, using a combination of the motorised and piezo x and y translation stages, until it can be aligned with a single microsphere. Once a silica microsphere is located within close proximity to the tapered optical fibre tip, then the laser is activated and the microsphere is observed. If the optical fibre taper fails to create an optical trap, then it is discarded.

However, once optical trapping takes place, the taper is then subjected to a simple test to validate whether it is indeed capable of 3D optical trapping and not merely 2D, as discussed above. The validation is achieved by elevating the tapered optical fibre tip whilst in the process of optically trapping a microsphere. If 3D optical trapping occurs then both the fibre taper and the microsphere are synchronously elevated. This is evident since the microsphere is maintained at the tip of the fibre and both are seen to become unfocused to the eye as they leave the focal view of the microscope objective. However if only 2D manipulation is

observed, then the behaviour of the fibre taper and the micro-sphere differs, as depicted in Figure 7-1 . Here the optical fibre is inserted at an angle of  $45^\circ$  with position (1) showing it at its initial location with the microsphere located at position (a). As the fibre is elevated to position (2) the image of the tapered fibre tip becomes unfocused as it moves out of the focal region of the microscope objective. The microsphere, on the other hand, is guided along the laser beam and pushed away from the fibre's end face to position (b). The higher the tapered fibre tip is elevated, i.e. up to position (3); its image becomes more indistinct as it moves further from the focal region of the microscope objective. However this is not the case for the microsphere, which fails to be elevated, since it is only under the influence of 2D optical forces. The microsphere's image therefore, is maintained in sharp focus, as it remains seated on the microscope chamber floor at position (c). Since the microsphere remains guided within the beam, by the gradient force, when the optical fibre descends back to its original position (1), then the microsphere also returns back to its origin at position (a).

The higher the tapered fibre tip is elevated, i.e. up to position (3); its image becomes more indistinct as it moves further from the focal region of the microscope objective. However this is not the case for the microsphere, which fails to be elevated, since it is only under the influence of 2D optical forces. The microsphere's image therefore, is maintained in sharp focus, as it remains seated on the microscope chamber floor at position (c). Since the microsphere remains guided within the beam, by the gradient force, when the optical fibre descends back to its original position (1), then the microsphere also returns back to its origin at position (a).

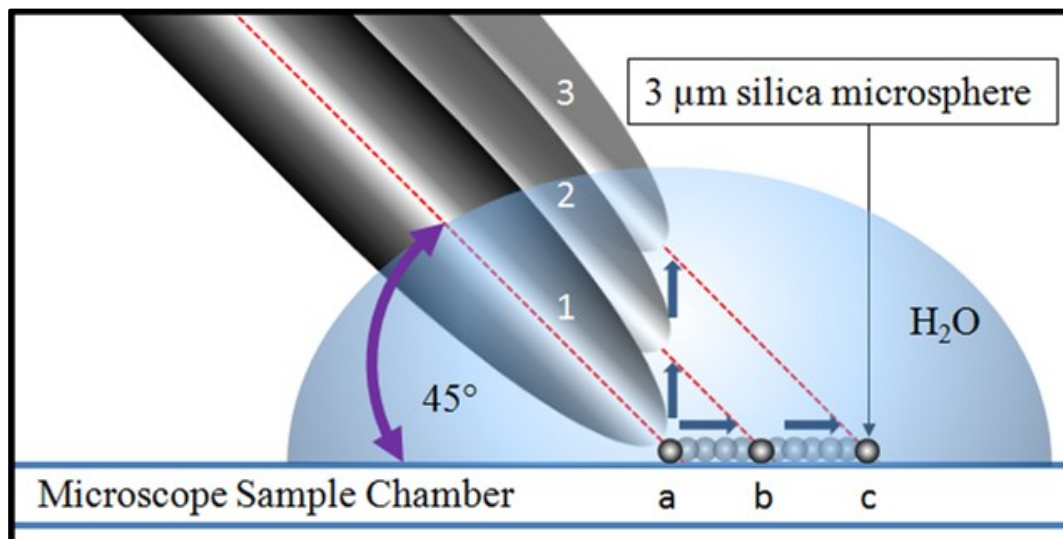


Figure 7-1 trapping in 2D; as the tapered optical fibre taper is elevated in the +ve Z direction the microsphere is driven away from the tapered optical fibre tip in the

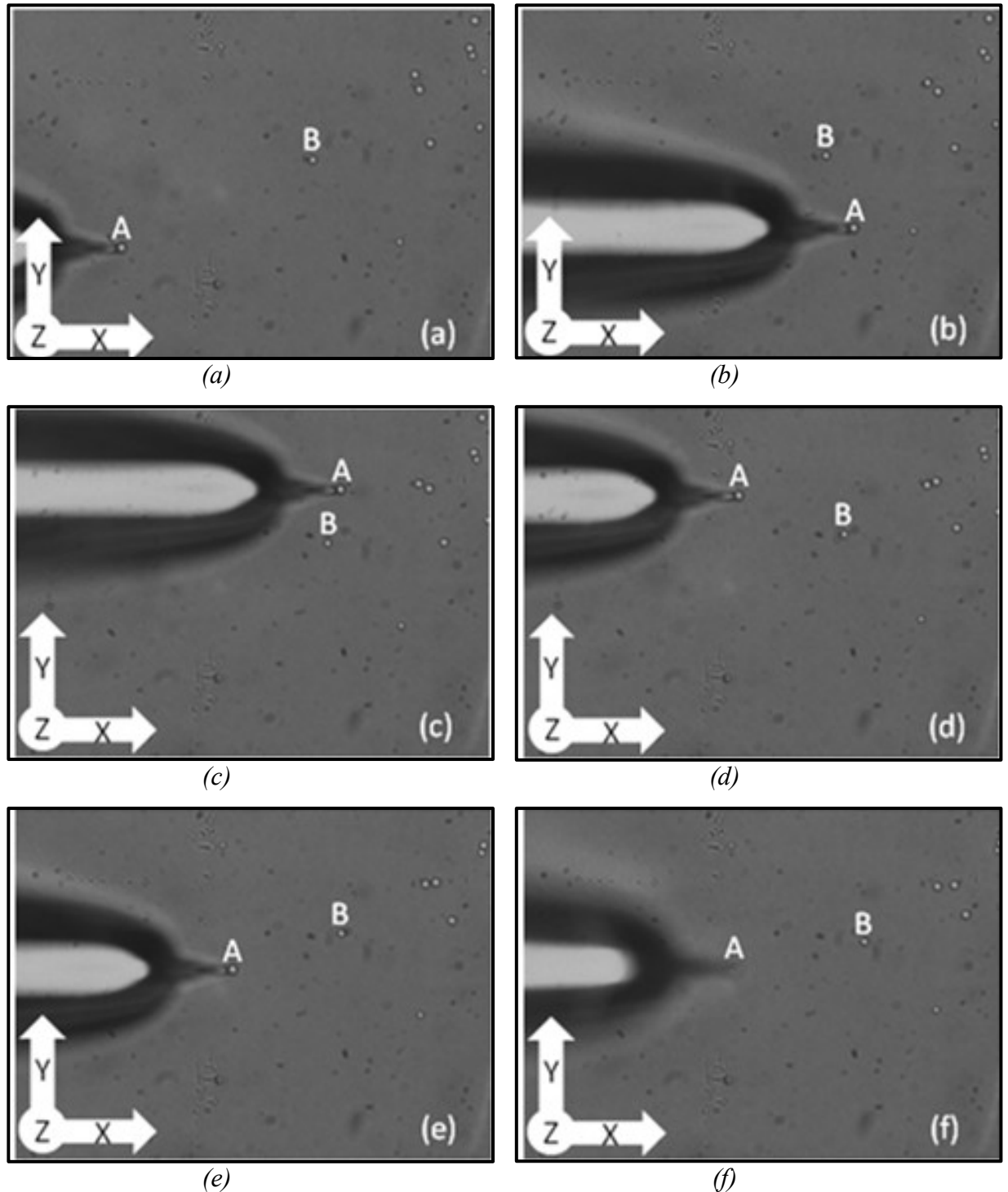
*direction of the laser beam's propagation and remains seated on the microscope sample chamber floor.*

During 3D optical trapping events both the tapered optical fibre tip and an optically trapped particle will synchronously elevate. This outcome is clearly detectable since both the tip and the microsphere depart from the focal plane, resulting with an image that is no longer in focus, such as that demonstrated in Figure 7-2(f).

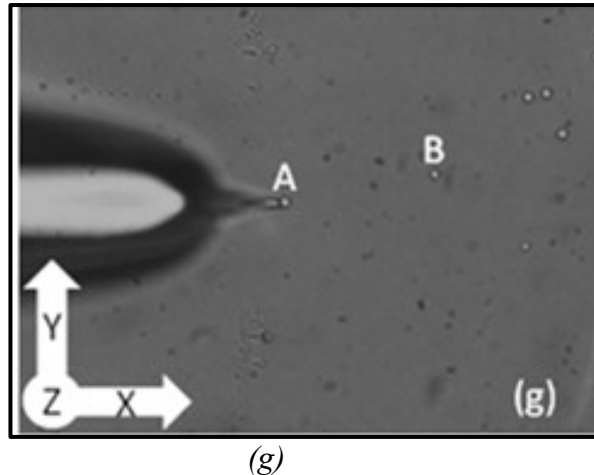
### **7.2.2 RESULTS - 3D TRAPPING TEST**

Figure 7-2 shows images (a) - (f) and Figure 7-3 shows image (g) taken from the video sequence of the first successful trapping experiment, recorded at 30 fps using the DeltaPix Infinity X CMOS video camera. The images show the tapered fibre optic tip number 44, at an insertion angle of  $45^\circ$  to the sample chamber floor. At the end of the tapered fibre is an optically trapped  $3\ \mu\text{m}$  diameter silica micro-sphere labelled (A).

A  $3\ \mu\text{m}$  diameter silica microsphere labelled (B) is located on the microscope sample chamber floor and is free to drift in the surrounding medium (water) due to Brownian motion. Microsphere B is used as a reference point, the optically trapped sphere A is moved in an anti-clockwise direction around microsphere B at a velocity of  $10\ \mu\text{m/s}$ . The directional sequence of the tapered fibre optic tip is (a) origin (b) +X direction (c) +Y direction (d) -X direction (e) -Y direction (f) +Z direction (g) -Z direction. During vertical translations in the +Z direction it is clear in (f) that both the taper and the silica microsphere both travel together. This is evident as they both leave the focal view of the microscope. Returning the tapered fibre optic tip back in the -Z direction drives both the tapered tip and microsphere back towards to the focal point as shown in (g).



*Figure 7-2 X-Y trapping (a) the tapered fibre probe and 3µm diameter silica micro-sphere trapped at the fibre end, (b)-(e) The Piezo translation stage moves the fibre probe, directing sphere A in an anti-clockwise direction around sphere B, in the directional sequence +X, +Y, -X, -Y (f)-(g) Z-Trapping (f) the trapping fibre is moved in the +Z direction and both the fibre and the silica sphere can be seen to be out of focus (image (g) continued on the following page in Figure 7-3(g))*



*Figure 7-3 (continued from previous page in Figure 7-2 (a)-(f)) (g) the trapping fibre is moved in the  $-Z$  direction and both the fibre and particle A are seen to have come back into focus*

Elevation of a trapped microsphere could be achieved with laser output powers of as little as 20 mW. Also the microsphere could be maintained in the elevated position when the laser power was reduced down to 1mW. For laser intensities below 1mW the microsphere would break free from the optical trap and fall back to the sample chamber floor. This experiment demonstrates that the  $3\mu\text{m}$  diameter optically trapped microsphere, labelled (A) in Figure 7-2 and Figure 7-3, has been confined and manipulated in a single beam gradient force 3D optical trap, or fibre based optical tweezers.

### 7.3 OPTICAL TRAPPING AT $10^\circ$ INSERTION ANGLE

The information from literature suggesting that 3D optical trapping is not possible, using a single optical fibre, at insertion angles of  $<20^\circ$ , led the author to investigate why this could be happening? Was it purely an optical problem? Or could there be some other underlying reason for this limitation? On reflection it is not immediately obvious as to why the insertion angle should have any bearing on the outcome, especially considering that the laser beam is

incident upon a spherical dielectric object. So what additional factors could possibly contribute to this phenomenon?

Regardless of the perceived limitations expressed in the literature the following attempt was made to optically trap in 3D using tip number 44 at an insertion angle of  $10^\circ$ . However initially 3D optical trapping no longer occurred when using the moderate optical power outputs that had previously successfully trapped in 3D at a fibre insertion angle of  $45^\circ$ . Undeterred by this initial and expected response, the optical power was subsequently increased by 10 mW increments until a threshold value of 600mW. Initially and as expected, optical trapping failed to materialise. However, an output power of 520 mW, as monitored by the in-line optical tap, the unexpected happened and the fibre taper number 44 successfully optically trapped a  $3\mu\text{m}$  silica micro-sphere in 3D. This unanticipated but positive result opened up a new line of investigation, which led to the following hypothesis as to why gradient force 3D optical trapping failed at low insertion angles.

### ***7.3.1 INVESTIGATIONS INTO TRAPPING DEGRADATION AT INSERTION ANGLES BELOW $20^\circ$***

Consider that the diameter of a cleaved single mode fibre (SMF), inclusive of its acrylate outer buffer coating, is  $\approx 245\ \mu\text{m}$ , as shown in Figure 7-4. If the fibre is resting upon a flat horizontal surface, the axis of the core would be at a height of  $122.5\ \mu\text{m}$  running parallel to the surface. If a silica microsphere of  $3\ \mu\text{m}$  diameter was at rest on the microscope sample chamber floor, then the centre of the sphere would still be  $\approx 121\ \mu\text{m}$  below the centre of the beam axis emerging from the fibre core.

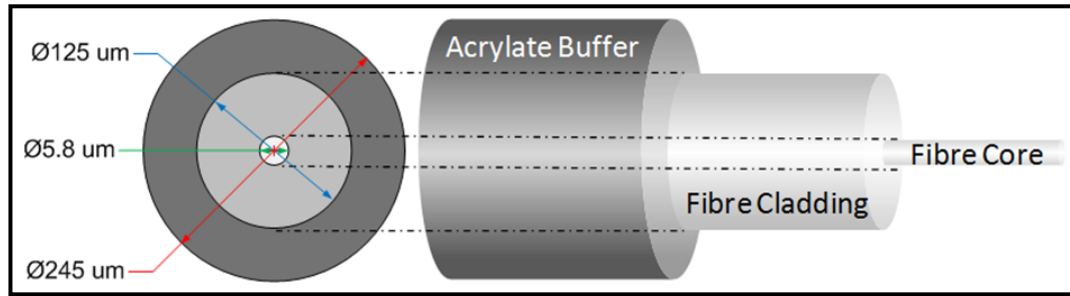


*Figure 7-4 Dimensions of Nufern 1060XP single mode optical fibre*

Strictly speaking this is not an exact description of the optical trapping scenario for two key reasons. Firstly the intention is to incline the optical fibre with an insertion angle of  $10^\circ$  to the base of the sample chamber, rather than being horizontally placed along the sample chamber floor; secondly the fibre is to be tapered to a smaller diameter and not simply cleaved and maintaining its natural diameter. This simple examination of the fibre dimensions provided an avenue for further investigation as to why fibre based optical trapping should fail at insertion angles of  $\leq 20^\circ$ .

The use of an inverted optical microscope provides the user with a view from below the specimen plane, which results in an inverted plan view. To fully understand the above problem, through the visualization of the optical fibre taper's geometric profile, a view from a side elevation is required. Figure 7-5 and Figure 7-6 portray a large diameter, short tapered optical fibre tip that is oriented incident to the microscope sample chamber at insertion angles of  $45^\circ$  and  $10^\circ$  respectively. The diagrams are not exact in terms of taper length, shape, and diameter, or to scale with respect to the size of the microsphere. However they serve as a visual aid to understanding the optical trapping problems associated with the optical fibre taper at low insertion angles. At an optical fibre insertion angle of  $45^\circ$ , and when sufficiently elevated, the fibre taper sits directly above the subject microsphere allowing easy 3D trapping to occur as shown in Figure 7-5. However, when using the same large diameter, short tapered

tip at the shallower insertion angle of  $10^\circ$  difficulties ensue when attempting to achieve 3D trapping.

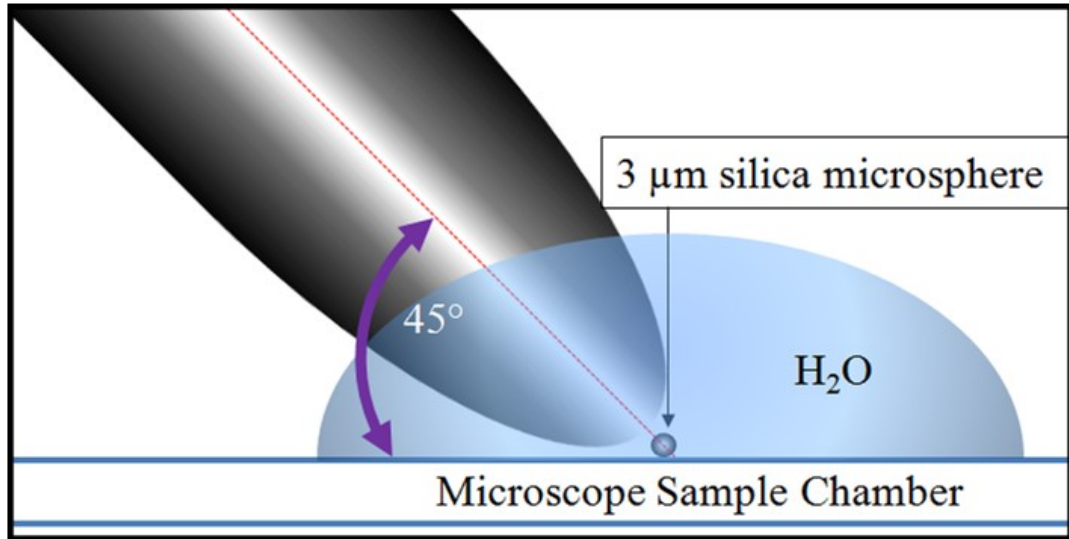


*Figure 7-5 large diameter, tapered optical fibre tip at an insertion angle of  $45^\circ$*

The implications of adopting such a tip at an insertion angle of  $10^\circ$  can be seen in Figure 7-6. The underlying problem is that the fibre is now almost parallel to the microscope sample chamber floor. As a result the combination of the short taper length, the large diameter tip and the low insertion angle means that that the trapping zone, which is located around the central axis of the tapered fibre's end face, is now somewhat elevated above the surface of the sample chamber's base surface.

This means that in order for the microsphere to enter the trapping zone it has to undergo a significant elevation in the vertical positive  $Z$  direction. Unsurprisingly such an elevation can only be achieved through the generation of very high optical forces, as previously demonstrated. However the high laser intensities associated with such forces are not acceptable for use in cell trapping applications, such as the one envisaged here. The reason for

this is that extremely high laser intensities, such as those recorded earlier, will undoubtedly result in cell damage or even cell death.

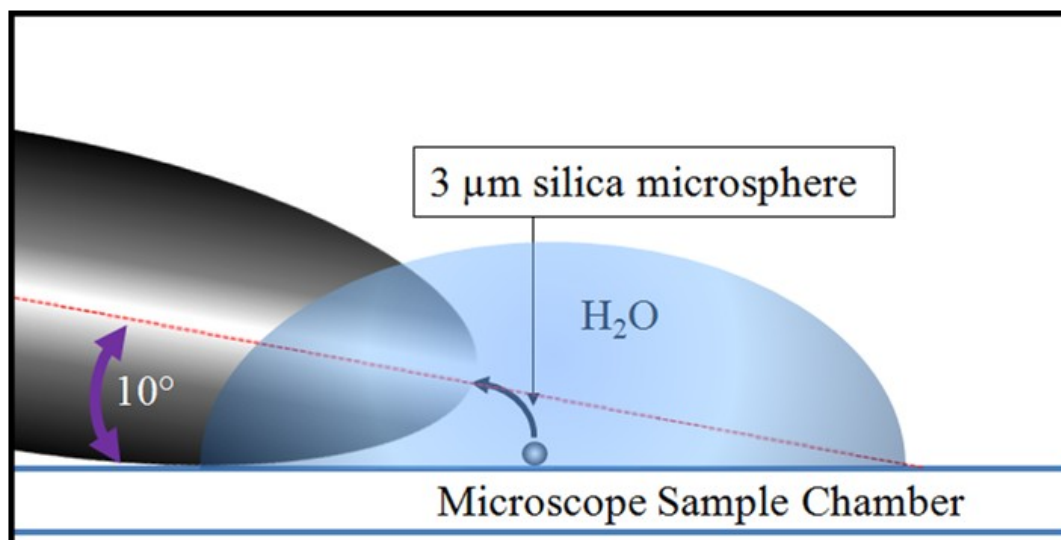


Figure 7-6 large diameter tapered optical fibre tip at an insertion angle of  $10^\circ$

### 7.3.2 FIBRE TAPER OPTIMISATION FOR 3D OPTICAL TRAPPING AT AN INSERTION ANGLE OF $10^\circ$

For biological samples, such as cells, to maintain viability during optical trapping procedures laser intensities must be maintained below a certain threshold. The typical laser intensities that can be employed may be as high as 340 mW, at a wavelength ( $\lambda$ ) of 1064 nm, depending on the experiment conducted ([Gross, 2003](#)). Therefore, it is clear that increasing the optical power beyond this value would not be a viable solution. This excludes tip number 44 as a feasible option since it requires in excess of 500 mW of focused laser output power at the sample to optically trap in 3D at a  $10^\circ$  insertion angle.

An alternative method to increase the optical forces being produced would be to optimize the laser beam's focus. This in turn would generate a steeper intensity gradient and thus facilitate an increased gradient force. This could be achieved by altering the geometric profile

of the tapered optical fibre tip. Moreover by tapering the fibre in such a way so as to coerce the laser beam's focal point so as to be nearer to the trapping subject 3D optical trapping at low insertion angles could be realised using only moderate laser intensities. This course of action would potentially offer a superior and "cell safe" alternative to simply increasing the optical output power. Such a fibre taper would be required to exhibit a longer taper length and a reduction in tip diameter similar to that portrayed in Figure 7-7 .

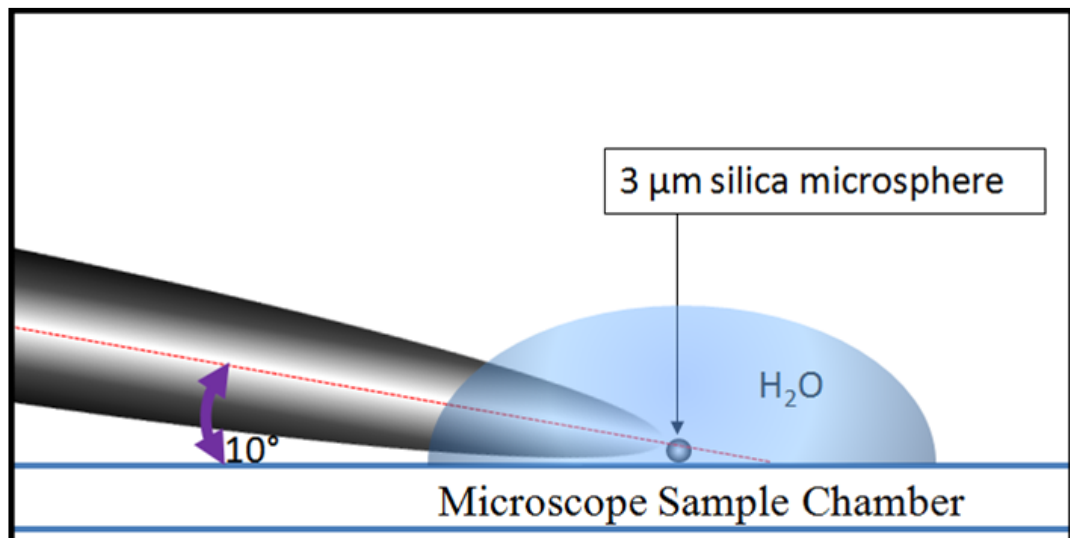


*Figure 7-7 proposed optimized optical fibre taper geometry possessing a longer taper length combined with a smaller diameter tip to gain closer proximity to the sample*

However, there is the danger that this type of taper profile could also prove to be unfeasible for optical trapping, since the long taper and small diameter, tip may result in the optical fibre losing its integrity. This would lead to the fibre becoming predisposed to high optical losses. Such losses would effectively reduce the taper's ability to efficiently transport the laser light along its length due to TIR. The knock on effect of this however, would be the tapered fibre tip's inability to focus the light, which would inhibit its capability to form an effective 3D optical trap.

### 7.3.3 *DEVELOPMENT OF NOVEL OPTIMISED TAPERED FIBRE OPTIC TIPS FOR 3D OPTICAL TRAPPING AT AN INSERTION ANGLE OF 10°*

In an attempt to increase the likelihood of 3D optical trapping at the near horizontal insertion angle of 10° three additional working tips were successfully developed. The parameter values for the P2000/F programs that were used to develop the tapered optical fibre tips can be seen in Table 7-2. Each of the tips underwent and passed the required testing to determine their suitability for 3D trapping of a 3µm silica microsphere at a fibre insertion angle of 10°.

*Table 7-2 parameter values for the P2000/F Micro-Pipette Puller Used to Fabricate the Optical Fibre Tapers<sup>18</sup>*

<b>Program Number</b>	<b>Heat</b>	<b>Filament</b>	<b>Velocity</b>	<b>Delay</b>	<b>Pull</b>
<b>44</b>	<b>320</b>	<b>002</b>	<b>022</b>	<b>128</b>	<b>000</b>
	320	002	022	128	175
92	340	002	023	128	000
	340	002	023	127	175
94	325	002	023	128	000
	325	002	023	127	175
96	320	002	023	128	000
	320	002	023	127	175

The three new custom tapered fibre tips that were developed are named tip numbers 92, 94 and 96 respectively. The tips are an improvement on the original tip number 44, because they have a longer taper and a reduced diameter tip. However, and more importantly, they can each perform the required 3D optical trapping at a fibre insertion angle of 10°. Figure 7-8 (a) shows the dimensions of the original tip number 44 in comparison to the three new tips that are numbered 92, 94 & 96, which are shown in Figure 7-8 (b, c and d) respectfully. It must be noted here that the dimensions of the fibre tapers differ somewhat from the dimensions given in ([Ross et al., 2014](#)). The reason for this is that it has since become apparent that the system magnification was found to be nearer to x35 rather than x40.

<sup>18</sup> The parameter values of the P2000/F micropipette puller are discrete values only and have no SI units assigned to them.

At the end of tip number 44 there is a needle-like-like portion protruding from the parabolic end. However during the development of the three additional tapers 92, 94 and 96 the needle-like portion became deformed. The curly deformation is a result of the elastic recoil of the extremely thin tapered region as the narrow viscous material of the fibre is divided into two parts.

As a result the deformed section was physically removed, using a fairly coarse method, to diminish any unwanted optical effects. This involved snapping off the deformed region by wiping an Isopropanol soaked wipe along the fibre in the direction towards the taper's distal end. In an effort to provide an even and smooth end-face finish the fibre taper was then subjected to polishing using a piece of final polishing sheet (LCFC, ThorLabs, UK). These polyester film sheets are coated with precision-grade silicon dioxide and are normally used in the last step in the process of polishing fibre end-faces that have been glued into a ceramic ferrule.

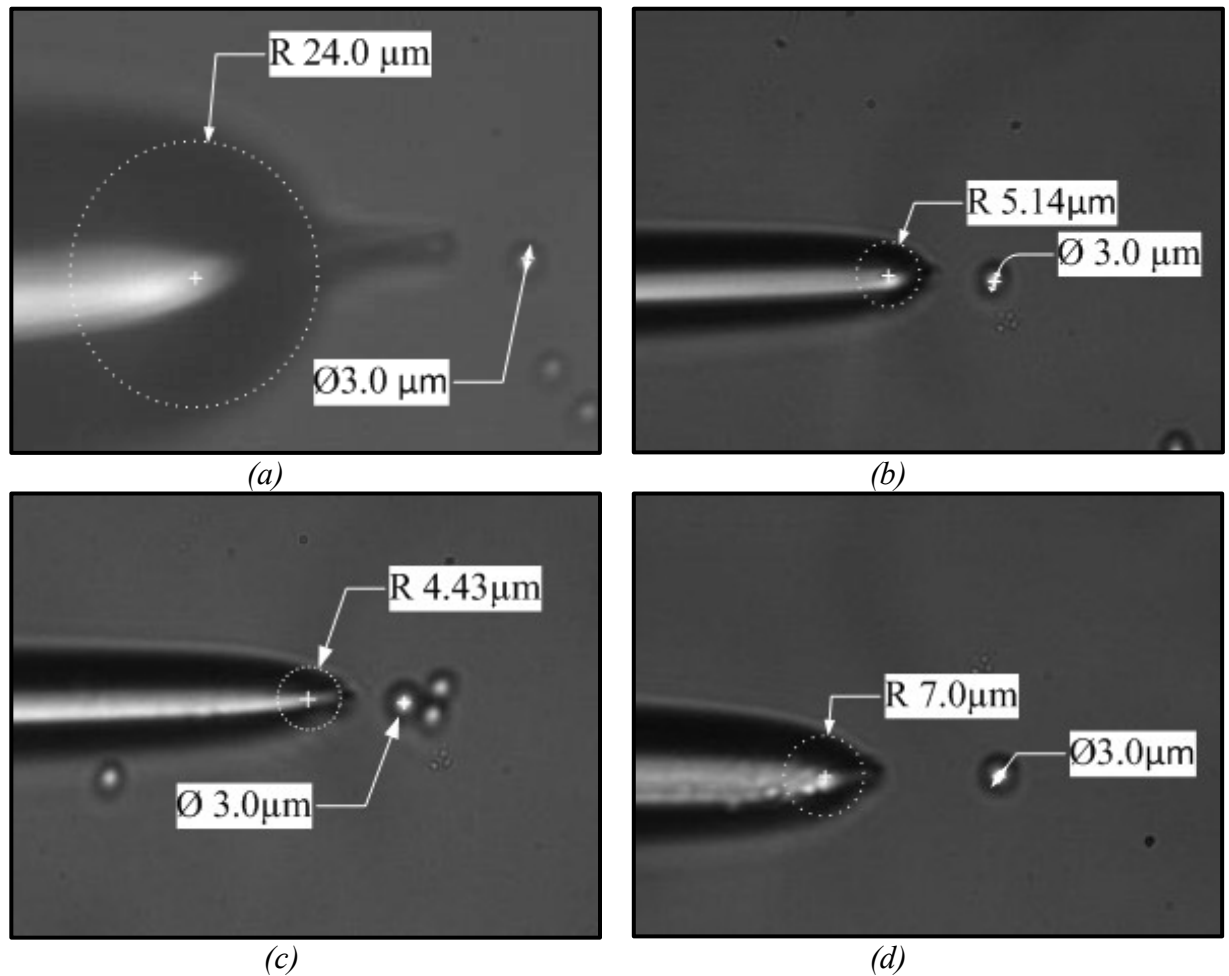


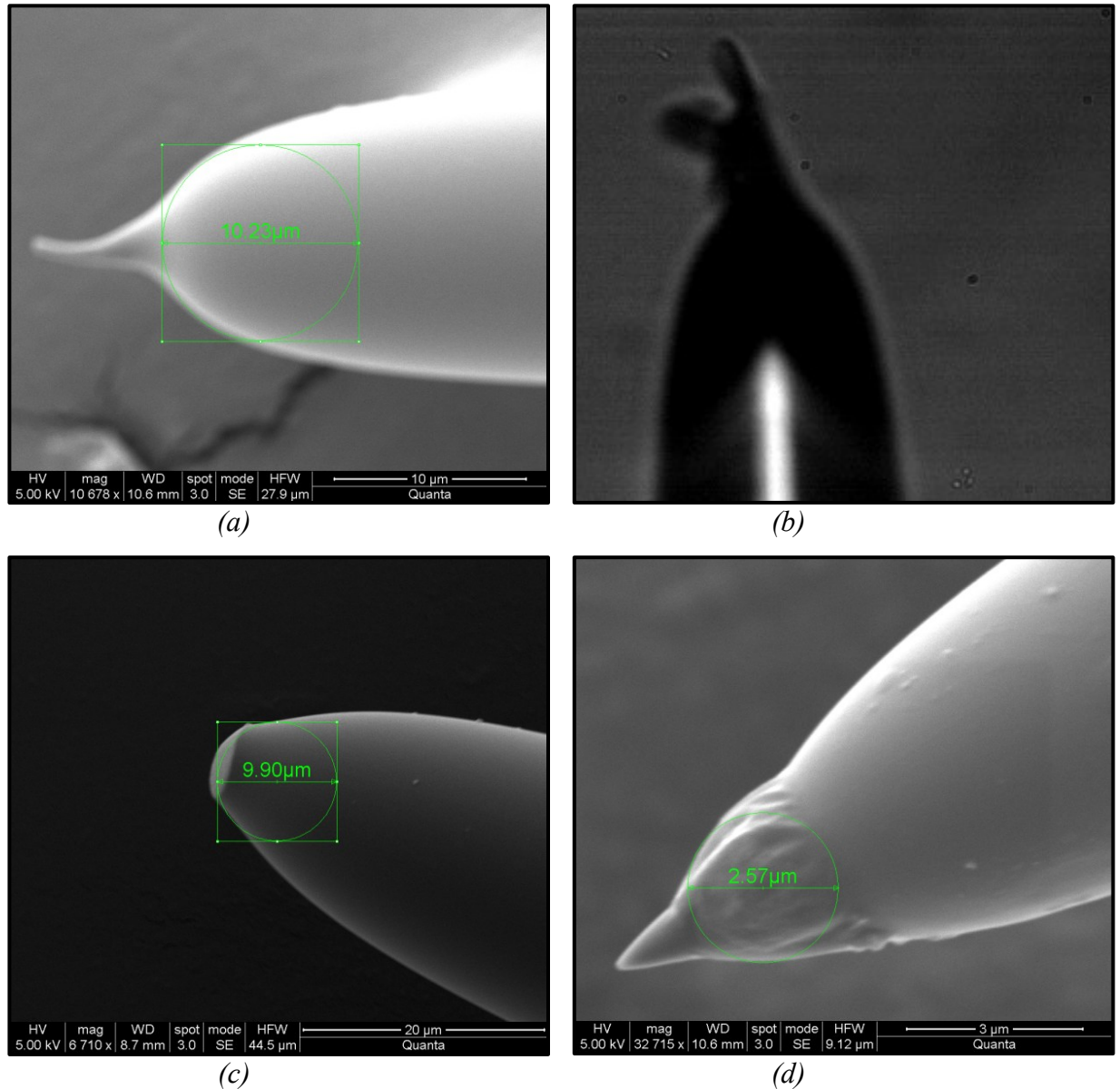
Figure 7-8 dimensions of the tapered fibre optic tips numbered (a) 44, (b) 92, (c) 94 and (d) 96

Figure 7-9 (a) shows a scanning electron microscopy (SEM) image of a slight elastic recoil deformation of a relatively large diameter taper. For significantly smaller diameter tapers the deformation is much more pronounced, creating at least one full curl, such as that shown in the light microscopy image in Figure 7-9 (b).

Figure 7-9 (c) shows a SEM image of a hand polished end-face following the removal of a deformed needle-like region. The polishing is conducted by hand. The fibre is held, as one would hold a pencil for instance, and a length of polishing sheet is bent in half. The two ends

of the polishing sheet, which have been brought together, are held between the thumb and index finger. The central portion of the sheet is not bent sufficiently to cause a crease and therefore maintains an arc-like geometry, and thus maintains the flexibility of the polishing sheet during the polishing process. The fibre end face is used, as you would a pencil, to lightly draw a single figure of eight on to the flexible polishing sheet structure, thus lightly polishing the fibre's end-face.

Figure 7-9 (d) is a high magnification (x32715) SEM image of a fibre taper and it can be seen that the region near to the very end of the tip is distorted due to the heating and pulling process. This type of distortion could be the reason for tapers that superficially look capable of 3D trapping, following the initial visual inspection, but ultimately fail to trap.



*Figure 7-9 SEM Image of (a) slight bend in the needle-like region due to elastic recoil (b) distortion seen in a light microscopy image of a tapered tip with pronounced elastic recoil (c) hand polished finish to the taper end-face (d) taper showing signs of heat distortion*

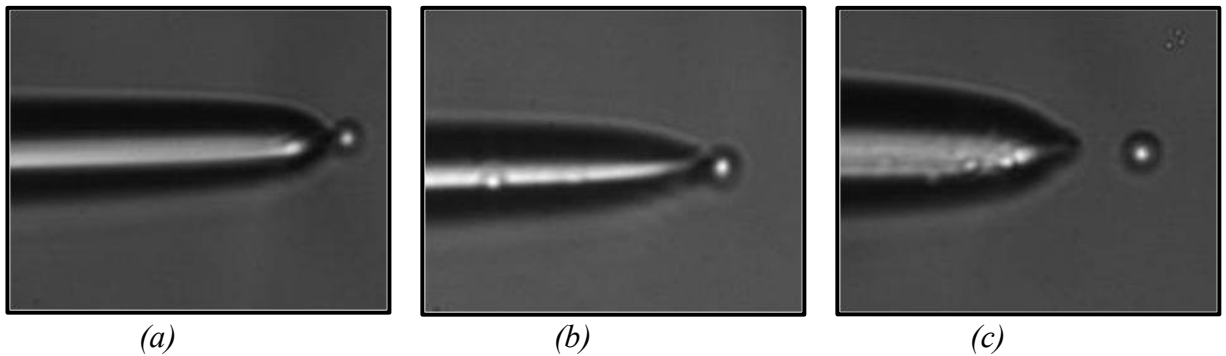
#### 7.4 INITIAL OPTICAL TRAPPING OBSERVATIONS

Figure 7-10 (a), (b) and (c) show the three optimized tapered optical fibre tips numbered 92, 94 and 96 respectively. Each of the three images represent the final frame from an optical trapping video sequence recorded using the Photron MC-1 Fastcam, CMOS high speed video

camera. The significance of viewing images of the final frame is that they each visually indicate the position of the stable 3D trapping zone with respect to the fibre taper tip.

It can be seen that, for tips numbered 92 and 94, the focal points, or trapping zones, are in similar locations. Both can be seen to be confining a  $3\ \mu\text{m}$  silica microsphere at the fibre end-face where the microsphere appears to be in contact with the tip of the optical fibre. In contrast the trapping zone for the tapered optical fibre tip numbered 96 can be seen to be located at a distance of about  $7.4\ \mu\text{m}$  away from the end of the optical fibre tip.

The significance of the trapping zone being located away from the fibre end-face is that it is ideally suited for the non-contact manipulation and optical trapping of live biological material. It is estimated that by using this type of tip cells with diameters in the region of  $10\text{-}14\ \mu\text{m}$  could easily be confined without making physical contact with the fibre.



*Figure 7-10 tapered optical fibre tips, corresponding to program numbers (a) 92 (b) 94 and (c) 96, optically trapping  $3\ \mu\text{m}$  silica microspheres, showing their respective trapping zones*

#### **7.4.1 CHANGE IN TRAP DYNAMICS**

Initial testing of the new tapered fibre tips, inserted at an angle of  $10^\circ$ , exhibited radical changes to the trapping dynamics compared to those observed during optical trapping at an insertion angle of  $45^\circ$ . The first noticeable change was that there was a significant reduction

in the trapping volume, which is the amount of microspheres that the optical trap could confine at any one time. When trapping at a fibre insertion angle of  $45^\circ$  it is difficult to trap and isolate a single microsphere. There is a tendency for multiple microspheres to be drawn into the optical trap together, forming a V-formation about the tip. After initial observations it would be easy to assume that the shape of the microsphere formation corresponds with the divergence in the far field beyond the focal point of the laser beam. This is an assumption that is supported by theory, since the microspheres are held in position by a combination of the laser beam's gradient force, which draws the particles transversely into its central axis, and the microscope's sample chamber floor, which acts to resist the propulsion of the microspheres in the direction of the beam's propagation due to the scattering force.

In contrast, whilst optical trapping at an insertion angle of  $10^\circ$  it is usual for only a single microsphere to be observed within the trap at any one time. Any additional microspheres that are drawn towards the trap are seen to be guided away from the trapping zone, in the direction of the beam's propagation. However, and in direct contradiction to the above statement, there have been occasions when two or three microspheres have been observed to be simultaneously optically trapped due to optical binding. Optical binding is a phenomenon in which a trapped micro-particle acts as a focusing lens, thereby creating an additional optical trapping zone beyond its boundary, such as that shown in Figure 7-11 . However, during this observation it was found that the optical binding was only maintained momentarily, for a few seconds, before the additional microspheres are eventually ejected from the trap.

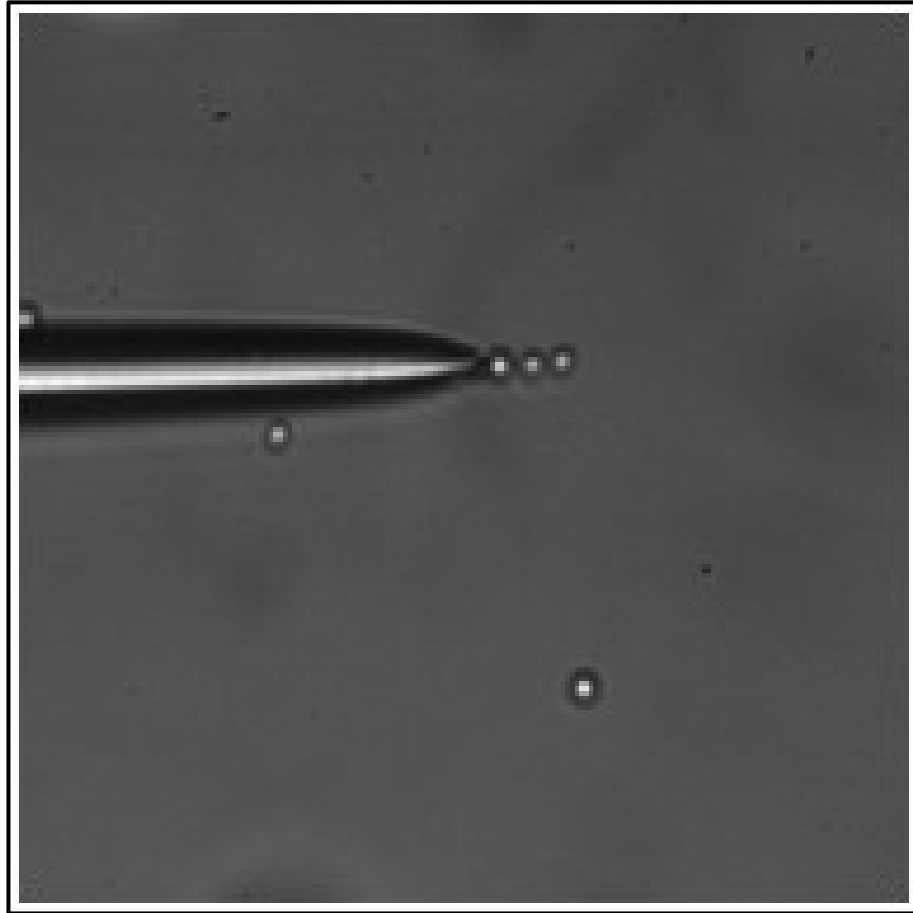


*Figure 7-11 TFOT's system demonstrating the optical trapping of three microspheres simultaneously due to optical binding*

Additionally Figure 7-12 shows the introduction of a maximum trapping range (MTR). The MTR became observable due to the new shallower insertion angle of  $10^\circ$ . The reason for this is that there is no longer the same physical impedance that was previously provided by the glass microscope sample slide. This is because the propagation of the beam now runs at a near parallel plane to the glass slide as opposed to its previously semi-perpendicular orientation. The result is that the full range of the optical trap's potential now becomes clear, since its direction is both parallel to the plane of the microscope's sample chamber floor, and orthogonal to the orientation of the microscope's viewing optics.

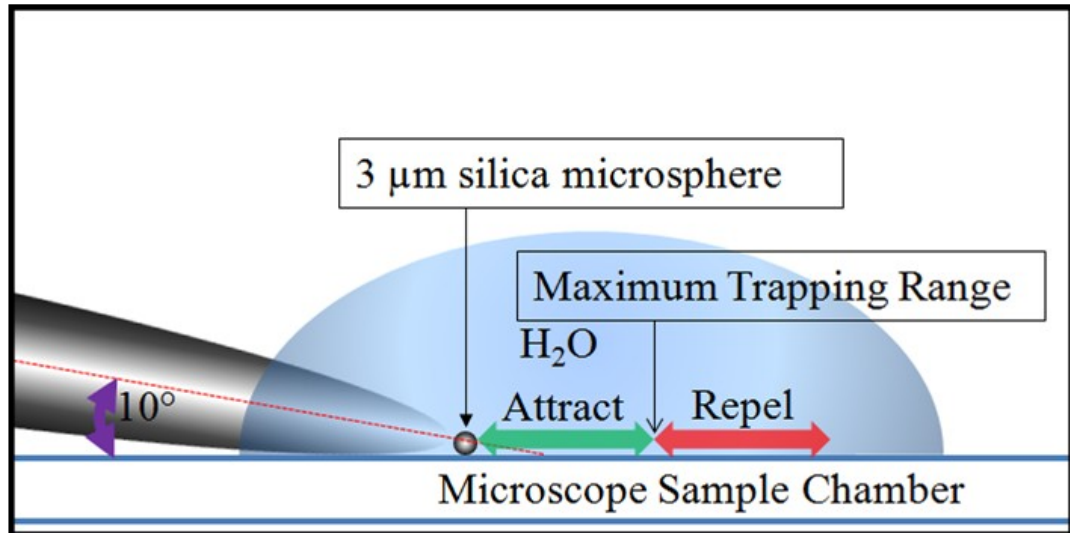


*Figure 7-12 change in trapping dynamics with the introduction of a maximum trapping range*

The MTR's maximum trapping distance is located at the point where the gradient and scattering forces cancel each other out resulting in a zero net force. To either side of this equilibrium point there are two areas where either gradient, or scattering, forces dominate respectively. A microsphere's position in one or the other of these two areas dictates the direction in which the microsphere will subsequently move. If microsphere's position is located to the side characterised by a dominant gradient force, then the microsphere is attracted towards the focal point of the laser beam and becomes optically trapped. If the microsphere is located towards the side characterised by a dominant scattering force, then the microsphere is repelled in the direction of the laser beams propagation.

The additional benefit of this configuration is that there is no longer a requirement to conduct the 3D optical trapping test. The reason for this is that it is evident whether, or not, 3D trapping occurs, since any particle will be repelled if the latter is true. However one must first be certain that the target particle is not situated just beyond the MTR of the tested tip before discarding the tip as not being capable of 3D trapping.

### 7.4.2 *EXPERIMENT - DETERMINING THE MAXIMUM TRAPPING RANGE*

The experimental measurement of a given taper's MTR was achieved by using the following experimental protocol. The tapered optical fibre is first manoeuvred into position close to a target microsphere, using a combination of the motorised and piezo x and y translation stages. Once the optical fibre's tapered tip is in position, the laser is activated and the microsphere is optically trapped as depicted in Figure 7-13 (top). The laser is then deactivated and the optical fibre taper is moved, initially by just a short distance of about 1 $\mu$ m-3 $\mu$ m, at a rate of 100 nm/s in the -ve X direction, as shown in Figure 7-13 (middle). When the tapered optical fibre occupies its new position, the laser is reactivated and the microsphere, if it is located within the MTR, will undergo optical trapping and be drawn into the trapping zone near the taper end-face, as depicted in Figure 7-13 (bottom).

The initial short distance that the tapered optical fibre tip is moved away from the microsphere is first required to establish a base point. It is important that this distance is less than the yet unknown maximum trapping range. The reason for this is that if the distance is too large then the microsphere may be repelled, in the direction of the laser beam's propagation, since it may sit beyond the trap's MTR. Upon establishment of the base point the process of trapping from a distance is repeated. Each time the process is repeated the -ve X distance of the optical fibre taper is increased by increments of 1 $\mu$ m. At the point at which trapping no longer occurs and the microsphere is repelled then the previous distance is deemed to be the extremity that represents the MTR.

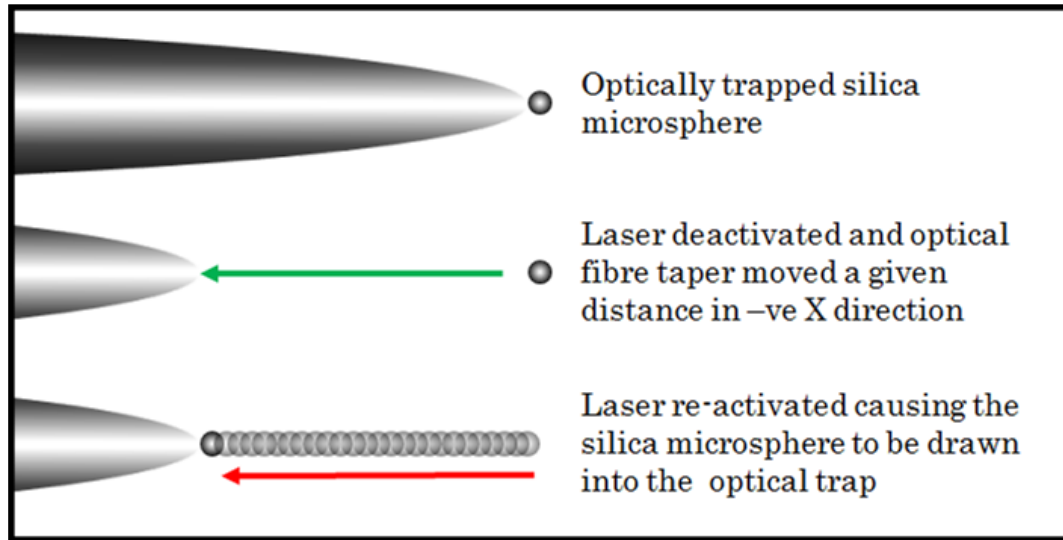


Figure 7-13 experimental procedure carried out to determine the maximum trapping range (MTR)

Videos of the optical trapping procedures are recorded and analyzed using a particle tracking (PT) software package. The PT software tracks the microsphere's course through each frame of video. An array of X and Y coordinate values of the particle's centre of mass is determined for each frame. A mathematical model is used to convert the X and Y coordinate data into real world micrometer values, thus providing distance information of the microsphere's trajectory back into the optical trapping zone. The microsphere's trajectory data, along with the associated timestamps, are recorded to enable further velocity and force analysis. The micrometer conversion is achieved by:

$$\text{Distance } (\mu\text{m}) = \frac{P_n \times P_s}{\text{Mag}} \quad (7-1)$$

Where  $P_n$  is the coordinate pixel value,  $P_s$  is the effective pixel size at the camera sensor and  $\text{Mag}$  is the magnification of the microscope's objective lens.

### 7.4.3 RESULTS: DETERMINING THE MAXIMUM TRAPPING RANGE

Table 7-3 shows that the maximum trapping range for the three optical fibre tapers were found to be 9 $\mu\text{m}$ , 9 $\mu\text{m}$  and 13 $\mu\text{m}$  for the optical fibre tapered tips 92, 94 and 96 respectively. However in the case of tip number 96, the actual maximum distance from the end of the tapered optical fibre, at which a microsphere can be drawn into the optical trap, is actually 20.4 $\mu\text{m}$ . This is due to the trapping zone, or the focal point, being located 7.4 $\mu\text{m}$  from the taper's end. The MTR has been determined by the distance that the fibre is moved by the piezo translation stage. Therefore it is not affected by the system magnification and thus remains the same as stated in ([Ross et al., 2014](#)). However what does change is the distance from the end of the taper to the optical trapping zone of tip 96, which is given in the preceding article as 6.5 $\mu\text{m}$  and is actually reported as being 7.4 $\mu\text{m}$  here due to the previously discussed magnification difference.

*Table 7-3 trapping range uncertainty*

<b>P2000/F Program Number</b>	<b>92</b>	<b>94</b>	<b>96</b>
Maximum Trapping Range ( $\mu\text{m}$ )	9	13	13
Tip Movement Piezo Value ( $\mu\text{m}$ )	9	9	10
Tip Movement PT Value ( $\mu\text{m}$ )	7.17	6.98	9.37
Percentage Uncertainty %	20.3	22.4	6.3

Following a comparison of the data for the piezo monitoring and control software with the PT software coordinate values, it was apparent that the two sets of data were unequal and inconsistent. The distance that the tapered optical fibre was moved in the -ve X direction and the distance that the microsphere was displaced when being drawn back towards the fibre tip and into the optical trap, during optical trapping, were expected to be relatively similar. This recorded uncertainty exposed a problem, which could have either been due to a mathematical error in the PT software, or due to a fault with the piezo monitoring and control software.

To check that the uncertainty was not due to the PT software the experiment was repeated. The fibre taper was moved in the  $-ve$  X direction away, from the previously trapped microsphere, by a distance of  $9\mu\text{m}$  for tapers 92 and 94 and  $10\mu\text{m}$  for taper 96. On each occasion the microsphere's path back into the optical trapping zone was recorded, using a high-speed video camera at x35 magnification, for later analysis using the PT software.

Table 7-3 shows that there is a displacement difference associated with the compared values given by the piezo control software and the PT software. Of the three tapered optical fibre tips, number 96 is seen to have the least displacement difference with an uncertainty of 6.3% compared with uncertainties of 20.3% and 22.4% for tips 92 and 94 respectively. Unfortunately this course of action failed to distinguish the source of the displacement uncertainties, which was a discovery that prompted a further test to validate the MTR.

#### ***7.4.4 FURTHER TESTING TO VALIDATE THE MAXIMUM TRAPPING RANGE***

In an effort to discover the origin of the above uncertainty a further test was conducted. This involved optically trapping a  $3\mu\text{m}$  silica microsphere and moving the tapered optical fibre tip a distance of  $10\mu\text{m}$ . Since the microsphere is optically trapped in 3D, both it and the fibre synchronously move along the  $-ve$  X direction. It is obvious then that they should both move exactly the same distance as each other. The associated video data was then analysed using the PT software. It was found that the distance travelled by the trapped microsphere was also  $10\mu\text{m}$ , and equal to the distance of the piezo translation. This finding eliminated the piezo monitoring and control of the translation stage, or the particle tracking data, as the source of uncertainty in the previous experiment. Therefore there must be an additional influence within the experimental environment that accounts for the ambiguity.

#### **7.4.5 POSSIBLE EXPLANATION FOR THE MAXIMUM TRAPPING RANGE ERROR**

The reason for the displacement uncertainty, discussed previously, can be explained by the following hypothesis. When the taper is moved away from the microsphere the relatively large size and shape of the tapered optical fibre causes a disturbance in the surrounding medium. The microsphere, which is free from optical trapping forces, is then dragged in the tapered optical fibre's "wake", i.e. the disturbance within the medium due to the tapered optical fibre's physical movement. Therefore the microsphere's original position is not maintained. This phenomenon is compounded as the effects of Brownian motion may also contribute to the microsphere's new starting position immediately prior to the laser's reactivation. Furthermore, additional forces, such as an electrostatic force, which could maintain the microsphere and tapered fibre's contact, following laser deactivation can also contribute to moving the microsphere from its original starting point.

This hypothesis is strongly supported by the results, which confirm that the percentage of uncertainty for taper 96 is far less than that of tapers 92 & 94. The reduced percentage of uncertainty for taper number 96 can be attributed to its focal point being a distance of about 7.4  $\mu\text{m}$  away from the fibre end face. This is in contrast to that of tapers 92 & 94, in which both have a trap focal point that is in an extremely close to the end of the tapered tip. The distance of the centre of the microsphere from the fibre's taper end-face during optical trapping is in the range of approximately 1.4-1.7 $\mu\text{m}$  for both tips 92 and 94, which is a distance that corresponds to being  $\geq$  the approximate radius of the microsphere at  $\approx 1.5\mu\text{m}$ . Consequently any potential tip disturbance effects for the tapered optical fibre tip numbered 96 would impinge less upon the microsphere compared to the corresponding cases for tapered optical fibre tips numbered 92 and 94.

The measured maximum trapping ranges of the three optimized tapered fibre optic tips numbered 92, 94 & 96 are given as  $9\mu\text{m}$ ,  $13\mu\text{m}$  and  $13\mu\text{m}$  respectfully. The measured values are in good agreement with the simulated data presented by Liu et al., where the simulated value was given as being  $12\mu\text{m}$  ([Liu et al., 2006](#)). However Liu et al. also suggested that particles located at a distance of  $15\mu\text{m}$  from the optical fibre would be propelled away from the tip due to the scattering force. Their simulation therefore implied that there is a  $3\mu\text{m}$  range, between  $12\mu\text{m}$  and  $15\mu\text{m}$  from the end of the tapered optical fibre tip, within which they fail to state whether a particle would be optically trapped, or repelled, due to radiation pressure forces.

Here the author has attempted to experimentally determine the maximum trapping range to an accuracy of  $1\mu\text{m}$ . Such accuracy was achieved as the incremental distance steps that the fibre was moved away from the particle were of  $1\mu\text{m}$  in length. Taking into account the magnification factor and the pixel size of the camera sensor, the accuracy to which the maximum trapping range could have been determined may have been as low as  $\approx 286\text{nm}$  at a magnification of  $\times 35$ . However in light of the ambiguities associated with the previously discussed “wake” phenomenon, caused by the taper being moved within the liquid medium, together with the effects of Brownian motion, the larger resolution of  $1\mu\text{m}$  increments was deemed to be satisfactory.

By modifying the T-FOTs system it is believed that the displacement uncertainty can be eliminated altogether allowing the exact measurement of the MTR to be recorded. The modification would require the addition of a second tapered optical fibre tip employed as a second and static optical trap. This second trapping fibre could hold the microsphere in position, whilst the first trapping fibre is moved away during MTR determination tests.

Elimination of the particles movement would be achieved activating the first fibre's beam whilst simultaneously deactivating the second fibre's beams.

A second trapping site can easily be created using a 1x2 50/50 fibre splitter in conjunction with a pair of in-line electronically controlled optical fibre attenuators for precise and independent control of the laser, within each of the two trapping fibres.

## 7.5 CHARACTERISING THE OPTICAL TRAPPING FORCE

Determining the optical trapping forces in a COT system requires the trapped object to be displaced by some external force to give a drag force equivalent optical trapping force. The external force is usually due to the drag force of the fluid medium acting on the trapped particle as the microscope sample stage is driven in a given direction. Conversely the optical trap itself may be used to drag the particle through the medium to generate a drag force that is suitably large to displace the particle from the optical trap. The velocity of the medium taken to displace the particle from the optical trap, which is equal to the translation velocity of the microscope sample chamber, or of the optical trap's movement itself, is multiplied by the Stokes drag coefficient to give the drag force at the point which the particle is displaced, and is given as:

$$F_d = 6\pi\eta r v \quad (7-2)$$

where  $\eta$  is the viscosity of the fluid medium,  $r$  is the radius of the particle and  $v$  is the velocity. The optical trapping force, for the given optical power, is equivalent to the drag force that is capable of displacing the particle from the optical trap and is said to increase linearly with the optical power.

However, one of the fundamental advantages that COT systems have over their fibre counterparts is that they don't have any physical entity, not counting the light itself, operating within the trapping medium. As discussed earlier, any movement of the optical fibre within the medium produces unwanted and disruptive fluid flow disturbances. Therefore, the practice of driving the fluid medium, or the fibre itself through the medium, to cause a fluid velocity which is sufficient to displace a trapped particle, would inherently have a negative influence upon experimental accuracy and would increase the complexity of determining the optical trapping forces.

In order to determine the optical forces for this project the same method that was used to determine the MTR is adopted, in that the particle is initially trapped then released by deactivating the laser. The taper is then moved a predetermined distance in the -ve X direction before the laser is re-activated and the particle is drawn back into the optical trapping zone. The particle's movement, as it is drawn into the optical trap, is recorded using a high speed video camera. This was repeated eight times for each of the three tapered tips 92, 94 and 96. On each occasion the optical power of the laser was increased in intervals of 5% from 25%  $\approx$  50mW up to 60%  $\approx$  600 mW.

The frames of the recorded video sequences were first decompiled into individual Joint Photographic Experts Group (.jpeg) images using the commercially available software suite Blaze Media Pro V.9.10 ([Media, 2009](#)). The decompiled video is then read into the particle tracking software Traps.pro ([Skydan, 2009](#)) that was developed here at the GERI in the Interactive Data Language (IDL) version 7.0 software package. The particle tracking software locates a user defined particle within each of the recorded frames. The X and Y pixel coordinate data of the particle's centre of mass, along with converted real world micrometer X

and Y coordinates, and the associated frame time stamps are recorded in a text file (.txt) for later analysis. The timestamps of the individual image frames are given at the rate of 30 fps, which is the decompiling software's limit; this is later converted to the appropriate frame rate at which the video was recorded.

The optical force is determined using the Stokes drag force coefficient, the difference here being that the velocity of the particle's trajectory as it is drawn into the optical trap is used rather than the velocity of the fluid that is used to displace the particle as discussed previously. The velocity of the particle is determined by taking the first derivative of the particle's displacement with respect to time. An additional term has been included in the Stokes law from Equation (7-2) that takes into account the effects of the microscope sample chamber floor, which is parallel to the direction of the drag force and is given by:

$$F_d = 6\pi\eta r v \gamma \quad (7-3)$$

where  $\gamma$  is given by:

$$\gamma = \frac{1}{1 - \frac{9}{16}\left(\frac{r}{h}\right) + \frac{1}{8}\left(\frac{r}{h}\right)^3 - \frac{45}{256}\left(\frac{r}{h}\right)^4 - \frac{1}{16}\left(\frac{r}{h}\right)^5} \quad (7-4)$$

where  $r$  is the radius of the particle and  $h$  is the distance between the centre of the particle and the flat microscope sample chamber surface ([Ha and Pak, 2010](#)).

The total force acting on a trapped particle is given by:

$$F_{Total} = F_d + F_i \quad (7-5)$$

where  $F_d$  is the drag force given by the Stokes equation presented in Equation (7-3) and  $F_i$  is the inertia force given by Newton's second law of motion, shown in Equation (7-6)

$$F_i = ma \quad (7-6)$$

where  $m$  is the mass of the trapped particle and  $a$  is its acceleration given by the second derivative of the particle's position with respect to time. However the inertia force  $F_i$  can be neglected if the Reynolds number,  $R_e$ , as given in Equation (7-7), is  $\leq 1$ .

$$R_e = \frac{DV\rho}{\eta} \quad (7-7)$$

where  $D$  is the particle diameter,  $\rho$  is the density of the medium,  $V$  is the maximum velocity of the particle and  $\eta$  is the viscosity of the medium. The forces acting on a trapped particle have been determined using the program `Optical_trap_force1.pro` that was developed specifically for this application in the IDL programming language ([Ross, 2014c](#)).

During the processing of the force data it was sometimes found that the data possessed uncharacteristic data spikes, which were subsequently removed using the IDL program `clipdata1.pro` ([Ross, 2014a](#)). The program allows the user to manually select the data to be removed. This is achieved using left and right mouse clicks on a plot image (see Figure 7-14 (a) for a typical plot image that requires clipping), to define invalid clipping regions on either side of the data to be saved. Images of a set of spiked data before and after clipping can be seen in Figure 7-14 (a) and (b) respectively. Data that does not require to be clipped is run through `clipdata2.pro` ([Ross, 2014b](#)) and saved in its original unclipped format. Both programs were developed in the IDL programming language.

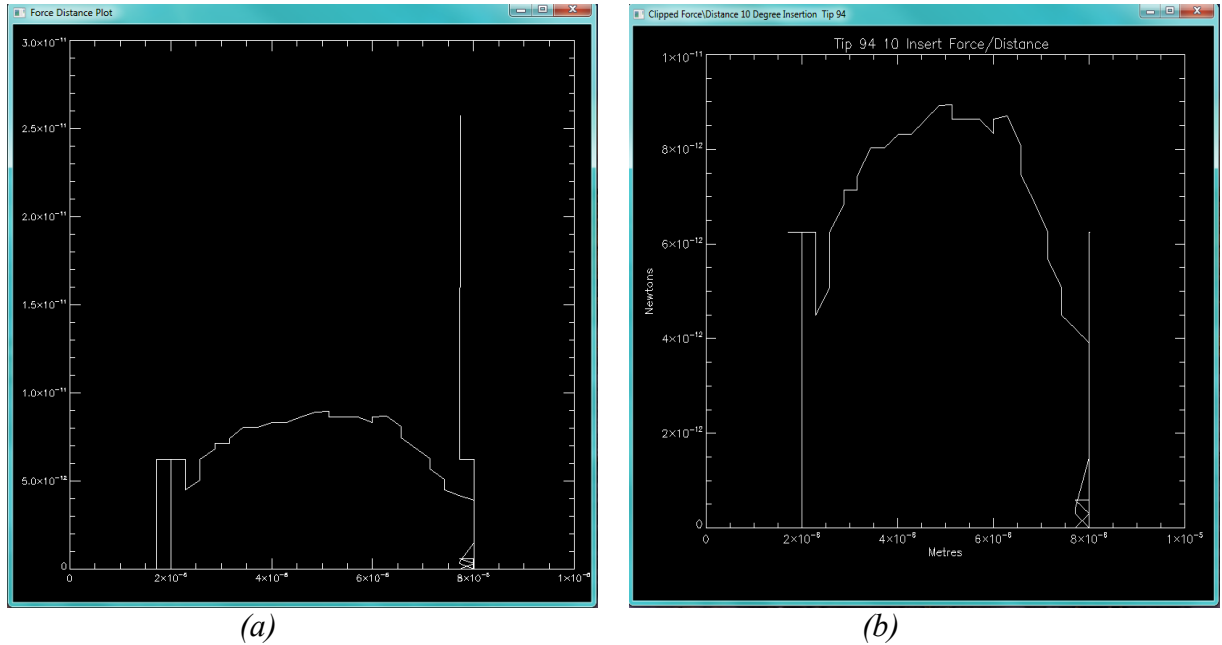


Figure 7-14 (a) plot of data with uncharacteristic data spike (b) plot of data after using *clipdata1.pro* to eradicate the data spike

## 7.6 RESULTS - CHARACTERISING THE OPTICAL TRAPPING FORCE

Figure 7-15 shows the gradient of the laser's optical power output versus the optical trapping force. Included is the data for tapered tip number 44 at an insertion angle of  $45^\circ$  and tapered tips numbered 92, 94 and 96 at an insertion angle of  $10^\circ$ . The force was measured for increasing optical powers as per the discussion given in Section 7.5. Each of the data sets has a trend line fitted and the tapers that have been employed at an insertion angle of  $10^\circ$  show the strongest fit with  $R^2$  values ranging between 0.88 and 0.96. This is in comparison to taper number 44 with an  $R^2$  value of -2.698, which was employed at an insertion angle of  $45^\circ$ . The  $R^2$  values show the goodness of fit of the line-fitting procedure and serve to highlight inconsistent data associated with taper number 44.

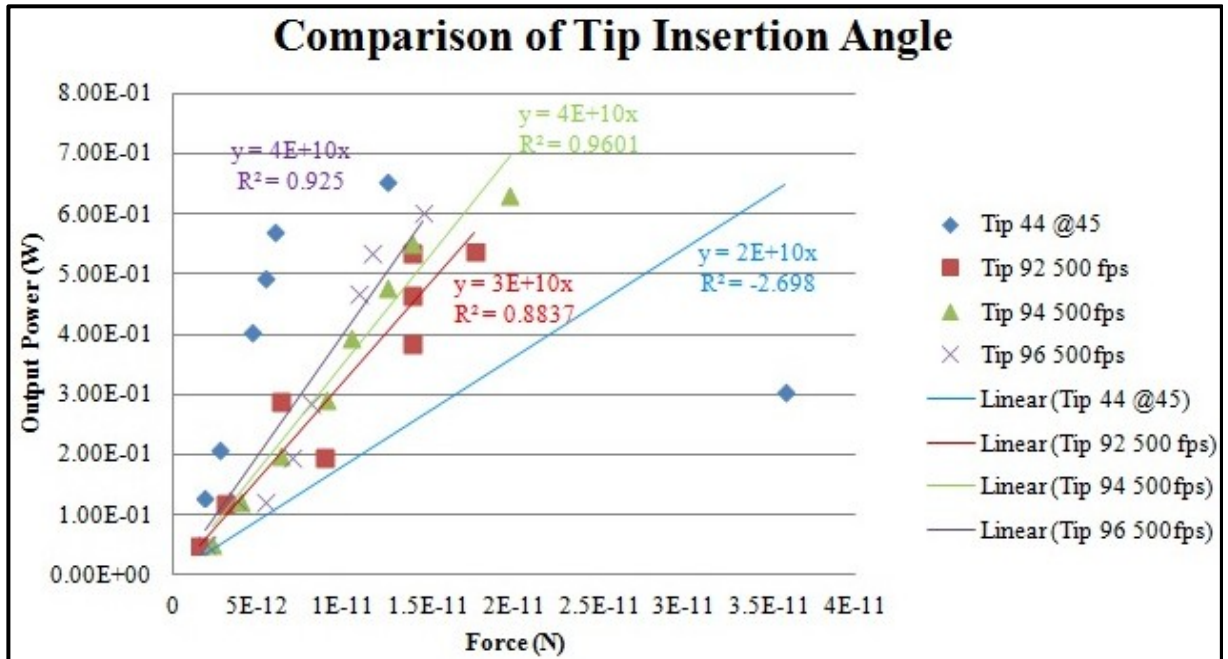


Figure 7-15 force v optical power gradients for tip number 44 at 45° insertion angle and tips numbered 92, 94 and 96 at an insertion angle of 10°

The gradient of the force versus power plots provides an indicator of the trapping quality that is similar to that of the optical trapping efficiency (Q) of the system. However the gradient values are not dimensionless as was the case with the Q values, with the gradient being able to predict real force values.

Table 7-4 shows each of the measured force/power gradients (FPG) and the equivalent Q values for all of the tapers. Taper number 94a exhibits the best trapping efficiency, with a value of 0.015, which also corresponds to the best FPG value; this predicts that the trap using tip number 94a could potentially produce a force of 82pN per 1W of laser power. Whereas, the taper with the lowest Q value, of 0.0013 corresponding to a FPG value of 8.8pN/W, was taper number 92a, which is an order of magnitude less efficient than the most efficient taper in the range.

*Table 7-4 force v power gradient (FPG) values and optical trapping efficiency (Q) values*

<b>Tip Number</b>	<b>44</b>	<b>92</b>	<b>92a</b>	<b>94</b>	<b>94a</b>	<b>941k</b>	<b>96</b>
<b>Insertion angle</b>	45°	10°	10°	10°	10°	10°	10°
<b>FPG (N/W)</b>	21e-12	30.3e-12	8.8e-12	28.1e-12	82e-12	54.6e-12	24.2
<b>Trapping efficiency Q</b>	0.0025	0.0066	0.0013	0.0060	0.0150	0.0149	0.0045

### **7.6.1 TAPERED OPTICAL FIBRE TIP NUMBER 44**

Surprisingly the only taper that had been investigated at an insertion angle of 45° was not recorded as being the worst performer, as per Table 7-4. This taper was taper number 44, which is not capable of optical trapping at 10°. Furthermore, it was only surpassed, with respect to poor optical performance, i.e. FPG and Q values, by taper number 92a, which was the replica taper of the original tip 92, and shown to be the most inefficient of all the tapers.

During the trapping experiments to determine the optical forces for taper number 44, the tip was moved 20µm away from the particle. At a 45° insertion angle there is no measured, or definite, MTR and particles are drawn into the optical trap from relatively long distances in excess of 20µm. To verify this particles have been observed to be drawn into the optical trap from outside the FOV of the viewing optics. If the tapered fibre tip is located within the centre of the FOV then the shortest distance that a particle that is located outside the FOV could travel is at least 73µm. Figure 7-16 shows the force v distance curves for taper number 44 at an insertion angle of 45°. It can be seen that the particle starts its journey at about 20µm away from the tip of the fibre, which is located at the origin of the axis. What is clear is that, for the first half of its trajectory, the forces are low and only begin to increase significantly after the particle had travelled a distance of 10µm from its original starting point. Also noticeable from Figure 7-16 is the fact that large spikes of data are evident and located just before the particle has reached the trapping zone, which is where the tapered optical fibre tip is

located. For the data recorded at 60% of the laser output, shown as the white dotted line, the spiked data was clipped since it seemed uncharacteristic compared to the rest of the data set. However on closer examination one can clearly see that the clipped data (shown as the black line) now falls short of the trapping zone which should be in the region of about 2  $\mu\text{m}$  from the origin. The force associated with the unclipped data is 39.48 pN, compared to 12.48pN after it was clipped. It can be seen to be uncharacteristically large compared with the other optical forces. The question naturally arises as to what is the cause of these spikes of data. Furthermore should they be clipped, since the clipping of this data removes information concerning the particle's trajectory, as its data excludes the final recorded destination by about 2 $\mu\text{m}$ ?

One theory that may explain the data spikes just before the fibre tip could be that when the fibre is orientated at an insertion angle of 45° the particle being drawn into the optical trapping zone is pulled along the sample chamber floor. Therefore an additional opposing force that is due to friction could be imposing an influence. This is because the particle is recorded as being drawn into the trapping region at low velocity and thus low force. However if the height of the tapered tip is larger than the expected set up height of 1 $\mu\text{m}$  above the particle diameter, which may of have arisen due to some external influence, such as a differences in medium volume, or movement of the fibre within the fibre holder. Then at the point where the particle is drawn into the optical trapping zone, it might undergo elevation, and thus remove the restrictive frictional forces, for the final duration of its trajectory, producing increased optical trapping force values at the fibre end-face.

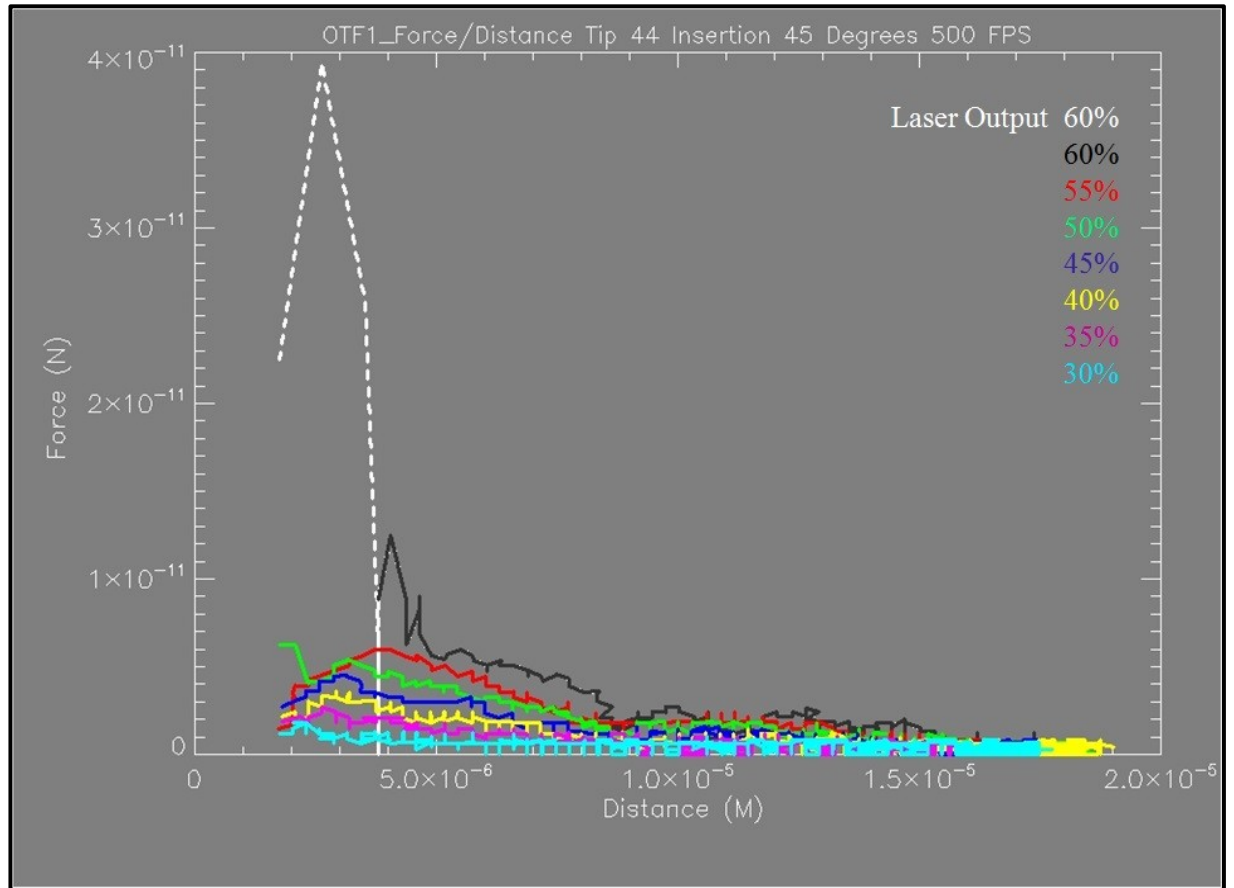
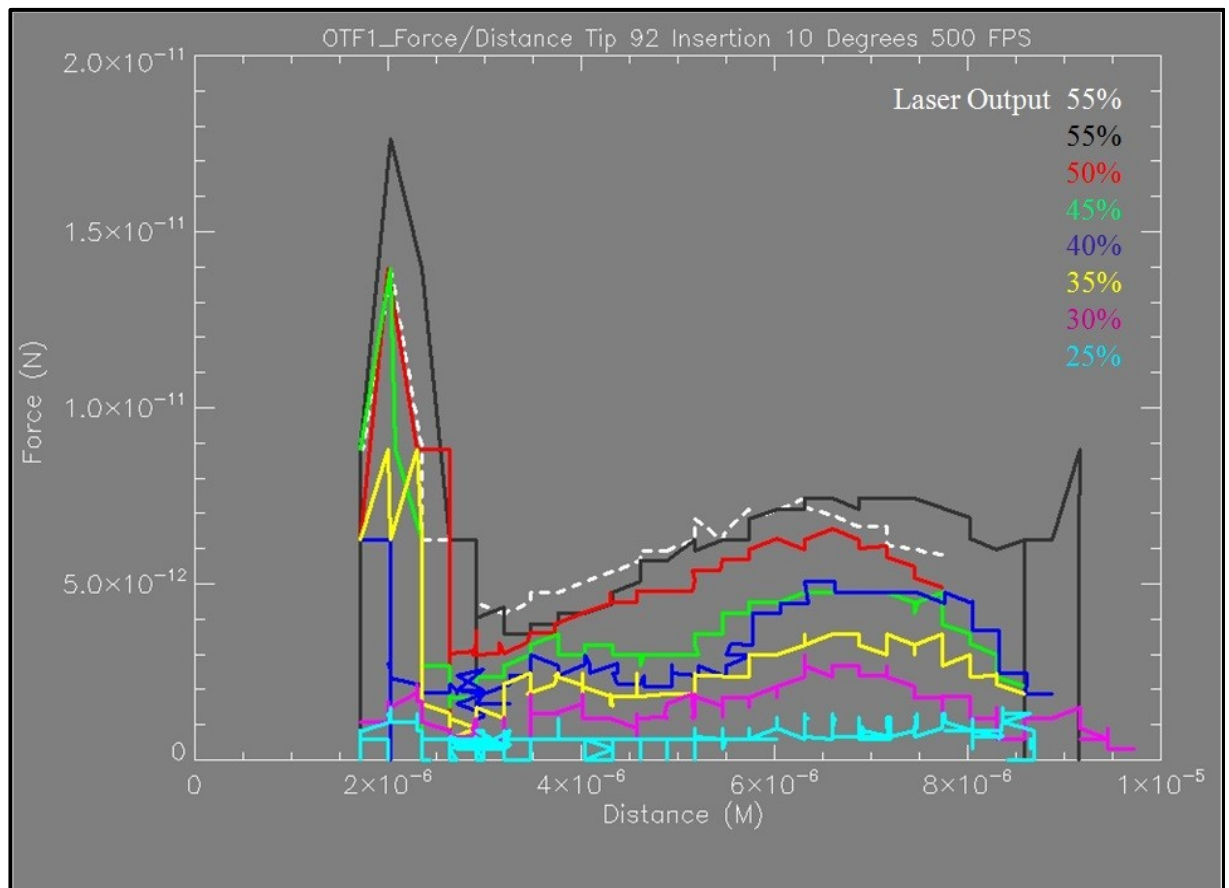


Figure 7-16 force - distance curves of ascending optical powers for tip numbered 44 at an insertion angle of  $45^\circ$

### 7.6.2 TAPERED OPTICAL FIBRE TIP NUMBER 92

Figure 7-17 presents the force/distance curves for taper number 92, which also shows force spikes that are close to the origin similar to those exhibited by tip 44. This suggests that the data spikes are not a feature associated with a fibre taper being orientated at higher insertion angles, since taper 92 was inserted at  $10^\circ$ . Furthermore some of the large spikes of data all seem to have similar maximum values even though the optical powers used to create the forces are different. As an example the data recorded at 55% of laser power (white dashed

line)<sup>19</sup>, 50% (red line) and 45% (green line) of laser output power each record comparable maximum force values, whilst the force curve for a duplicated 55% laser output power (black line)<sup>20</sup> exhibits a spike that is greater in magnitude than all of the force curves stated above, including that of the force curve that was generated using a similar optical power. Interestingly all the curves above 35% of the maximum laser output exhibit this sharp rise in forces when nearing the fibre tip.



*Figure 7-17 force - distance curves of ascending optical powers for tip numbered 92 at an insertion angle of 10°*

<sup>19</sup> This should have been 60% laser output power but due to an operator error during the experiment only 55 %, output power was used which is  $\approx 537.7$  mW at the sample.

<sup>20</sup> Intended 55% laser output power  $\approx 539.4$  mW at the sample (see Table 7-6)

### **7.6.3      *TAPERED OPTICAL FIBRE TIP NUMBER 94***

Figure 7-18 shows a significantly improved optical trap performance compared to those offered by tips 44 and 92. The force curves exhibit a better shape, in that from the particles original starting point until the region prior to the data spikes a clear bell like structure of all the data sets is evident. This bell like shape of the plot is similar in shape to what can be expected from a velocity curve and is what is expected here since the force is determined by the Stokes drag force coefficient multiplied by the velocity. Although what is still inexplicably evident is the steep rise in force as the particle approaches the fibre tip. The performance is also highlighted in Table 7-4, where the Q and FPG values are slightly greater than those for tips 44 and 92, with values of 0.006 and 28.1pN/W respectively.

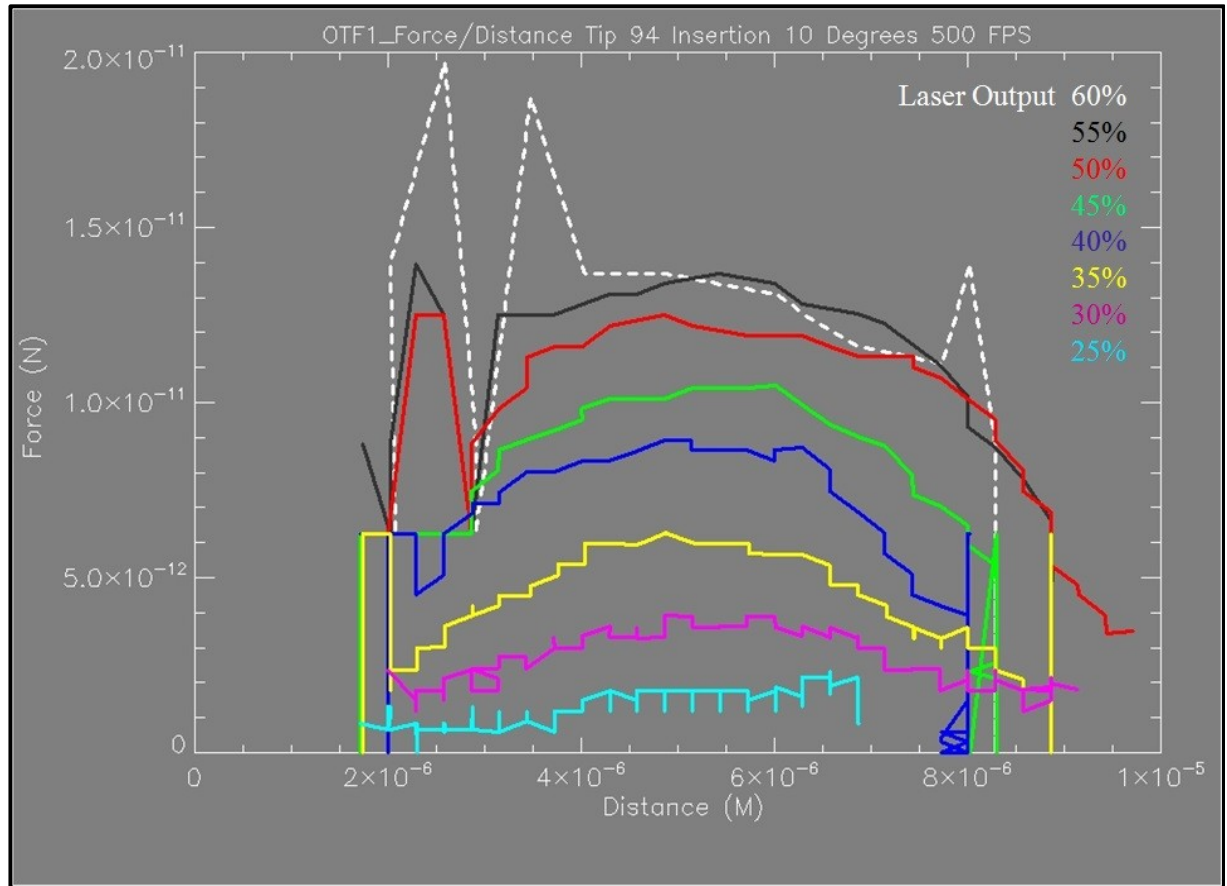


Figure 7-18 force - distance curves of ascending optical powers for tip numbered 94 at an insertion angle of  $10^\circ$

#### 7.6.4 TAPERED OPTICAL FIBRE TIP NUMBER 96

The force distance curves for tip number 96 show little evidence of the data spikes that have been inherent previously. Figure 7-19 shows that the different forces are clearly defined in a bell-like curve. Of interest here is the location of the trapping zone, which can be seen to be in the region of approximately  $7-8\mu\text{m}$  away from the end of the tapered fibre that is located at the axis origin. This suggests that the spike data that was exhibited previously could be a direct result of trapping near the taper itself. The Q and Force Power Gradient values for tip 96 are 0.0045 and  $24.2\text{pN/W}$  respectively. So although no data spikes are evident, and the plot looks clean when compared to those presented previously, this tip doesn't perform as well as initially expected. On the other hand, the data spikes in the previous force diagrams may well

be giving a false impression of their true performance for example other factors may be affecting the measured forces. For example additional electrostatic forces between the taper and the particle could be contributing and would explain why the data spikes are not evident for taper 96.

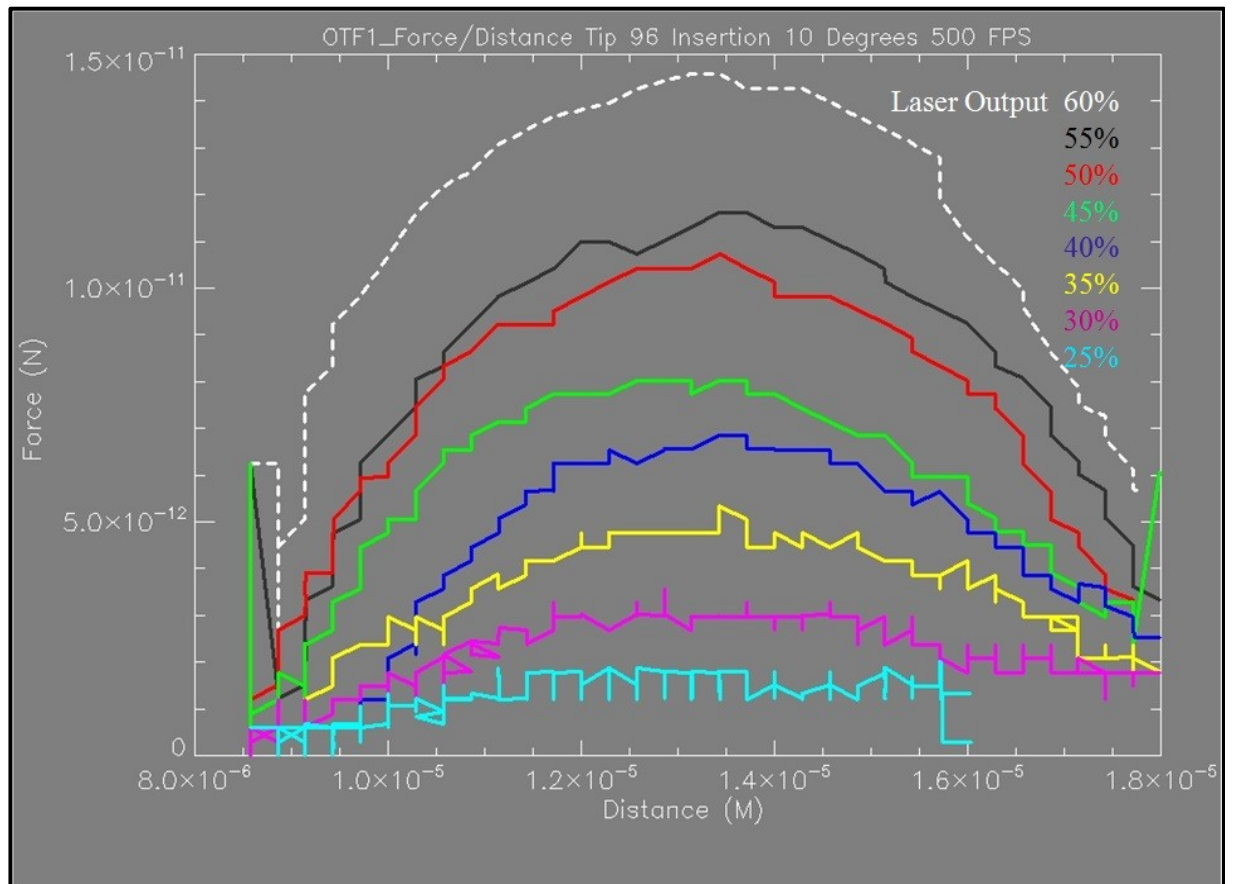


Figure 7-19 force - distance curves of ascending optical powers for tip numbered 96 at an insertion angle of  $10^\circ$

### 7.7 EFFECTS OF FRAME RATE ON MEASURED OPTICAL TRAPPING FORCE

Figure 7-20 shows two force-distance plots for tip 94, where the first plot shown in Figure 7-20 (a) was recorded at 500fps and this is also shown previously at full size in Figure 7-18. The second plot Figure 7-20 (b) was recorded at 1000 fps using exactly the same tip at the exact same insertion angle. It can be seen that, at the increased frame rate, the recorded

optical trapping forces shown in Figure 7-20 (b) are somewhat higher than the corresponding optical trapping forces recorded at 500 fps shown in Figure 7-20 (a).

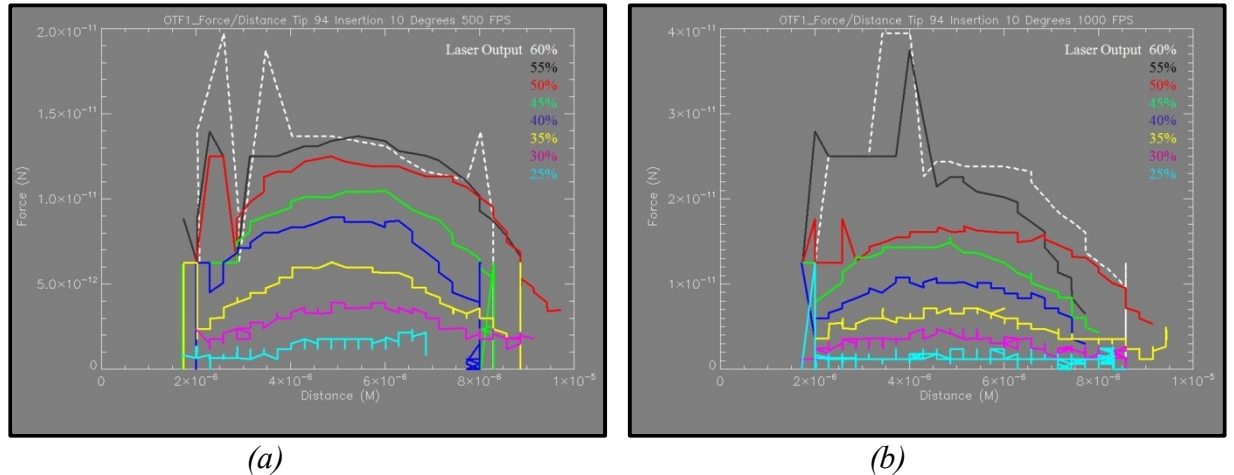


Figure 7-20 comparison of alternative frame rates - force - distance curves of ascending optical powers for tip numbered 94 at an insertion angle of  $10^\circ$  (a) 500fps and (b) 1000fps

Furthermore the empirically recorded force values for the laser output values of 55% and 60% are shown to be of similar magnitude. Such inconsistencies serve to demonstrate the difficulties faced when attempting to predict optical trapping forces via simulation.

Unfortunately such inconsistencies are inherent in optical trapping, as replicating and maintaining constant environmental conditions is nearly impossible. The reason for this is that the variables that dictate the quality and efficiency of optical trapping are not constant. For example micro, even nano, changes in the size of a trapped a particle's diameter from one experiment to the next will have a dramatic impact on the outcome. So too will changes in the viscosity of the medium, which can be brought about by changes in temperature, or the addition of sample particles. Needless to say the evaporation of the medium, leading to altered medium volume/depth will also have an effect on proceedings. Inconsistent data may also result from laser instabilities, although the majority of inconsistent data being recorded

here seems to be occurring in a pattern such that it appears to mainly be evident when trapping occurs near a tip end-face.

A comparison of the average optical output powers for tip number 94 at 500 and 1000 fps can be seen in Table 7-5. This shows that there is little, or no, difference between the laser outputs for the lower value output powers. For example at 25% laser output the power is given as 53.6 and 52.6 mW for tip 94 at 500 fps and 1000fps respectively. At a laser output power of 60% of the maximum, there is a larger disparity between the two optical power values, with a 630.8mW power output at 500 fps and 611.1 mW at 1000 fps.

*Table 7-5 average optical power output of laser for tip 94 at 500fps and 1000fps*

Frame-rate (fps)	Tip #	Optical power output at the sample							
		25% (mW)	30% (mW)	35% (mW)	40% (mW)	45% (mW)	50% (mW)	55% (mW)	60% (mW)
500	94	53.6	123.7	201.0	295.3	396.4	478.1	554.7	630.8
1000	94	52.5	122.5	194.7	287.9	379.1	467.3	541.9	611.1

Furthermore, since the higher of the two outputs was recorded at 500 fps, then the marked increase of trapping force recorded at 1000 fps cannot be attributed to increased optical power at the sample. The values shown in Table 7-4 for Q and the FPG are given as 0.0060 and 28.1pN/W respectively for tip94 at 500fps and 0.0149 and 54.6pN/W respectively for the same tip at 100fps. This indicates that at 500 fps the accuracy of the force results is questionable, since the temporal resolution is insufficient to adequately model the trajectory. As shown above, by doubling the frame rate, this has increased the accuracy of the recorded force values. Even so there is no guarantee that this latter result is at all accurate. Higher frame rates will be required to improve the force values to the point where it can no longer be improved upon. However, such frame rates may be out of the reach of the MC-1 high speed camera, where the maximum frame rate at maximum resolution is 2000 fps.

The reason that there is a different force value recorded between the two different camera frame rates is because the optical system suffers from inadequate resolution. The resolution is determined by a combination of the size of the pixels within the camera sensor and the magnification of the microscope's objective lens. Whereas the temporal resolution is limited by the recording frame rate, which has an interval of 0.002 and 0.001 seconds between recorded frames for the 500 fps and 1000 fps frame rates respectively. There are two main ways that may be used to improve the accuracy of the optical trap force measurements. The first method involves increasing either the resolution, by choosing a camera with a smaller pixel size, and/or increasing the magnification, or by sub-pixel image processing via software. The second method involves increasing the temporal resolution, which requires an increase in frequency of the data acquisition, which is the frame-rate of the camera in this case. The true optical trapping force will only be achieved when sufficient resolution is exercised such that a maximum force value is reached and can no longer be increased.

## **7.8 FIBRE TAPER REPEATABILITY TEST**

A working tapered tip can be damaged due to its reduced diameter and its brittle nature. If for example a tapered fibre tip should be damaged midway through a set of optical trapping experiments, then an exact replica of the tapered tip in terms of its geometric profile and its optical output properties must be produced in order to maintain continuity and accuracy of results. Failure to meet the exacting taper properties could lead to conflicting results within data-sets. This section therefore, looks at the micropipette puller's ability to accurately replicate a given fibre taper. Two original tapers, numbered 92 and 94, are measured here with regard to parameters such as physical dimensions, maximum trapping ranges (MTR), position of their focal point and optical trapping forces. These are then compared with the

corresponding values for two replica tapered fibre tips numbered 92a and 94a. Additionally the laser output power is taken into account when discussing the trapping forces.

### **7.8.1 RESULTS – COMPARISON OF THE PHYSICAL DIMENSIONS**

Figure 7-21 (a) and (b) show a comparison of the physical dimensions between the two tapered optical fibre tips developed using the P2000/F micropipette puller's program number 92. It can be seen that tapers are of a similar shape however, they differ in terms of their physical dimensions. Taper number 92 is shown in Figure 7-21 (a) has a tapered tip radius of approximately  $5.14\mu\text{m}$  compared to its replica taper, named 92a, whose radius is only  $3.71\mu\text{m}$ , as shown in Figure 7-21 (b). Looking at Table 7-4, the Q and FPG values are 0.0060 and 30.3pN/W for taper 92, and 0.0013 and 8.8pN/W for taper 92a respectively. These values, coupled with the dimensions of the tapers, only serve to highlight the concerns made earlier in the thesis. It is evident from the values presented in this table that taper 92a, with its smaller diameter taper, has the poorest operating performance, not only between the original and replica tested here, but out of all of the tapers presented thus far.

Figure 7-21 (c) and (d) shows the same comparison for two optical fibre tapered tips produced using program number 94. Tip 94, shown in Figure 7-21 (c), has a taper radius of  $4.43\mu\text{m}$ , whilst its replica counterpart, tip 94a, is slightly larger with a radius of  $4.85\mu\text{m}$  as shown in Figure 7-21 (d). The Q values and FPG values, from Table 7-4, show that the replica taper outperforms not only the original taper 94 but all of the other tapers presented thus far. With Q and FPG values of 0.006 and 28.1pN/W for taper number 94 and Q and FPG values of 0.0150 and 82pN/W for taper number 94a, the replica taper 94a even outperforms taper 94 at 1000 fps, which has a similar Q value at 0.0149, but a value of only 54.6pN/W for the FPG.

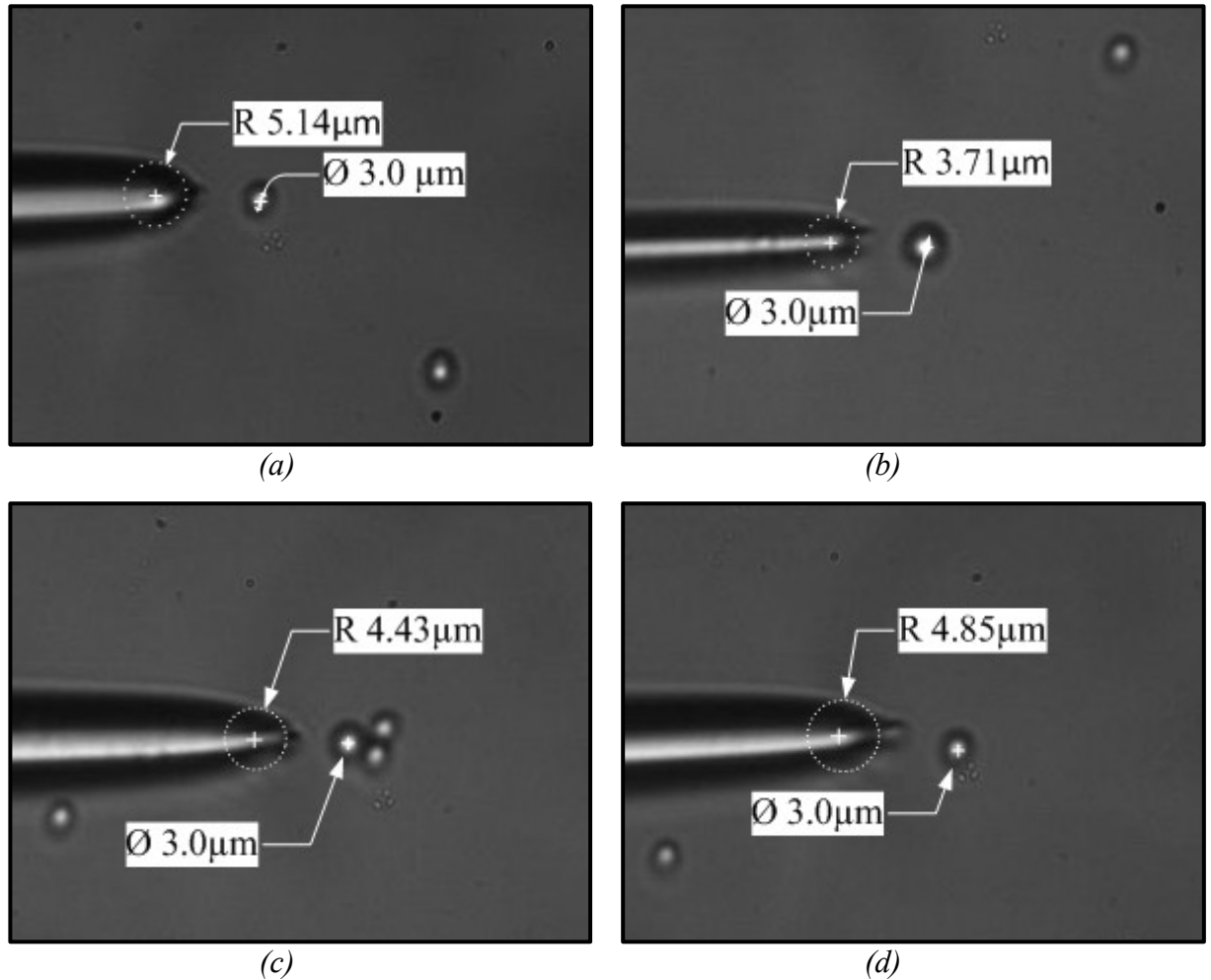


Figure 7-21 (a) original fibre taper dimensions for tip number 92 (b) attempt to recreate tip 92 - fibre taper dimensions for tip 92a (c) original fibre taper dimensions for tip number 94 (d) attempt to recreate tip 94 - fibre taper dimensions for tip 94a

### 7.8.2 RESULTS – COMPARISON OF THE MAXIMUM TRAPPING RANGE

Further comparisons between replica tips consist of the maximum trapping range (MTR) and the optical trapping forces that are deliverable by the taper. The MTRs for tapers 92, 92a, 94 and 94a are  $9 \mu\text{m}$ ,  $6 \mu\text{m}$ ,  $13 \mu\text{m}$  and  $8 \mu\text{m}$  respectively, providing evidence that, as expected, shows that the difference in physical dimensions naturally has an effect on the optical properties of the tapers. This is the case for tips 92 and 94a, as both tips do exhibit reduced MTR; however this is where the similarity ends. As we have seen previously, tip 94a

outperforms every taper with regard to Q and FPG values, whereas tip 92 is the worst performer. The reduced MTR in tip 94a could be due a wider focusing angle, which is more conducive for stable efficient optical trapping. In COT OT's systems a beam converging angle of  $\geq 60^\circ$  has been demonstrated to exhibit the best optical trapping Q value ([Sonek and Wang, 1996](#)).

### **7.8.3 RESULTS – COMPARISON OF THE TAPERS OPTICAL TRAP FOCAL POINTS**

Figure 7-22 compares the position of the tapered optical fibre's focal point, which is the point where the optical trap is located with respect to the tapered tip. Each of the four images represents the final frame taken from individual optical trapping sequences and therefore captures the particle trapped at the focal point of the laser exiting the fibre. The different trapping sequences represent each of the four tips 92, 92a, 94 and 94a respectively. It can be seen that the original tip 92, and the replica tip 92a, have trapping zones that are immediately at the fibre's end-face, as shown in Figure 7-22 (a) and Figure 7-22 (b) respectively. Similarly the original tip 94 and its replica tip 94a, as shown in Figure 7-22 (c) and Figure 7-22(d) follow the same pattern of trapping the particle at the taper's end-face. The images also clearly show that for both of the replica tapers 92a, shown in Figure 7-22 (b), and 94a, shown in Figure 7-22 (d), the needle-like portion of the tip has not been fully removed, unlike the original tips, 92 in Figure 7-22(a) and 94 in Figure 7-22 (c), where the particle is trapped at the parabolic like end face.

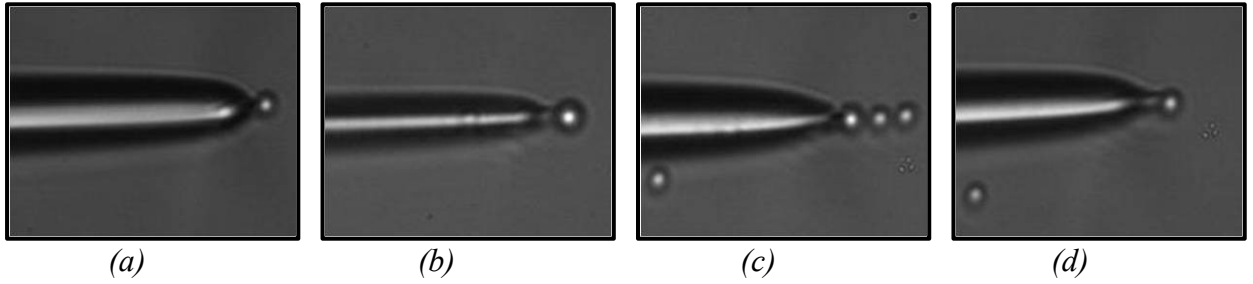


Figure 7-22 comparison of the optical tweezers trapping zone for (a) tip 92 (b) tip 92a (c) tip 94 and (d) tip 94a

#### 7.8.4 RESULTS – COMPARISON OF THE OPTICAL FORCE OUTPUT

The final taper comparison is an assessment of the optical trapping force curves, for the contrasting original tapered tips numbered 92 and 94 and the replica tapered tips numbered 92a and 94a. Figure 7-23 (a) and (b) show the force curves for the original taper number 92 and its replica taper 92a respectively, whilst Table 7-6 tabulates the average optical power output of the laser during the optical trapping experiments that yielded the force curves from Figure 7-20 .

The average laser optical output power, as shown in Table 7-6, is cross referenced with the force curves. This assessment ensures that any significant losses in optical force between the original and replica tapers is not due to significant differences in optical power at the sample. Take tip 92 shown in Figure 7-23 (a) for example; if we assume that the spike data is real force data then its force magnitude is almost double that of tip 92a in Figure 7-23 (b). This is contrary to the fact that throughout the experiment tip 92a exhibited larger laser output powers, apart from the values that range between 35% and 45% of the laser's output.

Table 7-6 average optical power output of laser for tips and 92, 94 and replica tapers 92a and 94a

Tip #	Optical power output at the sample							
	25% (mW)	30% (mW)	35% (mW)	40% (mW)	45% (mW)	50% (mW)	55% (mW)	60% (mW)
92	51.3	121.9	196.5	289.6	387.9	467.6	539.4	537.7
92a	52.2	123	196.2	288.8	384.1	473.1	547.7	620.7
94	53.6	123.7	201.0	295.3	396.4	478.1	554.7	630.8
94a	51.1	122.7	194.1	290.1	380.1	468.4	539.5	616.1

Similarly the laser output power is greater across the board for tip 94 and yet the generated optical trapping forces for tip 94a are more than double for tip 94.

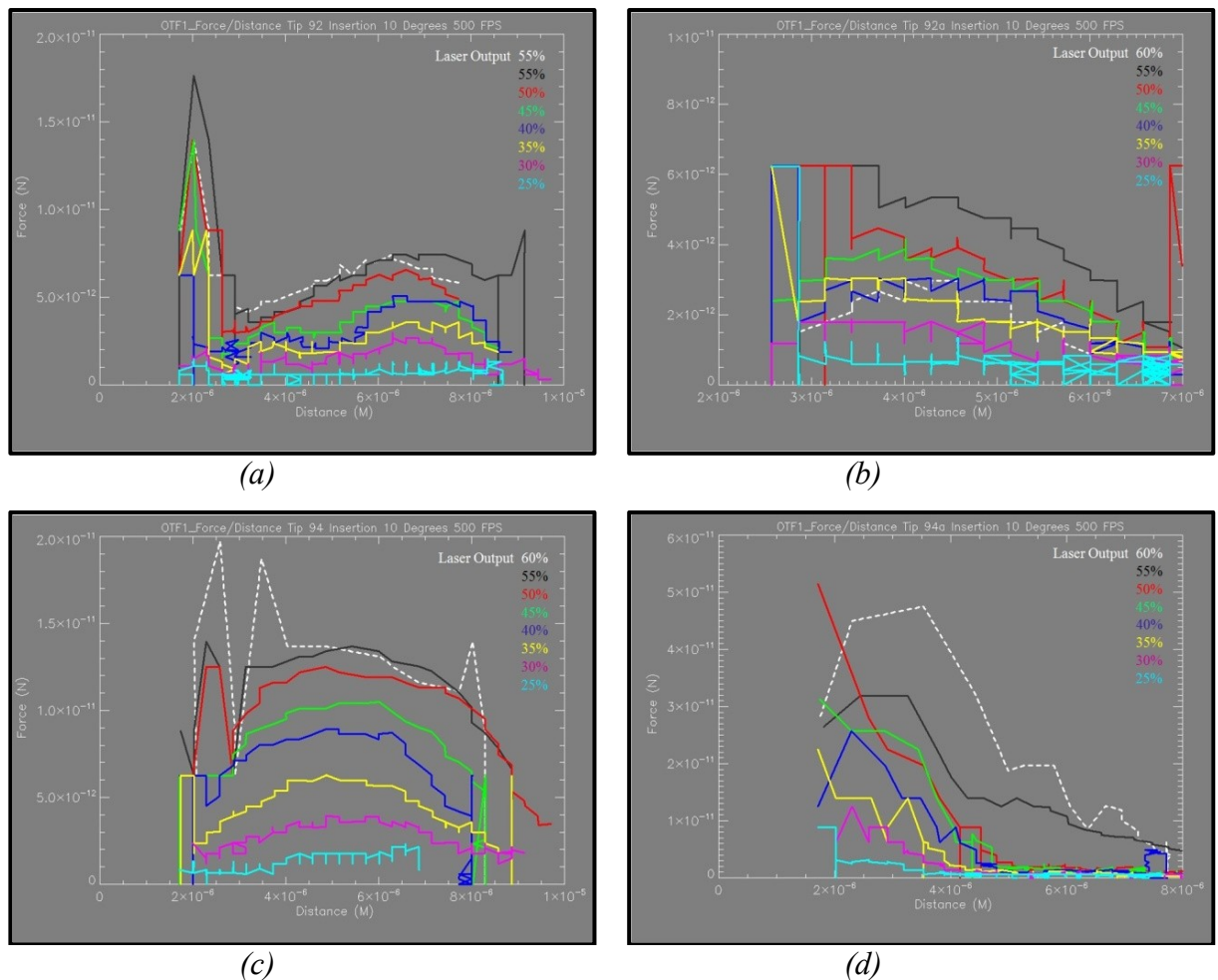


Figure 7-23 comparison of the optical forces produced by the original and replica tapers (a) tip 92 and its replica (b) tip 92a; and the original tip 94 (c) and its replica tip 94a (d)

Figure 7-24 shows the FPG gradient plots for tips 92 and 92a. Considering that each of the increasing laser power increments of 5% corresponds to a significant laser power increase of  $\approx 70\text{-}100\text{mW}$ , as shown in Table 7-6, it is difficult to conceive that lower laser power outputs can outperform higher laser outputs within the same experimental setting. However in some cases this can be seen to be so. The poor goodness of fit,  $R^2 = 0.543$ , for tip 92a from the FPG plot highlights such inconsistencies. Such anomalies are also observed in the force-distance plot. It can be seen that the data from 25% to 55% of the laser's output all show higher values in optical trapping forces than those at the maximum 60% of the laser's output power.

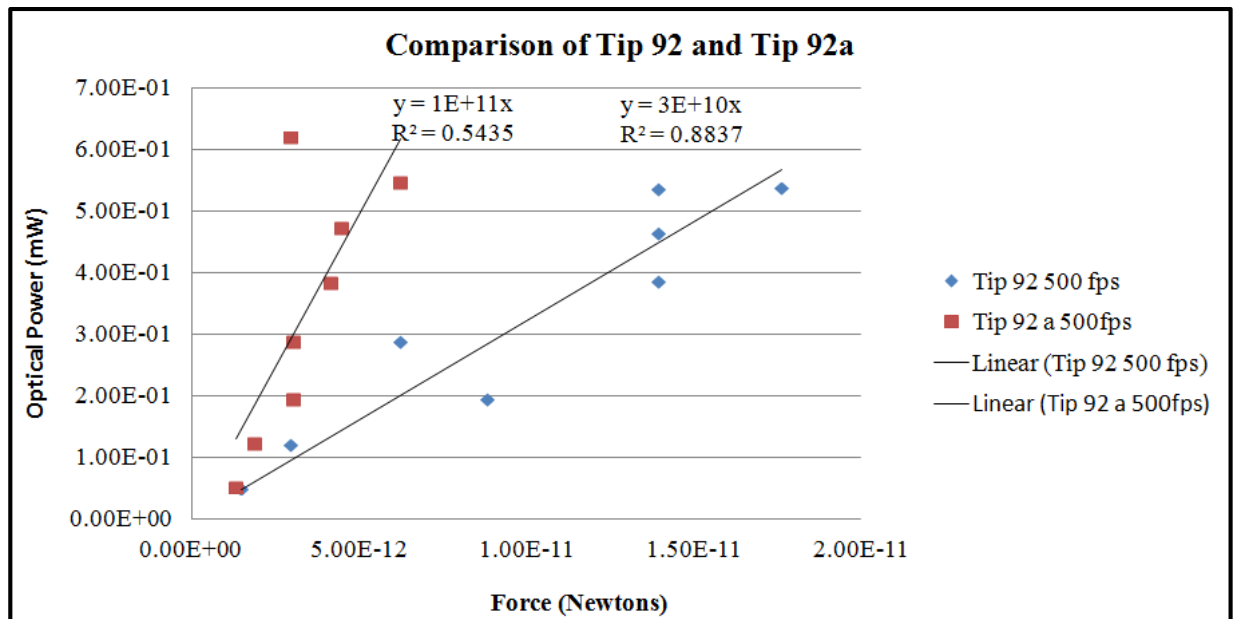


Figure 7-24 force v optical power gradients for tip number 92 and 92a at  $10^\circ$  insertion angle

Figure 7-25 shows the FPG plots for tips 94 and 94a. Although tip 94a is the superior taper in terms of trapping efficiency and FPG, it is not free from inconsistent behaviour. The plot shows that the largest optical trapping force was generated using  $468.4\text{mW}$  of optical power at the sample even though two higher optical power outputs of  $539.5\text{mW}$  and  $616.1\text{mW}$  respectively were utilised during the same experiment. On the other hand tip 94 acts as one

would expect with regard to force versus optical power gradient as the force increases linearly with increasing laser output optical power. Both of these findings are easily confirmed by looking at the force distance plots in Figure 7-23 .

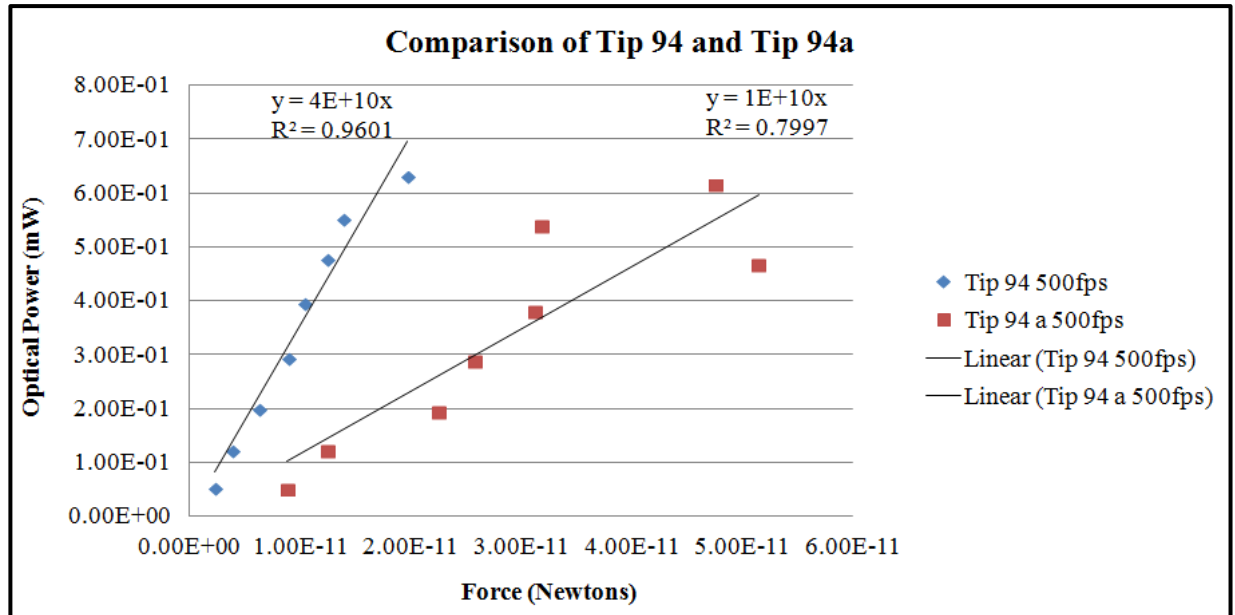


Figure 7-25 force v optical power gradients for tip number 94 and 94a at 10° insertion angle

### 7.8.5 DISCUSSION

These experiments show conclusively that optical trapping forces can be extremely difficult to predict. One would expect an increase in optical trapping forces by significantly increasing the laser's optical power by 70, or even 100 mW, especially when the experimental set up appears not to have changed, however, as these results show, this does not always seem to be the case.

From all of the tapers developed, two tapers stand out in terms of optical trapping efficiency, namely tip 94 (at 1000fps) and 94a, with Q values of 0.0149 and 0.0150 and FPG values of 54.6pN/W and 82pN/W respectively. However taper tip 94a, which has proven to be the best of the tapers in terms of offering the highest optical forces and thus the best optical

trapping efficiency  $Q$  and FPG values, does show some inconsistency in its force/power values. However these inconsistencies are most probably due to environmental changes within the system, such as different particle diameters, or changes in the refractive index of the medium, either due to temperature change, evaporation, or replenishment of the medium for example. Tip 94a also possesses a reduced MTR, which although posing no problems when trapping small diameter particles, such as the  $3\mu\text{m}$  diameter microspheres here, the reduced MTR may result in the T-FOTs inability to trap larger objects or to trap biological material without causing physical damage.

On the other hand tip 96 initially looked like a contender for being the best tip. Showing excellent stability during optical trapping experiments, it had an  $R^2$  goodness of fit value of 0.925, which was only surpassed by the original tip number 94. This high quality was also exhibited in its force distance curves, which showed excellent bell-like shape and constant force values throughout the incremental laser output power increases. Additionally tip 96 has a trapping zone that is located  $\approx 7.4\mu\text{m}$  away from the tapered fibre end-face. This could prove to be an advantage when applying it to work with large biological specimens, where non-contact manipulation would be seen as an advantage. Combining the favourable attributes of the high efficiency force generating tips 94 and 94a and the long working distance of taper 96 would be an advantage in any future work.

Additionally the use of a higher frame rate of 1000fps, as opposed to the 500 fps usually employed during this project, has highlighted the fact that at the lower frame rate there is a reduced magnitude, in the determined optical force, compared to when a higher frame rate was adopted, which is due to the limited spatial and temporal resolutions of the camera. It is believed that the accuracy of the measured optical trapping force could be improved by

increasing the frame rate, and thus the temporal precision, or by exploring the possibility of incorporating a device such as a quadrant photo diode (QPD) photo-detector into the T-FOTs system, which has far superior spatial and temporal resolutions at a fraction of the computational and monetary cost. However, as discussed earlier, implementing a QPD into the T-FOTs system may be difficult to achieve, but still warrants further investigation to the possibility.

Finally, this exercise has demonstrated that the micropipette puller does not possess the ability to reproduce identical optical fibre tapers in terms of shape size and optical properties. Therefore it is not suitable for the development of replica tapers subsequent the start of an experimental set. With the advice here being that once an experiment set has begun, extreme care must be taken to maintain the same fibre tip throughout the duration of the entire experiment. If a taper should be compromised in any way during an experiment, then in the interest of the integrity and consistency of the experiment it should be halted and restarted with a new taper.

## **7.9 TRAPPING OF BIOLOGICAL SAMPLES**

The trapping of biological samples has been limited to an attempt to trap large,  $\approx 20\mu\text{m}$  diameter, diseased human prostate cells and yeast cells with a diameter of  $\approx 6\text{-}7\ \mu\text{m}$ . In the case of the prostate cells optical trapping failed to occur. Figure 7-26 shows the yeast cell optically trapped and elevated above the general population of other yeast cells, demonstrating the developed T-FOTs successful 3D trapping ability. It can be seen that the cell's nucleus is clearly visible and the trapping zone is immediately at the optical fibre taper's end-face. Again this highlights the pipette puller's inability to repeat exact replica tapers, since this taper

was also created using program number 96, the same program number that produced a tapered tip with a focal point, or trapping zone, located about  $7.4\mu\text{m}$  from its end-face.



*Figure 7-26 optically trapped yeast cell elevated above the general population of cells demonstrating 3D trapping in the process*



**CHAPTER EIGHT CONCLUSION**

## CONCLUSION

This thesis is the culmination of several years' research to deliver a bespoke, portable, fibre-optic based optical trapping system that is suitable for integration with other advanced microscopy applications. From the early onset it was obvious that this practical experimental research programme was not going to be an easy task. First of all the existing literature stated that optical trapping using a single optical fibre inserted at an angle below  $20^\circ$  was not possible. And since the principal aim was to integrate the said system with our AFM, a feat that would require an insertion angle of  $10^\circ$  to allow the fibre to pass under the AFM head, then this was going to be a challenging project!

This early negativity was further compounded whilst attending a conference that was hosted by a well known company, whose primary business concerned the manufacture of commercial AFM's and optical tweezers systems. During an interval a conversation was struck up between the author and one of their principal design engineers who, after asking about my research, informed me "that it was an impossible task that could not be achieved". Nonetheless this is a happy conclusion, as against all the odds, a single optical fibre based; 3D optical trapping system has been successfully developed. Furthermore the tapered fibre optic tweezers system, or (T-FOTs), is also capable of operating at a fibre insertion angle of  $10^\circ$ . This is a fact that offers experimental proof that the system is capable of performing in conjunction with an AFM as requested, albeit subsequent to some further modifications to the AFM. Such modifications would include the addition of an optical IR filter to ensure that the trapping laser does not interfere with the AFM's optical detection system.

The system uses single mode fibre to deliver the trapping laser light to the sample chamber. Since optical tweezers require a tightly focused laser beam for 3D trapping, the divergent

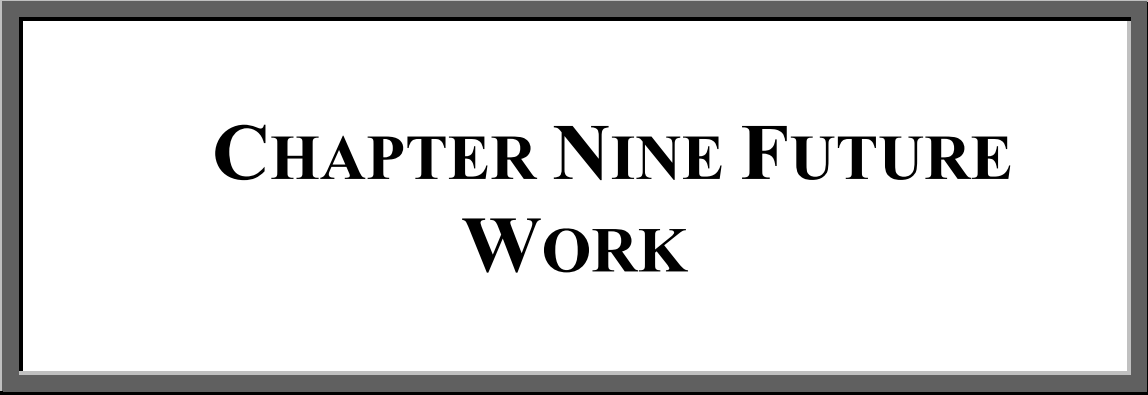
nature of the light exiting the optical fibre is altered by tapering the optical fibre. The tapering of the optical fibre is achieved by the heating and drawing process using a commercially available micropipette puller that has been modified for working with smaller diameter glass material such as optical fibre. Several novel working tapered tips, of various taper profiles, have been developed with some showing promise that could potentially lead to improvements that will see the system become as optically efficient as other more complex and expensive alternatives. Already optical trapping efficiencies  $Q$  of 0.0150 have been achieved, with the potential to produce  $82\text{pn/W}$ . Alternatively a novel tapered fibre tapered tip with a long working distance has been developed. What is novel about this tip is the fact that the trapping zone is located approximately about  $7.4\mu\text{m}$  away from the tapered fibre's end-face. Such a taper would be ideally suited for working with large biological material that requires no contact with the sample whatsoever. Generally the optical trapping zone produced by tapered optical fibre is located right at the fibre's end-face, where some form of contact, however small, is inevitable.

However knowledge of the true optical trapping force values is still unclear. At this time the T-FOTs system's particle detection subsystem has been identified as the weak point, which after significant improvement should see improved precision and accuracy in acquiring the improved optical trapping force data. Work therefore must be carried out to develop a solution that will allow high resolution monitoring equipment, such as QPD's, to be employed for 3D particle tracking.

During optical trapping at the desired insertion angle of  $10^\circ$  changes to the dynamics of the optical trap were observed, which were previously not obvious at the more vertical orientation of  $45^\circ$ . These changes were due to the trapping fibre now being at a near horizontal

orientation to the microscope's sample chamber floor. Because of this novel fibre arrangement, a maximum trapping range has now become apparent. Particles that are within this maximum trapping range are drawn into the optical trap by the trapping laser. Conversely those that are located beyond the maximum trapping range are guided by and propelled, via the electromagnetic radiation pressure forces, in the direction of the beam's propagation. This opens up new possibilities, for example in particle sorting applications.

The maximum trapping range has been found to be different for the diverse taper profiles and thus is tuneable, with trapping ranges to date being measured empirically and ranging from  $6\mu\text{m}$  up to  $13\mu\text{m}$ . However taper 96, which was discussed earlier and which has a relatively long working distance of about  $7.4\mu\text{m}$  and a maximum trapping range of  $13\mu\text{m}$ , has an overall maximum trapping range in the region of  $20.4\mu\text{m}$ .



**CHAPTER NINE FUTURE  
WORK**

## **FUTURE WORK**

It has become abundantly clear from this research programme that the use of a high speed camera within an optical trapping system is possibly limited in terms of providing a level of both spatial and temporal resolution that is required for accurate optical trapping force measurements. Coupled to the fact that its use comes along with a high computational and monetary cost, then finding an alternative method of recording the particle displacement for force analysis is imperative. A quadrant photo detector is such a low cost high resolution alternative. Therefore methods for integration of a QPD into this system should be sought to increase system resolution and improve optical trapping force measurements.

Currently the system only tracks the particle of interest in the 2D X and Y planes. However, if one considers the optical trapping of 3 $\mu$ m diameter particles using fibre tapers that have a radius at the tip ranging from 4-6  $\mu$ m, then there will be some elevation of the particle as it is drawn into the trap. Thus there is a third z force component present, which is currently being grossly overlooked, that should be included in all of the force calculations. By tracking the particle in 3D, the resultant additional force component may go some way to bring the trapping efficiency of the system into line with other and more efficient, but more complex and costly systems.

The experiments conducted for this thesis have shown one or two taper designs that could be explored further to improve their overall design. For example by combining the long working distance of taper 96 with the high efficiency tapers from program 94, this could result in an 'ultimate' fibre taper. Therefore increased work should be carried out to determine the ultimate taper in terms of optical properties and trapping efficiency. Already there is a good fundamental starting point in place, with regard to tapers 94 and 96, however much more detailed testing and analysis over a larger data set of tapers is still required.

This comprehensive research should not just look at the taper profile generation, but also new ways of removing controlled amounts of material from the taper's end-face, since the relatively crude methods employed here to date are detrimental to advancement. When controlled material removal is possible, then tapers could be developed with complete, with partial, or completely without needle-like tips and could be tested to find the best solution. This would go some way to help answer questions such as; 'Does the reduction of the needle-like improve trapping efficiency?'; 'Is the focal point somewhere inside the needle-like tip and closer to the radius of the larger diameter of the taper, or does the needle like tip perform as a conduit delivering the focused beam at the fibre medium interface?' Specific lengths of needle-like tips can be removed and tested in optical trapping experiments against versions with their complete removal. Of course this will be not be easy to accomplish when one considers the challenges involved in reproducing 'identical' replica tapers.

A further suggestion for future work concerns mapping the output beam exiting the fibre's end-face. Visualisation of the beam's output shape, either in terms of an optical force map, or an image of the actual beam profile as it exits the fibre, would provide vital data to assist in the development of the ultimate fibre taper profile. The reason for this is that vital beam parameters, such as the beam's focal distance and convergence angle would be more readily available using such imagery and could be utilised to aid in gaining the best geometric profile for the tapered optical fibre. The groundwork for mapping the optical forces emanating from a fibre tip has already been set in motion. For example the particle tracking software allows the user to set the optical fibre taper's tip as the image origin. This allows the user to perform optical trapping of a particle from various locations surrounding the tip, i.e. from anywhere in the FOV, and enables the appending all of the force data into a single array, as it is acquired. This accumulated and appended force data

can then be used to produce a 3D map of the optical forces emanating from the fibre's tip. Figure 9-1 shows the starting positions of multiple optically trapped microspheres (30 in total). Each of the microspheres was trapped from different locations around the optical fibre tip. The central axis of the end face of the tapered fibre tip was set to be the image origin.

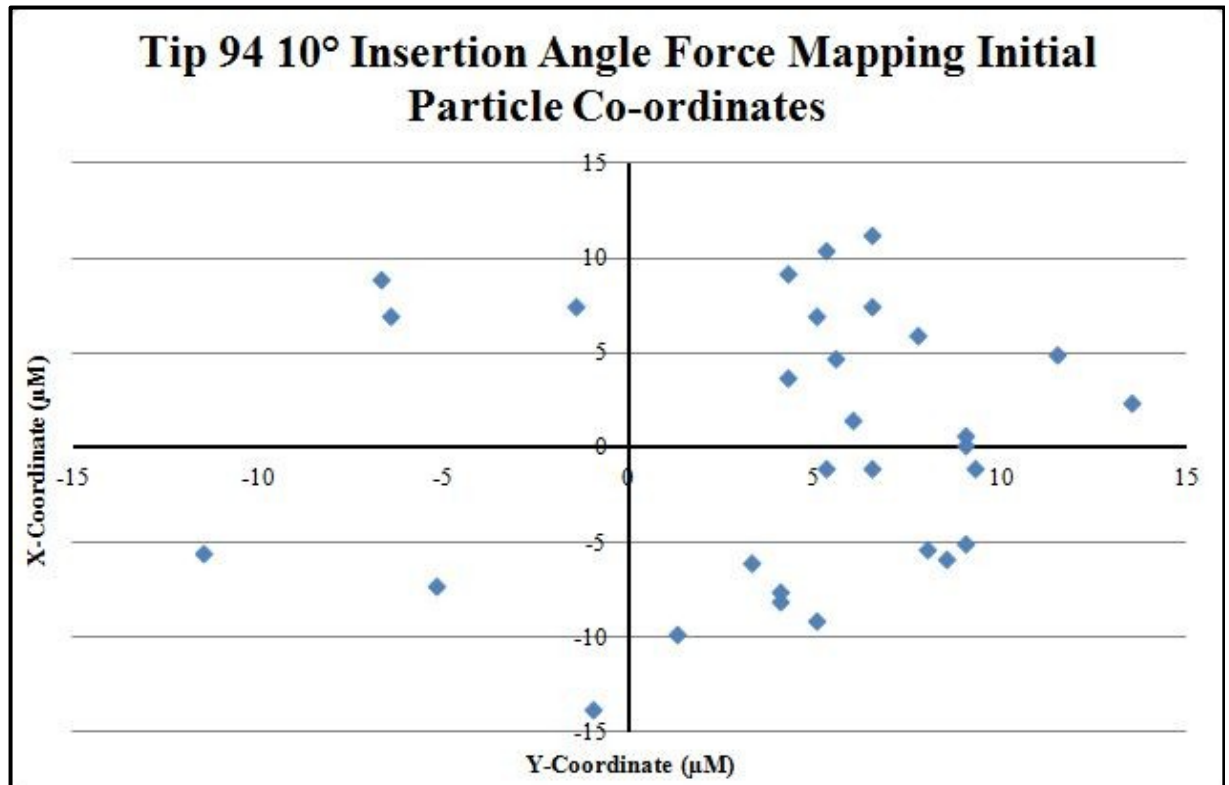


*Figure 9-1 particle distribution plot showing the starting position of 3µm silica microspheres recorded during multiple location optical trapping procedures*

The use of multimode fibre should also be explored and is an idea that was formulated following the critical analysis of a journal article ([Liu et al., 2006](#)). In this article a single fibre trap was created with a SMF that had a large core diameter whilst using a laser wavelength for which single mode operation should not have been achievable. However it appears that single mode output was actually achieved in this case, since they demonstrated 3D optical trapping with their tip. This formed the author's idea that maybe the laser beam could be spatially filtered, by the tapered end of a MMF, to produce a single mode Gaussian output suitable for Optical Trapping. If this was the case, then coupling of the

laser to fibre will become much easier, with additional benefits in that a high power connector would not be required as burning of the optical components would be less prevalent. The use of MMF, for laser to fibre coupling, could hold the potential to significantly improve the stability of the optical trap, with regard to unwanted power fluctuations, a problem that is due to the back-reflections associated with the use of the hollow metal ferrule high power connector currently employed by the coupling system. This would be a simple and relatively low cost exploration, which if successful would revolutionise the coupling of the laser to fibre.

Currently the system records video for later analysis. The video is decompiled into JPEG images using Blaze Media Pro software. These are then run through particle tracking software created in IDL. The resultant data is then processed through three, or four, additional IDL software programs, before force data is output. Additionally temperature and laser power monitoring is done using a LabView .vi program and the result is about six different software programs, each operating independently of one another, although all are reliant on each other to get the results. Therefore work should progress to develop a bespoke single optical trapping software platform that can run in real time to determine forces and conduct other calculations during live experiments.

Improved characterisation of the system must be achieved for accurate force analysis and optical trapping analysis to be realised and should include a larger range of particle sizes. Subsequent to the improved system characterisation, significant biological studies should be conducted on a variety of material of differing sizes, shapes and compositions.

This system was envisaged as a tool to aid investigations into the mechanical properties of cells. The main driving force for this system design was so that it could be incorporated easily with other advanced microscopy applications employed during these investigations.

Therefore preparatory work should also be carried out to make ready these additional microscopy applications for the T-FOTs integration. Such work would include the insertion of IR filter systems, so that the trapping laser light does not interfere with the optical systems of the AFM, or the laser scanning confocal microscope, etc.

The writing of this thesis has opened up more new questions regarding the future direction of this project and the work that still has to be undertaken before the system's true potential can be realised. Future T-FOTs system development will also be dependent on any future applications, as the development of yet smaller devices are increasingly in demand and are prevalent in today's society. Development of micro and nano technologies is technically demanding and requires the correct precision tools to meet the requirements.

At present optical tweezers are somewhat limited in the way that they can move and thus be applied within applications. In COT tweezers, many tweezers can be used independently in a 2D array to manipulate and move objects in the x, y and z directions. However since they are all orientated parallel to one another, their freedom of movement imposes limits when it comes to manipulating components in a manufacturing or assembly environment. Fibre based systems are limited to the amount of trapping sites that can be realistically imposed on the limited confines of a microscope's sample chamber. Nonetheless, this type of configuration offers increased flexibility in terms of trap arrangement, as two trapping fibres can be arranged orthogonally to one another. However this orientation is also limited in terms of the way the fibre end-faces are manipulated within the working area via the use of linear translation devices.

Greater freedom of movement and dexterity could be provided to the system through its union with a miniaturised robot that mimics the large scale production techniques down at the micro/nano manufacturing level. The system robot would have two arms each, with

shoulders elbows and wrists, which may also rotate and incorporate fibre bundles that carry various laser beams that could be used for different applications. The robotic “optical hands” could be used to assemble and fix nano/micro manufactured devices from many components. Additional fibres located in the robot hands could be used to transport additional “laser tools”, for example an optical hand can be used to hold a microsphere in place, whilst a second laser is used to fuse, drill, or cut it. For example the method of fusing a component to a substrate could be automatically repeated over and over again to build a structure with high precision and with the dexterity of a human operator.

Of course such a scheme would require significant research and development to overcome the technical challenges involved, for example, the reduction a robotic arm complete with moveable joints down to a size that is compatible with the working arena of a microscope stage. Similarly, delivering the laser light via optical fibre would also be an issue. The reason for this is because the rotation and bending of the robotic joints would have undesirable effects on the fibre itself. Therefore, at this moment in time such a scheme exists merely as a fanciful dream. However, the history tells us that such things can become reality with the advent of new technology. A prime example is optical trapping, which could never have been realised without the invention of the laser, so there is always hope for future developments. Who knows what the future holds? With the timely discovery of new super materials, such as Graphene, for example, entering the research arena at this juncture anything is possible.

Such future work offers the opportunity for industrial and academic collaboration, such as with one of the large scale robotic manufacturers, who have been instrumental in applying robotic production lines within automotive production plants. One thing is for sure, that optical trapping is no longer in its infancy, but it still has potential for growth

both in terms of technological advancement and in reaching out to new and innovative applications.

A large, horizontally-oriented rectangular box with a thick, dark gray border. The text "SECTION TEN REFERENCES" is centered within the box in a bold, black, serif font.

**SECTION TEN REFERENCES**

**REFERENCES**

- ABDELRAFIK, M., RENAUD, B. & FREDERIC VAN, L. 2001. Two-step process for micro-lens-fibre fabrication using a continuous CO<sub>2</sub> laser source. *Journal of Optics A: Pure and Applied Optics*, 3, 291
- ACAMPORA, A. S. 1994. The scalable lightwave network. *Communications Magazine, IEEE*, 32, 36-42.10.1109/35.335998.
- AGRAWAL, G. P. 1989. Nonlinear Fiber Optics. In: LIAO, P. F. & KELLEY, P. L. (eds.) *Quantum Electronics - Principles and Applications*. London: Academic Press Inc.
- ARLT, J., GARCES-CHAVEZ, V., SIBBETT, W. & DHOLAKIA, K. 2001. Optical micromanipulation using a Bessel light beam. *Optics Communications*, 197, 239-245
- ASHKIN, A. 1970. Acceleration and Trapping of Particles by Radiation Pressure. *Physical Review Letters*, 24, 156-159
- ASHKIN, A. 1992. Forces of a single-beam gradient laser trap on a dielectric sphere in the ray optics regime. *Biophysical Journal*, 61, 569-582[[http://dx.doi.org/10.1016/S0006-3495\(92\)81860-X](http://dx.doi.org/10.1016/S0006-3495(92)81860-X)].
- ASHKIN, A. 1997. Optical trapping and manipulation of neutral particles using lasers. *Proceedings of the National Academy of Sciences*, 94, 4853-4860 [<http://dx.doi.org/10.1073/pnas.94.10.4853>].
- ASHKIN, A. 2000. History of optical trapping and manipulation of small-neutral particle, atoms, and molecules. *Selected Topics in Quantum Electronics, IEEE Journal of*, 6, 841-856.10.1109/2944.902132.
- ASHKIN, A. & DZIEDZIC, J. M. 1971. Optical Levitation by Radiation Pressure. *Applied physics Letters*, 19, 283-285[<http://dx.doi.org/10.1063/1.1653919>].
- ASHKIN, A. & DZIEDZIC, J. M. 1987. Optical trapping and manipulation of viruses and bacteria. *Science*, 235, 4[<http://dx.doi.org/10.1126/science.3547653>].

- ASHKIN, A. & DZIEDZIC, J. M. 1989. Internal cell manipulation using infrared laser traps. *Proceedings of the National Academy of Sciences*, 86, 7914-7918 [<http://dx.doi.org/10.1073/pnas.86.20.7914>].
- ASHKIN, A., DZIEDZIC, J. M., BJORKHOLM, J. E. & CHU, S. 1986. Observations of a Single-Beam Gradient Force optical Trap for Dielectric Particles. *Optics Letters*, 11, 288-290 [<http://dx.doi.org/10.1364/OL.11.000288>].
- ASHKIN, A., DZIEDZIC, J. M. & YAMANE, T. 1987. Optical trapping and manipulation of single cells using infrared laser beams. *Nature*, 330, 769-771
- ASHKIN, A., SCHUTZE, K., DZIEDZIC, J. M., EUTENEUER, U. & SCHLIWA, M. 1990. Force generation of organelle transport measured in vivo by an infrared laser trap. *Nature*, 348, 346-348 [<http://dx.doi.org/10.1038/348346a0>].
- BARNARD, C. W. & LIT, J. W. Y. 1991. Single-mode fiber microlens with controllable spot size. *Applied Optics*, 30, 1958-1962 10.1364/ao.30.001958.
- BARNES, T., SHULMAN, A., FARONE, A., FARONE, M. & ERENDO, D. 2013. Assessment of the Elasticity of Erythrocytes in Different Physiological Fluids by Laser Traps. *Optics and Photonics Journal*, 3, 6 [<http://dx.doi.org/10.4236/opj.2013.32034>].
- BEAR, P. D. 1980. Microlenses for coupling single-mode fibers to single-mode thin-film waveguides. *Applied Optics*, 19, 2906-2909 10.1364/ao.19.002906.
- BELLINI, N., VISHNUBHATLA, K. C., BRAGHERI, F., FERRARA, L., MINZIONI, P., RAMPONI, R., CRISTIANI, I. & OSELLAME, R. 2010. Femtosecond laser fabricated monolithic chip for optical trapping and stretching of single cells. *Optics Express*, 18, 4679-4688 10.1364/oe.18.004679.
- BEZOMBES, F. A., LALOR, M. J. & BURTON, D. R. 2007. Contact microphone using optical fibre Bragg grating technology. *Journal of Physics: Conference Series*, 76, 012017
- BLACK, B. J. & MOHANTY, S. K. 2012a. Fiber-optic spanner. *Optics Letters*, 37, 5030-5032 10.1364/ol.37.005030.
- BLACK, B. J. & MOHANTY, S. K. Rotation of microscopic objects in fiber optic trap. Imaging, Manipulation, and Analysis of Biomolecules, Cells and Tissues, 2012b San Francisco. Proc. of SPIE, 82250B-82250B-82256,

- BLOCK, S. M., GOLDSTEIN, L. S. B. & SCHNAPP, B. J. 1990. Bead movement by single kinesin molecules studied with optical tweezers. *Nature*, 348, 348-352
- BRAGHERI, F., MINZIONI, P., CRISTIANI, I., LIBERALE, C., DE ANGELIS, F. & DI FABRIZIO, E. Numerical and experimental demonstration of a single fiber for optical trapping and analysis. Conference on Lasers and electro-Optics (CLEO)/Quantum Electronics and Laser Science Conference (QELS) and Photonic Applications Systems Technologies, 2008 San Jose, California. Optical Society of America,
- BRAGHERI, F., MINZIONI, P., LIBERALE, C., DI FABRIZIO, E. & CRISTIANI, I. 2008a. Design and optimisation of a reflection based fiber optic tweezers. *Optics Express*, 16, 17647-17653
- BRAGHERI, F., MINZIONI, P., LIBERALE, C., DI FABRIZIO, E. & CRISTIANI, I. 2008b. Design and optimization of a reflection-based fiber-optic tweezers. *Opt. Express*, 16, 17647-17653 [<http://dx.doi.org/10.1364/OE.16.017647>].
- BRAMBILLA, G. & XU, F. 2007. Adiabatic submicrometric tapers for optical tweezers. *Electronic Letters*, 43, 204-206 [<http://dx.doi.org/10.1049/el:20073709>].
- BROUHARD, G. J., SCHEK, H. T., III & HUNT, A. J. 2003. Advanced optical tweezers for the study of cellular and molecular biomechanics. *Biomedical Engineering, IEEE Transactions on*, 50, 121-125 [<http://dx.doi.org/10.1109/TBME.2002.805463>].
- CABRINI, S., LIBERALE, C., COJOC, D., CARPENTIERO, A., PRASCIOLU, M., MORA, S., DEGIORGIO, V., DEANGELIS, F. & DIFABRIZIO, E. 2006. Axicon lens on optical fiber forming optical tweezers, made by focused ion beam milling. *Microelectronic Engineering*, 83, 804-807 [<http://dx.doi.org/10.1016/j.mee.2006.01.247>].
- CAPITANIO, M., CICCHI, R. & SAVERIO PAVONE, F. 2007. Continuous and time-shared multiple optical tweezers for the study of single motor proteins. *Optics and Lasers in Engineering*, 45, 450-457 [<http://dx.doi.org/10.1016/j.optlaseng.2005.02.011>].
- CHAIGNEAU, M., MINEA, T. & LOUARN, G. 2007. Comparative study of different process steps for the near-field optical probes manufacturing. *Ultramicroscopy*, 107, 1042-1047 [<http://dx.doi.org/10.1016/j.ultramic.2007.02.047>].
- CHU, S. 1998. Nobel Lecture: The manipulation of neutral particles. *Reviews of Modern Physics*, 70, 685-706

- CHU, S., BJORKHOLM, J. E., ASHKIN, A. & CABLE, A. 1986. Experimental Observation of Optically Trapped Atoms. *Physical Review Letters*, 57, 410.1103/PhysRevLett.57.314.
- CISCO, S. 2005. Introduction to Optical Fibers, dB, Attenuation and Measurements. *Technical Support & Documentation – Cisco Systems* [Online]. Available: [http://www.cisco.com/image/gif/paws/29000/db\\_29000.pdf](http://www.cisco.com/image/gif/paws/29000/db_29000.pdf).
- COHEN-TANNOUJJI, C. N. 1998. Nobel Lecture: Manipulating atoms with photons. *Reviews of Modern Physics*, 70, 707-719
- COHEN, E. A. 1994. The Mystique of U.S. Air Power. *Foreign Affairs*, 73, 109-124
- COLLINS, S. D., BASHKIN, R. J. & HOWITT, D. G. 1999. Microinstrument Gradient-Force Optical Trap. *Applied Optics*, 38, 6068-6074 [<http://dx.doi.org/10.1364/AO.38.006068>].
- COLLINS, S. D., SIDICK, E., KNOESEN, A. & BASKIN, R. J. Micromachined optical trap for use as a microcytology workstation. In: GOURLEY, P. L., ed. *Micro and Nanofabricated Electro-Optical Mechanical Systems for Biomedical and Environmental Applications*, 1997 San Jose, CA. Proc. SPIE, 69-74,
- COLLINS, S. D., SIDICK, E., KNOESEN, A. & BASKIN, R. J. Micromachined optical trap for use as a microcytology workstation. In: PAUL, L. G., ed., 1997. SPIE, 69-74,
- CONSTABLE, A., KIM, J., ZARINETCHI, F. & PRENTISS, M. 1993. Demonstration of a fiber optical light-force trap. *Optics Letters*, 18, 1867-1869 [<http://dx.doi.org/10.1364/OL.18.001867>].
- DOYLE, A., CROSBY, S. R., BURTON, D. R., LILLEY, F. & MURPHY, M. F. 2011. Actin bundling and polymerisation properties of eukaryotic elongation factor 1 alpha (eEF1A), histone H2A–H2B and lysozyme in vitro. *Journal of Structural Biology*, 176, 370-378 [<http://dx.doi.org/10.1016/j.jsb.2011.09.004>].
- DOYLE, A., MURPHY, M. & CROSBY, S. Investigation of the structural components of the cellular scaffolding using transmission electron microscopy and fluorescence microscopy. The 6th GERI Annual Research Symposium GARS2010 2010 Liverpool UK. GERI Annual Research Symposium, 3-8, ISSN: 1757-6717.

- DUFRESNE, E. R. & GRIER, D. G. 1998. Optical tweezer arrays and optical substrates created with diffractive optics. *Review of Scientific Instruments*, 69, 1974[<http://dx.doi.org/10.1063/1.1148883>].
- FALLMAN, E. & AXNER, O. 1997. Design of a Fully Steerable Dual-Trap Optical Tweezers. *Applied Optics*, 36, 7[<http://dx.doi.org/10.1364/AO.36.002107>].
- FONTES, A., CASTRO, M. L. B., BRANDÃO, M. M., FERNANDES, H. P., THOMAZ, A. A., HURUTA, R. R., POZZO, L. Y., BARBOSA, L. C., COSTA, F. F., SAAD, S. T. O. & CESAR, C. L. 2011. Mechanical and electrical properties of red blood cells using optical tweezers. *Journal of Optics*, 13, 044012
- GAHAGAN, K. T. & SWARTZLANDER, G. A. 1996. Optical vortex trapping of particles. *Optics letters*, 21, 3
- GALAJDA, P. & ORMOS, P. 2001. Complex micromachines produced and driven by light. *Applied Physics Letters*, 78, 249
- GALLAGHER, R. P., SPINELLI, J. J. & LEE, T. K. 2005. Tanning Beds, Sunlamps, and Risk of Cutaneous Malignant Melanoma. *Cancer Epidemiology Biomarkers & Prevention*, 14, 562-566
- GAMBLING, W. A., PAYNE, D. N., MATSUMURA, H. & DYOTT, R. B. 1976. Determination of core diameter and refractive-index difference of single-mode fibres by observation of the far-field pattern. *Microwaves, Optics and Acoustics, IEE Journal on*, 1, 13-1710.1049/ij-moa:19760002.
- GAUTHIER, R. C. & FRANGIOUDAKIS, A. 2000. Optical Levitation Particle Delivery System for a Dual Beam Fiber Optic Trap. *Applied Optics*, 39, 26-3310.1364/ao.39.000026.
- GRIER, D. G. 2003. A revolution in optical manipulation. *Nature*, 424, 810-816[<http://dx.doi.org/10.1038/nature01935>].
- GRIER, D. G. & ROICHMAN, Y. 2006. Holographic optical trapping. *Appl. Opt.*, 45, 880-887[<http://dx.doi.org/10.1364/AO.45.000880>].
- GROSJEAN, T., SALEH, S. S., SUAREZ, M. A., IBRAHIM, I. A., PIQUEREY, V., CHARRAUT, D. & SANDOZ, P. 2007. Fiber microaxicons fabricated by a polishing technique for the

generation of Bessel-like beams. *Applied Optics*, 46, 8061-8067 [10.1364/ao.46.008061](https://doi.org/10.1364/ao.46.008061).

GROSS, S. P. 2003. Application of optical traps in Vivo. In: GERARD, M. & IAN, P. (eds.) *Methods in Enzymology*. Academic Press.

GUCK, J., ANANTHAKRISHNAN, R., MAHMOOD, H., MOON, T. J., CUNNINGHAM, C. C. & KAS, J. 2001. The optical Stretcher: A Novel Laser Tool to Micromanipulate Cells. *Biophysical Journal*, 81, 767-784 [[http://dx.doi.org/10.1016/S0006-3495\(01\)75740-2](http://dx.doi.org/10.1016/S0006-3495(01)75740-2)].

GUCK, J., ANANTHAKRISHNAN, R., MOON, T. J., CUNNINGHAM, C. C. & KAS, J. 2000. Optical deformity of Soft Biological Dielectrics. *Physical Review Letters*, 84, 5451-5454 [<http://dx.doi.org/10.1103/PhysRevLett.84.5451>].

GUCK, J., SCHINKINGER, S., LINCOLN, B., WOTTAWAH, F., EBERT, S., ROMEYKE, M., LENZ, D., ERICKSON, H. M., ANANTHAKRISHNAN, R., MITCHELL, D., KAS, J., ULVIC, S. & BILBY, C. 2005. Optical deformity as an inherent cell marker for testing malignant transformation and metastatic competence. *Biophysical Journal*, 88, 3689-3698

HA, C. & PAK, H. K. 2010. Observation of Colloidal Particle Dynamics Near a Flat Wall by Using Oscillating Optical Tweezers. *Journal of the Korean Physical Society*, 56, 5doi: 10.3938/jkps.56.977

HAHN, D. W. 2009. Light Scattering Theory. Florida: University of Florida.

HARUN, S. W., LIM, K. S., TIO, C. K., DIMYATI, K. & AHMAD, H. 2013. Theoretical analysis and fabrication of tapered fiber. *Optik - International Journal for Light and Electron Optics*, 124, 538-543 [<http://dx.doi.org/10.1016/j.ijleo.2011.12.054>].

HÉNON, S., LENORMAND, G., RICHERT, A. & GALLET, F. 1999. A New Determination of the Shear Modulus of the Human Erythrocyte Membrane Using Optical Tweezers. *Biophysical Journal*, 76, 1145-1151 [[http://dx.doi.org/10.1016/S0006-3495\(99\)77279-6](http://dx.doi.org/10.1016/S0006-3495(99)77279-6)].

HOFFMANN, P., DUTOIT, B. & SALATHÉ, R.-P. 1995. Comparison of mechanically drawn and protection layer chemically etched optical fiber tips. *Ultramicroscopy*, 61, 165-170 [[http://dx.doi.org/10.1016/0304-3991\(95\)00122-0](http://dx.doi.org/10.1016/0304-3991(95)00122-0)].

- HU, Z., WANG, J. & LIANG, J. 2004. Manipulation and arrangement of biological and dielectric particles by lensed fiber probe. *Optics Express*, 12, 4123-4128[<http://dx.doi.org/10.1364/OPEX.12.004123>].
- HU, Z., WANG, J. & LIANG, J. 2005. Manipulation of Yeast Cells by a Tapered Fiber Probe and Measurement of Optical Trapping Force. *Journal of the Korean Physical Society*, 47, 4
- HU, Z., WANG, J. & LIANG, J. 2006. Theoretical and experimental investigation of the optical trapping force in single lensed fibre trapping. *Journal of Optics A: Pure and Applied Optics*, 8, 891-896
- HU, Z., WANG, J. & LIANG, J. 2007. Experimental measurement and analysis of the optical trapping force acting on a yeast cell with a lensed optical fiber probe. *Optics and Laser Technology*, 39, 475-480
- IKEDA, M., TANAKA, K., KITAKA, M., TANAKA, M. & SHOHATA, T.-A. 2004. Rotational manipulation of a symmetrical plastic micro-object using fiber optic trapping. *Optics Communications*, 239, 103-108[<http://dx.doi.org/10.1016/j.optcom.2004.05.057>].
- JÄCKLE, H. & JAHN, R. 1998. Vesicle transport: Klarsicht clears up the matter. *Current Biology*, 8, R542-R544[[http://dx.doi.org/10.1016/S0960-9822\(07\)00343-0](http://dx.doi.org/10.1016/S0960-9822(07)00343-0)].
- JENSEN-MCMULLIN, C., LEE, H. P. & LYONS, E. R. L. 2005. Demonstration of trapping, motion control, sensing and fluorescence detection of polystyrene beads in a multi-fiber optical trap. *Optics Express*, 13, 2634-2642[10.1364/opex.13.002634].
- JESS, P. R. T., GARCÉS-CHÁVEZ, V., SMITH, D., MAZILU, M., PATERSON, L., RICHES, A., HERRINGTON, C. S., SIBBETT, W. & DHOLAKIA, K. 2006. Dual beam fibre trap for Raman micro-spectroscopy of single cells. *Opt. Express*, 14, 5779-5791
- JOHNSTON, G., BURTON, D. R., LILLEY, F., DOYLE, A., MURPHY, M. F., MADDEN, G., GDEISAT, M. A., MOORE, C. J., MARCHANT, T. & MATUSZEWSKI, B. Analysis of microscopy and reconstructive images for applications in medicine and biology. 18th IEEE International Conference on Image Processing (ICIP), 11-14 Sept. 2011 2011. 3069-3072, 1522-4880.
- JONG, Y. C., CHEN, J. H., HSU, J. H. & FANN, W. S. 1995. Constructions and Applications of a Simple Optical Tweezers. *Zoological Studies*, 34, 2

- KALOGIROU, S. A. 2009. *Solar Energy Engineering: Processes and Systems*, Elsevier Science.
- KAUPPILA, A., KINNUNEN, M., KARMENYAN, A. & MYLLYLÄ, R. 2012. Measurement of the trapping efficiency of an elliptical optical trap with rigid and elastic objects. *Appl. Opt.*, 51, 5705-5712
- KAWATA, S., SUN, H.-B., TANAKA, T. & TAKADA, K. 2001. Finer features for functional microdevices. *Nature*, 412, 697-698 [<http://dx.doi.org/10.1038/35089130>].
- KÖNIG, K., TADIR, Y., PATRIZIO, P., BERNS, M. W. & TROMBERG, B. J. 1996. Andrology: Effects of ultraviolet exposure and near infrared laser tweezers on human spermatozoa. *Human Reproduction*, 11, 2162-2164
- KREYSING, M. K., KIEBLING, T., FRITSCH, A., DIETRICH, C., GUCK, J. R. & KÄS, J. A. 2008. The optical cell rotator. *Optics Express*, 16, 16984-16992.10.1364/oe.16.016984.
- KRONER, A., KARDOSH, I., RINALDI, F. & MICHALZIK, R. 2006. Towards VCSEL-based integrated optical traps for biomedical applications. *Electronics Letters*, 42, 93-94.10.1049/el:20063821.
- KUMAR DE, A., ROY, D., SAHA, B. & GOSWAMI, D. 2008. A simple method for constructing and calibrating an optical tweezer. *Current Science*, 95, 2
- LANG, M. J. & BLOCK, S. M. 2003. Resource Letter: LBOT-1: Laser-based optical tweezers. *American Journal of Physics*, 71, 14 [<http://dx.doi.org/10.1119/1.1532323>].
- LEE, Y.-C. & WU, C.-Y. 2007. Excimer laser micromachining of aspheric microlenses with precise surface profile control and optimal focusing capability. *Optics and Lasers in Engineering* 45, 9
- LI, J., DOU, J., HERMAN, P. R., FRICKE-BEGEMANN, T., IHLEMANN, J. & MAROWSKY, G. 2007. Deep ultraviolet laser micromachining of novel fibre optic devices. *Journal of Physics: Conference Series*, 59, 691
- LI, Y., WEN, C., XIE, H., YE, A. & YIN, Y. 2009. Mechanical property analysis of stored red blood cell using optical tweezers. *Colloids and Surfaces B: Biointerfaces*, 70, 169-173 [<http://dx.doi.org/10.1016/j.colsurfb.2008.11.012>].

- LIAO, G.-B., BAREIL, P. B., SHENG, Y. & CHIOU, A. 2008. One-dimensional jumping optical tweezers for optical stretching of bi-concave human red bloodcells. *Optics Express*, 16, 1996-2004. [10.1364/oe.16.001996](https://doi.org/10.1364/oe.16.001996).
- LIAO, S., GONG, M. & ZHANG, H. 2009. Theoretical calculation of beam quality factor of large-mode-area fiber amplifiers. *Laser Physics*, 19, 437-444. [10.1134/s1054660x09030141](https://doi.org/10.1134/s1054660x09030141).
- LIBERALE, C., MINZIONI, P., BRAGHERI, F., DE ANGELIS, F., DI FABRIZIO, E. & CRISIANI, I. 2007. Minaturised all fiber probe for three dimensional optical trapping and manipulation. *Nature Photonics*, 1, 723-727 [<http://dx.doi.org/10.1038/nphoton.2007.230>].
- LIN, S. I. E. 2005. A lensed fiber workstation based on the elastic polishing plate method. *Precision Engineering*, 29, 146-150 [<http://dx.doi.org/10.1016/j.precisioneng.2004.05.008>].
- LIU, Y., CHENG, D. K., SONEK, G. J., BERNS, M. W., CHAPMAN, C. F. & TROMBERG, B. J. 1995. Evidence for localized cell heating induced by infrared optical tweezers. *Biophysical Journal*, 68, 2137-2144. [10.1016/s0006-3495\(95\)80396-6](https://doi.org/10.1016/s0006-3495(95)80396-6).
- LIU, Y. & YU, M. Fiber Optical Tweezers for Cell Manipulation and Force Sensing. Conference on Lasers and Electro-Optics/Quantum Electronics and Laser Science Conference and Photonic Applications Systems Technologies, 2007/05/06 2007 Baltimore, Maryland. Optical Society of America, CMAA6,
- LIU, Y. & YU, M. 2009. Investigation of inclined dual-fiber optical tweezers for 3D manipulation and force sensing. *Optics Express*, 17, 13624-13638
- LIU, Z., GUO, C., YANG, J. & YUAN, L. 2006. Tapered fiber optical tweezers for microscopic particle trapping: fabrication and application. *Opt. Express*, 14, 12510-12516 [<http://dx.doi.org/10.1364/OE.14.012510>].
- LYONS, E. R. & SONEK, G. J. 1995. Confinement and bistability in a tapered hemispherically lensed optical fiber trap. *Applied Physics Letters*, 66, 1584 [<http://dx.doi.org/10.1063/1.113859>].
- MADDEN, G., JOHNSTON, G., MURPHY, M., LILLEY, F. & BURTON, D. 2010. The effects of ionising radiation on the biometrics of living human cells. *The 6th GERI Annual*

*Research Symposium GARS2010*. Liverpool UK: The Proceedings Of The GERI Annual Research symposium.

MAIMAN, T. 1960. Stimulated optical radiation in ruby *Nature*, 187, 493-494

MAINSTER, M. A., STUCK, B. E., BROWN, J. & JR 2004. ASsessment of alleged retinal laser injuries. *Archives of Ophthalmology*, 122, 1210-1217.1001/archopht.122.8.1210.

MALIGNINO, N., PESCE, G., SASSO, A. & ARIMONDO, E. 2002. Measurements of trapping efficiency and stiffnes in optical tweezers. *optics Commiunications*, 214, 15-24[[http://dx.doi.org/10.1016/S0030-4018\(02\)02119-3](http://dx.doi.org/10.1016/S0030-4018(02)02119-3)].

MAMEREN, J., WUITE, G. L. & HELLER, I. 2011. Introduction to Optical Tweezers: Background, System Designs, and Commercial Solutions. *In*: PETERMAN, E. J. G. & WUITE, G. J. L. (eds.) *Single Molecule Analysis*. Humana Press.

MARUO, S., IKUTA, K. & KOROGI, H. 2003. Force-controllable, optically driven micromachines fabricated by single-step two-photon microstereolithography. *Microelectromechanical Systems, Journal of*, 12, 533-539.10.1109/jmems.2003.817894.

MEDIA, M. 2009. Blaze Media Pro. 9.10 ed.: Mystic Media.

MINZIONI, P., BRAGHERI, F., LIBERALE, C., DI FABRIZIO, E. & CRISTIANI, I. 2008. A novel approach to fiber-optic tweezers: numerical analysis of the trapping efficiency. *IEEE Journal of Selected Topics in Quantum Electronics*, 14, 151-157[<http://dx.doi.org/10.1109/JSTQE.2007.912910>].

MISAWA, H., SASAKI, K., KOSHIOKA, M., KITAMURA, N. & MASUHARA, H. 1992. Multibeam Laser Manipulation and Fixation of Microparticles. *Applied Physics Letters*, 60, 310-312[<http://dx.doi.org/10.1063/1.106695>].

MOHANTY, S. K., VERMA, R. S. & GUPTA, P. K. 2007. Trapping and controlled rotation of low-refractive-index particles using dual line optical tweezers. *Applied Physics B: Lasers and Optics*, 87, 211-215.10.1007/s00340-007-2617-7.

MOLLOY, J. E. & PADGETT, M. 2002. Lights, action:optical tweezers. *Contemporary Physics*, 43, 17

- MURPHY, D. B. & DAVIDSON, M. W. 2012. *Fundamentals of Light Microscopy and Electronic Imaging*, Hoboken, New Jersey, John Wiley and Sons Inc.
- MURPHY, M. F. 2007. *Investigating the Mechanical & Structural Properties of Human Cells Using Atomic Force & Confocal Microscopy* PhD PhD, Liverpool John Moores University.
- MURPHY, M. F., LALOR, M. J., MANNING, F. C. R., LILLEY, F., CROSBY, S. R., RANDALL, C. & BURTON, D. R. 2006. Comparative study of the conditions required to image live human epithelial and fibroblast cells using atomic force microscopy. *Microscope Research and technique*, 69, 757-765 [<http://dx.doi.org/10.1002/jemt.20339>].
- MURPHY, M. F., LILLEY, F., LALOR, M. J., CROSBY, S. R., MADDEN, G., JOHNSTON, G. & BURTON, D. R. 2012. Evaluation of a nonlinear Hertzian-based model reveals prostate cancer cells respond differently to force than normal prostate cells. *Microscopy Research and Technique*, n/a-n/a [<http://dx.doi.org/10.1002/jemt.22132>].
- NAWAZ, S., SÁNCHEZ, P., BODENSIEK, K., LI, S., SIMONS, M. & SCHAAP, I. A. T. 2012. Cell visco-elasticity measured with AFM and optical trapping at sub-micrometer deformations. *PLoS ONE*, 7, e45297
- NEUMAN, K. C. & BLOCK, S. M. 2004. Optical Trapping. *Review of Scientific Instruments*, 75, 23 [<http://dx.doi.org/10.1063/1.1785844>].
- NEUMAN, K. C., CHADD, E. H., LIU, G. F., BERGMAN, K. & BLOCK, S. M. 1999. Characterization of Photodamage to Escherichia coli in Optical Traps. *Biophysical Journal*, 77, 2856-2863
- NUGENT-GLANDORF, L. & PERKINS, T. T. 2004. Measuring 0.1-nm motion in 1 ms in an optical microscope with differential back-focal-plane detection. *Optics Letters*, 29, 2611-2613
- O'NEIL, A. T. & PADGETT, M. J. 2000. Three-dimensional optical confinement of micron-sized metal particles and the decoupling of the spin and orbital angular momentum within an optical spanner. *Optics Communications*, 185, 139-143 10.1016/s0030-4018(00)00989-5.
- PHILLIPS, W. D. 1998. Nobel Lecture: Laser cooling and trapping of neutral atoms. *Reviews of Modern Physics*, 70, 721-741

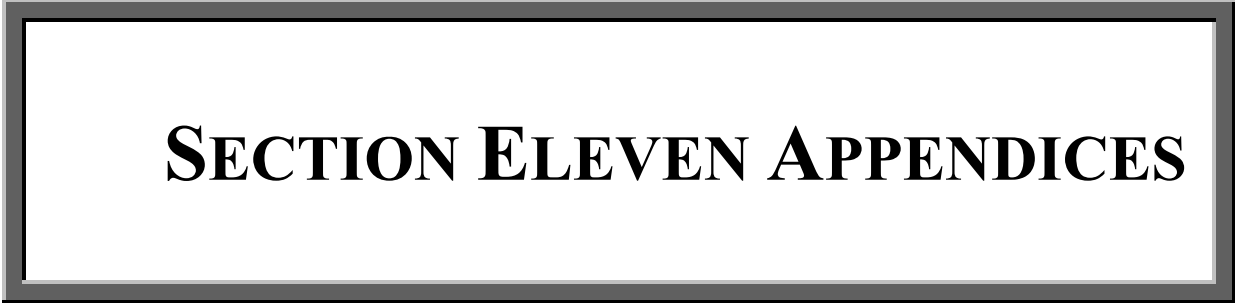
- PITT, G. D., EXTANCE, P., NEAT, R. C., BATCHELDER, D. N., JONES, R. E., BARNETT, J. A. & PRATT, R. H. 1985. Optical-fibre sensors. *Optoelectronics, IEE Proceedings J*, 132, 214-24810.1049/ip-j:19850047.
- PRESBY, H. M., BENNER, A. F. & EDWARDS, C. A. 1990. Laser Micromachining Of Efficient Fiber Microlenses. *Applied Optics*, 29, 2692-269510.1364/ao.29.002692.
- RANDALL, C. & MURPHY, M. Mechanical response and properties of human MRC5 and MRC5-SV2 transformed cell. 4th GERI Annual Research Symposium GARS2008, 2008 Liverpool UK. Proceedings Of The GERI Annual research symposium 3-8, ISSN: 1757-6717.
- RANDALL, C. M. 2009. *Investigating the Mechanical and Structural Properties of Human Cells by Atomic force Microscopy*. PhD PhD, Liverpool John Moores University.
- RAO, Y. J., D.J, W., JACKSON, D. A., ZHANG, L. & BENNION, I. 1998. Optical In-Fiber Bragg Grating Sense Systems for Medical Applications. *Journal of Biomedical Optics*, 3, 6
- RAZAGHI, M. R., MOKHTARPOUR, H. & MAZLOOMFARD, M. M. 2012. *Diode Laser Treatment of Human Prostates*.
- ROSS, S. 2011. OpticalTap25degrees.vi. Liverpool: LabView.
- ROSS, S. 2014a. clipdata1.pro. Liverpool: IDL V7.0.
- ROSS, S. 2014b. clipdata2.pro. Liverpool: IDL V7.0.
- ROSS, S. 2014c. Optical\_trap\_force1.pro. Liverpool: IDL V7.0.
- ROSS, S., MURPHY, M. F., LILLEY, F., LALOR, M. J. & BURTON, D. R. 2014. Single-beam three-dimensional optical trapping at extremely low insertion angles via optical fiber optimization. *Optical Engineering*, 53, 085107-08510710.1117/1.oe.53.8.085107.
- ROUNDY, C. 1999. Beam Profile Analysis: Propagation Factor Quantifies Laser beam Performance. *Laser Focus World*.

- RUDD, D., LOPEZ-MARISCAL, C., SUMMERS, M., SHAHVISI, A., GUTIÉRREZ-VEGA, J. C. & MCGLOIN, D. 2008. Fiber based optical trapping of aerosols. *Optics Express*, 16, 14550-14560. [10.1364/oe.16.014550](https://doi.org/10.1364/oe.16.014550).
- RUSSO, V., RIGHINI, G. C., SOTTINI, S. & TRIGARI, S. 1984. Lens-ended fibers for medical applications: a new fabrication technique. *Applied Optics*, 23, 3277-3283. [10.1364/ao.23.003277](https://doi.org/10.1364/ao.23.003277).
- SAKAI, K. & NODA, S. 2007. optical trapping of metal particles in doughnut-shaped beam emitted by photonic-crystal laser. *Electronics Letters*, 43, [210.1049/el:20073012](https://doi.org/10.1049/el:20073012)
- SIDICK, D., COLLINS, S. D. & KNOESEN, A. 1997. Trapping Forces in a Multiple-Beam Fiber-Optic Trap. *Applied Optics*, 36, 6423-6433
- SIEGMAN, A. E. 1993. Defining, measuring, and optimizing laser beam quality. 2-1210.1117/12.150601.
- SIEGMAN, A. E. How to (Maybe) Measure Laser Beam Quality. In: DOWLEY, M., ed., 1998. Optical Society of America, MQ1,
- SKYDAN, S. 2009. Traps.Pro. Liverpool: IDL V7.0.
- SOLMAZ, M. E., BISWAS, R., SANKHAGOWIT, S., THOMPSON, J. R., MEJIA, C. A., MALMSTADT, N. & POVINELLI, M. L. 2012. Optical stretching of giant unilamellar vesicles with an integrated dual-beam optical trap. *Biomedical optics express*, 3, 2419
- SONEK, G. J. & WANG, W. 1996. Theory of Optical Trapping Forces: A Review. *Review of Laser Engineering*, 24, 9
- SONI, G. V., HAMEED, F. M., ROOPA, T. & SHIVASHANKAR, G. V. 2002. Development of an optical tweezer combined with micromanipulation for DNA and protein nanobioscience. *Current Science*, 83, 1464-1470
- STEEN, W. M. & MAZUMDER, J. Diode-pumped Solid-state Lasers. Laser Material Processing, 2010 London. Springer, 45-50, 978-1-84996-062-5.
- SVOBODA, K. & BLOCK, S. M. 1994. Biological applications of optical forces. *Annual Review of Biophysics and Biomolecular Structure*, 23, 38 [<http://dx.doi.org/10.1146/annurev.bb.23.060194.001335>].

- SYKES, M. 1984. The compact disc, player and system. *Electronics and Power*, 30, 367-372 [10.1049/ep.1984.0202](https://doi.org/10.1049/ep.1984.0202).
- TAGUCHI, K., ATSUTA, K., NAKATA, T. & IKEDA, M. 2000. Levitation of a microscopic object using plural optical fibers. *Optics Communications*, 176, 43-47 [[http://dx.doi.org/10.1016/S0030-4018\(00\)00499-5](https://doi.org/10.1016/S0030-4018(00)00499-5)].
- TAGUCHI, K., OKADA, J., NOMURA, Y. & TAMURA, K. 2012. Three-Dimensional Optical Trapping for Cell Isolation Using Tapered Fiber Probe by Dynamic Chemical Etching. *Journal of Physics: Conference Series*, 352, 012039 [[http://dx.doi.org/10.1088/1742-6596/352/1/012039](https://doi.org/10.1088/1742-6596/352/1/012039)].
- TAGUCHI, K., TANAKA, M. & M, A. I. 2001. Theoretical study of an optical levitation using dual beam from optical fibres inserted at an angle. *Optics Communications*, 194, 67-73 [[http://dx.doi.org/10.1016/S0030-4018\(01\)01273-1](https://doi.org/10.1016/S0030-4018(01)01273-1)].
- TAGUCHI, K., UENO, H. & IKEDA, M. 1997. Optical Trapping of Dielectric Particle and Biological Cell Using optical Fibre. *Electronics Letters*, 33, 413-414
- TAGUCHI, K. & WATANABE, N. Single beam optical fiber trap. International Conference on Nanoscience and Technology (ICN&T 2006), 2007. Institute of Physics (IOP), 1137-1141,
- TAGUCHI, K. & WATANBE. Experimental and Theoretical Investigation of an Optical Levitation Using Dual-Beam from Optical Fibers Inserted at an Angle. International Conference on Nanoscience and technology (ICN&T 2006), 2007. Institute of Physics (IOP), 1127-1131,
- TAM, J., BIRAN, I. & WALT, D. R. 2004. An imaging fiber-based optical tweezer array for microparticle array assembly. *Applied Physics Letters*, 84, 11
- TAYLOR, R. & HNATOVSKY, C. 2003. Particle trapping in 3-D using a single fiber probe with an annular light distribution. *Opt. Express*, 11, 2775-2782 [[http://dx.doi.org/10.1364/OE.11.002775](https://doi.org/10.1364/OE.11.002775)].
- THUAL, M., MOREAU, G., RIBETTE, J., ROCHARD, P., GADONNA, M. & SIMON, J. C. 2005. Micro-lens on polarization maintaining fibre for coupling with 1.55  $\mu\text{m}$  quantum dot devices. *Optics Communications*, 255, 278-285 [[http://dx.doi.org/10.1016/j.optcom.2005.06.040](https://doi.org/10.1016/j.optcom.2005.06.040)].

- VALKAI, S., OROSI, L. & ORMOS, P. 2009. Optical tweezers with tips grown at the end of fibers by photopolymerization. *Applied optics*, 48, 4[<http://dx.doi.org/10.1364/AO.48.002880>].
- VISSCHER, K. & BRAKENHOFF, G. J. 1991. Single beam optical trapping integrated in a confocal microscope for biological applications. *Cytometry*, 12, 486-491[<http://dx.doi.org/10.1002/cyto.990120604>].
- VISSCHER, K., BRAKENHOFF, G. J. & KROL, J. J. 1993. Micromanipulation by “multiple” optical traps created by a single fast scanning trap integrated with the bilateral confocal scanning laser microscope. *Cytometry*, 14, 105-114[<http://dx.doi.org/10.1002/cyto.990140202>].
- VISSCHER, K., GROSS, S. P. & BLOCK, S. M. 1996. Construction of multiple-beam optical traps with nanometer-resolution position sensing. *Selected Topics in Quantum Electronics, IEEE Journal of*, 2, 1066-1076[<http://dx.doi.org/10.1109/2944.577338>].
- WANG, S., ARELLANO-SANTOYO, H., COMBS, P. A. & SHAEVITZ, J. W. 2010. Actin-like cytoskeleton filaments contribute to cell mechanics in bacteria. *Proceedings of the National Academy of Sciences*, 107, 9182-9185
- WARD, J. M., O'SHEA, D. G., SHORTT, B. J., MORRISSEY, M. J., DEASY, K. & CHORMAIC, S. G. N. 2006. Heat-and-pull rig for fiber taper fabrication. *Review of Scientific Instruments*, 77, 083105
- WATANABE, T. M., IWANE, A. H., TANAKA, H., IKEBE, M. & YANAGIDA, T. 2010. Mechanical Characterization of One-Headed Myosin-V Using Optical Tweezers. *PLoS ONE*, 5, e12224[<http://dx.doi.org/10.1371/journal.pone.0012224>].
- WAZENBOECK, H. D. & WADE, S. 2011. Focused Ion Beam Lithography, Recent Advances in Nanofabrication Techniques and Applications *In: CUI, P. B. (ed.). InTech*.
- WEBER, H. P., KALTENBRUNNER, W., HEINZE, A. & STEINBACH, K. 1997. Laser catheter coagulation of atrial myocardium for ablation of atrioventricular nodal reentrant tachycardia. *European Heart Journal*, 18, 487-495
- WEI, M. T., YANG, K., KARMENYAN, A. & CHIOU, A. 2006. A Three-Dimensional Optical Force Field on a Chinese Hamster Ovary Cell in Fibre-Optical Dual Beam Trap. *Optics Express*, 14, 3056-3064

- WELTE, M. A., GROSS, S. P., POSTNER, M., BLOCK, S. M. & WIESCHAUS, E. F. 1998. Developmental Regulation of Vesicle Transport in Drosophila Embryos: Forces and Kinetics. *Cell*, 92, 547-557 [http://dx.doi.org/10.1016/S0092-8674\(00\)80947-2](http://dx.doi.org/10.1016/S0092-8674(00)80947-2).
- XIN, H., SHI, P. & SHIFA, W. Fabrication of Optical Fiber Probe Nano-tips by Heated Micro-pulling Combined with Static Chemical Etching. *Nano/Micro Engineered and Molecular Systems*, 2006. NEMS '06. 1st IEEE International Conference on, 18-21 Jan. 2006 2006. 254-257,
- YING-CHIEN, T., YU-DA, L., CHIEN-LIANG, C., YU-KUAN, L. & WOOD-HI, C. 2008. A new scheme of fiber end-face fabrication employing a variable torque technique. *Journal of Micromechanics and Microengineering*, 18, 055003
- YU, Z., ZHIHAI, L., JUN, Y. & LIBO, Y. 2012. Four-Core Optical Fiber Micro-Hand. *Lightwave Technology, Journal of*, 30, 1487-1491 [10.1109/jlt.2012.2187772](http://dx.doi.org/10.1109/jlt.2012.2187772).
- YUAN, L., LIU, Z., YANG, J. & GUAN, C. 2008. Twin core fiber optical tweezers. *Optics Express*, 17, 4551-4558 <http://dx.doi.org/10.1364/OE.16.004559>.
- ZHAN, Q. 2003. Radiation forces on a dielectric sphere produced by highly focused cylindrical vector beams. *Journal of Optics A: Pure and Applied Optics*, 5, 229
- ZHANG, G., ZHU, Z., LI, Y., XIA, G. & LIN, Q. 2000. Numerical analysis of near-field optical trapping using tapered fiber probe. 321-328 [10.1117/12.390565](http://dx.doi.org/10.1117/12.390565).
- ZHANG, Y., LIU, Z., YANG, J. & YUAN, L. A new real non-invasive single fiber tweezers. Third Asia Pacific Optical Sensors conference, 2012a Sydney, Australia. Proc. SPIE 83512X-83512X-83515,
- ZHANG, Y., LIU, Z., YANG, J. & YUAN, L. 2012b. A non-contact single optical fiber multi-optical tweezers probe: Design and fabrication. *Optics Communications*, 285, 4068-4071 [10.1016/j.optcom.2012.06.025](http://dx.doi.org/10.1016/j.optcom.2012.06.025).

A large, horizontally-oriented rectangular box with a thick, dark gray border. The text "SECTION ELEVEN APPENDICES" is centered within the box in a bold, black, serif font.

**SECTION ELEVEN APPENDICES**

## APPENDICES

### 11.1 APPENDIX - A – PUBLICATIONS

#### 11.1.1 *NON-PEER REVIEWED*

Ross, S., Burton, D. R., Lalor, M. J., Lilley, F. & Murphy, M. F. An introduction to state of the art optical fibre trapping and its applications for studying the mechanical properties of cells. The 4th GERI Annual Research Symposium GARS 2008, 2008 Liverpool UK. Proceedings Of The GERI Annual Research Symposium 9-14, ISSN: 1757-6717.

Ross, S., Murphy, M. F., Lilley, F. & Burton, D. R. The Development of a 3 Dimensional LASER Light Force Optical Trap using a Tapered Optical Fibre Delivery System. The 5th GERI Annual Research Symposium GARS2009, 23rd June 2009 2009 Liverpool, UK. Proceedings of the GERI Annual Research Symposium, ISSN: 1757-6717.

Ross, S., Burton, D. R., Lalor, M. J., Lilley, F., Murphy, M. F., Bezombes, F. & Skydan, S. A fibre based "optical tweezers" system for the investigation of cell mechanics. *The 6th GERI Annual Research Symposium GARS2010*, 2010 Liverpool UK. The Proceedings Of The GERI Annual Research Symposium, 22-28, ISSN: 1757-6717.

Ross, S., Murphy, M. F., Lilley, F. & Burton, D. R. 2012. Fibre taper optimisation for single-beam 3-D optical trapping at near horizontal insertion angles. *7th GERI Annual Research Symposium GARS2012*. Liverpool, UK: Proceedings of the GERI Annual Research Symposium, ISSN: 1757-6717.

Ross, S., Lilley, F., Murphy, M. F. & Burton, D. R. Optical trapping: Evolution from free-beam to optical fibre "tweezers". *8th GERI Annual Research Symposium GARS2013*, 26th June 2013 2013 Liverpool, UK. Proceedings of the GERI Annual Research Symposium, ISSN: 1757-6717.

Ross, S., Lilley, F., Murphy, M. F. & Burton, D. R. Tapered fibre optic tweezers (T-FOTs) system for trapping at extremely low fibre insertion angles, *9th GERI Annual Research Symposium GARS2014*, Liverpool, UK: Proceedings of the GERI Annual Research Symposium, ISSN: 1757-6717.

**11.1.2 PEER REVIEWED**

Ross, S., Murphy, M. F., Lilley, F., Lalor, M. J. & Burton, D. R. 2014. Single-beam three-dimensional optical trapping at extremely low insertion angles via optical fibre optimization, *Optical Engineering*, 53, 085107-08510710.1117/1.oe.53.8.085107.

Ehtezazi, T., Davies, M. J., Seton, L., Morgan, M. N., Ross, S., Martin, G. D. & Hutchings, I. M. Optimizing the primary particle size distributions of pressurized metered dose inhalers by using inkjet spray drying for targeting desired regions of the lungs, *Drug Development and Industrial Pharmacy*, 10.3109/03639045.2013.858741.

**11.1.2.1 SINGLE-BEAM THREE-DIMENSIONAL OPTICAL TRAPPING AT EXTREMELY LOW INSERTION ANGLES VIA OPTICAL FIBER OPTIMIZATION**

Ross, S., Murphy, M. F., Lilley, F., Lalor, M. J. & Burton, D. R. 2014. Single-beam three-dimensional optical trapping at extremely low insertion angles via optical fibre optimization, *Optical Engineering*, 53, 085107-08510710.1117/1.oe.53.8.085107.

Copyright XXXX (2014) Society of Photo-Optical Instrumentation Engineers. One print or electronic copy may be made for personal use only. Systematic reproduction and distribution, duplication of any material in this paper for a fee or for commercial purposes, or modification of the content of the paper are prohibited.

DOI Abstract link:

<http://dx.doi.org/10.117/1.OE.53.8.085107>

# Optical Engineering

OpticalEngineering.SPIEDigitalLibrary.org

## **Single-beam three-dimensional optical trapping at extremely low insertion angles via optical fiber optimization**

Steven Ross  
Mark F. Murphy  
Francis Lilley  
Michael J. Lalor  
David R. Burton

**SPIE.**

Downloaded From: <http://opticalengineering.spiedigitallibrary.org/> on 09/18/2014 Terms of Use: <http://spiedigitallibrary.org/terms>

# Single-beam three-dimensional optical trapping at extremely low insertion angles via optical fiber optimization

Steven Ross,<sup>a,\*</sup> Mark F. Murphy,<sup>a,b</sup> Francis Lilley,<sup>a</sup> Michael J. Lalor,<sup>a</sup> and David R. Burton<sup>a</sup>

<sup>a</sup>Liverpool John Moores University, Faculty of Technology and Environment, General Engineering Research Institute, Byrom Street, Liverpool, L3 3AF, United Kingdom

<sup>b</sup>Liverpool John Moores University, The School of Pharmacy and Biomolecular Sciences, Byrom Street, L3 3AF, United Kingdom

**Abstract.** Employing optical fiber to deliver the trapping laser to the sample chamber significantly reduces the size and costs of optical tweezers (OT). The utilization of fiber decouples the OT from the microscope, providing scope for system portability, and the potential for uncomplicated integration with other advanced microscopy systems. For use with an atomic force microscope, the fiber must be inserted at an angle of 10 deg to the plane of the sample chamber floor. However, the literature states that optical trapping with a single fiber inserted at an angle  $\leq 20$  deg is not possible. This paper investigates this limitation and proposes a hypothesis that explains it. Based on this explanation, a tapered-fiber optical tweezer system is developed. This system demonstrates that such traps can indeed be made to function in three-dimensions (3-D) at insertion angles of  $\leq 10$  deg using relatively low optical powers, provided the fiber taper is optimized. Three such optimized tapered fiber tips are presented, and their ability to optically trap both organic and inanimate material in 3-D is demonstrated. The near-horizontal insertion angle introduced a maximum trapping range (MTR). The MTR of the three tips is determined empirically, evaluated against simulated data, and found to be tunable through taper optimization. © 2014 Society of Photo-Optical Instrumentation Engineers (SPIE) [DOI: [10.1117/1.OE.53.8.085107](https://doi.org/10.1117/1.OE.53.8.085107)]

Keywords: optical trapping; tapered optical fiber; applied optics; micro-optics; microlens.

Paper 140161 received Jan. 28, 2014; revised manuscript received Jun. 30, 2014; accepted for publication Jul. 22, 2014; published online Aug. 21, 2014.

## 1 Introduction

We aim here to develop an optical trapping system to aid our investigations into the mechanical properties of cells.<sup>1–6</sup> We currently employ atomic force microscopy (AFM) to carry out force-indentation experiments on adherent cells. However, we would also like to use AFM to study the force response of nonadherent cells, e.g., blood cells. In order to achieve this, the nonadherent cells would be required to be held in place while the AFM cantilever is brought into contact with them. This is one of the driving forces behind the design of our optical trap. The system should be physically decoupled from the microscope and exhibit a certain degree of portability to ensure its interoperability with other such microscopy systems. With this in mind, an optical fiber based system configuration has been proposed here.

Existing literature suggests that full three-dimensional (3-D) optical trapping is not possible using a single optical fiber inserted at an angle  $< 20$  deg to the plane of the sample chamber floor.<sup>7</sup> Previously, single optical fiber traps have also shown a significant reduction of trapping efficiency at insertion angles of  $< 40$  deg to the plane of the sample chamber.<sup>8</sup> To date, these limitations have not been investigated in order to discover their cause. This paper investigates these limitations and proposes a hypothesis that is based on the geometric profile of the optical fiber's distal end. Consequently, a solution is proposed whereby the geometry of the tapered optical fiber's distal end is optimized to allow 3-D optical trapping at an insertion angle of 10 deg for silica

particles 3  $\mu\text{m}$  in diameter. To the authors' knowledge, this is the first time that a fiber-based single-beam 3-D optical trapping system has been employed at such extremely low insertion angles for the particle sizes given above.

The authors are not claiming to have developed a new method for fiber taper fabrication here. Indeed, the method proposed in Ref. 9 was deemed to be an ideal solution for optical trapping of small particles at low insertion angles. However, it was found that replication of this work could not be achieved. An alternative method has been proposed in Ref. 10. By applying this latter dual heating method, the authors found that it was possible to achieve 3-D optical trapping, initially at an insertion angle of 45 deg, using low optical powers. At an insertion angle of 10 deg, 3-D optical trapping was still achieved. However, this was possible only when using exceptionally high optical output powers that were in excess of 500 mW. It was this finding that led to the hypothesis that will be described later in Sec. 5—a finding that spawned the development of the three optimized tapered fiber tips that are capable of 3-D optical trapping at extremely low insertion angles, using optical output powers of  $< 20$  mW.

The near horizontal orientation of the fiber has led to observable changes in the trapping dynamics when compared to those encountered at larger insertion angles. One such change was in the form of a maximum trapping range. Computer simulations of the optical trapping range for similar shaped optical fiber tapers have previously been performed.<sup>10</sup> However, since optical trapping at

\*Address all correspondence to: Steven Ross, E-mail: [s.ross@2002.ljmu.ac.uk](mailto:s.ross@2002.ljmu.ac.uk)

insertion angles  $<20$  deg have previously been perceived to be unattainable, determining these results experimentally has thus far been neglected.

## 2 Origins of Optical Trapping

The origins of optical trapping can be traced back to 1969 when Ashkin initiated investigations into the effects of electromagnetic radiation pressure upon microscopic particles.<sup>11</sup> It was during these experiments that unusual and extraordinary phenomena were observed. These observations led to a full appreciation of the optical forces at play during the interaction between light and matter, which led Ashkin to develop the first optical trapping systems.<sup>11,12</sup> In 1986, Ashkin developed the first single-beam, gradient force 3-D optical trap, which has since become known as optical tweezers.<sup>13</sup> Since then, these initial optical trapping systems have been built upon and improved, offering systems that provide multiple and flexible optical trapping sites.<sup>14–21</sup>

Optical traps are capable of generating optical forces  $>100$  pN with subnanometer resolution,<sup>22</sup> while simultaneously measuring the displacement of particles of sizes ranging between the Rayleigh and Mie regimes. As a consequence, optical trapping systems have since become invaluable tools within the physical<sup>23,24</sup> and biological sciences.<sup>25–28</sup> A full description of the theory, design, and construction of optical tweezers has been well covered in the literature and the reader is guided to Refs. 29–34.

### 2.1 Optical Fiber Based Optical Trapping System Configurations

The first optical fiber based optical trapping system was developed in 1993 in an effort to reduce both the system size and building costs. This simple system comprised two counterpropagating and cleaved optical fibers.<sup>35</sup> However, this configuration lacked stability in the longitudinal direction, leading to two different approaches being taken to address the issue. The first employed tapered hemispherical lenses fabricated onto the end of the optical fibers.<sup>36–39</sup> The second setup utilized a further two optical fibers, which were added to the system to provide a cross-hair configuration.<sup>40,41</sup>

The hemispherical lensed approach failed to provide 3-D trapping using a single fiber, since the necessary high numerical aperture could not be achieved. In an attempt to replicate optical tweezers, the first single optical fiber based full 3-D optical trap was developed.<sup>42</sup>

3-D trapping was claimed to have been achieved using a tapered optical fiber.<sup>43</sup> A description of the trapping experiment in a prior publication suggests that it was capable of only two-dimensional (2-D) trapping.<sup>8</sup> An axicon lens was fabricated directly onto the end of a single-mode fiber (SMF) using focused ion beam (FIB) lithography to create a Bessel mode beam output for optical trapping.<sup>44</sup>

A single-beam 3-D optical trap, with a trapping efficiency that was an order of magnitude less than that of the optical tweezers system, was designed by tapering a single-mode optical fiber using a heating and drawing method.<sup>10</sup> The trapping efficiency of 3-D optical fiber trapping systems was improved using an FIB milling machine to make incisions to the optical fiber core at its end-face, the result of which is that the output from either a four fiber bundle or

a fiber with an annular core is redirected to a centralized focal spot.<sup>45–48</sup>

Single-fiber 3-D trapping was demonstrated using a custom-built optical fiber consisting of four cores that were tapered by chemical etching. The thin taper was then melted using an electric arc to cause a lens effect.<sup>49</sup> A single-fiber 3-D optical trap was produced by chemically etching the end of an SMF to form a taper.<sup>7</sup> However, no attempt was made by the author to trap at insertion angles  $<20$  deg due to the perceived notion that it was not possible.

### 2.2 Limitations and Challenges of Using Optical Fiber

Optical fiber based systems offer certain advantages, such as reduced size and building costs. However, they also possess limitations when compared to classical systems, such as a reduction in trapping efficiency.<sup>10</sup> Although this limitation has been eradicated with novel fiber modifications, the requirement for intricate shaping of the fiber end-face can only be achieved using expensive equipment such as an FIB milling machine.<sup>44,45,47,48</sup> A FIB milling machine can cost in the region of £400,000. Alternative methods for shaping of the fiber, such as chemical etching, require the use of harmful and toxic chemicals,<sup>7</sup> while other configurations require the use of specialized optical fibers,<sup>45–49</sup> a factor that could also lead to increased system cost.

The heating and drawing method provides a nonhazardous and relatively low-cost option to focus the exiting laser light. The cost of the P2000/F micropipette puller used here is 50 times less than an FIB milling machine. For these reasons and because it is already a proven method that permits 3-D optical trapping,<sup>10</sup> a tapered fiber configuration was selected for this project.

Additionally, this method maintains the optical fiber's integrity as the core/cladding ratio is maintained. This is an important factor when one considers the laser light's mode of transport along the fiber is due to total internal reflection (TIR).<sup>50</sup> Furthermore, this method can be performed relatively quickly while still offering a certain degree of repeatability. These are desirable characteristics when one considers that the fragile tapered optical fiber tips can be easily subjected to damage.

The inability of fiber based systems to trap at insertion angles of  $<20$  deg to the microscope sample chamber<sup>7</sup> was the most significant challenge to this project. The intended integration of the tapered optical fiber trapping



Fig. 1 Asylum research molecular force probe three-dimensional (3-D) atomic force microscope head that houses the optical lever detection system located above the microscope's sample chamber.

system with our AFM (Asylum Research Molecular Force Probe atomic force microscope) requires the insertion angle of the fiber's distal end to be  $\leq 10$  deg. This would allow the fiber a clear passage under the AFM head, which is shown in Fig. 1, permitting the delivery of the laser light to the sample chamber of the microscope.

### 3 Tapered Fiber Optic Tweezers System Setup

The basic setup of the tapered fiber optic tweezers (T-FOTs) system is shown in Fig. 2. The laser source is a Ventus IR diode pumped solid state neodymium-doped yttrium aluminum garnet laser. It has a variable output power of up to 3 W and a wavelength of 1064 nm (Laser Quantum, Stockport, United Kingdom). The laser is coupled into a SMF via a laser to fiber coupler (Oz Optics Ltd., Ottawa, Canada).

To eliminate burning of the optical fiber during coupling, an SMF patch cord terminated with a high-power optical fiber connector consisting of a hollow metal ferrule is employed. The output of the high-power patch cord is fusion spliced to the input of a high-power PIN InGaAs 1% inline optical tap. Fusion spliced to the output end of the inline optical tap is a 10 m length of 1060XP SMF (Thorlabs Ltd., Ely, United Kingdom) for delivery of the laser to the sample chamber. The optical tap's output voltage is received by a USB-2404-UI DAQ module (Adept Scientific, Letchworth Garden, United Kingdom) and transmitted to the custom-built PC. The output signal from the optical tap is imported into a LabView virtual instrument and provides real-time monitoring of the optical power at the sample.

The 1060XP SMF's distal end was tapered using a Sutter P2000/F micropipette puller (Intracell Ltd., Shepreth, United Kingdom) to enable focusing of the laser light. The tapered optical fiber tip can be maneuvered within the sample chamber of a GXD-30 inverted microscope (Masarek Optical Systems Ltd., Southam, United Kingdom) in the  $X$ ,  $Y$ , and  $Z$  planes. Distances of up to 5 mm of coarse travel can be achieved using three motorized compact M-110.1DG microtranslation stages configured for  $X$ ,  $Y$ , and  $Z$  axis translations. Alternatively, movement of a finer nature can be achieved over 100  $\mu\text{m}$  distances in both the  $X$  and  $Y$  directions using the P-621.2CD PIHera XY Piezo stage and using the P-621.ZCD PIHera Precision Z stage in

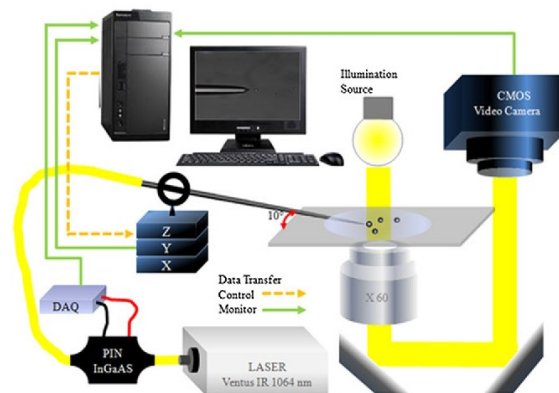


Fig. 2 Schematic diagram showing the setup of the single tapered optical fiber tweezers system.

Table 1 Tapered fiber optic tweezers system insertion losses.

Component	Insertion loss	Quantity	Total insertion loss
Laser to fiber coupler	1.25 dB	1	1.25 dB
HP Patch-cord	0.3 dB	1	0.3 dB
1060 XP single-mode fiber	1.5 dB/km	10 m	0.015 dB
Inline optical tap	0.15 dB	1	0.15 dB
Fusion splice	0.05 dB	2	0.1 dB
Additional losses	0.29 dB	1	0.29 dB
<b>Total system losses</b>			<b>2.855 dB</b>

the  $Z$  direction (Lambda Photometrics, Harpenden, United Kingdom). A miniature rotation stage 07 TRT 508 (CVI Laser Optics & Melles Griot, Cambridge, United Kingdom) allows changes to the insertion angle to be quickly and accurately achieved.

A CMOS video camera, DeltaPix Infinity X (Kane Computing Ltd., Northwich, United Kingdom), is used to monitor the microscope sample chamber, provide position detection, and record optical trapping procedures for later analysis.

Table 1 shows the insertion loss power budget for the T-FOT system. The given insertion losses for the system components are totaled to be 2.855 dB. This equates to a possible maximum output power at the sample of  $\sim 1558$  mW, which is an overall power loss of 48%. In reality, the system has a maximum power output of 1425 mW at the sample, which is a loss of 52.5%. Therefore, the actual system insertion losses are closer to 3.2 dB.

### 4 Experimental Test for 3-D Trapping

The tapered optical fiber tip is aligned within the microscope sample chamber. A sample solution of de-ionized water and 3  $\mu\text{m}$  diameter silica microspheres are added to a microscope slide. The tapered optical fiber tip is maneuvered about the sample chamber and aligned close to a microsphere. Then the laser is activated and the microsphere is observed. If the optical fiber taper is capable of only a 2-D optical trap, then it is disregarded.

The action of a 2-D optically trapped microsphere is depicted in Fig. 3. Here the optical fiber is inserted at an

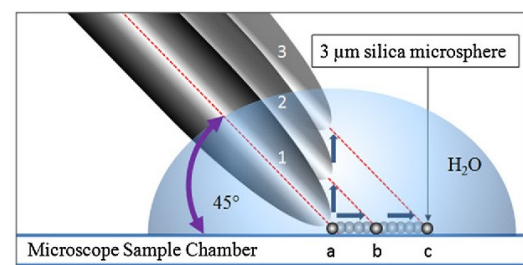


Fig. 3 The effect of optical fiber elevation on a microsphere that is optically trapped in only two dimensions.

Ross et al.: Single-beam three-dimensional optical trapping at extremely low insertion angles...

angle of 45 deg. The fiber can be seen to be at its initial location, denoted as position (1), with the microsphere located at position (a). As the fiber is elevated to position (2), the microsphere, guided by the laser beam, is pushed away from the fiber's end-face to position (b). As the fiber is further elevated, e.g., to position (3), it becomes indistinct as it gradually moves out of the focal region of the microscope objective. However, this is not the case for the microsphere, which, as it is only trapped in 2-D, fails to be elevated and, thus, is maintained clearly in focus as it remains seated on the microscope chamber floor at position (c). Since the microsphere remains guided within the beam by the gradient force, if the optical fiber is descended back to its original position (1), then the microsphere also returns back to the origin (a).

However, if optical trapping occurs at an insertion angle of 45 deg, then that taper is subjected to further testing to validate its capability for 3-D optical trapping. This involves elevating the trapping fiber in the positive  $z$  direction. If 3-D trapping occurs, then both the fiber and the microsphere will synchronously elevate. This is detectable by both the tip and the microsphere departing from the focal plane as exhibited in Fig. 4(f).

At near horizontal insertion angles, only 3-D optical trapping can stably hold a target. The reason for this is that the fiber's orientation is such that the sample chamber floor offers almost no resistance and, therefore, the particle will be propelled in the direction of the laser beam's propagation rather than being optically trapped.

#### 4.1 Result: Experimental 3-D Optical Trapping Test

Figure 4 shows images [Figs. 4(a) to 4(g)] taken from the video sequence of a 3-D optical trapping test experiment, recorded at 30 fps using the DeltaPix Infinity X CMOS video camera. The images show the tapered fiber optic tip number 44 at an insertion angle of 45 deg to the sample chamber. At the end of the tapered fiber optic tip is an optically trapped 3- $\mu\text{m}$  silica microsphere labeled A. The 3- $\mu\text{m}$  silica microsphere labeled B in the image sequences is free to drift in the surrounding medium (water). Sphere A is moved in an anticlockwise direction around the reference sphere B.

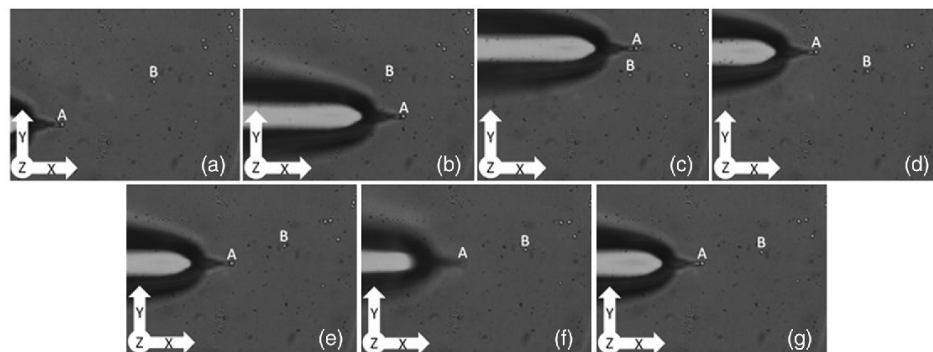


**Fig. 4** Tip number 44 3-D optical trapping at 45-deg insertion angle; X-Y trapping (a) the tapered fiber probe and 3- $\mu\text{m}$ -diameter silica microsphere trapped at the fiber end. (b) to (e) The piezo translation stages move the tapered fiber tip, directing sphere A in an anticlockwise direction around sphere B, in the directional sequence  $+X$ ,  $+Y$ ,  $-X$ ,  $-Y$ . (f) and (g) Z-Trapping. (f) The trapping fiber is moved in the  $+Z$  direction and both the fiber and the silica sphere can be seen to be out of focus. (g) The trapping fiber is moved in the  $-Z$  direction and both are now seen to be back in focus.

The directional sequence of the tapered fiber optic tip is (a) origin, (b)  $+X$  direction, (c)  $+Y$  direction, (d)  $-X$  direction, (e)  $-Y$  direction, (f)  $+Z$  direction, (g)  $-Z$  direction. When the translation stage was moved in the  $+Z$  direction, it is clear in (f) that both the tapered fiber optic tip and the silica microsphere travel together as they both leave the focal point of the microscope, returning to the focal point in (g) when moved in the  $-Z$  direction. Thus, it is evident that the sphere is confined and manipulated in a gradient force 3-D optical trap.

#### 5 Investigation of Trapping Degradation at Sub-45-Deg Insertion Angles

When the insertion angle for tip number 44 was altered from 45 to 10 deg, it was found that 3-D optical trapping could only be realized at an extremely high optical power output, which was in excess of 500 mW. It was this observation that led to the following hypothesis regarding a single fiber optical trap's inability to trap below 20 deg.

Figure 5 portrays a tapered optical fiber tip incident on the microscope sample chamber at an insertion angle of 45 deg. Once the fiber taper is sufficiently elevated, it sits directly above the subject microsphere allowing easy 3-D trapping to occur.

The implications of adopting such a short tapered, large-diameter tip at an insertion angle of 10 deg can be seen in Fig. 6. The underlying problem is that the fiber is now at an almost parallel plane to the microscope sample chamber.

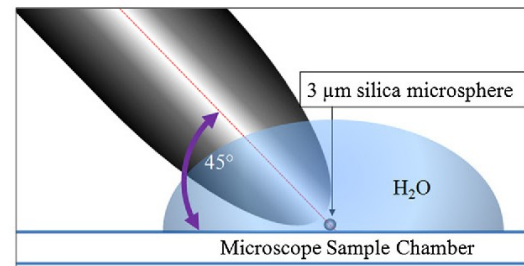


**Fig. 5** Large diameter, tapered optical fiber tip at an insertion angle of 45 deg.

Ross et al.: Single-beam three-dimensional optical trapping at extremely low insertion angles. . .

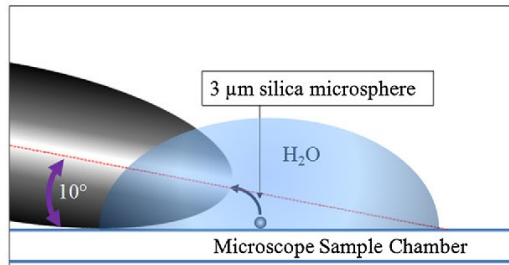


**Fig. 6** Large-diameter tapered optical fiber tip at an insertion angle of 10 deg.

This combination constitutes a fiber tip geometry for which the trapping zone is significantly elevated above the surface of the sample chamber's base surface. The result of this is that the microsphere has to be significantly elevated in the vertical +Z direction to enter the trapping zone. Unsurprisingly, this can only be achieved through the generation of very high optical forces, which are not acceptable for use in cell trapping applications such as the one envisaged here, as they result in cell damage.

### 5.1 Fiber Taper Optimization for 3-D Optical Trapping at a 10-Deg Insertion Angle

For biological samples, such as cells, to maintain viability during optical trapping procedures, typical optical powers employed can be as high as 340 mW at a wavelength ( $\lambda$ ) of 1064 nm and depend on the experiment conducted.<sup>51</sup> Therefore, increasing the optical power beyond this value is not a viable solution. Initial tests show that it would take focused laser light with optical powers in excess of 500 mW to 3-D optically trap at an insertion angle of 10 deg using tip number 44.

An alternative method to increase the optical forces being produced would be to optimize the laser beam's focus. This, in turn, would generate a steeper intensity gradient and, thus, facilitate an increased gradient force. This could be achieved by altering the geometric profile of the tapered optical fiber tip. Furthermore, shaping the taper profile in such a way as to coerce the laser beam's focal point closer to the subject to be trapped could also aid optical trapping. This action would potentially offer a superior and cell safe alternative to simply increasing the optical output power. Such a fiber taper would be required to exhibit a longer taper length and a reduction in tip diameter similar to that portrayed in Fig. 7.

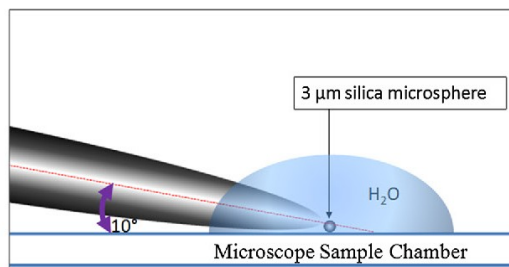


**Fig. 7** Proposed optimized optical fiber taper geometry possessing a longer taper length combined with a smaller diameter tip to gain closer proximity to the sample.

However, this type of taper profile could also prove to be unfeasible, since the long-taper, small-diameter tip may result in the fiber losing its integrity. This would inherently lead to the fiber becoming predisposed to high optical losses at the tapered tip. Such losses would effectively reduce the taper's ability to efficiently transport the laser light along the entirety of the taper due to TIR. Such losses would hinder the tapered fiber tip's ability to focus the light and, therefore, its ability to form an effective optical trap.

### 5.2 Development of Fiber Tapers for Optical Trapping at a 10-Deg Insertion Angle

Three additional working tips, numbered 92, 94, and 96, respectively, were successfully developed in an attempt to increase the likelihood of 3-D trapping at an insertion angle of 10 deg. The parameter values for the P2000/F programs can be seen in Table 2. Each of the tips underwent and passed the required 3-D optical trapping test as previously discussed in Sec. 4. Figures 8(b) to 8(d) show the dimensions of the three new tips, numbered 92, 94, and 96, in comparison with the original tip number 44 in Fig. 8(a).

**Table 2** Parameter values for the P2000/F micro-pipette puller used to fabricate the optical fiber tapers.

Program number	Heat	Filament	Velocity	Delay	Pull
44	320	002	022	128	000
	320	002	022	128	175
92	340	002	023	128	000
	340	002	023	127	175
94	325	002	023	128	000
	325	002	023	127	175
96	320	002	023	128	000
	320	002	023	127	175

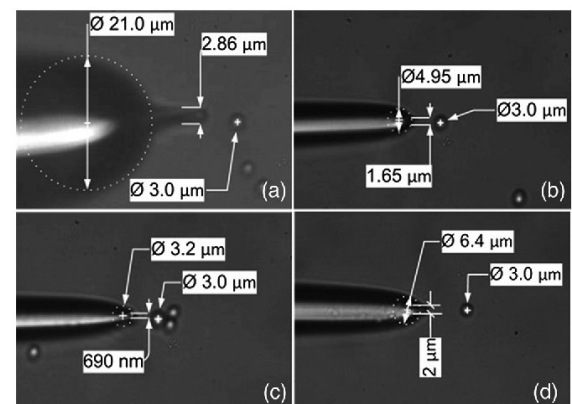


**Fig. 8** Dimensions of the tapered fiber optic tips numbered (a) 44, (b) 92, (c) 94, and (d) 96.

## 6 3-D Optical Trapping Test at 10-Deg Insertion Angle

Each of the three new tips demonstrated 3-D optical trapping of 3- $\mu\text{m}$ -diameter silica microspheres at an insertion angle of 10 deg to the microscope sample chamber. Each of the optimized optical fiber tapers could elevate and hold 3- $\mu\text{m}$ -diameter silica microsphere using optical powers as low as 10 mw. The microsphere could remain elevated by the optical trap after reducing the optical powers down to 1 mW.

### 6.1 Change in Trap Dynamics

When compared to optical trapping at an insertion angle of 45 deg, trapping at an insertion angle of 10-deg bore witness to changes in the trapping dynamics. First, while optical trapping at an insertion angle of 45 deg, it is difficult to trap and isolate a single particle. There is a tendency for multiple particles to be drawn into the optical trap. However, at an insertion angle of 10 deg, only a single particle could usually be trapped, with any additional particles being propelled in the direction of the beam. However, occasionally, two or three particles were observed to be simultaneously trapped.

The second change can be seen in Fig. 9, in which the introduction of a maximum trapping range (MTR) is depicted. The MTR comes into effect and is observable as the fiber is closer to a horizontal orientation. Therefore, there is no longer the same physical impedance provided by the glass microscope sample slide.

The image shows that there is a point at which the gradient and scattering forces cancel each other out, resulting in a zero net force. To either side of this equilibrium point are areas where either gradient or scattering forces dominate, respectively, and a particle's position in one or the other of these two areas dictates the direction in which the particle will subsequently move. If the particle is located on the side characterized by a dominant gradient force, then the particle is attracted toward the focal point of the laser beam and becomes optically trapped. If the particle is located toward the side characterized by a dominant scattering force, then the particle is repelled.

### 6.2 Experimental Method for Determining the Maximum Trapping Range

Discovery of a given taper's MTR was achieved by first optically trapping the subject microsphere as depicted in Fig. 10 (top). The laser is then deactivated and the optical fiber taper is moved a short distance in the negative  $X$  direction as depicted in Fig. 10 (middle). This short distance must be

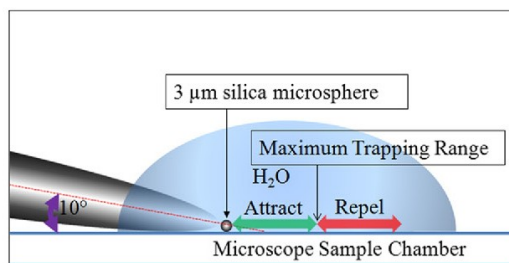


Fig. 9 Change in trapping dynamics with the introduction of a maximum trapping range.

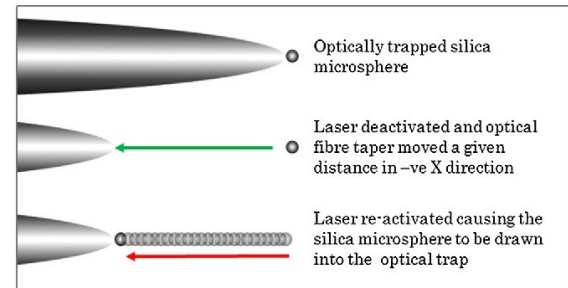


Fig. 10 Experimental procedure carried out to determine the trapping range.

less than the yet unknown maximum trapping range to ensure retrapping of the microsphere. When the tapered optical fiber occupies its new position, the laser is reactivated and the microsphere is attracted to the trapping zone as shown in Fig. 10 (bottom).

Initially, the distance between the tapered optical fiber's tip and the sphere is relatively short in order to establish a base point. If the distance is too great, the particle is repelled as it sits beyond the maximum trapping range. When the base point has been established, the process of trapping from a distance is repeated. Each time the process is repeated, the negative  $X$  distance of the optical fiber taper is systematically increased by 1- $\mu\text{m}$  increments from the established base point. At the point at which trapping no longer occurs and the microsphere is repelled, the previous distance is deemed to be the extremity of the maximum trapping range.

Videos of the optical trapping procedures are recorded and analyzed using a particle tracking (PT) software package which tracks the particle's course through each frame of video. The PT software calculates the coordinate data in both pixel and real distance values for the particle's trajectory along with the associated timestamps to enable further velocity and force analysis.

When attempting to determine the trapping range, a discrepancy was noted. It was found after running the associated video data through the PT software. The experimental data showed that the actual distance the particle travelled did not correctly correspond with the distance that the optical fiber taper was moved in the negative  $X$  direction, as determined by the Piezo translation monitoring and control software.

To further investigate this apparent anomaly, the experiment was repeated for a predetermined distance. The fiber was moved in the negative  $X$  direction away from the previously trapped microsphere by a distance of 9  $\mu\text{m}$  for tapers 92 and 94, and 10  $\mu\text{m}$  for taper 96. On each occasion, the microsphere's path back into the optical trapping zone was recorded using a high-speed video camera for later analysis using the PT software.

After comparison of the associated PT and Piezo monitoring and control data, a displacement error was determined, as shown in Table 3. To test that the discrepancy was not due to the Piezo actuator not translating for the required distance, a further check was made. This involved a 3- $\mu\text{m}$  silica microsphere being optically trapped and the fiber being moved in the negative  $X$  direction by a distance of 10  $\mu\text{m}$ , while the silica microsphere was still under the

Ross et al.: Single-beam three-dimensional optical trapping at extremely low insertion angles. . .

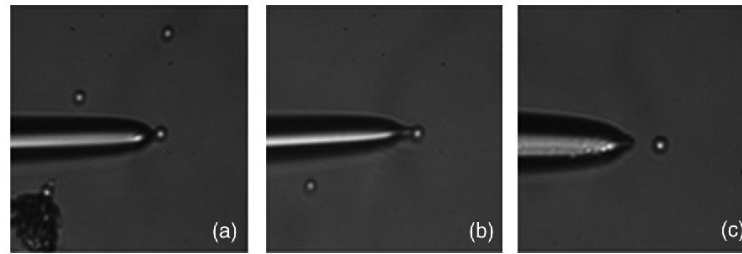


Fig. 11 Tapered optical fiber tips optically trapping 3- $\mu\text{m}$  silica microspheres showing their trapping zones corresponding to program numbers (a) 92, (b) 94, and (c) 96.

influence of the optical forces. The associated video data were then passed through the PT software and the distance travelled by the microsphere was found to be equal to the distance of the Piezo translation, thus eliminating any possibility of Piezo error.

### 6.3 Results: Determining the Maximum Trapping Range

Figures 11(a), 11(b), and 11(c) show the three optimized tapered optical fiber tips numbered 92, 94, and 96, respectively. It can be seen that for tips numbered 92 and 94, the focal points or trapping zones are in similar locations. Both can be seen to be trapping a 3- $\mu\text{m}$  silica microsphere at the fiber end with the microsphere actually coming into contact with the tip of the optical fiber. In contrast, the trapping zone for the tapered optical fiber tip numbered 96 can be seen to be at a distance of  $\sim 6.5 \mu\text{m}$  away from the end of the optical fiber tip.

Table 3 shows that the maximum trapping range for the three optical fiber tapers were found to be 9, 9, and 13  $\mu\text{m}$  for the optical fiber tapered tips 92, 94, and 96, respectively. However, in the case of tip number 96, the actual maximum distance from the end of the tapered optical fiber, from which a particle can be drawn into the optical trap is 19.5  $\mu\text{m}$ . This is due to the trapping zone or the focal point being located 6.5  $\mu\text{m}$  from the taper's end.

The disparity between the distance that the tapered optical fiber was moved in the negative  $X$  direction and the actual distance that the particle was displaced when being drawn back toward the fiber tip and into the optical trap can be seen in Table 3. It shows that there is a displacement error associated with the compared values. Tapered tip number 96 is seen to have the least error with 18% error, compared with 30.3 and 32.1% errors for tips 92 and 94, respectively.

Table 3 Trapping range error.

P2000/F program number	92	94	96
Maximum trapping range ( $\mu\text{m}$ )	9	13	13
Tip movement piezo value ( $\mu\text{m}$ )	9	9	10
Particle movement particle tracking value ( $\mu\text{m}$ )	6.27	6.11	8.20
Percentage error %	30.3	32.1	18

## 7 Trapping of Organic Material

Silica microspheres provide a good optical trapping subject that is ideal for system characterization. The reason for this is their uniformity in size, shape, and optical characteristics, i.e., refractive index. Live biological materials, such as cells, are dynamic. They can change shape and grow. Their optical characteristics are complex since their makeup consists of many dynamic components and materials. Therefore, optical fiber tips that are suitable for the trapping of silica microspheres might not be suitable for the trapping of complex biological systems.

The three tapered tips were tested to see if they could optically trap yeast cells in 3-D. This is by no means a thorough examination, since there are many different cells of all shapes and sizes which will be featured during future work. All three tips successfully trapped and elevated yeast cells of  $\sim 6 \mu\text{m}$  in diameter as shown in Fig. 12, where the fiber tip and the optically trapped yeast cell are both in focus and elevated above the general population of yeast cells. The nucleus of the trapped yeast cell is clear. Since the untrapped yeast cells are not in the focus of the microscope objective, they are seen as the dark shadow-like features.

## 8 Discussion

Three optimized optical fiber tapered tips have been developed for optical trapping at extremely shallow insertion angles of  $\leq 10$  deg. This orientation can be considered to be nearly horizontal and almost parallel to the plane of the sample chamber's base. All three of the optimized tapers could successfully trap, elevate, and hold 3- $\mu\text{m}$  silica microspheres using as little as 1 mW of optical power, a significant improvement compared with the original optical fiber taper number 44 that required in excess of 500 mW in order to trap

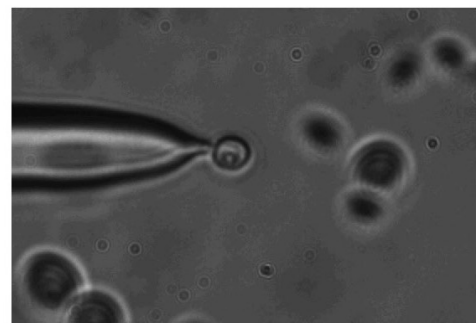


Fig. 12 Optical trapping and elevation of a yeast cell.

a similar silica microsphere in 3-D at an insertion angle of 10 deg.

The result of being able to trap at low optical powers is that the system is ideally suited for the optical trapping of organic biological material. The fact that optical trapping at low powers can now occur at insertion angles of  $\leq 10$  deg offers proof of concept that the fiber based optical trapping system developed here can be successfully integrated with an AFM. However, further work is still required before this realization can be implemented. For example, an IR optical filter would have to be retro-fitted in order to block the scattered optical trapping laser light from interfering with the AFM head optical lever detection system.

The contrast in maximum trapping ranges for the three optimized optical fiber tapered tips suggests that the maximum trapping range is tunable and is dependent upon the geometrical profile of the optical fiber taper. Furthermore, the trapping range can be exploited to offer a solution to particle sorting. The reduction in the optical trapping volume associated with near horizontal trapping at an insertion angle of 10 deg compared to trapping at a 45-deg insertion angle, will potentially offer a great advantage for applications involving single cell manipulation or particle sorting.

The observation that the distances are unequal for the optical fiber movement in the negative  $X$  direction and the actual particle displacement as it is drawn into the optical trap, can be explained through the following hypothesis. When the taper is moved away from the microsphere, the relatively large size and shape of the optical fiber taper causes a disturbance in the medium. The microsphere, which is then free from optical trapping forces, is then dragged in the tapered optical fibers wake, i.e., the disturbance within the medium caused by the relatively large tapered optical fiber's physical movement. Therefore, the microsphere's original position is not maintained. This phenomenon is compounded as the effects of Brownian motion may also contribute to the microsphere's new starting point.

This hypothesis is strongly supported as it is evident that the percentage error for taper 96 is far less than that of tapers 92 and 94. This can be attributed to the focal point of taper 96 being a distance of  $\sim 6.5 \mu\text{m}$  away from the fiber end-face, unlike that of tapers 92 and 94, both of which have a trapping point that is in extreme close proximity (equal to the radius of a microsphere  $\approx 1.5 \mu\text{m}$ ) to the end of the tapered tip. Consequently, any potential tip disturbance effects for tapered optical fiber tip numbered 96 would impinge less upon the microsphere as it is at a greater distance from the tip in comparison to tapered optical fiber tips numbered 92 and 94.

The maximum trapping ranges offered by the three optimized tapered fiber optic tips numbered 92, 94, and 96 are given as 9, 13, and 13  $\mu\text{m}$ , respectfully. The measured values are in good agreement with the simulated data presented in Ref. 10, in which the predicted values for the trapping range of a tapered optical fiber were stated to be in the range of 0 to 12  $\mu\text{m}$ . However, this simulated data suggested that particles located at a distance of 15  $\mu\text{m}$  from the optical fiber would be propelled away from the tip due to the scattering force. This simulation implies then that there is a 3  $\mu\text{m}$  distance between 12 and 15  $\mu\text{m}$  from the fiber tip over which it is not clear whether a particle would be either trapped or repelled.

Here the authors have experimentally determined the maximum trapping range to an accuracy of 1  $\mu\text{m}$ . Such accuracy was achieved as the incremental distances that the fiber was moved away from the particle were 1  $\mu\text{m}$  in length. Taking into account the simulated data's uncertainty of 3  $\mu\text{m}$ , the accuracy provided by the 1- $\mu\text{m}$  increments was deemed satisfactory.

The trapping region of tip number 96 is also of great interest as its distance from the tip is ideally suited for noncontact manipulation of larger and biological material since the physical optical fiber would not cause interference with the specimen.

It is believed that the variances in maximum trapping range could also offer an indication as to the quality of the optical trapping efficiency, the reasoning being that increases in trapping ranges could be due to increases in the gradient forces being generated through optimized focusing of the beam.

## 9 Conclusion

The literature suggests that single optical fiber 3-D optical trapping systems cannot operate at fiber insertion angles of  $< 20$  deg. In order for a single fiber based system to be integrated within an AFM, this assumption must be contradicted; otherwise the amalgamation of the two systems cannot be realized. The reason is that in order for the fiber to pass under the AFM head, it must enter the sample chamber at an insertion angle of 10 deg.

A comprehensive review of the various optical trapping system configurations that are currently available and a description of the tapered fiber optic tweezers (T-FOT's) system developed here is presented. This is followed by an investigation as to why optical trapping, for single fiber based systems, fails at low insertion angles and a hypothesis based on the findings is offered.

The investigations found that the geometric profile of the tapered optical fiber tip number 44 was too large. The result of this meant that any potential trapping targets would have to be elevated up into the trapping zone. This required in excess of 500 mw of optical power and was, therefore, unfeasible as such high intensities would be highly damaging to living biological samples. This finding led to the development of three optimized optical fiber taper profiles. Consisting of longer taper lengths and reduced tip diameters. By using these optimized tapers, 3-D optical trapping at an insertion angle of 10 deg and with reduced optical power outputs of a little as 1 mW was achieved. The results offer proof of concept that the T-FOT's system could be successfully integrated with a typical AFM, subject to modifications being made to protect its optical lever detection system from the trapping laser.

When compared to optical trapping at a 45-deg insertion angle, optical trapping at the near horizontal insertion angle of 10 deg produced a change in the optical trapping dynamics.

First, there was the introduction of a maximum trapping range, which is the maximum distance from the focal point or trapping zone in which the particle can be drawn in and trapped. Beyond this point the particle is repelled due to the influence of the greater scattering force. The maximum trapping ranges for the tips numbered 92 and 94 are both given as 9  $\mu\text{m}$  and that for tip number 96 is 13  $\mu\text{m}$ . Such variances in

the maximum trapping ranges of the optimized tapered optical fiber tips suggest that the maximum trapping range is tunable, is dependent on the geometric profile of the optical fiber taper, and could possibly be an indicator for trapping efficiency.

Second, the trapping volume was found to be substantially reduced in that only a single particle could be trapped at any one time. Being able to target a specific particle in this manner could be used for single particle analysis and particle sorting applications.

Finally, the optimized tapers also exhibited varying focal distances from the end of the optical fiber tip. Tips 92 and 94 both trapped the particle at the end of the fiber at a distance equal to the radius of the microsphere. Tip 96, on the other hand, trapped a particle  $\sim 6.5 \mu\text{m}$  away from the tip's end-face, which could be exploited for noncontact manipulation of biological cells, or large-diameter targets.

### Acknowledgments

This research was supported by the Engineering and Physical Sciences Research Council (EPSRC) under Grant No. R66311G. The authors thank EPSRC, Engineering Instrument Loan Pool, Rutherford Appleton Laboratory, United Kingdom, for the loan of the Photron FASTCAM MC-1 and the Photron Ultima APX, CMOS high-speed video cameras.

### References

1. A. Doyle et al., "Actin bundling and polymerisation properties of eukaryotic elongation factor 1 alpha (eEF1A), histone H2A-H2B and lysozyme in vitro," *J. Struct. Biol.* **176**(3), 370–378 (2011).
2. G. Johnston et al., "Analysis of microscopy and reconstructive images for applications in medicine and biology," in *18th IEEE Int. Conf. on Image Processing*, Brussels, pp. 3069–3072, IEEE (2011).
3. M. F. Murphy, "Investigating the mechanical & structural properties of human cells using atomic force & confocal microscopy," PhD Thesis, General Engineering Research Institute, Liverpool John Moores University, Liverpool (2007).
4. M. F. Murphy et al., "Comparative study of the conditions required to image live human epithelial and fibroblast cells using atomic force microscopy," *Microsc. Res. Tech.* **69**(9), 757–765 (2006).
5. M. F. Murphy et al., "Evaluation of a nonlinear Hertzian-based model reveals prostate cancer cells respond differently to force than normal prostate cells," *Microsc. Res. Tech.* **76**(1), 36–41 (2013).
6. C. M. Randall, "Investigating the mechanical and structural properties of human cells by atomic force microscopy," PhD Thesis, General Engineering Research Institute, Liverpool John Moores University, Liverpool (2009).
7. K. Taguchi et al., "Three-dimensional optical trapping for cell isolation using tapered fiber probe by dynamic chemical etching," *J. Phys.: Conf. Ser.* **352**(1), 012039 (2012).
8. Z. Hu, J. Wang, and J. Liang, "Manipulation and arrangement of biological and dielectric particles by lensed fiber probe," *Opt. Express* **12**(17), 4123–4128 (2004).
9. G. Brambilla and F. Xu, "Adiabatic submicrometric tapers for optical tweezers," *Electron. Lett.* **43**(4), 204–206 (2007).
10. Z. Liu et al., "Tapered fiber optical tweezers for microscopic particle trapping: fabrication and application," *Opt. Express* **14**(25), 12510–12516 (2006).
11. A. Ashkin, "Acceleration and trapping of particles by radiation pressure," *Phys. Rev. Lett.* **24**(4), 156–159 (1970).
12. A. Ashkin and J. M. Dziedzic, "Optical levitation by radiation pressure," *Appl. Phys. Lett.* **19**(8), 283–285 (1971).
13. A. Ashkin et al., "Observations of a single-beam gradient force optical trap for dielectric particles," *Opt. Lett.* **11**(5), 288–290 (1986).
14. D. G. Grier and Y. Roichman, "Holographic optical trapping," *Appl. Opt.* **45**(5), 880–887 (2006).
15. E. R. Dufresne and D. G. Grier, "Optical tweezer arrays and optical substrates created with diffractive optics," *Rev. Sci. Instrum.* **69**(5), 1974 (1998).
16. M. Capitano, R. Cicchi, and F. S. Pavone, "Continuous and time-shared multiple optical tweezers for the study of single motor proteins," *Opt. Lasers Eng.* **45**(4), 450–457 (2007).
17. K. Visscher, G. J. Brakenhoff, and J. J. Krol, "Micromanipulation by 'multiple' optical traps created by a single fast scanning trap integrated with the bilateral confocal scanning laser microscope," *Cytometry* **14**(2), 105–114 (1993).
18. K. Visscher, S. P. Gross, and S. M. Block, "Construction of multiple-beam optical traps with nanometer-resolution position sensing," *IEEE J. Sel. Topics Quantum Electron.* **2**(4), 1066–1076 (1996).
19. E. Fallman and O. Axner, "Design of a fully steerable dual-trap optical tweezers," *Appl. Opt.* **36**(10), 7 (1997).
20. H. Misawa et al., "Multibeam laser manipulation and fixation of microparticles," *Appl. Phys. Lett.* **60**(3), 310–312 (1992).
21. G. V. Soni et al., "Development of an optical tweezer combined with micromanipulation for DNA and protein nanobiotechnology," *Curr. Sci.* **83**(12), 1464–1470 (2002).
22. D. G. Grier, "A revolution in optical manipulation," *Nature* **424**(6950), 810–816 (2003).
23. A. Ashkin, "Trapping of atoms by resonance radiation pressure," *Phys. Rev. Lett.* **40**(12), 729–732 (1978).
24. S. Kawata et al., "Finer features for functional microdevices," *Nature* **412**(6848), 697–698 (2001).
25. A. Ashkin and J. M. Dziedzic, "Optical trapping and manipulation of viruses and bacteria," *Science* **235**(4795), 4 (1987).
26. A. Ashkin and J. M. Dziedzic, "Internal cell manipulation using infrared laser traps," *Proc. Natl. Acad. Sci.* **86**(20), 7914–7918 (1989).
27. A. Ashkin, J. M. Dziedzic, and T. Yamane, "Optical trapping and manipulation of single cells using laser beams," *Nature* **330**(24), 3 (1987).
28. A. Ashkin et al., "Force generation of organelle transport measured in vivo by an infrared laser trap," *Nature* **348**(6299), 346–348 (1990).
29. A. Ashkin, "Forces of a single-beam gradient laser trap on a dielectric sphere in the ray optics regime," *Biophys. J.* **61**(2), 569–582 (1992).
30. A. Ashkin, "Optical trapping and manipulation of neutral particles using lasers," *Proc. Natl. Acad. Sci.* **94**(10), 4853–4860 (1997).
31. K. Svoboda and S. M. Block, "Biological applications of optical forces," *Annu. Rev. Biophys. Biomol. Struct.* **23**, 247–285 (1994).
32. G. J. Brouhard et al., "Advanced optical tweezers for the study of cellular and molecular biomechanics," *IEEE Trans. Biomed. Eng.* **50**(1), 121–125 (2003).
33. K. C. Neuman and S. M. Block, "Optical trapping," *Rev. Sci. Instrum.* **75**(9), 23 (2004).
34. N. Malignino et al., "Measurements of trapping efficiency and stiffness in optical tweezers," *Opt. Commun.* **214**(1–6), 15–24 (2002).
35. A. Constable et al., "Demonstration of a fiber optical light-force trap," *Opt. Lett.* **18**(21), 1867–1869 (1993).
36. E. R. Lyons and G. J. Sonek, "Confinement and bistability in a tapered hemispherically lensed optical fiber trap," *Appl. Phys. Lett.* **66**(13), 1584 (1995).
37. K. Taguchi et al., "Levitation of a microscopic object using plural optical fibers," *Opt. Commun.* **176**(1–3), 43–47 (2000).
38. K. Taguchi, M. Tanaka, and M. Ikeda, "Theoretical study of an optical levitation using dual beam from optical fibres inserted at an angle," *Opt. Commun.* **194**(1–3), 67–73 (2001).
39. M. Ikeda et al., "Rotational manipulation of a symmetrical plastic micro-object using fiber optic trapping," *Opt. Commun.* **239**(1–3), 103–108 (2004).
40. S. D. Collins, R. J. Bashkin, and D. G. Howitt, "Microinstrument gradient-force optical trap," *Appl. Opt.* **38**(28), 6068–6074 (1999).
41. S. D. Collins et al., "Micromachined optical trap for use as a micro-cytology workstation," *Proc. SPIE* **2978**, 69–74 (1997).
42. R. Taylor and C. Hnatovsky, "Particle trapping in 3-D using a single fiber probe with an annular light distribution," *Opt. Express* **11**(21), 2775–2782 (2003).
43. Z. Hu, J. Wang, and J. Liang, "Manipulation of yeast cells by a tapered fiber probe and measurement of optical trapping force," *J. Korean Phys. Soc.* **47**, S9–S12 (2005).
44. S. Cabrini et al., "Axicon lens on optical fiber forming optical tweezers, made by focused ion beam milling," *Microelectron. Eng.* **83**(4–9), 804–807 (2006).
45. C. Liberale et al., "Minaturised all fiber probe for three dimensional optical trapping and manipulation," *Nat. Photonics* **1**(12), 723–727 (2007).
46. P. Minzioni et al., "A novel approach to fiber-optic tweezers: numerical analysis of the trapping efficiency," *IEEE J. Sel. Topics Quantum Electron.* **14**(1), 151–157 (2008).
47. F. Bragheri et al., "Numerical and experimental demonstration of a single fiber for optical trapping and analysis," in *Lasers and Electro-Optics/Quantum Electronics and Laser Science Conference and Photonic Applications Systems Technologies*, San Jose, California, pp. 1–2, Optical Society of America (2008).
48. F. Bragheri et al., "Design and optimisation of a reflection based fiber optic tweezers," *Opt. Express* **16**(22), 17647–17653 (2008).
49. L. Yuan et al., "Twin core fiber optical tweezers," *Opt. Express* **17**(7), 4551–4558 (2008).
50. G. Zhang et al., "Numerical analysis of near-field optical trapping using tapered fiber probe," *Proc. SPIE* **4082**, 321–328 (2000).

Ross et al.: Single-beam three-dimensional optical trapping at extremely low insertion angles...

51. S. P. Gross, "Application of optical traps in vivo," in *Methods in Enzymology*, M. Gerard and P. Ian, Eds., pp. 162–174, Academic Press, Miamisburg, OH (2003).

**Steven Ross** is a PhD student and a member of the Cell Mechanics Group, which is a multidisciplinary team of engineers and life scientists at the General Engineering Research Institute, Liverpool John

Moore's University. Research interest in optical fiber based optical trapping—optical tweezers. He received an MSc in telecommunications engineering from Liverpool John Moore's University (LJMU) in 2007 with a BEng in electronics and communications engineering also from LJMU in 2005.

Biographies of the other authors are not available.

## **11.2 APPENDIX – B - OPTICAL TRAPPING DATA SOURCES (ON DISK)**

### ***11.2.1 DISK 1 VIDEO DATA FOR TIP NUMBER 44***

Video recordings for optical trapping using tip number 44 at an insertion angle of 45° recorded at a video frame rate of 500 fps<sup>21</sup>

C001H001S0001.avi – 25% laser output

C001H001S0002.avi – 30% laser output

C001H001S0003.avi – 35% laser output

C001H001S0004.avi – 40% laser output

C001H001S0005.avi – 45% laser output

C001H001S0006.avi – 50% laser output

C001H001S0007.avi – 55% laser output

C001H001S0008.avi – 60% laser output

### ***11.2.2 DISK 1 DECOMPILED VIDEO DATA FOR TIP NUMBER 44***

Folders containing decompiled JPEG images for the videos of tip number 44 at an insertion angle of 45°.

C001H001S0001

C001H001S0002

C001H001S0003

C001H001S0004

C001H001S0005

C001H001S0006

---

<sup>21</sup> To view these videos at their true frame rate of 500fps please use the Photron FASTCAM Viewer.3 (PFV.3) software which can be downloaded free from: [http://www.photron.com/?cmd=product\\_general&product\\_id=16](http://www.photron.com/?cmd=product_general&product_id=16)

C001H001S0007

C001H001S0008

### ***11.2.3 DISK 2 VIDEO DATA FOR TIPS NUMBERED 92, 94 AND 96***

Video recordings for optical trapping using tip 92 at a fibre insertion angle of  $10^\circ$  recorded at a video frame rate of 500fps.

C001H001S0001.avi – 25% laser output

C001H001S0002.avi – 30% laser output

C001H001S0003.avi – 35% laser output

C001H001S0004.avi – 40% laser output

C001H001S0005.avi – 45% laser output

C001H001S0006.avi – 50% laser output

C001H001S0007.avi – 55% laser output

C001H001S0008.avi – 60% laser output

Video recordings for optical trapping using tip 94 at a fibre insertion angle of  $10^\circ$  recorded at a video frame rate of 500fps.

C001H001S0001.avi – 25% laser output

C001H001S0002.avi – 30% laser output

C001H001S0003.avi – 35% laser output

C001H001S0004.avi – 40% laser output

C001H001S0005.avi – 45% laser output

C001H001S0006.avi – 50% laser output

C001H001S0007.avi – 55% laser output

C001H001S0008.avi – 60% laser output

Video recordings for optical trapping using tip 96 at a fibre insertion angle of 10° recorded at a video frame rate of 500fps.

C001H001S0001.avi – 25% laser output

C001H001S0002.avi – 30% laser output

C001H001S0003.avi – 35% laser output

C001H001S0004.avi – 40% laser output

C001H001S0005.avi – 45% laser output

C001H001S0006.avi – 50% laser output

C001H001S0007.avi – 55% laser output

C001H001S0008.avi – 60% laser output

Video recordings for optical trapping using tip 92a at a fibre insertion angle of 10° recorded at a video frame rate of 500fps.

C001H001S0001.avi – 25% laser output

C001H001S0002.avi – 30% laser output

C001H001S0003.avi – 35% laser output

C001H001S0004.avi – 40% laser output

C001H001S0005.avi – 45% laser output

C001H001S0006.avi – 50% laser output

C001H001S0007.avi – 55% laser output

C001H001S0008.avi – 60% laser output

Video recordings for optical trapping using tip 94a at a fibre insertion angle of 10° recorded at a video frame rate of 500fps.

C001H001S0001.avi – 25% laser output

C001H001S0002.avi – 30% laser output

C001H001S0003.avi – 35% laser output

C001H001S0004.avi – 40% laser output

C001H001S0005.avi – 45% laser output

C001H001S0006.avi – 50% laser output

C001H001S0007.avi – 55% laser output

C001H001S0008.avi – 60% laser output

Video recordings for optical trapping using tip 94 at a fibre insertion angle of 10° recorded at a video frame rate of 1000fps.

C001H001S0001.avi – 25% laser output

C001H001S0002.avi – 30% laser output

C001H001S0003.avi – 35% laser output

C001H001S0004.avi – 40% laser output

C001H001S0005.avi – 45% laser output

C001H001S0006.avi – 50% laser output

C001H001S0007.avi – 55% laser output

C001H001S0008.avi – 60% laser output

#### ***11.2.4 DISK 2 DECOMPILED VIDEO DATA FOR TIPS NUMBERED 92, 94 AND 96***

Folders containing the decompiled JPEG images from the video recordings of optical trapping using tip 92 at a fibre insertion angle of 10° recorded at a video frame rate of 500fps.

C001H001S0001

C001H001S0002

C001H001S0003

C001H001S0004

C001H001S0005

C001H001S0006

C001H001S0007

C001H001S0008

Folders containing the decompiled JPEG images from the video recordings of optical trapping using tip 94 at a fibre insertion angle of  $10^\circ$  recorded at a video frame rate of 500fps.

C001H001S0001

C001H001S0002

C001H001S0003

C001H001S0004

C001H001S0005

C001H001S0006

C001H001S0007

C001H001S0008

Folders containing the decompiled JPEG images from the video recordings of optical trapping using tip 96 at a fibre insertion angle of  $10^\circ$  recorded at a video frame rate of 500fps.

C001H001S0001

C001H001S0002

C001H001S0003

C001H001S0004

C001H001S0005

C001H001S0006

C001H001S0007

C001H001S0008

Folders containing the decompiled JPEG images from the video recordings of optical trapping using tip 92a at a fibre insertion angle of 10° recorded at a video frame rate of 500fps.

C001H001S0001

C001H001S0002

C001H001S0003

C001H001S0004

C001H001S0005

C001H001S0006

C001H001S0007

C001H001S0008

Folders containing the decompiled JPEG images from the video recordings of optical trapping using tip 94a at a fibre insertion angle of 10° recorded at a video frame rate of 500fps.

C001H001S0001

C001H001S0002

C001H001S0003

C001H001S0004

C001H001S0005

C001H001S0006

C001H001S0007

C001H001S0008

Folders containing the decompiled JPEG images from the video recordings of optical trapping using tip 94 at a fibre insertion angle of 10° recorded at a video frame rate of 1000fps.

C001H001S0001

C001H001S0002

C001H001S0003

C001H001S0004

C001H001S0005

C001H001S0006

C001H001S0007

C001H001S0008

### **11.3 APPENDIX - C – DISK 2 T-FOTs SYSTEM SOFTWARE PROGRAMS**

IDL

clipdata1.pro

clipdata2.pro

optical\_trap\_force1.pro

Overplot.pro

Traps.pro

LabView

OpticalTap25degrees.vi

### **11.4 APPENDIX - D – DISK 2 SYSTEM COMPONENTS SPECIFICATION SHEETS**

1060\_XP\_spec\_20111220.pdf

DTS0042.pdf

DTS0108.pdf

Fastcam MC1.pdf

GX\_Microscopes\_GXD-20\_30\_series\_Datasheet.pdf

Infinity X Digital Camera for Microscopes.pdf

M110\_Datasheet.pdf

Omega thermocouple SA1XL-KI-2Mpdf

Oz optics standard tables.pdf

P620\_z\_Datasheet.pdf

P-2000\_OpMan.pdf

PI\_Specifications\_P-620\_1\_-\_P-629\_1\_30\_10\_2014.pdf

PM100 power monitor.pdf

T-FOTs Optical fibre light force trap components.xls

USB-2404UI-spec.pdf

VentusIR.pdf